Cardiff
Catalysis Institute

Sefydliad Catalysis
Caerdydd

Catalytic Methodologies for C(sp^3)-F Bond Formation with Heterogeneous Catalysts

Thesis submitted in accordance with the requirements of Cardiff University for the degree of doctor of philosophy by

Giulia Tarantino

School of Chemistry

Cardiff University

2018

Supervisor

Dr. Ceri Hammond

Abstract

Fluorinated compounds are extremely desirable in several fields of the chemical industry, such as pharmaceuticals, materials and agrochemicals. Consequently, the development of novel methods of fluorination represents a major challenge in contemporary chemistry. Although several breakthroughs have been achieved in this area in recent years, the development of an active, stable, reusable and truly heterogeneous catalyst, able to perform selective $C(sp^3)$-F formation, has not yet been achieved. Accordingly, this thesis explores the applicability of heterogeneous catalysts, to perform novel and selective $C(sp^3)$-F bond formations. Different strategies to achieve $C(sp^3)$-F bond synthesis were explored, including: i) fluorination of pre-activated substrates (*e.g.* carboxylic acids), and ii) direct $C(sp^3)$-H fluorination.

Firstly, the applicability of heterogeneous materials, such as Ag_xO/TiO_2 and pure TiO_2, were investigated for decarboxylative fluorination reactions (R-COOH $\rightarrow$ R-F), with (photo-fluorination) and without the employment of light sources. Following an investigation of the catalytic performances of Ag_xO/TiO_2 and pure TiO_2 for fluorination of pre-activated substrates, an alternative route, whereby the applicability of heterogeneous materials for direct $C(sp^3)$-H fluorination, was explored. Although more elegant and desirable, direct $C(sp^3)$-H fluorination represents an immense challenge, mainly due to the scarce substrate reactivity, which typically results in a requirement of harsher reaction conditions. Due to the challenges associated with activation of $C(sp^3)$-H bonds, two different systems to achieve direct $C(sp^3)$-H fluorination were investigated. Firstly, the viability of benzylic fluorinations was explored, as these substrates represent excellent model substrates with slightly activated C-H bonds. Secondly, substrates possessing less active $C(sp^3)$-H bonds, such as cyclooctane, were investigated for direct alkane fluorination.

Acknowledgements

First and foremost, I would like to thank Dr. Ceri Hammond for his guidance, support, and providing me with the opportunity to grow as a researcher, academic and professional. Furthermore, I am grateful for the opportunity to work on such an interesting PhD project, which facilitated a host of opportunities including the chance to spend a month working at Stanford University in collaboration with Prof. Edward Solomon, to whom I would also like to thank for welcoming me and his supervision during my stay.

Secondly, I would like to extend my deepest thanks to Dr. Nikolaos Dimitratos for his valuable advice, and to all the Hammond and Dimitratos group for their support and their friendship throughout my PhD. My PhD wouldn't have been so enjoyable without all of you guys, thanks.

I also would like to thank my whole family for their love, support and encouragement even from Italy. To my Mum and my Dad, thank you for everything that you have done for me, I couldn't have completed any of this without you, I owe you not only this PhD, but all the achievements in my life.

Special acknowledgments are for Francesco, Elly and Susana, thank you all for your understanding, love and support, for always helping me and for the amazing memories we've made and will continue to make in the future.

Last, but not least, I would like to thank Jonathan for everything, starting with all of your emotional support, standing me even in my worst mood, and always being there for me, I don't think I could have finished this thesis without you. Thank you.

Table of Contents

Chapter 1 – Introduction

Chapter 4 – Photocatalytic Decarboxylative Fluorination

Chapter 5 – Direct C(sp³)-H Fluorination: Benzylic Fluorination

Chapter 6 – Direct C(sp³)-H Fluorination: Alkane Fluorination

Chapter 7 – Conclusions and Pertaining Challenges

Chapter 8 – Appendix

Introduction

1

1.1 Fluorination

In recent decades, fluorinated materials and compounds have rapidly emerged as essential components and compounds in several fields of chemistry. In fact: i) methyl fluoride, a hydrofluorocarbon (HFC), widely used in semiconductor processing; ii) tetrafluoroethane, another HFC, used as a refrigerant; iii) perfluorooctanesulfonic acid, widely employed in the industry as a surfactant; and iv) Teflon, a polymer with many applications, are just a few examples of the broad range of applications found by fluorinated compounds. Consequently, the functionalisation of molecules to introduce fluorine functionality has gained increasing attention in recent years.

The first medicinal compound containing synthetic carbon-fluorine bonds was, 5-fluorouracil, reported in 1957, discovered during a study on the activities of fluorine derivatives of natural purine and pyrimidines.[1] Indeed, the biological, physical and chemical properties of an organic molecule can be significantly affected by the addition of a fluorine atom. Such effects include improved lipophilicity, bioavailability, metabolic stability, and increased protein-ligand interactions.[2] As such, fluorination reactions can be a highly useful tool when synthesising new pharmaceutical materials. Chemists have thus sought to develop new pathways to perform fluorination reactions efficiently, resulting in the formation of new, pharmaceutically active compounds.[3,4] However, although a substantial amount of all pharmaceuticals contain fluorine (approximately 20%),[4] only 21 natural molecules containing carbon-fluorine bonds are known, resulting in a low supply of natural fluorine containing compounds. This illustrates the significance of fluorine chemistry within the pharmaceutical industry.[1-4] An example of the impact of fluorine on the medicinal properties of compounds is given by fluorooxindole, a novel drug that is used for the treatment of stroke.[5] This discovery highlights the link between sustained research in C-F bond formation and the discovery of new pharmaceuticals for the treatment of diseases.

In addition to the key role played by fluorine in the pharmaceutical field, fluorine is also used to great effect in a variety of other chemical industries. The polymer industry alone contains several examples of the efficient use of fluorine chemistry. One of them is Teflon, a polymer used as a non-stick coating for cooking and kitchen equipment. Fluorine atoms are known to be responsible for the commercially desirable attributes of Teflon, such as hydrophobicity, low coefficient of friction and non-reactivity.[6] Another example of a perfluorinated polymer is Nafion, which is used in the fuel cell industry and produced through the addition of sulfonic acid groups into the Teflon polymeric structure. Nafion displays excellent thermal and mechanical stability and has therefore been used in fuel cell industry for over 40 years.[7] Fluorinated graphene is a new material that is also receiving significant interest despite being commercially unavailable at present. In fact, this material is considered as a 2D counterpart of Teflon, with potential applications in electronics and medicine.[8,9]

Another well-known application of fluorine chemistry is Positron Emission Tomography (PET).[10] PET scans are used to monitor metabolic processes and aid in the identification of disease. As such, PET scans are an integral part of modern medicine with many millions of scans performed every year. PET imaging uses positron emitting radionuclides as detectors, with ^{18}F isotopes typically used in the form of 2-[^{18}F]fluoro-2-deoxyglucose ([^{18}F]FDG), due to its low energy positron emission, resulting in high-quality 3D images. The wide employment of ^{18}F in PET mainly arises from the 110 minute half-life of ^{18}F, ideal for PET imaging as during this timeframe it is possible to perform a synthesis, administer the sample, and perform the imaging without causing a great deal of disruption to the patient. The benefit of using ^{18}F is therefore easy to see when comparing with other radionuclides such as ^{11}C, which has a half-life of only approximately 20 minutes.[11]

The use of fluorine in the examples noted above, and the dependence on fluorine in several other fields, including agrochemicals and perfluorinated solvents, has led to a high demand for the development of novel selective fluorination methods. Consequently, this pressure has inspired research into the realisation of new methods of fluorination, particularly facilitated by the development of several novel fluorinating reagents such as Selectfluor® and diethylaminosulfur trifluoride (DAST), which present many advantages over the highly dangerous F_2 and XeF_2 (see Section 1.2.3 for further discussion). Nevertheless, a large part of the fluorination methods reported in

literature (around 90%) are not catalytic, and often stoichiometric amounts of metals and/or metal complexes are used to convert substrates into the desired fluorinated compounds. Furthermore, despite the many goals recently achieved in this area, heterogeneous catalysts for the industrialisation of selective fluorination processes, have not yet been developed. The main target of this work is therefore to develop highly active, selective and stable solid catalysts for fluorination reactions, particularly focusing on selective $C(sp^3)$-F bond formation, which represents the major challenge in the field.

1.2 General methods of fluorination

The literature on novel fluorination reactions can be separated into three main reaction pathways: electrophilic, nucleophilic and radical fluorination. Each of these fields have benefitted greatly from the development of easy-to-handle fluorinated reagents such as Selectfluor® and XtalFluor-E. Prior to the development of such reagents, there was little progress regarding the development of C-F bond forming methods, primarily due to the safety concerns associated to the aggressive nature of the reagents needed for fluorination reactions. Perchloryl fluoride is an example of such a reagent. Indeed, it was linked to the death of two researchers and consequently caused the pharmaceutical industry to shut down production of its fluorinated products. Hence, an increase in the demand for safer fluorinating agents led to the search for safer reagents that are non-explosive, less toxic and preferentially inexpensive such as DAST, one of the major S-F fluorinating reagent. The development of such reagents represents one of the major breakthroughs in the field of nucleophilic fluorinations.[12]
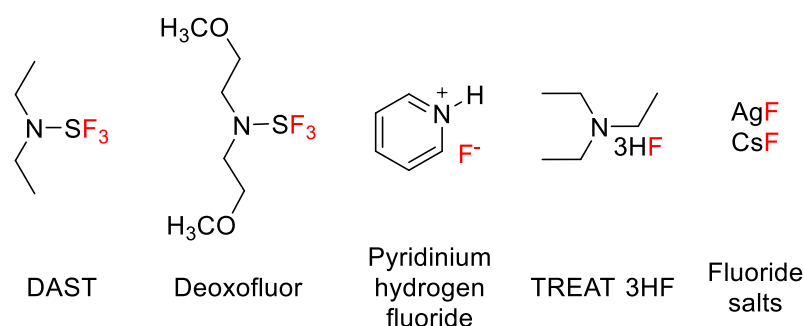
Figure 1.1: Examples of nucleophilic fluorinating agents.
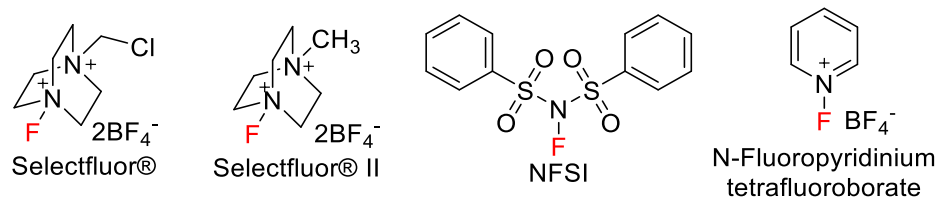
Figure 1.2: Examples of electrophilic fluorinating agents.

1.2.1 Nucleophilic fluorination

DAST has successfully been used for many years in an array of highly efficient and selective fluorination reactions. Notably, DAST has been shown to be an effective deoxofluorination reagent, as it is able to produce high product yields from a wide range of substrates.[13,14] One of the most important applications for DAST is the synthesis of allylic fluorides from allylic alcohols.[15] Allylic fluorides are important fluorinated compounds as they are commonly found in radioactive tracers and bioactive molecules. However, DAST is not without drawbacks; upon heating it readily decomposes, forming $(NEt_2)_2SF_2$, a dangerous and explosive compound. Additionally, it is unable to illicit regioselective or enantioselective control during reactions, and mixtures of isomers are typically formed. Furthermore, DAST exhibits poor reaction selectivity in the site-specific monofluorination of allylic alcohols, yielding unwanted dehydrated and rearranged products. These drawbacks have therefore led to the development of crystalline nucleophilic fluorinating agents that are safer to employ, such as XtalFluor-E and simlar reagents.[16,17] XtalFluor-E is non-explosive and less moisture sensitive than DAST. It is also far easier to handle, being solid at room temperature. Furthermore, XtalFluor-E has been shown to perform deoxofluorination reactions with higher selectivity than DAST, and has also been successfully used in other fluorination reactions such as aminofluorinations.[18] It is also worthy of note that XtalFluor-E has been shown to be active not only in fluorination reactions, but also as an efficient coupling agent in the amidation of carboxylic acids.[19]
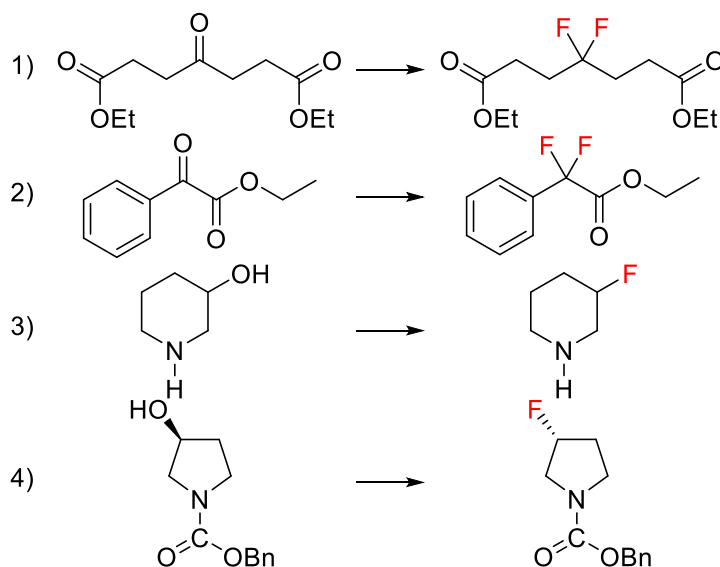
Figure 1.3: Examples of deoxofluorination reactions catalysed by DAST: **1)** deoxofluorination of diethyl 4-oxoheptanedioate to diethyl 4-difluoroheptanedioate, **2)** deoxofluorination of ethyl 2-oxo-2-phenylacetate to ethyl 2-difluoro-2-phenylacetate, **3)** deoxofluorination of piperidin-3-ol to 3-fluoropiperidine and **4)** enantioselective deoxofluorination of benzyl (S)-3-hydroxypyrrolidine-1-carboxylate to benzyl (R)-3-fluoropyrrolidine-1-carboxylate.

1.2.2 Electrophilic fluorination

In addition to the achievements observed in the field of nucleophilic fluorination, the development of the electrophilic fluorinating agent, 1-chloromethyl-4-fluoro-1,4-diazoniabicyclo[2.2.2]octane bis(tetrafluoroborate) (Selectfluor®, F-TEDA-BF$_4$), has also resulted in increased interest in electrophilic fluorination processes.[20] Electrophilic fluorinations have been traditionally performed using gaseous fluorine (F$_2$) or xenon difluoride (XeF$_2$), both of which present a number of safety concerns due to their high toxicity and strongly oxidising nature. Nevertheless, modern electrophilic fluorinating agents such as Selectfluor® and N-fluorobis(phenyl)sulfonamide (NFSI)[21] have opened a whole host of research opportunities regarding the electrophilic fluorination of functional groups. Selectfluor® is far safer than fluorine gas, and is consequently a milder and more efficient electrophilic fluorinating agent. Furthermore, it is generally less expensive to produce than traditional fluorinating agents.[22]

This ease of handling has led to an increased variety and a greater exploration of the capabilities of electrophilic fluorination. It has been recently shown that Selectfluor® is able to fluorinate a wide range of functional groups including aromatics, alkenes and

enamines (Figure 1.4). Unfortunately, such fluorinations are only reported to work with sp^2 carbons and, as with DAST, are not suitable for selective C(sp^3)–F bond formation when using the fluorinating reagent alone, *i.e.* in the absence of a catalyst. However, Selectfluor® can be used in combination with an organocatalyst to perform enantioselective monofluorination of alkyl compounds, which is not possible when using DAST.[23] Despite this breakthrough, it should be noted that this methodology is restricted to a limited number of substrates, and more general and versatile methods are therefore needed. It is for this reason that novel electrophilic pathways for the selective formation of alkyl fluorides are highly sought after, and is an area of fluorination chemistry that is of great interest to the scientific community.
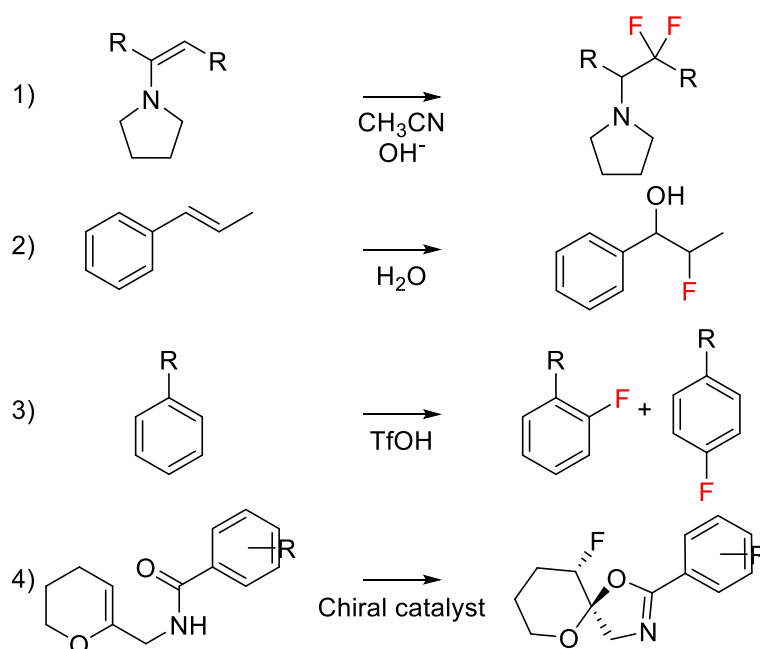
Figure 1.4: Examples of electrophilic fluorinations using Selectfluor®: **1)** synthesis of fluorinated carbonyl compounds from enamines,[24] **2)** synthesis of alkoxyfluorides from alkenes,[25] **3)** synthesis of aryl fluorides from aromatics,[26] and **4)** synthesis of fluorinated heterocycles *via* enantioselective fluorocyclisation.[23]

1.2.3 Radical fluorination

Unlike other methods of fluorination, radical fluorination has received much less attention in the literature. This type of reaction involves the generation of high energy free radicals that are produced through the scission of chemical bonds, resulting in an unpaired valence electron. Unlike electrophilic fluorinations, radical fluorination pathways are rapid and often proceed with low selectivity and poor reaction control,

due to the high energy nature of the radical species in question. For this reason, the development of synthetic methodologies based upon radical reaction pathways have been somewhat ignored.

Radical fluorination reactions typically involve fluorine radical (F$^\bullet$) species, generated by homolytic dissociation of F-F bond in F$_2$. Comparing the dissociation energies related to homolytic and heterolytic scission of the F-F bond, it is clear that homolytic dissociation, thus forming F$^\bullet$ radical species, is highly favoured over heterolytic dissociation where F$^+$ and F$^-$ species are formed. This is mainly due to the poor stability of F$^+$ species. Nevertheless, the low barrier towards homolytic dissociation of the fluorine-fluorine bond in F$_2$, coupled with the high ΔH_f values related to C-F bonds (around 116 kcal/mol), usually results in highly exothermic and difficult to control reactions. This is shown below in Scheme 1.1:

Homolysis: F$_2 \rightarrow$ 2 F$^\bullet$ $\Delta H° = 38.0$ kcal/mol

Heterolysis: F$_2 \rightarrow$ F$^+$ + F$^-$ $\Delta H° = 420.7-59.4 = 361.3$ kcal/mol

Scheme 1.1: Scheme illustrating bond dissociation energies for homolytic and heterolytic dissociation of F$_2$.

Whilst such reactions have been considered uncontrollable for the reasons outlined above, a few examples have proven to be applicable, provided that suitable conditions are employed.[27] Indeed, although radical fluorinations are far less prevalent in the literature than nucleophilic and electrophilic fluorinations, a number of successful examples do exist, helping to demonstrate the validity of this approach. One such example is the radical fluorination of aryl silanes using XeF$_2$ as the radical fluorinating species.[28] This process is interesting as it demonstrates that site-specific products can be achieved *via* radical fluorinations instead of uncontrollable perfluorinations. A second example involves radical decarboxylative fluorination using F$_2$ [29] and XeF$_2$,[30,31] examples of which date back to the late '60s and early '80s respectively. A C(sp^3)-F bond can indeed be formed via decarboxylative fluorination in a way that is applicable to a wide-range of substrates, as carboxylic acid groups are commonly found in many natural compounds of interest and can be easily synthesised in few reaction steps. It is for this reason that radical decarboxylative fluorinations present an exciting opportunity for the formation of novel C-F bonds. It should be noted, however, that reactions involving F$_2$ and XeF$_2$ are very inefficient, and these reagents are highly toxic and

unstable, greatly reducing the applicability of these methods for use in industry. It was a lack of other safer radical fluorinating reagents that caused research progress on radical fluorinations to stall up until very recently.

In the past few years, the ability of an N-F electrophilic fluorinating reagent such as Selectfluor® to transfer fluorine to alkyl radicals has been demonstrated. In 2012, Rueda-Becerril *et al.*[32] were the first to report the potential of classic electrophilic fluorinating agents (like NFSI and Selectfluor®) as radical fluorine transfer reagents. This is due to the relatively low bond dissociation energies of the N-F bonds (for example, 63.4 kcal/mol and 64 kcal/mol for N-Fluorobenzenesulfonimide (NFSI) and Selectfluor®, respectively).[33] These bond dissociation energies are also low enough to allow reaction with most alkyl radicals *via* a single electron transfer (SET) process illustrated below in Scheme 1.2:

$$R_2N\text{-}F + [R^{\bullet}] \rightarrow R_2N^{\bullet} + R\text{-}F$$
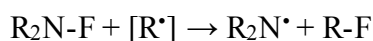
Scheme 1.2: SET process between alkyl radical species and fluorinating agent yielding an R-F species.

As a result of these predictions, the fluorination of *tert*-butyl peresters *via* radical pathways has been reported in the literature, using NFSI as a fluorinating reagent.[32] Whilst this work represents significant progress as the first published example of radical fluorination using a safer and more stable fluorination agent (Selectfluor®), it should be noted that a number of additional reaction steps are required, as the perester substrates need to first be prepared from carboxylic acids. In addition, the general applicability of the system to the selective fluorination of other systems is unknown. However, the findings of Rueda-Becerril *et al.*[32] has led to progress in research focused on easier access to $C(sp^3)$-F bonds *via* decarboxylative fluorination. A new synthetic strategy for decarboxylative fluorination was recently reported by Yin *et al.* employing Selectfluor® as the fluorinating agent and a homogeneous silver salt ($AgNO_3$) as catalyst.[34]
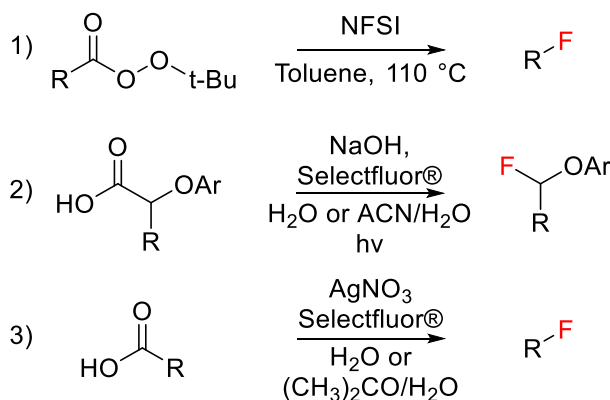
Figure 1.5: Examples of radical fluorinations using electrophilic fluorinating agent containing N-F bonds (Selectfluor® and NFSI): **1)** fluorination of *tert*-butyl peresters to form C(sp³)-F bonds,[32] **2)** photo-decarboxylic fluorination of 2-aryloxy and 2-aryl carboxylic acids,[35] and **3)** decarboxylative fluorination of aliphatic carboxylic acid with AgNO₃.[34]

1.3 Strategies to form new C(sp³)-F bonds

Amongst strategies to synthesise new C(sp³)-F bonds, two major distinctions can be made: i) conversion of pre-activated substrates (R-X to R-F), and ii) direct C-H fluorination (including direct alkane fluorination and benzylic/allylic fluorination). The first route involves the conversion of a pre-activated functional group to a fluorine atom. Amongst all the different functional groups, carboxylic groups have been identified as the most promising candidates to be substituted with a fluorine, mainly due to the lower toxicity and availability of the substrates. The second, and more elegant, route involves the direct conversion of stable C-H bonds into C-F bonds. Indeed, novel homogeneous pathways have recently been explored for such direct C(sp³)-H fluorinations, starting from both activated C-H bonds (benzylic and allylic), and more inert alkane C-H bonds.[36,37] However, whilst many breakthroughs have been achieved for allylic and benzylic fluorination, attempts to achieve direct fluorination from inactivated C(sp³)-H bonds are still very scarce, with only few examples of limited detail being present in the literature.

The great success observed for both allylic and benzylic C-H fluorination arises from the lower energy required to homolytically or heterolytically break, allylic and benzylic C-H bonds. Firstly, such bonds are weaker than those found in less active alkanes (pK$_a$ value of 43 and 41 for allylic and benzylic protons respectively compared with pK$_a$ values > 50 for alkyl protons). Furthermore, the intermediate radical species, generally involved in these reactions, are stabilised by resonance delocalisation of the electrons.

9

Hence, allowing allylic and benzylic substrates to be fluorinated at milder reaction conditions when compared with alkyl counterparts. Nevertheless, although more challenging, direct alkane fluorination would be an incredible achievement from both a mechanistic and industrial perspective. In fact, the broad range of alkanes, *i.e.* the high availability of a large range of relatively inexpensive substrates, makes direct alkane fluorination preferable from an industrial perspective.

The next section highlights the state of the art methods for the formation of $C(sp^3)$-H fluorinations, starting from pre-activated and non-activated substrates. However, further critical discussion of systems pertinent to results Chapters 3 - 6 is provided during the introduction of each individual chapter.

1.3.1 Decarboxylative fluorination of aliphatic carboxylic acids

As described above, new $C(sp^3)$-F bonds can be formed using various pre-activated substrates. Amongst these, carboxylic acids present several advantages, including lower toxicity, and ready availability. As such, it is unsurprising that the decarboxylative fluorination of aliphatic carboxylic acids represents the most explored route for the synthesis of $C(sp^3)$-F bonds. Amongst the variety of methodologies developed to perform this reaction, the most efficient and pursued methods are: i) silver catalysed decarboxylative fluorinations, ii) photocatalytic decarboxylative fluorinations, and iii) metalloporphyrin catalysed reaction for the synthesis of targeted $C(sp^3)$-^{18}F bonds.

1.3.1.1 Silver mediated decarboxylative fluorination

The first example of decarboxylative fluorination with sustainable fluorinating agents was published in 2012 by Yin *et al.*[34] who reported a novel and highly chemo-selective route for aliphatic decarboxylative fluorination using Selectfluor® as fluorinating reagent and the homogeneous silver nitrate salt ($AgNO_3$) as catalyst. To demonstrate the efficiency and the versatility of this systems, the authors demonstrated good yields (from 40 to 95%) of fluorinated products from a broad array of carboxylic acid substrates.[34] According to the reaction mechanism proposed by Yin *et al.*,[34] the reaction pathway involves the formation of an active Ag(III) intermediate species, formed by the oxidation of the Ag^+ cationic species present in solution by Selectfluor®, giving a Ag(III)-F complex. This Ag(III)-F complex reportedly undergoes a single electron transfer (SET) following interaction with the carboxylic acid group, leading to the

formation of a Ag(II)-F intermediate and an alkyl radical species. In the final step of the catalytic cycle, fluorine atom transfer occurs from the Ag(II) complex to the alkyl radical, resulting in the formation of the fluorinated product, and renewing the Ag(I) species. Unlike other methods of conversion of pre-activated substrates, the regeneration of Ag(I) results in a closed catalytic process, with TON > 1 being reported by the authors.
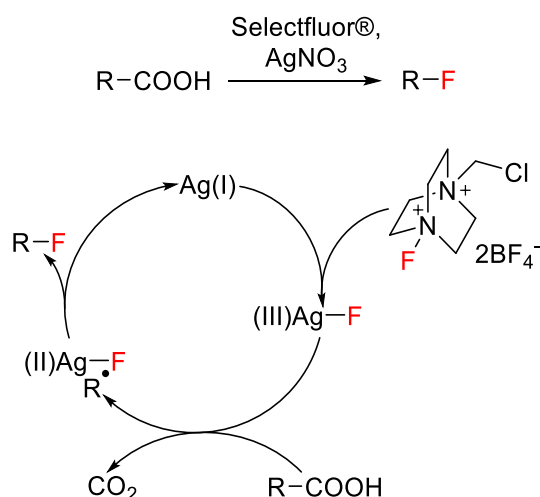
Figure 1.6: The Ag-catalysed decarboxylative fluorination of aliphatic carboxylic acid and the reaction mechanism proposed by Yin et *al.*[34]

The innovative approach of Yin *et al.*[34] resulted in increased interest in metal-catalysed fluorination, and two additional mechanistic studies of this system were recently reported. Notably, both studies offer an alternative mechanism to the one previously proposed by Yin *et al.*[34] Initially, Patel *et al.*[38] performed a kinetic and spectroscopic investigation, and proposed that the reaction is initiated *via* the formation of a Ag(I)-carboxylate intermediate, Ag(I)-OOCR, which is then oxidised by Selectfluor® giving a Ag(II) species, Ag(II)-OOCR, and a TEDA-BF4 radical cation. The Ag(II)-OOCR complex then oxidises the carboxylate, yielding CO_2 and an alkyl radical, restoring the silver (I) cation. The alkyl radical formed then undergoes a SET by Selectfluor® forming the desired fluorinated product (Figure 1.7). Furthermore, this mechanism was supported by recent DFT calculations by Zhang.[39]
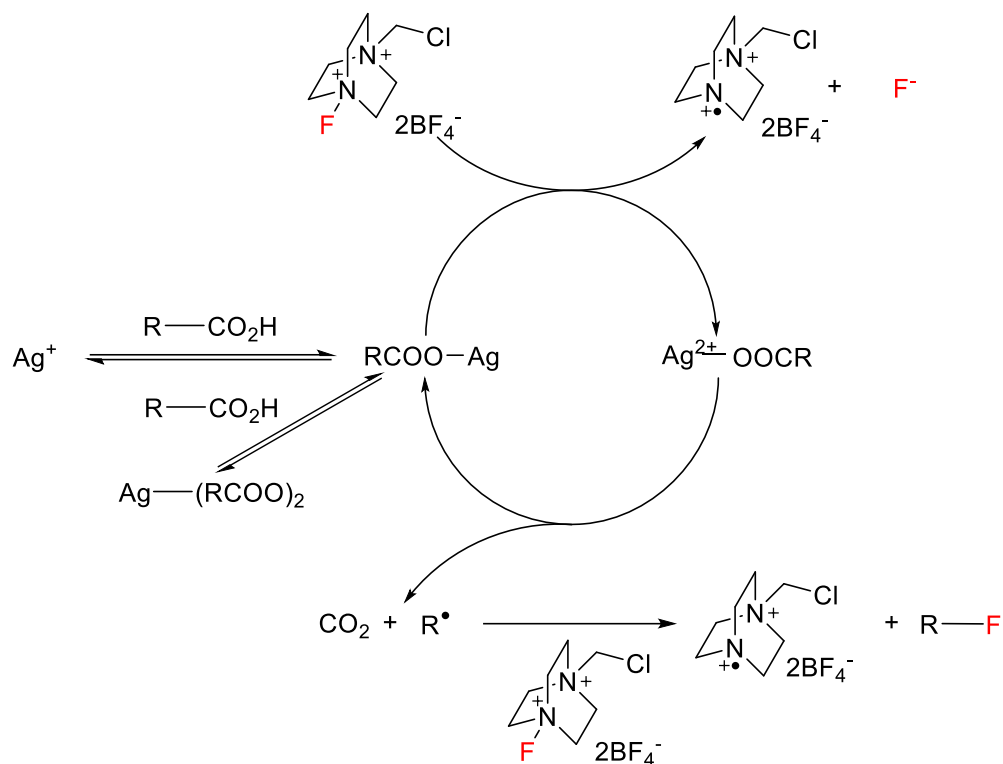
Figure 1.7: Mechanism for the decarboxylative fluorination of aliphatic carboxylic acids, as proposed by Patel *et al*.[38]
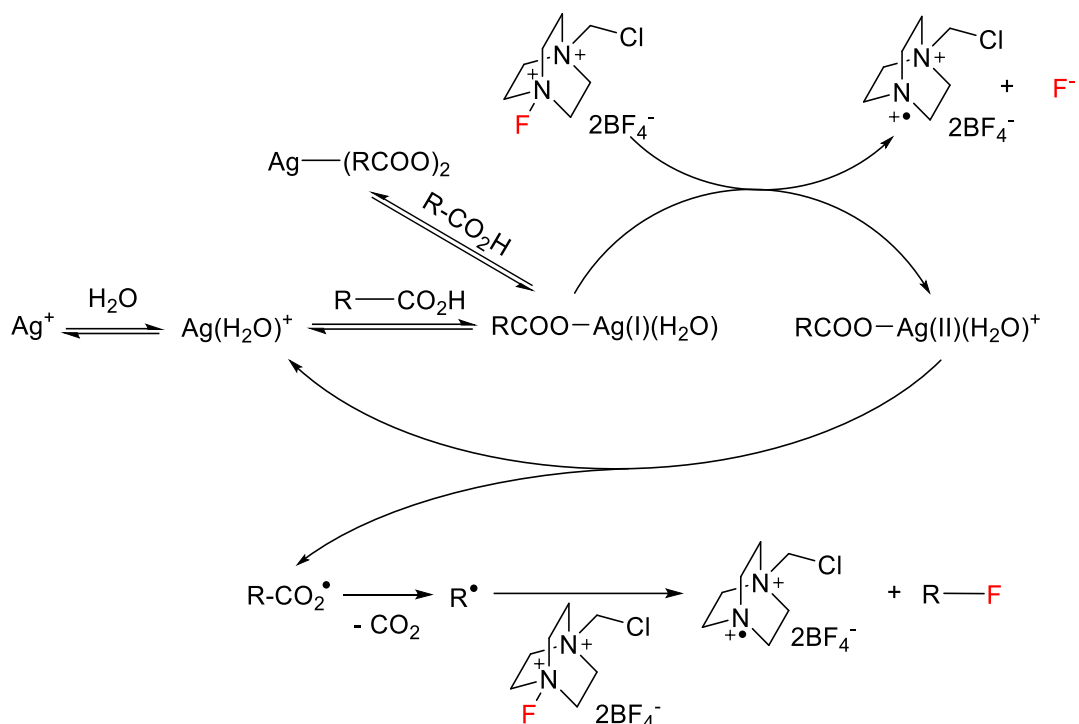
Figure 1.8: Mechanism for the decarboxylative fluorination of aliphatic carboxylic acids, as proposed by Zhang.[39]

Crucially, these studies contradict the Ag(III) mediated reaction pathway originally proposed by Yin *et al.*,[34] and suggest that the formation of both Ag(II)-F and Ag(III)-F species is unlikely. Furthermore, these findings imply that only Ag(I) is catalytically active for the fluorinations. Hence, any silver present in a catalyst with a different oxidation state maybe inactive or even detrimental to the reaction. The novel findings reported by Yin *et al.*[34] not only demonstrates the possibility of a radical-based route to selectively form C(sp³)-F bonds, but also provides a useful mechanistic insight into radical fluorination reactions, providing a good platform for future catalytic developments.

Nevertheless, to scale-up Ag-catalysed fluorination reactions for industrial applications, in order to develop fluorination processes able to satisfy the high demand of fluorinated compounds, the cost of materials and the overall sustainability of the technology must be minimised. A key step in achieving increased sustainability would be the ease of recovery and subsequent regeneration of the catalyst. This would preferably involve a heterogeneous catalytic system, such as a supported solid catalyst, such systems are typically characterised by increased sustainability and economic feasibility (see section 1.4).

1.3.1.2 Radical decarboxylative fluorination activated *via* photocatalysis

Recent studies have successfully identified photocatalysis as an alternative way to form C(sp³)-F bonds *via* decarboxylative fluorination reactions with Selectfluor® as a fluorinating agent and a homogeneous species as photocatalysts. In fact, following the discovery in 2012 that 2-aryloxy and 2-aryl carboxylic acids can undergo decarboxylative fluorination when irradiated with light in the presence of Selectfluor®,[35] several other works have focussed on the development of photocatalytic systems able to convert more general carboxylic acids. Noteworthy examples have been reported by Rueda-Becerril *et al.*[40] and Ventre *et al.*,[41] using a Ru or an Ir complex as photocatalysts, respectively. Organic dyes have also been employed to perform photocatalytic decarboxylative fluorination.[42] Another recent example of an Ir complex used as a catalyst for both the photo-fluorination of carboxylic acids and also for hydrogen generation has been reported by Porras *et al.* in 2016.[43] However, the complicated preparation protocols for the synthesis of these complexes in addition to

the use of expensive metals, make these catalysts unsuitable for industrial applications. Heterogeneous materials, ideal for industrial scale-up, to perform photo-fluorination, are yet to be successfully developed, despite the great deal of interest in heterogeneous photocatalysts.
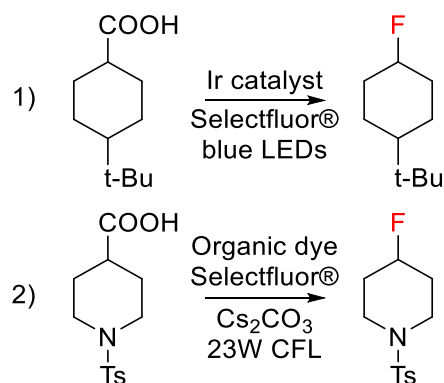
Figure 1.9: Examples of photocatalytic fluorinations mediated by: **1)** Iridium catalysts,[41] and **2)** organic dyes.[42]

1.3.1.3 Metal-porphyrin catalysed decarboxylative fluorination

Metalloporphyrin catalysed decarboxylative fluorination of aliphatic carboxylic acids represents another route to convert R-COOH into R-F. This route, recently discovered by Huang *et al.*[44] allowed targeted ^{18}F-C bond formation to be achieved. However, despite the interesting nature of this mechanism, which employs a reportedly biomimetic compound (a manganese(III)-porphyrin, (TMP)Mn(III)Cl), stronger oxidising conditions are required. Indeed, instead of the easy to handle fluorinating reagent Selectfluor®, strong oxygen donors such as iodosylbenzene (PhIO) are required to activate the catalyst, and fluoride ions are employed as fluorine sources.

R-COOH $\xrightarrow[\substack{[18F]F^- \\ CH_3CN, 50°C}]{\substack{(TMP)Mn(III)Cl \\ PhIO}}$ R-^{18}F

(TMP)Mn(III)Cl

R = mesityl
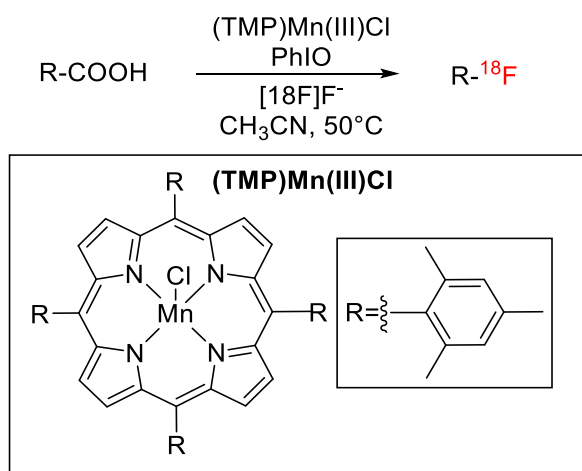
Figure 1.10: Targeted fluorination *via* decarboxylative fluorination catalysed by (TMP)Mn(III)Cl.[44]

1.3.2 Direct C(sp^3)-H bonds fluorination

Despite the promising results recently reported for conversion of pre-activated substrates to C-F bonds, direct C(sp^3)-H functionalisation to C(sp^3)-F remains the most ideal and desirable target. However, direct C(sp^3)-H fluorination to achieve C(sp^3)-F bonds represents a difficult task, due to the high energy required for activation of the substrates. Generally, the activation of the substrates requires fluorinating reagents that possess a high oxidation potential, and harsh reaction conditions are also typically required. Despite this, some achievements have recently been made for direct C(sp^3)-H fluorination of more activated C-H bonds, such as benzylic C-H bonds. Moreover, a few promising examples have recently demonstrated that is possible to also selectively convert non-reactive alkanes into the corresponding fluorinated compounds employing two different routes: i) rebound chemistry involving H-atom abstraction with high valent transition metals, and ii) radical mechanisms involving use of radical initiators.

1.3.2.1 Benzylic fluorination

Amongst the different strategies to perform direct C(sp^3)-H fluorination using activated substrates, benzylic fluorination represents one of the most exploited routes. In recent years a large number of reports have been focussed on this topic and many breakthroughs have been achieved. Indeed, in addition to representing a good model system for selective direct C(sp^3)-H fluorination, due to the presence of the activated benzylic C-H bonds which require milder reaction conditions, this route is also

particularly desirable for pharmaceuticals applications, due to the high number of drugs containing benzylic $C(sp^3)$-F bonds. The first example of benzylic fluorination was reported by Hull *et al.*[45] in 2006, employing $Pd(OAc)_2$ as a catalyst and typical electrophilic fluorine sources, such as (2,4,6-Me_3-NFPy·BF_4). However, only in recent years this route has started to gain increased attention, with several recent reports published on this system.[46-53] Amongst the most promising of these are the Mn(salen) complexes, reported by the Groves group to be an active catalyst for benzylic fluorination using nucleophilic fluorine sources such as TREAT·HF and AgF.[47,48] In contrast, Bloom *et al.*[49,50] reported that benzylic activation can be achieved by using simple Fe(II) complexes, such as $Fe(acac)_2$, in the presence of Selectfuor® as fluorinating agent. Notably, a radical-involved mechanism with Selectfluor® and $AgNO_3$ for the synthesis of difluorinated benzylic molecules, has also been reported by Xu *et al.*[51] However, amongst the different strategies for the synthesis of benzylic fluorides, photocatalysed benzylic fluorination represents one of the most explored routes in recent years, demonstrating the good versatility of this system to undergo radical fluorinations in the presence of radical/electrophilic fluorinating agents such as Selectfluor®. Noteworthy examples of light mediated benzylic fluorination are the system developed by Xia *et al.*,[52] employing 9-fluorenone as photosensitive catalyst, and the system reported by Bloom et *al.*,[53] using tetracyanobenzene, TCB, as photocatalyst. Notably, a continuous flow system has also been reported using xanthone as photocatalyst.[54] However, it should be noted that despite the recent achievements made with respect to the fluorination of benzylic C-H bonds, no heterogeneous catalyst has yet been successfully reported. Moreover, low levels of catalytic activity, both in terms of rates (*i.e.* TOF) and productivity, have been achieved.
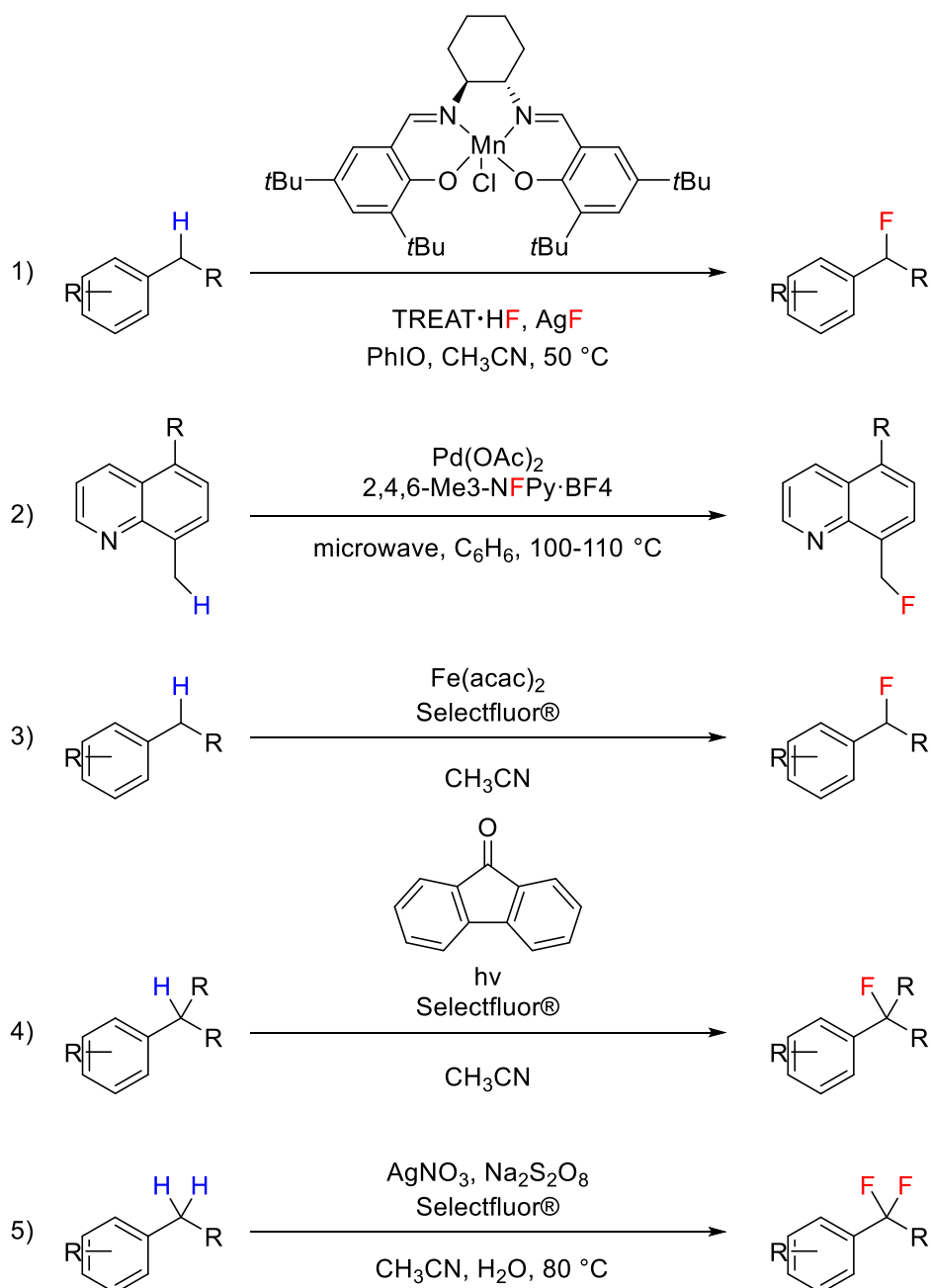
Figure 1.11: Examples of benzylic fluorinations reported by: **1)** Groves group,[47,48] **2)** Sanford group, [45] **3)** Lectka group,[49,50] **4)** Chen group, [53] and **5)** Tang group.[51]

1.3.2.2 Alkane fluorination *via* hydrogen abstraction followed by fluorine rebound chemistry

In 2012, Groves group[55] demonstrated that alkane fluorination can be achieved employing, (TMP)Mn(III)Cl (Figure 1.12). A mechanism involving a hydrogen abstraction step, generating an alkyl radical species, R•, followed by a F-rebound step, yielding the desired F-alkyl compound, was reported.[55]

$$R\text{-}H \xrightarrow[\substack{50°C, N_2 \\ CH_3CN/CH_2Cl_2\ (3:1)}]{\substack{PhIO,\ AgF \\ TBAF\cdot 3H_2O \\ (TMP)Mn(III)Cl}} R\text{-}F$$
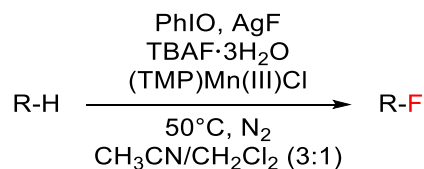
Figure 1.12: Alkane fluorination catalysed by Mn(III)-porphyrin chloride.[55]

According to the mechanism proposed by Groves,[55] the first step of the reaction pathway involves the exchange of the axial Cl⁻ ligand (bound to the manganese atom) with a fluoride ion, F⁻, giving the (TMP)Mn(III)F porphyrin. Subsequent oxidation of the porphyrin with iodosylbenzene (PhIO) results in the formation of an oxo-manganese (V) species. The proposed O=Mn (V) moiety is a strong oxidant, capable of abstracting a hydrogen atom from highly stable alkane species, such as cyclooctane and cyclohexane, yielding an alkyl radical species R• and subsequently forming a hydroxyl-Mn (IV) species, (TMP)Mn(IV)(OH)F. According to the reported mechanism, the (TMP)Mn(IV)(OH)F porphyrin is then subjected to another ligand exchange giving the difluoride porphyrin (TMP)Mn(IV)F₂, rather than immediately reacting with the alkyl radical R• *via* "classical" O-rebound which yields an R-OH species. The difluoride complex is thought to react with the generated alkyl radical, yielding the desired R-F product (F-rebound), concurrently restoring the Mn(III) porphyrin, (TMP)Mn(III)F.
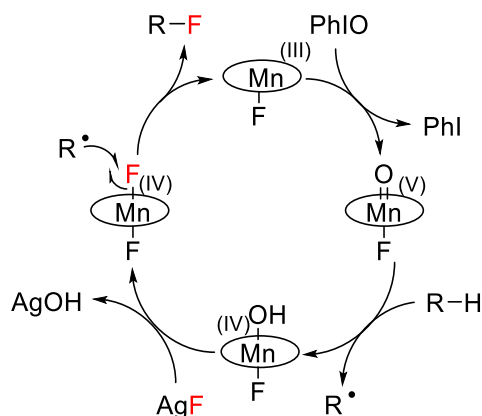
Figure 1.13: Reaction mechanism for alkane fluorination proposed by Groves.[55]

Interestingly, this mechanism resembles the enzymatic activity displayed by the monooxygenase family, such as methane mono-oxygenase (MMO) and cytochrome P450,[56] which are notably able to convert methane in methanol (or generally able to convert alkanes in the respective alcohols). Indeed, hydrogen atom abstraction followed

by oxygen rebound typically converts RH into ROH, even with very stable C-H species, *e.g.* CH$_4$ to CH$_3$OH.[57] However, whilst hydrogen atom abstraction (HAA) is prevalent in several biological processes, particularly during oxidation catalysis, no evidence for a similar mechanism for the insertion of a fluorine atom can be found in nature. However, a deep study of the reaction mechanism, and kinetic studies reporting eventual competition with the related oxidation pathways are still needed. Furthermore, the rules that govern both oxygen and fluorine rebound chemistry are still to be clarified. A full mechanistic understanding of the system could lead to the design of catalysts possessing tuneable catalytic activity; ideally active exclusively for either the fluorination route or the oxidation route, depending upon the identity of the targeted product.

1.3.2.3 Photocatalytic alkane fluorination *via* radical fluorination.

In parallel with fluorine rebound chemistry, another alkane fluorination pathway involving a radical initiator species has been explored. Following the report by Rueda-Becerril *et al.*,[32] in which electrophilic fluorinating reagents like Selectfluor® and NFSI were shown to react *via* SET with alkyl radicals, as discussed previously above, radical initiator species have been employed to achieve C(sp^3)-F bond formation directly from alkane substrates.

The first report of such reaction was by Bloom *et al.*,[58] who observed that the photocatalyzed aliphatic fluorination could be successfully employed using ultraviolet light and a photosensitiser, 1,2,4,5-tetracyanobenzene (TCB). Later, photocatalysed aliphatic fluorination was achieved using 9-fluorenone and acetophenone as photosensitiser, was reported by Xia *et al.*[59] More recently, in 2016, Neumann and Ritter,[60] reported the promising ability of uranium-based photocatalysts to activate simple alkanes, generating alkyl radicals which subsequently react *via* SET with NFSI, yielding to the F-alkyl compound.
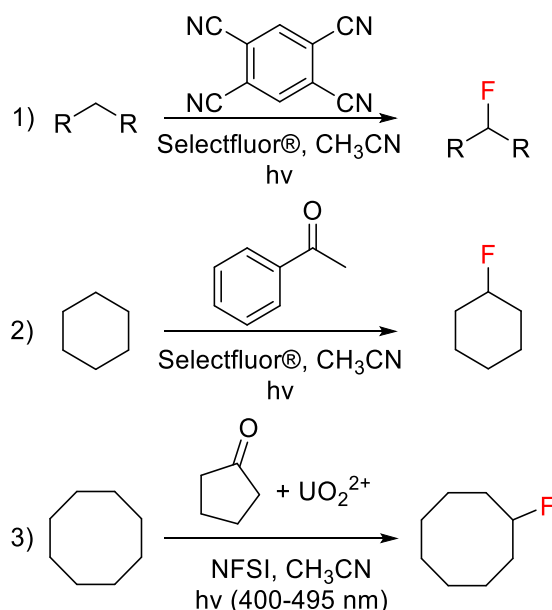
Figure 1.14: Examples of photocatalytic aliphatic fluorinations reported by: **1)** Bloom *et al.*[58] **2)** Xia *et al.*,[59] and **3)** Neumann and Ritter. [60]

1.3.3 Pertaining challenges

Despite the plethora of research published within the last five years, several challenges in the field of fluorination remain. Indeed, although fluorination is an important field, around 90% of the reports are still non-catalytic, and all the catalytic systems that have been developed up to now for the selective formation of $C(sp^3)$-F bonds employ homogeneous catalysts. Despite the high demand of fluorinated compounds for a wide range of applications (from drugs to fertilisers and PET application), the design of heterogeneous materials, suitable for industrial applications and active for the fluorination processes described above, has yet to be achieved. Thus, the focus of this work is the development of robust heterogeneous catalysts to form $C(sp^3)$-F bonds, demonstrating that selective fluorinations can be achieved also with heterogeneous materials, opening the way for an industrial exploitation of these systems. In this context, starting from pre-activated substrates, and leading to non-activated substrates (such as ethylbenzene), the capability of heterogeneous materials to perform selective fluorination reactions will be investigated. Notably, although the design of heterogeneous catalysts for fluorination reactions might not seem a difficult task, designing a truly heterogeneous catalyst, stable in the high acidic reaction conditions is extremely challenging. Indeed, the high acidic conditions typically related to these

reactions are very likely to cause i) deactivation, ii) decomposition of the heterogeneous material, and iii) metal leaching.

Despite the harsher reaction conditions and the stronger oxidising agents required for direct alkane fluorination, this route still represents a more elegant and desirable approach for the synthesis of $C(sp^3)$-F bonds. Hence, this approach not only removes the necessity of first functionalise the substrate, increasing the atom economy of the process, but is also applicable to a broad range of substrates. Also, the employment of easy available alkanes as raw materials for the industrial scale-up of selective fluorination processes for an industrial production of highly demanded fluorinated compounds would be a significant achievement with worldwide impact. Nevertheless, the design of heterogeneous catalysts for direct alkane fluorination represents an immense challenge mainly due to the scarce number of analogous homogeneous systems and the missing of detailed mechanistic and kinetic studies. Hence, kinetic studies of the homogeneous systems to perform alkane fluorinations are also performed in this project, in order to allow a better understanding of the system, essential for future design of heterogeneous catalysts active for selective direct alkane fluorination.

1.4 Heterogeneous catalysis

In a typical chemical reaction, whereby the reactants are transformed into the desired products, there is a minimum energy requirement that must be overcome for the reaction to proceed. This minimum energy value is known as the activation energy, E_a. A catalyst is "a substance that causes or accelerates a chemical reaction without itself being affected". A catalyst works by modifying the E_a of a process, either providing an alternative reaction pathway, or by stabilising the intermediate species. Both effects lead to decreasing of E_a, hence allowing an increase in the rate of reaction. In fact, E_a is related to the rate constant (k) of a reaction *via* the Arrhenius equation overleaf:

—

Where: k = rate constant
A = pre-exponential factor
R = universal gas constant
T = temperature
E_a = activation energy

A catalyst can also increase the selectivity to more desirable products by providing a reaction pathway that may have not been accessible in its absence, or by decreasing the activation energy for the desirable product. Another major benefit of a catalyst is that it is not consumed during the reaction, and as a result can continually participate in a reaction.
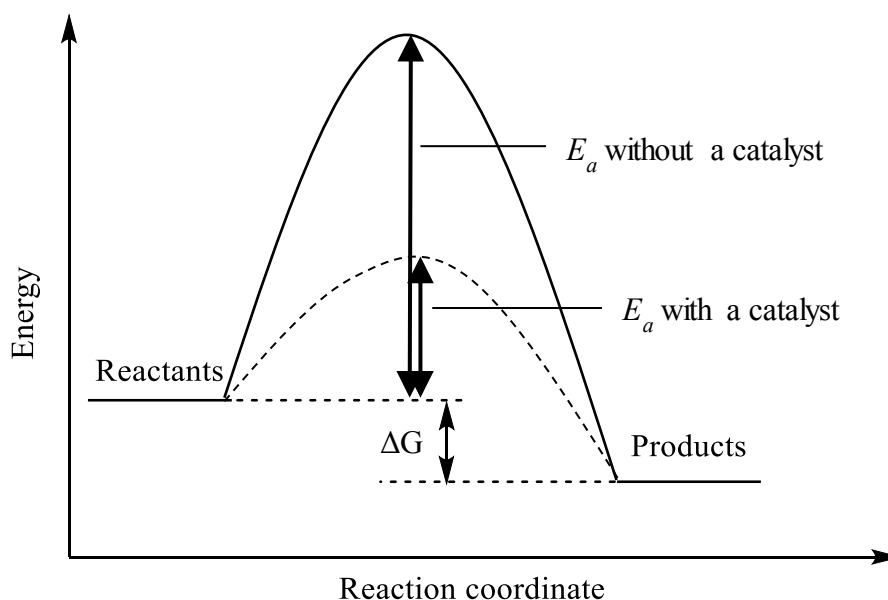
Figure 1.15: Energy diagram showing the difference in activation Energy of a process with and without catalyst.

Catalysts are generally divided into two categories, homogeneous and heterogeneous, depending from the phase of both catalyst and reactants; a catalyst is denoted homogeneous when it exists in the same phase as the reactants, and is denoted as heterogeneous if present in a different phase. Homogeneous catalysts generally exist in the liquid phase and can demonstrate high reaction selectivity, activity and atom economy. They also can exist in gas phase, reacting with other gases through atmospheric reactions. There is however a major drawback to homogeneous catalysis

that makes it unappealing from an industrial standpoint. The presence of both catalyst and substrate in the same phase means that complicated and energy intensive separation processes must be in place. Such procedures are time consuming and costly, consequently, heterogeneous catalysts that are easily recovered are preferred from an industrial standpoint. In fact, heterogenisation of homogenous catalysts provides a solution to this problem and therefore gives an opportunity to make these processes more sustainable.

Heterogeneous catalysts are usually solid materials and can be employed in reactions in which the substrate is either a liquid or a gas. The reaction between substrate and catalyst normally occurs at the solid-liquid (or solid-gas) interface and can be summarised into a few key steps. Firstly, the given substrate is adsorbed onto an active site situated on the surface of the solid catalyst. Then the reaction proceeds through bond breaking and bond forming *via* several key reaction intermediates on the surface of the catalyst, giving the product, which is subsequently desorbed from the catalyst surface. As mentioned earlier, a key advantage of heterogeneous catalysis is the ease of separation of the used catalyst from the products at the end of the reaction; this can typically be achieved via simple filtration, an important consideration from an industrial standpoint.

As previously mentioned, heterogeneous catalysis takes place at the solid liquid (or solid-gas) interface. Consequently, the performance of a heterogeneous catalyst is highly dependent upon the interactions occurring at the active site, the material itself, and the environment. Combining spectroscopic studies, especially *in-situ* spectroscopy, with kinetic studies, it is possible to determine many key features including; the active sites of the catalyst and the elucidation of the reaction mechanisms occurring on the catalytic active sites. Once these features have been determined it is then, in principle, possible to optimise and tune the catalyst to yield increases in key reaction parameters such as activity, selectivity, and catalyst stability. However, by its very nature, single site control represents a much greater challenge to achieve in heterogeneous catalysis than homogeneous catalysis, due to the heterogeneity of active sites, which often results in side reactions, decreasing the overall process selectivity when compared with homogeneous counterparts. As a result, catalyst preparation becomes a significant factor and optimisation of the preparation technique is often reaction specific and very important.

During this research, three different categories of catalysts were employed. These include: i) supported metal/metal oxide catalysts, ii) semiconductors and metal-doped semiconductors, and iii) metalloporphyrins based on bio-mimetic porphyrin scaffolds. The following sections provide a brief overview of the background of each of these different categories of catalysts.

1.4.1 Supported metal/metal oxide catalysts

Supported metals and metal oxides are perhaps the most well known heterogeneous catalysts, widely employed in several industrial applications.[61-63] The success of these materials in catalysis arises from their tuneable catalytic performances based on their readily modified shape, size, acidic or basic (Lewis and Brønsted) nature and surface area.[64] All these parameters can strongly affect the catalytic performances of the material and often simple treatments (*e.g.* thermal treatments) can lead to dramatic change in activity and selectivity. Also, the addition of small amounts of a different metal (metal-impregnation) finely dispersed on a supporting material can give new catalytic activity to the material.[65] The dimensions of the supported metal or metal oxide particles can also play an import role on the catalytic performances of the material. Particles of dimensions in a range of nanometers (nanoparticles) to micrometers can all exhibit excellent catalytic performances, depending on the nature of the catalytic system undergoing study.[66,67] Therefore, the catalytic performances of supported metal/metal oxide, especially supported nanoparticles, are strongly affected by their preparation method, including the metal sources, the deposition method of the active phase on the support and the choice of the support itself.

The use and choice of the supporting material is particularly important for the preparation of metal/metal oxide supported catalysts for a number of reasons. In fact, the supporting material helps to ensure that the particles are effectively dispersed all over the material surface, preventing the aggregation of particles. Achieving good dispersion is essential to ensure that the active species has the highest possible surface area, resulting in increased catalytic performance. Similarly, the support should also have a high surface area as this will allow the nanoparticles to be as finely dispersed as possible. Sintering is the aggregation of nanoparticles and is often caused by exposing the nanoparticles to the solvent, or to high temperatures below their melting point. The supporting material can help to prevent sintering as it can strongly interact with the

dispersed nanoparticles, often referred to as a strong metal support interaction. It is for these reasons that the choice of the supporting material is of utmost importance when designing a catalyst and when deciding upon which method of nanoparticle dispersion will be the most effective for optimum catalyst performance.

1.4.1.1 Impregnation

The easiest method of particle dispersion is known as wet impregnation and has the advantage of being applicable for any porous support.[68] In a typical wet impregnation procedure, a solution of the metal is prepared by dissolving known amounts of metal precursor salts into a suitable solvent, the requisite amount of metal solution is then mixed with the chosen support according to the desired weight loading. The metal nanoparticles will then nucleate within the pores and on the surface of the support material following the removal of the solvent and decomposition of the salt to its corresponding metal or metal oxide *via* calcination. Whilst the wet impregnation method is simple to perform and is applicable to almost all catalyst materials of interest, it does have several disadvantages. The main disadvantage is that precise control over the particle size distribution is difficult to achieve. It should however be noted that despite this, the impregnation method is commonly used in industry and academic research due to the minimal waste obtained in addition to the speed of synthesis.

1.4.1.2 Sol-Immobilisation

The sol-immobilisation technique has gained attention in the literature as it can be used to prepare highly dispersed nanoparticles, by using of a stabilising agent to yield greater control over particle size distribution than the wet impregnation method.[69] In this method, metals colloids are first formed by reducing a solution of metal salts in the presence of a reducing agent such as sodium borohydride. A stabilising agent such as PVA is then added to prevent aggregation and the resulting catalyst contains nanoparticles that are both finely dispersed and have a narrow size distribution.[70] A drawback to this method is that the stabiliser can sometimes be troublesome to remove, and the residual stabiliser can influence both the adsorption and the desorption of the substrates, affecting the catalytic performances of the catalyst.[71]

1.4.1.3 Mechanochemical milling

A less explored technique for the dispersion of particles involves the mechanochemical mixing of the metal precursor and the supporting material, a method known as mechanochemistry. Unlike typical laboratory or industrial reactions where energy is put into the system either thermally, electrolytically or photochemically, mechanochemistry uses mechanical energy to induce the chemical reaction.[72] Mechanochemistry is receiving increasing attention in the literature as it is able to induce chemical reactions between solid materials both rapidly and efficiently, in the absence, or with catalytic amounts, of liquid solvent.

Solvent-free mixing techniques have been shown in literature to produce catalysts that are effective, cheap and synthesised with little environmental impact.[73] In fact, there are a number of reported examples where synthetic mixing has produced catalysts with higher activities than conventional wet chemical methods such as wet-impregnation and sol immobilisation.[74,75]

Catalyst preparation *via* mechanochemistry ranges from techniques as facile as the manual grinding of the desired metal and support with a pestle and mortar to the use of sophisticated ball-milling instruments. A typical synthesis simply involves the mixing of a metal oxide of the active metal in a ball mill with the desired support for a set time; the resulting material prepared is then occasionally subjected to heat treatment. The high energy employed during the mechanochemical mixing can greatly affect a broad range of properties of the solid, such as, removal of the oxide film on the metal, the creation of new interfaces, heating, and the alteration of the particle size distribution.[76] It is the effects produced by mechanical activation that has generated interest into research on how mechanochemical synthesis methods can affect catalytic properties. As techniques such as mechanochemistry which limit, or may even exclude the use of solvents is highly interesting from an industrial perspective. Indeed, there is an increasing pressure for the development of reaction techniques that are more sustainable and environmentally friendly and the reduction of solvent use is of particular focus to industry, where a strong solvent dependency currently exists.[77]

1.4.2 Semiconductors and metal doped semiconductors

Another class of heterogeneous materials widely employed in catalysis is formed by semiconductors and doped-semiconductors. These materials are particularly employed in photocatalysis, due to their capabilities to interact with UV-Visible light. Amongst a range of semiconductor, titanium oxide (TiO_2), represents the most popular, and is employed for a large number of applications. Details of the properties and applications of TiO_2 will be further discussed in section 1.4.2.3.

1.4.2.1 Photocatalysis

A photoreaction is a chemical reaction involving interactions between the physical matter and light or electromagnetic radiation. The term "photocatalysis" can be applied to describe photochemical reactions accelerated by the presence of a substance able to absorb photons (photosensitiser). The photosensitiser in its excited state can then interact with the substrate or a primary photoproduct decreasing the activation energy of the overall process, without appearing in the stoichiometry of the reaction.

After the absorption of a photon, *hv*, the reaction can occur *via* energy transfer or electron transfer between the catalyst in its excited state and the substrate in its ground or excited state or the photoproduct. In the first case, energy transfer, the excited form of the catalyst, C*, interacts with the substrate, which goes from the ground state to an excited state S*, depicted in Scheme 1.3 below:

$$C + hv \rightarrow C*$$

$$C* + S \rightarrow S* + C$$

$$S* \rightarrow P$$
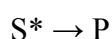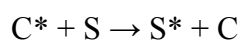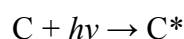
Scheme 1.3: Reaction scheme for photocatalysis of a substrate *via* energy transfer.

In the other case, when electron transfer takes place, the reaction proceeds through a new pathway and the catalyst acts as an electron donor/acceptor, interacting both with the substrate and the product. This is shown below in Scheme 1.4:

$$C + hv \rightarrow C*$$

$$*C + S \rightarrow S^- + C^+$$

$$S^- \rightarrow P^-$$

$$P^- + C^+ \rightarrow P + C$$
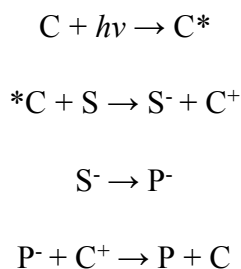
Scheme 1.4: Reaction scheme for photo catalysis of a substrate *via* electron transfer.

Since late 80s, the number of applications in the field of photocatalysis have been subjected to an exponential growth, due to the advantage of using renewable energy *i.e.* solar light to perform chemical reactions. Among the most exploited applications are the degradation of organic pollutants in water (wastewater purification)[78] and water splitting for new energy production.[79]

In this context, many breakthroughs have been achieved in the field of heterogeneous photocatalysis, particularly employing semiconductors as catalysts. The success achieved from the employment of semiconductor in photocatalysis arises from their stability, non-toxicity and low cost. In particular, amongst them, titanium dioxide, TiO_2, is known to be one the most suitable materials.

1.4.2.2 Semiconductors

To give a proper definition of semiconductors and describe their electronic properties it is necessary to start from the definition of electronic bands. Whilst in molecules the electrons are located in molecular orbitals with discrete energy values, formed by the overlapping of two or more atomic orbitals, for solids, the overlapping of a large number N of atomic orbitals creates a continuum of allowed energy values called "band". The occupied band at higher energy states is known as the "valence band", analogous to the highest occupied molecular orbital (HOMO) of a molecule, and the empty band at lower energies, analogous to the lowest unoccupied molecular orbital (LUMO) of a molecule, is defined as the "conduction band". The electronic properties of solids, and therefore their classification as insulators, semiconductors and conductors, is related to the separation, E_{bg}, between the valence and conduction bands. When these two bands are well separated and the Energy band gap, E_{bg}, between them is great enough to forbid any electron to reach the conduction band, the material behaves as an insulator. In contrast, when the E_{bg} is small enough such that thermal

energy, or photon irradiation, allows only some of the electrons to "jump" from the valence band to the conduction band, the material behaves as a semiconductor. In the last case, when the two bands overlap, electrons are free to move in the conduction band and the solid behaves as a conductor.
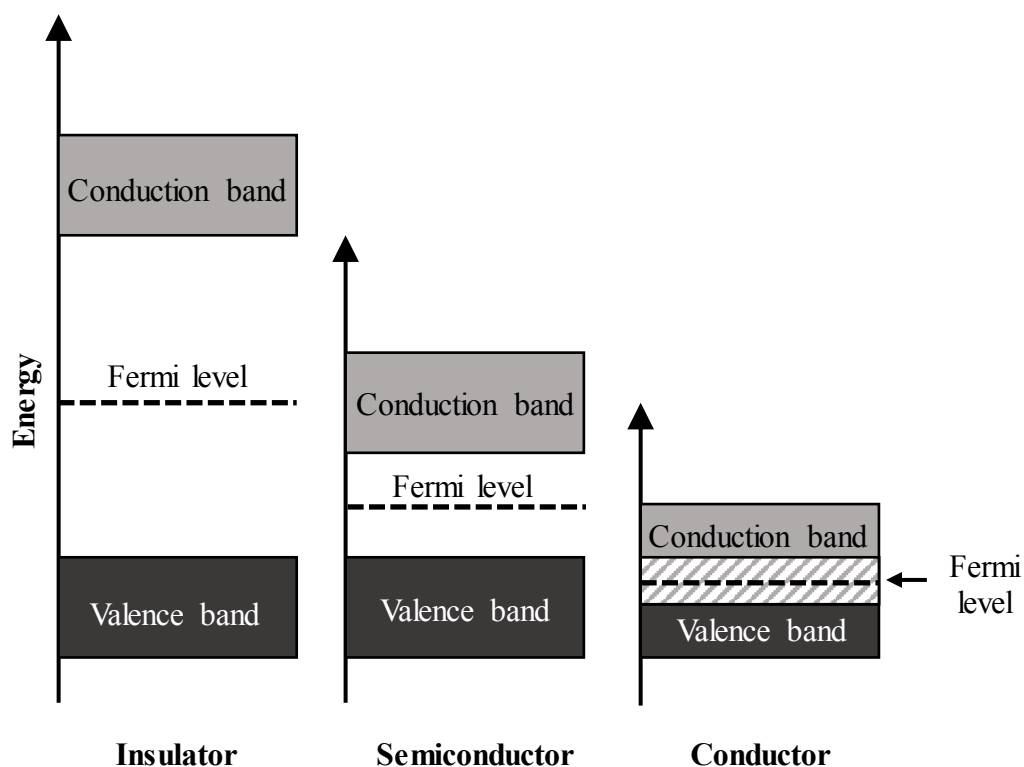
Figure 1.16: Schematic representation of E_{bg} between valence and conduction bands for insulators, semiconductors and conductors. The Fermi level represents the highest energy state occupied by electrons in a material at absolute zero temperature.

During a photocatalytic process, when the semiconductor is irradiated with a set of photons of energy higher than E_{bg}, the transition of electrons (e^-) from the valence band to the conduction band takes place, respectively generating holes (h^+) in the valence band. These species (e^-/h^+), denoted as charge carriers, can then recombine or react with the substrate starting the reaction process.

The activity of a semiconductor for photocatalysis is then related to the recombination time of the electron/hole pairs. The higher the time these pairs need to recombine, the higher the possibility that the electron(s) (e^-) react with and electron acceptor molecule adsorbed on the surface of the semiconductor, and that the hole (h^+) reacts with an electron donor species. To slow down the recombination time of the charge carriers, additional electron donor species (such as quinones and K_2CO_3) can be added to the

reaction mixture, removing the holes created in the valence band and allowing electrons to reach the catalyst surface, reacting with the substrate. The advantage of using semiconductors over conducting materials is their relatively slow recombination of holes/electron pair allowing the electron to reach the material surface and react with the substrates. In fact, in conducting materials, electrons are free to move in both bands, immediately recombining with the photogenerated holes, thus preventing the electron from reaching the material surface and subsequently reacting with the substrate(s).

1.4.2.3 Titanium dioxide for photocatalysis

Amongst the range of semiconductors, titanium dioxide (TiO$_2$) plays a central role. Because of its commercial availability, low cost, low-toxicity and good stability, in fact, TiO$_2$ is known to be the most investigated semiconductor in photocatalysis. From late 80s an increasing number of applications have been developed with this material. Following the discovery of the capability of TiO$_2$ to be employed for photoelectrochemical water splitting,[80] the first reported use of titanium dioxide as a photocatalyst was published in 1977 by Frank and Bard,[81] reporting an efficient way to purify water from CN$^-$. Subsequently, the utilisation of TiO$_2$ for both water and air purification through the employment of "green" solar energy attracted great interest in this field and several other applications were developed. Amongst them, anti-fogging and self-cleaning properties of titanium oxide surfaces were reported, as well as the efficiency of titanium oxide nanoparticles as dye sensitised solar cell.[82,83]

TiO$_2$ is intrinsically an n-type semiconductor, due to the intrinsic formation of oxygen vacancies (n-defects) and Ti interstitial atoms.[84] (The n-type semiconductors are materials in which electrons are the major carrier while holes h$^+$ are the minor ones.) Titanium oxide can be found in three different crystalline structures: rutile, anatase and brookite, with anatase and rutile being the main forms. For these crystalline structures the E_{bg} between the valence and the conduction band is different, and values of 3.0 eV, 3.2 eV and 3.2 eV can be attributed to rutile, anatase and brookite respectively.[85] Notably, E_{bg} of 3.2 eV is related to anatase, the most common crystalline form of titanium oxide, constituting the 73-85% of the total composition of commercial titanium oxide, P25 from Degussa. This means that wavelength with an energy higher than 3.2 eV, corresponding to a radiation of wavelength 387 nm ($\lambda \leq 387$ nm), are required to activate TiO$_2$, allowing the electron transfer from the valence to the

conduction band. Following irradiation with photons of energy higher than 3.2eV, electron/holes pairs are generated, conferring high reactivity to the material; whilst the electron so photo-generated in the conduction band is responsible for the reduction of an adsorbed acceptor molecule, the photo-induced vacancy h^+ in the valence band is able to oxidise a donor molecule adsorbed on the material surface. For example, in aqueous media, the positive vacancy h^+ is able to withdraw an electron from H_2O, *via* one-electron oxidation step, releasing the hydroxyl radical species $OH^\bullet$. At the same time, the free electron can reduce molecular oxygen, O_2, generating a superoxideradical, $O_2^{-\bullet}$. Both the hydroxyl radical and the superoxide ion radical are extremely oxidising species able to oxidise the organic pollutant agents present in water and air, giving to TiO_2 the characteristic anti-polluting properties.[86]
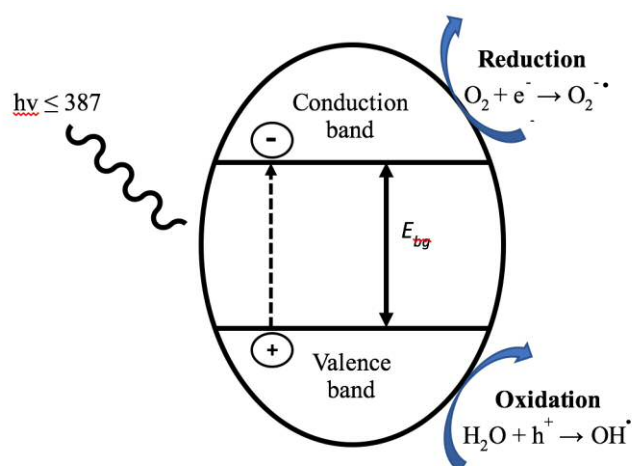
Figure 1.17: Schematic TiO_2 photocatalytic mechanisms.

1.4.2.4 Doped TiO₂ for photocatalysis

The major drawback of pure TiO_2 is the requirement for absorption at relatively high energy, at wavelengths lower than 387 nm, within the UV spectral range. Therefore, only a small portion of the solar light (380-780 nm) is efficiently absorbed by titanium oxide creating electron/hole pairs. Consequently, high energy light sources are often necessary to promote the catalytic activity of this material. Because of the need to move from UV light sources to solar light, hence minimising the energy requirements for the process and to use a renewable energy source (solar), in the recent years a broad range of research studies have been focussed on the synthesis and employment of metal-doped TiO_2. In fact, the incorporation of transition metals on a semiconductor surface can have

a considerable impact on the E_{bg} of the material, creating new energy levels between the valence band and the conduction band, hence consistently decreasing E_{bg}. Consequently, shifts of light absorption toward the visible light spectral range can be and therefore enhancements of catalytic activity due to the metal-doping are often observed. The effects arising from the M-doping of a semiconductor, possibly leading to the enhancement of the catalytic performances of the material, are related to i) alterations of interfacial charge transfer rate with the metal acting as an electron trap, consequently increasing the life time of electron/hole pairs, and ii) increasing the capability of the material to adsorb the substrates on its surface.[87]

In particular, upon doping titanium oxide with metal nanoparticles of noble metals such as Ag and Au, a new absorption band in the visible spectral region is generated. This new feature is related to the plasmonic resonance of the metal nanoparticles.[88] Therefore, irradiating Ag-doped titanium oxide with $\lambda \geq 400$ nm allows electron transfer on the metal sites occur, leading to electron transfer between TiO_2 and the metal nanoparticle, hence activating TiO_2 using visible light instead of UV light sources.[89]

1.4.3 Biomimetic catalysts

Biomimetic catalysis is a branch of chemistry that employs catalysts able to mimic the reactivity of natural enzymes. Indeed, enzymes are biological catalysts naturally able to catalyse the most challenging reactions, such as alkane oxidation and alkene epoxidation in the most benign environment. However, despite alkane functionalisation being one of the main goals of the chemical industry, and the intrinsic green nature of enzymatic catalysis, the fragility of these biological systems, particularly in terms of operational window flexibility (temperature, solvent, pH, pressure) complicates industrial scale-up. Therefore, a number of studies have focussed on the development of inorganic catalysts mimicking enzymatic reactivity and a broad number of biomimetic catalysts has been reported in literature.

Amongst homogeneous analogues, biomimetic catalysts are generally divided into two classes: i) heme and ii) non-heme catalysts. The first group of enzyme-like catalysts are simple metal-containing porphyrins, heterocyclic macrocycles composed of four modified pyrrole subunits interconnected at their α carbon atoms via =CH− bridges. The first example of a heme catalyst known to perform alkane oxidation and alkene

epoxidation is a chloro-α,β,γ,δ-tetraphenylporphinato-iron(III), (TPP)FeCl, species, reported by Groves *et al.*[90] in 1979 (Figure 1.18). After the discovery of the potential of these metalloporphyrins to mimic the activity of cytochrome P450, several other examples of Fe and Mn porphyrins have been studied and reported in literature.[91-96] Furthermore, examples of Ru-porphyrins have also been reported in literature.[97,98] These metalloporphyrins exhibit similar reactivity to P450 for alkane oxidation due to their ability to reach high valent oxo-species. Indeed, these oxo-species are capable of abstracting a hydrogen atom even from highly stable alkanes. This H-atom abstraction reportedly yields a transient alkyl radical species, which is almost immediately subjected to oxygen rebound, forming the desired hydroxylated compound.
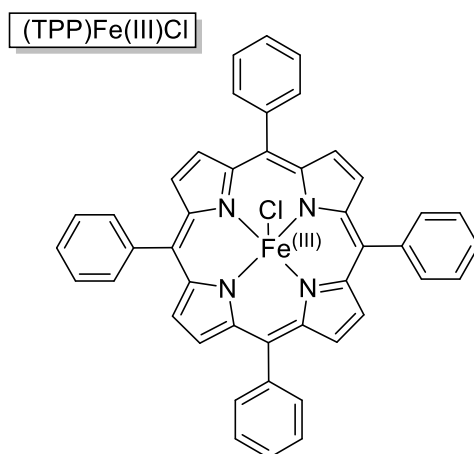
Figure 1.18: Structure of (TPP)Fe(III)Cl as an example of heme iron (III) catalyst reported by Groves *et al.*[90]

Concurrently to the development and catalytic study of metalloporphyrins for alkane oxidation, a consistent amount of studies has focussed on the development of less expensive and more robust catalysts with similar mono-oxygenase reactivity, but without the porphyrin ring, hence denoted as non-heme catalysts. Among them, metal complexes of Fe and Mn with Shiff bases where amongst the first examples of non-heme biomimetic catalysts reported in literature.[99] However, despite the immense breakthroughs achieved in homogeneous biomimetic catalysis, the number of heterogeneous catalysts able to efficiently mimic the enzymatic activity of P450 and MMO is still relatively scarce, and the design of biomimetic heterogeneous materials still represent a very challenging task. Nevertheless, some breakthroughs have been achieved by supporting heme and non-heme biomimetic compounds on different supporting materials, such as oxides, resins and metal organic framework (MOF).[100,101]

Although these heterogeneous catalysts represent a remarkable achievement in this area, their employment for industrial applications is still limited for several reasons, including: i) lack of activity, stability and selectivity, ii) their relatively expensive nature, and iii) their difficult synthetic procedures. Furthermore, a greater mechanistic understanding is needed to design proper heterogeneous enzyme-like catalysts.

1.5 Thesis targets

Following the increasing demand for the production of fluorinated compounds, particularly for selective $C(sp^3)$-F bond synthesis, and the lack of heterogeneous materials employed in these systems, the main focus of this thesis is the design and optimisation of heterogeneous materials able to perform selective fluorination reactions.

Among the different strategies to achieve $C(sp^3)$-F bonds, decarboxylative fluorination catalysed by Ag salts (AgNO$_3$), appears to be a suitable model system to begin to investigate the potential of heterogeneous catalysts to perform fluorination reactions.[91] However, although decarboxylative fluorination represents a good model system for the development of suitable and robust heterogeneous catalysts for selective $C(sp^3)$-F formations, highly activated substrates are required for efficient fluorination to be achieved. A more elegant, but more challenging, approach would be the generation of new $C(sp^3)$-F bonds from non-activated positions *i.e.* direct $C(sp^3)$-H fluorination. Therefore, an investigation of the catalytic performances of heterogeneous catalysts to perform direct $C(sp^3)$-H fluorination using activated $C(sp^3)$-H bonds such as benzylic C-H bonds, is also reported in this project.

Amongst the methodologies to perform direct $C(sp^3)$-H fluorination, direct alkane fluorination represents an ideal route from an industrial perspective, mainly due to the extremely broad range of substrates available in nature. However, the less reactive nature of typical C-H bonds makes such a process highly challenging. Indeed, there is a scarce number of reports in the literature focused upon this demanding process. Amongst the systems reported in Section 1.3.2.1, the one developed by Groves represents one of the most interesting one, performing alkane fluorination using a biocatalyst. However, no detailed mechanistic studies of this process have been reported, and the reasons behind the unique reactivity of the Mn-porphyrin system have

not yet been revealed. As such, strategies for designing solid catalysts for such a process are not evident. Accordingly, this thesis also focuses upon the catalytic performance of the Mn porphyrin system, with the aim of: i) understanding the true kinetic behaviour of the catalyst, ii) gaining an insight into the mechanism of the reaction, and iii) identifying suitable conditions for the future study of solid catalysts for direct $C(sp^3)$-F bond formation.

1.6 References

[1] C. Heidelberger, *Nature*, 1957, **179**, 663-666.

[2] M. Shimizu, T. Hiyama, *Ange. Chem. Int. Ed.*, 2005, **44**, 214-231.

[3] D. O'Hagan, *Chem. Soc. Rev.*, 2008, **37**, 308-319.

[4] D. Harper, D. O'Hagan, *Nat. Prod. Rep.*, 1994, **11**, 123-133.

[5] X. Xu, *J. Org. Chem.*, 2016, **81**, 6887-6892.

[6] L. Radulovic, Z. Wojcinski, *Encyclopedia of Toxicology*, 2014, 1133-1136.

[7] M. Pagliaro, R. Ciriminna, *J. Mater. Chem.*, 2005, **15**, 4981.

[8] J. T. Robinson, J. S. Burgess, C. E. Junkermeier, S. C. Badescu, T. L. Reinecke, F. K. Perkins, M. K. Zalalutdniov, J. W. Baldwin, J. C. Culbertson, P. E. Sheehan, E. S. Snow, *Nano Lett.*, 2010, **10** (8), 3001–3005.

[9] M. Dubecký, *J. Phys. Chem. Lett.*, 2015, **6**, 1430-1434.

[10] P. Miller, N. Long, R. Vilar, A. Gee, *Ange. Chem. Int. Ed.*, 2008, **47**, 8998-9033.

[11] S. Purser, P. Moore, S. Swallow, V. Gouverneur, *Chem. Soc. Rev.*, 2008, **37**, 320-330.

[12] W. Middleton, *J. Org. Chem.*, 1975, **40**, 574-578.

[13] W. Middleton, E. Bingham, *J. Org. Chem.*, 1980, **45**, 2883-2887.

[14] G. Posner, S. Haines, *Tetrahedron Lett.*, 1985, **26**, 5-8.

[15] A. Boukerb, D. Grée, M. Laabassi, R. Grée, *J. Fluorine Chem.*, 1998, **88**, 23-27.

[16] F. Beaulieu, L. Beauregard, G. Courchesne, M. Couturier, A. L'Heureux, *Org. Lett.*, 2009, **11**, 5050-5053.

[17] M. Pouliot, L. Angers, J. Hamel, J. Paquin, *Tetrahedron Lett.*, 2012, **53**, 4121-4123.

[18] D. Lu, G. Liu, C. Zhu, B. Yuan, H. Xu, *Org. Lett.*, 2014, **16**, 2912-2915.

[19] A. Orliac, D. Gomez Pardo, A. Bombrun, J. Cossy, *Org. Lett.* 2013, **15**, 902-905.

[20] R. Banks, N. Lawrence, A. Popplewell, *Chem. Commun.*, 1994, **0**, 343-344.

[21] E. Differding, H. Ofner, *Synlett*, 1991, (3), 187-189.

[22] P. Nyffeler, S. Durón, M. Burkart, S. Vincent, C. Wong, *Ange. Chem. Int. Ed.*, 2004, **44**, 192-212.

[23] V. Rauniyar, A. Lackner, G. Hamilton, F. Toste, *Science*, 2011, **334**, 1681-1684.

[24] W. Peng, J. M. Shreeve, *J. Org. Chem.*, 2005, **70**, 5760–5763.

[25] G. S. Lal, *J. Org. Chem.*, 1993, **58**, 2791–2796.

[26] M. Zupan, J. Iskra, S. Stavber, *J. Fluorine Chem.*, 1995, **70**, 7-8.

[27] J. Hutchinson, G. Sandford, *Elemental Fluorine in Organic Chemistry*, Springer, 1997.

[28] A. Lothian, C. Ramsden, *Synlett*, 1993, **10**, 753-755.

[29] V. Grakauskas, *J. Org. Chem.*, 1969, **34**, 2446-2450.

[30] T. Patrick, K. Johri, D. White, *J. Org. Chem.*, 1983, **48**, 4158-4159.

[31] C. Ramsden, M. Shaw, *Tetrahedron Lett.*, 2009, **50**, 3321-3324.

[32] M. Rueda-Becerril, C. Chatalova Sazepin, J. Paquin, G. Sammis, *J. Am. Chem. Soc.*, 2012, **134**, 4026-4029.

[33] J.-D. Yang, Y. Wang, X.-S. Xue, J.-P. Cheng, *J. Org. Chem.* 2017, **82**, 4129−4135.

[34] F. Yin, Z. Wang, Z. Li, C. Li, *J. Am. Chem. Soc.*, 2012, **134**, 10401-10404.

[35] J. C. T. Leung, C. Chatalova-Sazepin, J. G. West, M. Rueda-Becerril, J.-F. Paquin, G. M. Sammis, *Angew. Chem. Int. Ed.*, 2012, **51**, 10804–10807.

[36] T. Liang, C. N. Neumann, T. Ritter, *Angew. Chem. Int. Ed.,* 2013, **52**, 8214–8264.

[37] S. Bloom, C. R. Pitts, D. C. Miller, N. Haselton, M. G. Holl, E. Urheim, T. Lectka, *Angew. Chem. Int. Ed.*, 2012, **51**, 10580–10583.

[38] N. Patel, R. Flowers II, *J. Org. Chem.*, 2015, **80**, 5834-5841.

[39] X. Zhang, *Comp. Theor. Chem*, 2016, **1082**, 11-20.

[40] M. Rueda-Becerril, O. Mahé, M. Drouin, M. B. Majewski, J. G. West, M. O. Wolf, G. M. Sammis, J.-F. Paquin, *J. Am. Chem. Soc.*, 2014, **136** (6), 2637–2641.

[41] S. Ventre, F. R. Petronijevic, D. W. C. MacMillan, *J. Am. Chem. Soc.*, 2015, **137** (17), 5654-5657.

[42] X. Wu, C. Meng, X. Yuan, X. Jia, X. Qian, J. Ye *Chem. Commun.*, 2015, **51**, 11864-11867.

[43] J. A. Porras, I. N. Mills, W. J. Transue, S. Bernhard, *J. Am. Chem. Soc.*, 2016, **138** (30), 9460-9472.

[44] X. Huang, W. Liu, J. M. Hooker J. T. Groves, *Angew. Chem. Int. Ed.*, 2015, **54** (17), 5241-5245.

[45] K. L. Hull, W. Q. Anani, M. S. Sanford, *J. Am. Chem. Soc.* 2006, **128**, 7134−7135.

[46] K. B. McMurtrey, J. M. Racowski, M. S. Sanford, *Org. Lett*. 2012, **14**, 4094−4097.

[47] W. Liu, J. T. Groves, *Angew. Chem., Int. Ed*. 2013, **52**, 6024−6027.

[48] W. Liu, Z. Huang, J. T. Groves, *Nat. Protoc*. 2013, **8**, 2348−2354.

[49] S. Bloom, C. R. Pitts, R. Woltornist, A. Griswold, M. G. Holl, T. Lectka, *Org. Lett.* 2013, **15**, 1722−1724.

[50] S. Bloom, A. Sharber, M. G. Holl, J. L. Knippel, T. Lectka, *J. Org. Chem*. 2013, **78**, 11082−11086.

[51] P. Xu, S. Guo, L. Wang, P. Tang, *Angew. Chem. Int. Ed*. 2014, **53**, 5955 −5958.

[52] J.-B. Xia, C. Zhu, C. Chen, *J. Am. Chem. Soc*. 2013, **135**, 17494−17500.

[53] S. Bloom, M. McCann, T. Lectka, *Org. Lett*. 2014, **16**, 6338−6341.

[54] D. Cantillo, O. de Frutos, J. A. Rincon, C. Mateos, C. O. Kappe, *J. Org. Chem*. 2014, **79**, 8486−8490.

[55] W. Liu, X. Y. Huang, M. J. Cheng, R. J. Nielsen, W. A. Goddard, J. T. Groves, *Science*, 2012, **337**, 1322 −1325.

[56] P.R. Ortiz de Montellano, *Chem. Rev*. 2010, **110** (2), 932-948.

[57] J. T. Groves, *J. Chem. Educ.*, 1985, **62** (11), 928-931.

[58] S. Bloom, J. L. Knippel, T. Lectka *Chem. Sci.*, 2014, **5**, 1175−1178.

[59] J.-B. Xia, C. Zhu, C. Chen, *Chem. Commun.*, 2014, **50**, 11701-11704.

[60] C. N. Neumann, T. Ritter, *Nature Chemistry*, 2016, **8** (9), 822-823.

[61] C.N. Satterfield, *Heterogeneous Catalysis in Industrial Practice*, New York, 2nd ed., McGraw-Hill Inc., 1991.

[62] U. Diebold, *Surf. Sci. Rep*. 2003, **48** (5–8), 53-229.

[63] M. Haruta, *Catal. Today*, 1997, **36** (1), 153-166.

[64] R. K. Grasselli, A. W. Sleight, *Structure–Activity and Selectivity Relationships in Heterogeneous Catalysis*, Elsevier, New York, 1991.

[65] C. T. Campbell, *Surf. Sci. Rep*. 1997, **27**, 1-111.

[66] M.-C. Daniel, D. Astruc, *Chem. Rev*., 2004, **104** (1), 293−346.

[67] Y. Sun, Y. Xia, *Science*, 2002, **298** (5601), 2176-2179.

[68] G. Hutchings, R. Catlow, M. Davidson, N. Turner, *Modern developments in catalysis*, World Scientific, 1st ed., 2016.

[69] A. Villa, D. Wang, G. Veith, F. Vindigni, L. Prati, *Catal. Sci. Technol.*, 2013, **3**, 3036-3041.

[70] I. Gandarias, E. Nowicka, B. May, S. Alghareed, R. Armstrong, P. Miedziak, S. Taylor, *Catal. Sci. Technol.*, 2016, **6**, 4201-4209.

[71] N. Dimitratos, J. Lopez-Sanchez, D. Morgan, A. Carley, R. Tiruvalam, C. Kiely, D. Bethell, G. Hutchings, *Phys. Chem. Chem. Phys.*, 2009, **11**, 5142-5153.

[72] S. James, C. Adams, C. Bolm, D. Braga, P. Collier, T. Friščić, F. Grepioni, K. Harris, G. Hyett, W. Jones, A. Krebs, J. Mack, L. Maini, A. Orpen, I. Parkin, W. Shearouse, J. Steed, D. Waddell, *Chem. Soc. Rev.*, 2012, **41**, 413-447.

[73] K. Ralphs, C. Hardacre, S. James, *Chem. Soc. Rev.*, 2013, **42**, 7701-7718.

[74] L. Leite, V. Stonkus, K. Edolfa, L. Ilieva, L. Plyasova, V. Zaikovskii, *Appl. Catal. A.*, 2006, **311**, 86-93.

[75] U. Kamolphop, S. Taylor, J. Breen, R. Burch, J. Delgado, S. Chansai, C. Hardacre, S. Hengrasmee, S. James, *ACS Catal.*, 2011, **1**, 1257-1262.

[76] V. Boldyrev, *Rus. Chem. Rev.*, 2006, **75**, 177-189.

[77] R. Sheldon, *Green Chem.*, 2005, **7**, 267-278.

[78] M.N. Chong, B. Jin, C. W. K. Chow, C. Saint, *Water Research*, 2010, **44** (10), 2997-3027.

[79] T. Hisatomi, J. Kubota, K. Domen, *Chem. Soc. Rev.*, 2014, **43**, 7520–7535.

[80] A. Fujishima, K. Honda, *Nature*, 1972, **238**, 37–38.

[81] S.N. Frank, A. J. Bard, *J. Am. Chem. Soc.* 1977, **99**, 303–304.

[82] R. Wang, K. Hashimoto, A. Fujishima, M. Chikuni, E. Kojima, A. Kitamura, *Nature*, 1997, **388**, 431–432.

[83] B. O'Regan, M. Gratzel, *Nature*, 1991, **353**, 737–739.

[84] B. J. Morgan, G. W. Watson, *J. Phys. Chem. C*, 2010, **114**, 2321–2328

[85] M. Koelsch, S. Cassaignon, C. T. Thanh Minh, J.-F. Guillemoles, J.-P. Jolivet, *Thin Solid Films*, 2004, **451**, 86–92.

[86] A. Hoffman, E. R. Carraway, M. Hoffman, *Environ. Sci. Technol.* 1994, **28**, 776-785.

[87] X. Z. Li, F.B. Li, *Environ. Sci. Technol.* 2001, **35**, 2381–2387.

[88] X. Zhou, G. Liu, J. Yu, W. Fan, *J. Mater. Chem.* 2012, **22**, 21337–21354.

[89] C. Gunawan, W.Y. Teoh, C.P. Marquis, J. Lifia, R. Amal, *Small*, 2009, **5**, 341–344.

[90] J. T. Groves, T. E. Nemo, R. S. Myers, J. *Am. Chem. Soc.* 1979, **101**, 1032-1033.

[91] C. K. Chang, M. S. Kuo, *J. Am. Chem. Soc.*, 1979, **101**, 3413-3415.

[92] D. Mansuy, J.-F. Bartoli, J.-C. Chottard, M. Lange, *Angew. Chem. Int. Edit.*, 1980, **19**, 909-910.

[93] D. Mansuy, P. Dansette, F. Pecquet, J.-C. Chottard, *Biochem. Biophys. Res. Commun.*, 1980, **96**, 433-439.

[94] I. Tabushi, N. Koga, *J. Am. Chem. Soc*. 1979, **101**, 6456-6458.

[95] I. Tabushi, N. Koga, *Tetrahedron Lett.*, 1979, **38**, 3681-3684.

[96] E. Guilmet, B. Meunier, *Tetrahedron Lett*., 1980, **21**, 4449-4450.

[97] J. T. Groves, *Cytochrome P450: Structure, Mechanism and Biochemistry*, 3rd ed., P.R. Ortiz de Montellano (Ed.) Kluwer Academic/Plenum Publishers, New York, 2005.

[98] S.-I. Murahashi, D. Zhang, *Chem. Soc. Rev*., 2008, **37**, 1490-1501.

[99] W. Nam, *Acc. Chem. Res*., 2007, **40** (7), 522–531.

[100] S. Campestrini, B. Meunier, *Inorg. Chem.*, 1992, **31** (11), 1999–2006.

[101] M. H. Alkordi, Y. Liu, R. W. Larsen, J. F. Eubank, M. Eddaoudi, *J. Am. Chem. Soc*., 2008, **130** (38), 12639–12641.

2

Techniques

A summary of all the techniques employed in this project is provided in this chapter, alongside analytical details of the qualitative and quantitative analysis of the reactions reported in the whole project. Due to the variety of reactions reported throughout this thesis, specific experimental details regarding catalytic testing are provided in each particular chapter.

2.1 Catalyst characterisation

A range of analytical and spectroscopic techniques were employed throughout this project, for characterisation of the catalyst and mechanistic investigation of the reaction pathways. A summary of the theory behind every technique is provided, as well as specific experimental details of the analysis procedure employed.

2.1.1 Powder X-ray Diffraction (XRD)

Powder X-Ray Diffraction (pXRD) is a useful technique primarily employed for the characterisation of the crystallinity of materials *via* elastic scattering of X-ray photons. This technique provides information of the bulk crystalline phases present within a particular material, and the transformations during various processes, such as heat treatments and reaction. Moreover, it can be used to estimate the particle size of the crystallites present.

During XRD analysis, the sample is continuously irradiated with X-rays, electromagnetic waves with wavelengths in a range 0.1-10 Å. Such X-rays possess sufficient energy to penetrate solids and give information of their internal structures.[1] X-rays are typically generated in X-ray tubes in which an electrically heated filament emits high energy electrons which are subsequently accelerated toward a metallic target anode. The collision of the accelerated electron with the target causes the ejection of electrons from an inner shell of the target. These are immediately replaced by other electrons present in a higher shell, causing the release of X-ray photons of a specific

frequency that is characteristic of the given metal, known as characteristic radiation. Together with the generation of characteristic X-ray, the collision of the accelerated electrons with the metal target leads to a deceleration of these electrons (following the hit), generating a continuous flow of X-rays radiation known as *Bremsstrahlung* (from the German for "braking radiation") or *white* radiation. Since monochromatic radiation is an essential requirement for diffraction studies, the *Bremsstrahlung* is subsequently passed through a filter, through which only a monochromatic X-ray can pass. The λ of this X-ray is both target and filter dependent. Moreover, the incident radiation and the periodic spacings of the lattice are required to have the same order of magnitude.

Typical XRD diffractometers satisfy all these criteria by employing a copper (Cu) metal target paired with a nickel filter, essential to filter out most of the copper X-ray continuum, efficiently releasing only the intense Cu Kα maxima at $\lambda = 1.51$ Å as monochromatic X-ray source.[1]

Following interaction with a crystal, the incident monochromatic X-ray scatters elastically, giving diffracted radiations which must interact constructively to provide structural information, emerging from the crystal as a single beam. Notably, constructive interactions among the diffracted beams only occur when their difference in path length is an integer number (n) of the wavelength λ. This condition is known as Bragg condition, whose equation (Bragg equation, given below in equation 2.1) allows the measurement of the lattice spacings (d) of the material at a given glancing angle (2θ).[2] This is depicted below in Figure 2.1:
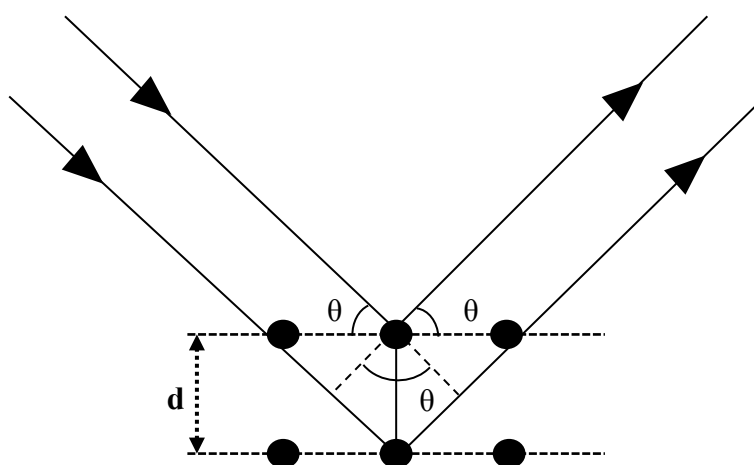

Figure 2.1: Diagram showing the diffraction of X-rays from lattice planes.

Where: n = integer
λ = wavelength
d = lattice spacing
θ = scattering angle

To measure the XRD pattern of the desired sample, which is typically ground to a fine powder, a stationary X-ray source is coupled with a moveable detector that monitors the intensity of the constructively interfering diffracted radiation at various diffraction angles, 2θ. The observed diffraction pattern of a sample strongly depends from the orientation of the single crystallites that have to be orientated at a specific angle (Bragg equation) to permit constructive interference of the scattered radiations: at a specific time, only the crystallites oriented at the right angle will contribute to the diffraction pattern. Therefore, the sample is generally rotated throughout the analysis duration, increasing the probability of the crystallites to contribute at the diffraction pattern, increasing the number of planes that satisfy Bragg condition and thus, increasing the intensity of the signals.

The signals obtained in an XRD pattern can then be compared with the diffraction patterns present in a large data-bank, allowing the identification of the crystalline phases present within the sample. An example of a commercial sample of titanium oxide (P25 from Degussa), which contains a mixture between two different phases, of TiO_2, anatase and rutile, is illustrated in Figure 2.2.[3]
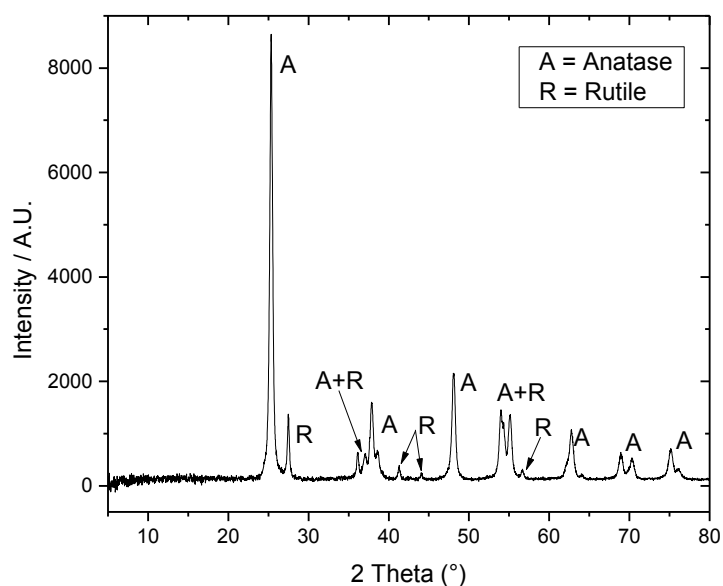
Figure 2.2: Powder XRD pattern of a commercial sample of TiO_2 P25 from Degussa with, assignment of the signals corresponding to anatase (A) and rutile (R), the two main crystalline phases present in P25.

In this study, X-Ray Powder Diffraction (XRPD) was performed on a PANalytical X'PertPRO X-ray diffractometer, with a CuK_α radiation source (40 kV and 30 mA) and Ni filter. Diffraction patterns were recorded between 5-80° 2θ at a step size of 0.0167° (time/step = 150 s, total time = 1.5 h).

2.1.2 Fundamentals of molecular spectroscopy

Spectroscopic techniques arise from energy exchange between the matter and electromagnetic radiations. Electromagnetic radiations can be described as simple harmonic waves transmitting through space, characterised by a specific amplitude and a specific wavelength (Figure 2.3).[4]
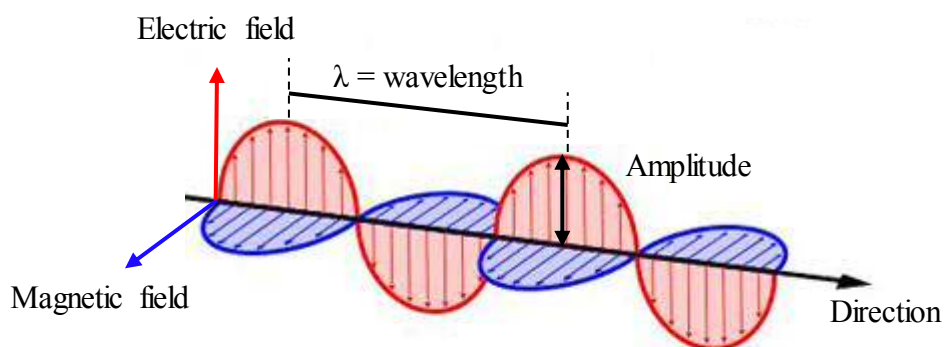
Figure 2.3: Schematic representation of an electromagnetic radiation.

The wavelength of an electromagnetic radiation is correlated to its frequency, and consequently to its energy *via* the following equations:

$$v$$

<div align="right">**Equation 2.2**</div>

$$E = h v$$

<div align="right">**Equation 2.3:** Planck's equation</div>

Where: c = speed of light
λ = wavelength
v = frequency
E = Energy
h = Planck's constant (h= 6.62607 x 10^{-34} J)

The energy of a molecule can be divided into several types of energies: electronic, rotational and vibrational. Each of the different energies is quantized, i.e. they can only possess discrete, specific values (known as "levels") and transitions among the different energy levels can only occur if specific amounts of energy (ΔE) are absorbed or emitted by the system.

$\Delta E = h\nu$
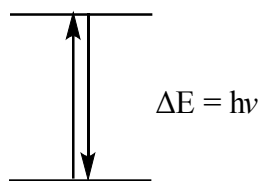
Figure 2.4: Example of transition between two different energy levels of a molecule or an atom during absorption or emission of a radiation of energy (ΔE).

Consequently, Planck's equation (Equation 2.3) can be employed to measure the frequency, and therefore the wavelength (Equation 2.2) of the electromagnetic radiation corresponding to the energy difference between the two different energy levels.

During spectroscopic analysis, the sample is generally irradiated with a beam of electromagnetic radiation, leading to the excitation of the system from a lower energy state (typically its ground state) to an upper (excited) one *via* the absorption of radiation of specific energy. Absorption spectra can, therefore, be generated measuring the eventual decreasing intensity of the electromagnetic beam by following its interaction with the sample, when the criterium $\Delta E = h\nu$ is satisfied.

When a molecule or atom exists in an excited state, energy is released to bring back the molecule in the lower energy (ground state) state. This energy can be released as electromagnetic radiation with a specific frequency as imposed by Planck's equation. Thus, following excitation of the sample, *via* irradiation, emission spectra can be generated detecting the radiation emitted from the sample.

Due to the relationship between adsorbed and emitted radiation with the energy gap of the different energy levels of a molecule, spectroscopic analysis allows information regarding the magnetic, vibrational, rotational and electronic properties of the analysed sample to be obtained.

2.1.3 Diffusive Reflectance Infra-red Fourier Transform (DRIFT) Spectroscopy

Fourier Transform - Infra-red (FT-IR) spectroscopy is a technique used to investigate the vibrational modes of molecules. FT-IR is a form of vibrational spectroscopy particularly useful for i) measuring bond lengths and force constants of small molecules

and ii) detecting and identifying the presence of specific functional groups situated in complicated molecular structures by characteristic absorptions.

Molecules possess a number of vibrational modes related to the number of atoms, N, present within the molecule: $3N - 6$ and $3N - 5$ vibrational modes are respectively observed for non linear and linear molecules. For a vibration to be amenable to study by FT-IR, its moment must correspond to a change in the electrical permanent dipole of the molecule.[5]
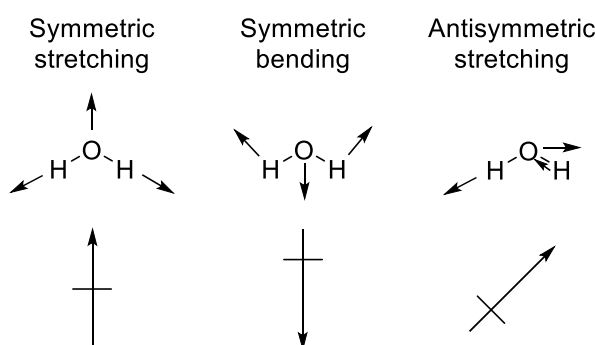
Figure 2.5: Illustrative vibrational modes of H_2O, divided in stretching and bending. The arrows below represent the changing in the electric dipole moment generated by the corresponding vibration.

The ΔE of such vibrational energy levels are of the order of 2500-25000 nm and hence, the vibrational information can be obtained when the energy of the radiation in a range $700 - 1 \times 10^6$ nm (IR) is used, therefore denoted as IR spectroscopy.

Irradiating the sample with electromagnetic radiation with wavelengths in a range 700 nm – 1 mm (infra-red radiation), the molecules can absorb vibrational energy and undergo to a transition from a vibrational state to an excited one. Notably, the vibrational frequency of a specific bond is strongly related to the mass of the atoms within the molecule, and the strength of the bond between them, according to the equations 2.4 and 2.5:

$$\overline{} \; \overline{}$$

<div align="right">**Equation 2.4**</div>

Where: v = frequency (cm^{-1})
k = force constant (N / cm)
μ = reduced mass (kg)

$$\overline{}$$

<div align="right">**Equation 2.5**</div>

Where: m_1, m_2 = the masses of the two vibrating atoms

Considering the broad number of vibrational modes possible for large molecules, FT-IR spectra generally show a large number of vibrations, typically separated into two classes; i) skeletal and ii) characteristic group vibrations. Notably, typical FT-IR spectra are plotted as a function of wavenumbers, equal to $1/\lambda$ (cm^{-1}). Skeletal vibrations, generally present in the range of wavelength 8300-25000 nm, corresponding to wavenumbers in a range $1200 - 400$ cm^{-1}, are related to the presence of linear or branched groups in the structures, possessing a large number of vibrational modes. Given that skeletal vibrational modes are highly sensitive to changes of the structure, such as the modification of a functional group. Therefore, this part of the spectrum ($1200 - 400$ cm^{-1}) is considered as the "fingerprint" region, characteristic of the analysing sample.

In addition to allowing the identification of a molecule *via* comparison of the absorption pattern observed in the fingerprint region of the spectrum, IR can also give more general information about the functional groups present in a complex molecule. The other part of the IR spectrum ($2500 - 8300$ nm, corresponding to $4000 - 1200$ cm^{-1}), generally shows the characteristic functional group vibrations present in the sample, such as C=O ~ 1700 cm^{-1}; O-H ~ 3500 cm^{-1}. These vibrations are typically independent from the molecular structure in its totality, but can strongly interact with other groups inside the structure, thus, helping to identify the structure of a sample.
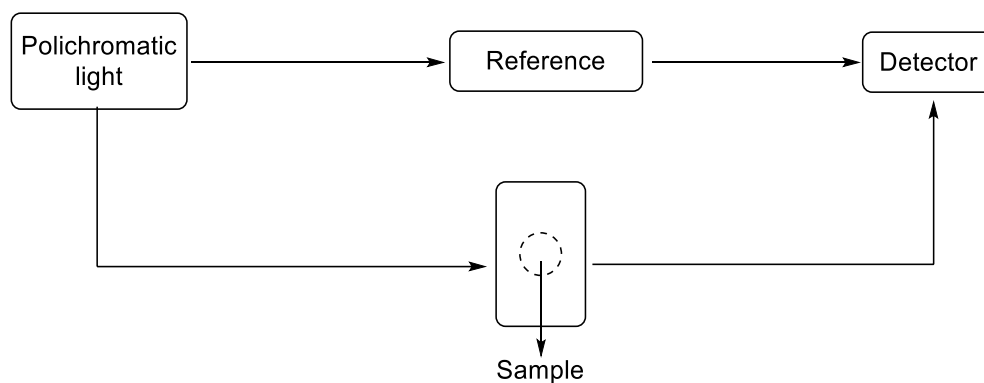
Figure 2.6: Schematic representation of a typical FT-IR setup.

To generate quality FT-IR spectra from bulk samples, such as solid catalysts, without any treatment of the material, diffuse reflectance spectroscopy is typically employed (DRIFT). In DRIFT spectroscopy, diffuse reflection arises by the roughness of the material surface, reflecting the IR light in all the directions. To measure the absorbed radiation, the scattered radiation is then collected *via* an ellipsoid or paraboloid mirror and re-directed to the detector.

In this project, DRIFT spectroscopy was employed to study the interactions between the catalyst (TiO_2) and pivalic acid ($(CH_3)_3CCOOH$), a carboxylic acid was employed as a substrate for decarboxylic fluorination. During the DRIFT experiment, pivalic acid was nebulised in N_2 and fluxed through the DRIFT cell containing the catalyst, adsorbing on the catalyst surface. The spectrum so observed (blue line, Figure 2.7) was compared with the IR spectrum of pure pivalic acid (red line, Figure 2.7), indicating that pivalic acid can be adsorbed on titanium oxide surface mainly as pivalate $(CH_3)_3CCOO^-$. This is indicated by the disappearing of the carboxylic group vibrations at $1694 \ cm^{-1}$ and $1197 \ cm^{-1}$ in the adsorbed spectrum (blue line).[6] The coordination and decomposition of the pivalate could subsequently be monitored as a function of time, temperature and UV light intensity / λ.
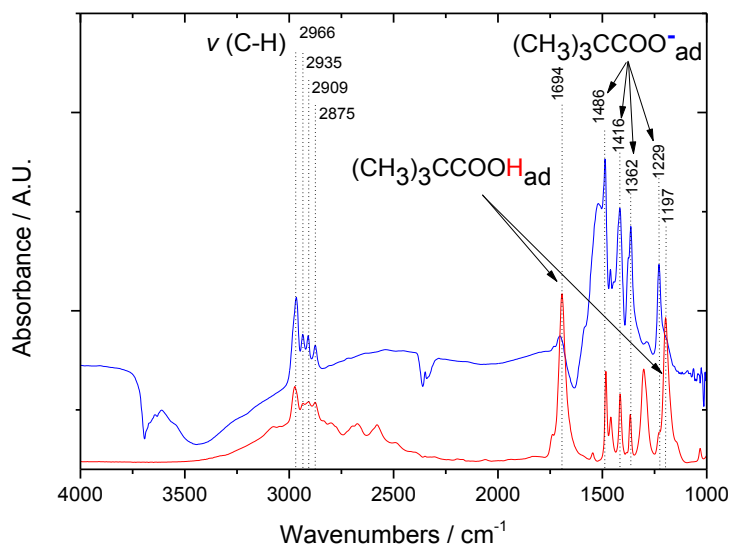
Figure 2.7: Diffuse Reflectance Infrared Fourier Transform (DRIFT) spectra of (red line) pivalic acid and (blue line) TiO₂ after adsorption of pivalic acid at 30 °C.

Diffuse Reflectance Infra-red Fourier Transform (DRIFT) spectroscopy was performed using a Harrick praying mantis cell. All the spectra were recorded on a Bruker Tensor spectrometer over a range of $4000 - 650$ cm^{-1} at a resolution of 2 cm^{-1}.

2.1.4 Magic-Angle Spinning Nuclear Magnetic Resonance (MAS-NMR)

Magic-Angle Spinning Nuclear Magnetic Resonance (MAS-NMR) is a spectroscopic technique suitable for the study of solids possessing nuclei with magnetic moments, generated by the presence of uneven numbers of nucleons (protons + neutrons) present in said nuclei. The nuclear spin (magnetic moment) possessed by a nucleus is also quantized and indicated by the quantum number *I*, represented by an integer or half-integer value depending from the number of unpaired nucleons present into the nucleus. In the absence of an external magnetic field, $2I + 1$ degenerate energy level are present, related to the nuclear spin of the particular nucleus. However, the application of an external magnetic field leads to the loss of degeneration of this energy level, which can subsequently split into different energy levels. The resultant energy levels can either align with, or be opposed to, the external field. The extent of this splitting of the energy level is directly proportional to the applied field and can be measured *via* the following equation 2.6:

$$B_0/2\pi$$

Equation 2.6

Where: giromagnetic ratio
    Planck costant
B₀   magnetic field
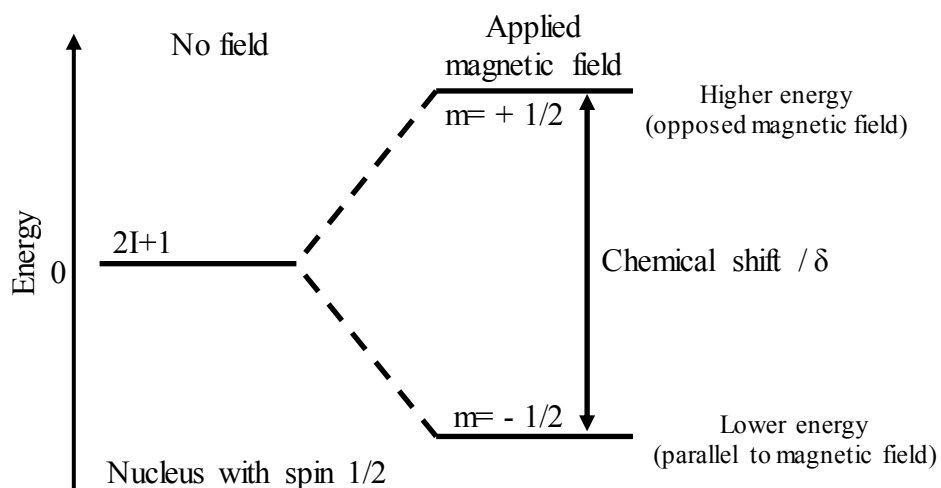
Figure 2.8: Splitting of the energy levels for a nucleus with spin ½, such as ^{1}H and ^{19}F in the presence of an applied magnetic field B₀. m = magnetic quantum number.

The splitting of energy levels for a nucleus with spin ½ is also depicted above in Figure 2.8. According to this schematic, it would seem that every nucleus has the same energy difference. However, it is essential to consider that every nucleus with a compound or molecule is surrounded by a slightly different electronic cloud, depending on the structure of the surrounding nuclei. Thus, every proton (or fluorine for ^{19}F) with different surroundings is subjected to very slightly different splitting between energy levels and will, therefore, resonate with a slightly different but specific frequency. The resonant frequency of a nucleus is known as its chemical shift, δ.

During NMR analysis, the sample, subjected to a magnetic field B₀, is irradiated with an electromagnetic radiation, promoting all the nuclei to their higher energy state. The energy subsequently released from the excited nuclei during the relaxation toward the lower energy states, is then measured. The NMR spectrum is obtained as a plot of the amount of the intensity as a function of energy, reported in terms of chemical shift.[7]

The resonance between the energy levels, arising by the application of a magnetic field, and the determination of the frequency necessary to achieve resonance are the fundamentals of NMR spectroscopy.

However, the NMR spectra can be affected by line broadening effects arising from several factors, including i) magnetic dipolar-dipolar interaction, ii) chemical shift anisotropy, and iii) quadrupolar interaction. Whilst in liquid samples these effects are easily removed by the fast molecular motion of the samples dissolved into the liquid, solid sample NMR are vulnerable to line broadening effects. To minimise line broadening issues, the analysing samples are quickly spun at an angle of 54.7 °, called "magic angle", mimicking the fast motions of the molecules dissolved in a solvent, thus increasing the spectra resolution.[8] Notably, the value 54.7° represents the angle at which the dipolar interaction, angular dependent, is minimised.

^{19}F MAS-NMR measurements were performed during this study in order to investigate the potential formation of Ti-F covalent bonds generated *in-situ* upon interaction of TiO_2 with the fluorinated reagent. An example of ^{19}F MAS-NMR on a used sample of TiO_2 is shown below in Figure 2.9. The spectrum reveals the presence of fluorine that is covalently bound to the catalyst surface, in fact, deconvolution of this spectra was performed and three main species were found, at 20, 12 and -9 ppm. All these species can be attributed to Ti-F species, in particular to Ti-F-Ti species (20 and 12 ppm) and "extra-framework" Ti-F species presents on defect sites of TiO_2 structure (-9 ppm) as reported by Dambournet group.[9-11]
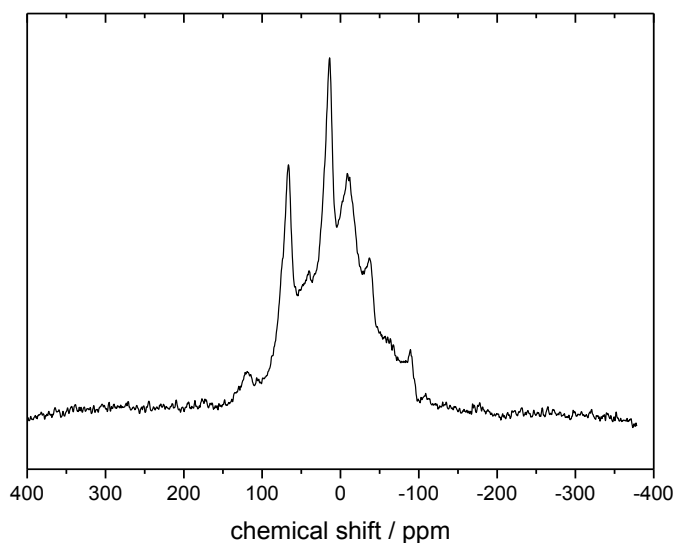
Figure 2.9: Magic-Angle Spinning NMR spectra of used TiO$_2$.

^{19}F MAS NMR experiments were performed in Durham University (GB) through the EPSRC UK National Solid-State NMR Service on a Bruker Avance III HD operating at 149 MHz, recorded using a rotor synchronised Hahn echo to improve the baseline. The samples (approximatively 60 - 100 mg placed in a 4 mm rotor) were analysed as received using a spinning of 20 kHz and CFCl$_3$ as reference (δ = 0.00 ppm). Measurements were performed in direct excitation mode (spin-echo 90x-t-180y), with a recycle delay of 1s.

2.1.5 X-ray Photoelectron Spectroscopy (XPS)

X-ray Photoelectron Spectroscopy (XPS) is a surface-specific spectroscopic technique based on the photoelectric effect, particularly employed to investigate the elemental composition of a sample and the oxidation states of the detected elements present within it. Irradiating a sample with X-ray radiation, the electrons of an atom, can be expelled from the atom with a kinetic energy (E_K) related to the binding energy of the electron (E_B) via the equation 2.7:
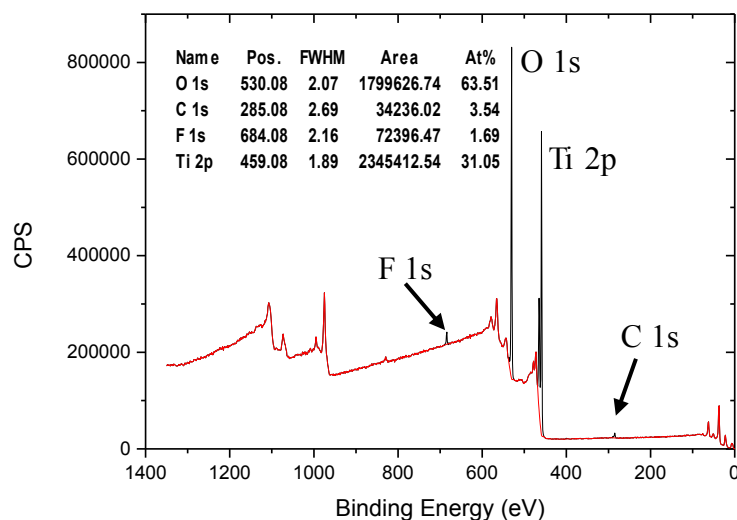
$$E_k = h\nu - E_b$$

<div align="right">**Equation 2.7**</div>

Where: E_K = kinetic energy
$h\nu$ = energy of the incident radiation
ν = frequency of radiation
E_B = binding energy of the electron
φ = XPS constant

The measurement of the kinetic energy of the expelled photoelectron can, therefore, be used to determine its binding energy, providing information about the nature of the emitted element. Apart from giving information about the identity of an element, subtle changes of the binding energies are observed when the oxidation state of the element is varied.[12] An example of the shift in binding energy due to the oxidation state of the element, is given by titanium (Ti). In fact, whilst a binding energy of 454.1 eV ($Ti2p_{3/2}$) is observed for metallic Ti, a higher binding energy, around 458.4 eV ($Ti2p_{3/2}$), is reported for $Ti^{(IV)}O_2$ in which the electrons are more tightly bound to the nucleus due to the higher oxidation state.

In this study, XPS analysis was employed for two different applications. In Chapter 3 it was essential to discriminate among two different types of silver oxides incorporated on the catalyst (Ag (I) oxide and Ag (I, III) oxide).[13-15] Whilst in Chapter 4, XPS analysis was performed to study the interactions between titanium oxide (TiO_2), and the fluorinating reagent, Selectfluor®.

An illustrative XPS spectrum of a used sample of TiO_2 post-treatment with Selectfluor® is shown below in Figure 2.10, generated by plotting the intensity of the expelled photoelectrons (N_E) against the binding energy:

Name	Pos.	FWHM	Area	At%
O 1s	530.08	2.07	1799626.74	63.51
C 1s	285.08	2.69	34236.02	3.54
F 1s	684.08	2.16	72396.47	1.69
Ti 2p	459.08	1.89	2345412.54	31.05

Figure 2.10: XPS spectrum of TiO_2 post-treatment with Selectfluor®. Titanium dioxide was treated under standard reaction conditions albeit in the absence of the substrate. After treatment the catalyst was filtered, washed with deionised water and dried in an oven for 2 hours.

XPS analysis was performed on a Thermo Scientific K-Alpha+ spectrometer. Samples were analysed using a monochromatic Al X-ray source operating at 72 W (6 mA x 12 kV), with the signal averaged over an oval-shaped area of approximately 600 x 400 microns. Data was recorded at pass energies of 150 eV for survey scans and 40 eV for high resolution scan with a 1 eV and 0.1 eV step size respectively. Charge neutralisation of the sample was achieved using a combination of both low energy electrons and argon ions (less than 1 eV) which gave a C(1s) binding energy of 284.8 eV.

All spectra were analysed using CasaXPS (v2.3.17 PR1.1) using Scofield sensitivity factors and an energy exponent of -0.6.

2.1.6 Ultraviolet-Visible Spectroscopy (UV-Vis)

Ultraviolet-Visible spectroscopy is a useful technique that gives important information about optically absorbing species in a sample. During UV-Vis analysis samples are irradiated with photons of wavelengths in a typical range 200-800 nm (UV-Visible spectral range).[16] This electromagnetic radiation possesses sufficient energy to allow electronic molecular transitions, providing several information about the nature of a chromophoric group present into the liquid or in the solid sample. This technique is

especially useful for transition metals, where several electronic transitions such as d-d orbital transitions and charge transfers between the ligand and the metal, may take place. Thus, information about the oxidation state and the geometry of the metallic centre, as well as indications about the nature of the coordinating ligand(s), can be inferred by the analysis of UV-Vis spectra, which can be measured in both absorbance or reflectance mode. UV-Vis is also widely employed to characterise Ag and Au colloidal solutions, providing useful information about size and shape of the particles dispersed in solution by monitoring a characteristic absorption peak known as plasmon resonance peak.[17]

UV-Vis spectroscopy can also be employed for quantitative analysis using the Beer-Lambert law, given below in equation 2.8, correlating the intensity of the absorbed radiation (at a given wavelength), with the concentration of the absorbing species:

Equation 2.8: Beer- Lambert Law

Where: A = absorbance
ε = molar extinction coefficient
[c] = concentration
l = path length of the sample cell

In this project, UV-Vis analysis was employed for several applications. It was mainly employed to study the behaviour of metallic silver, potentially present on the catalyst surface, upon interaction with the fluorinating agent mimicking the reaction conditions of a typical decarboxylative fluorination reaction albeit in the absence of the substrate. To study the behaviour of metallic silver, the plasmon resonance peak of a colloidal solution of metallic Ag nanoparticles was monitored *via* UV-Vis, following addition of the fluorinating agent, Seletfluor®, in solution (Figure 2.11).
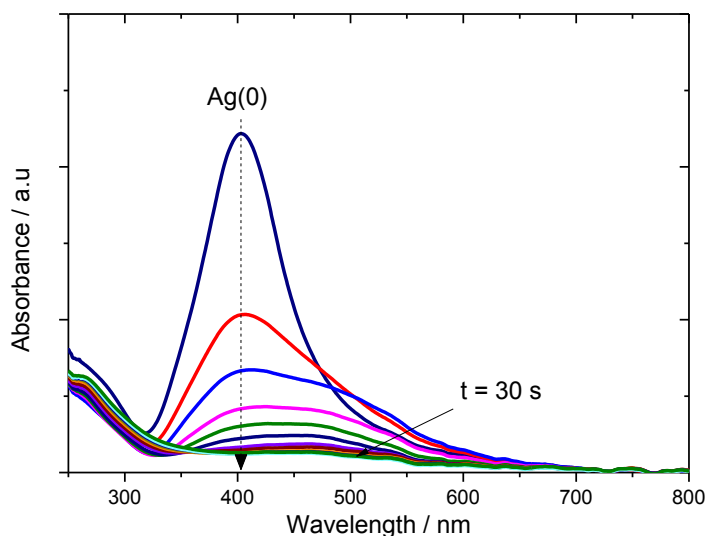
Figure 2.11: UV-Vis spectra of colloidal Ag(0) after addition of Selectfluor® and K_2CO_3.

UV-Vis analysis was performed with an Avantes AvaLight-DH-S-Bal light source and an Avantes, AvaSpec-2048 spectrometer in Absorbance mode.
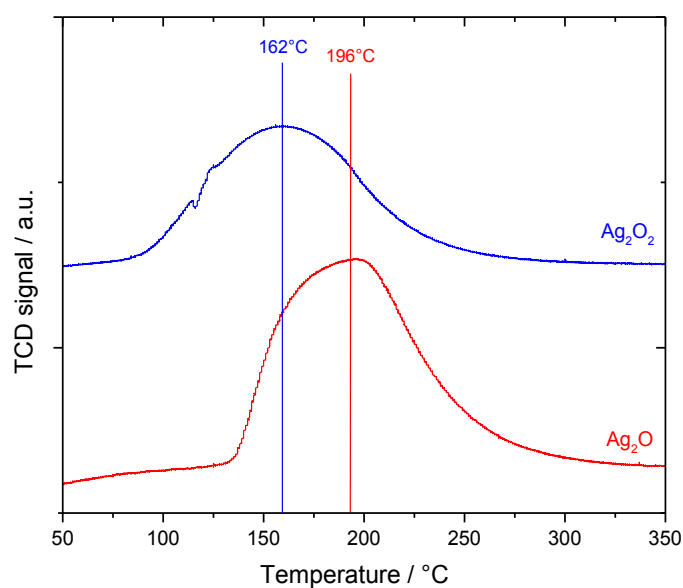
2.1.7 Temperature Programmed Reduction (TPR)

Temperature Programmed Reduction (TPR) is an analytical technique that provides useful information regarding the capability of a sample undergo reduction, giving information about the oxidation state of the metal(s) present on the catalyst. During TPR analysis, the analysing sample is heated with a linear ramp rate, under reducing atmosphere (generally 5-10% H_2/Ar). Part of the hydrogen flowing through the sample is then used to reduce the sample, and the quantity of H_2 consumed typically monitored throughout, by a thermal conductivity detector (TCD). TPR profiles are generally obtained by plotting the TCD signal versus the reduction temperature, in order to measure the temperature(s) necessary to reduce the sample. This allows information about the active species present on the catalyst (*e.g.* metal sites in their oxidized state) or bulk reduction (*e.g.* reduction of the catalytic support) to be obtained.[18] Also, this technique can provide useful information about the appropriate temperatures required to heat treatment the materials.
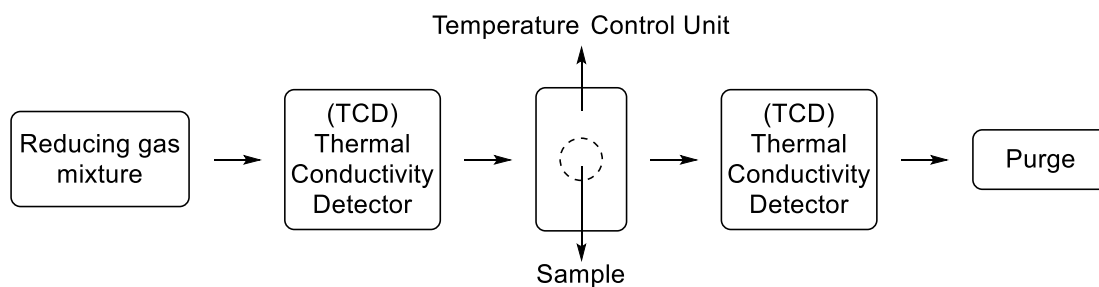
Figure 2.12: Schematic representation of a typical TPR setup.

TPR analysis was performed during this study in order to investigate the oxidation state of the Ag present in mechanochemical mixtures of Ag_xO/TiO_2, both of which exhibit specific reduction temperatures. An illustrative TPR profile is provided below in Figure 2.13:

Figure 2.13: Temperature Programmed Reduction (TPR) profiles of $1Ag_2O$ and Ag_2O_2 (Ag (I, III) oxide).

TPR analysis was carried out using a Thermo TPDRO 1100 instrument. The samples were fed with 10% H_2/Ar with a flow of 20 ml min^{-1} and the temperature was increased up to 550 °C at a rate of 5°C min^{-1}. Each measurement was performed on 100 mg of sample, pre-treated in Ar at 120 °C for 1 hour.

2.1.8 Microwave Plasma – Atomic Emission Spectroscopy

Microwave Plasma Atomic Emission Spectroscopy (MP-AES) is a powerful tool for the simultaneous identification and quantification of dissolved metallic species present in solutions (typically aqueous solutions). Despite the fact that it is less sensitive than Inductively Coupled Plasma (ICP) spectroscopy, with detectability limits arounds 1 ppm (part per million), MP-AES possesses several advantages over ICP-MS, including low operational cost, elimination of flammable gases, and smaller dimensions.

MP-AES is a spectroscopic method based on a microwave induced plasma (MP) interfaced with an atomic emission spectrophotometer (AES). Atomic emission spectroscopy (AES) is a technique involving the study of the radiation emitted by the atoms in their exited state, ionised by the effect of the high temperature of the plasma. In fact, in a typical MP-AES spectrometer, the atomised sample, previously nebulised in a nebuliser, interacts with the plasma, promoting electrons to their excited state. The subsequent relaxation of the excited electrons, returning to their ground state generates photons. The emitted photons are then dispersed by a grating and detected by a spectrometer that constantly monitor the changing in the emission at the desired line.

Given that each element emits radiation of specific wavelength, qualitative analysis *via* MP-AES can be performed. Moreover, measuring the intensity of the signals, related to the number of atoms in the exited state and the probability of the transition (Equation 2.9), allows quantitative analysis to be performed, measuring the amount of a given element in solution.[19]

$$N_i P_l$$

Equation 2.9

Where: I = intensity of the signal
K = Boltzmann constant
Ni = population of the electronic state *i*
Pi = probability of the transition

MP-AES analysis was performed in this study to detect the amount of metallic silver (Ag), eventually leached from the catalyst surface to the reaction solution. To analyse the free Ag present in solution, reaction mixtures were filtered and diluted with deionised water. The samples were then analysed with a 4100 MP-AES (Agilent

Technologies) and the eventual amount of metal was detected at two different wavelengths (338 nm and 328 nm for silver), giving the corresponding Ag leaching value as an average of the values obtained at the two different wavelengths (opportunely modified considering the dilution factor of the solution). For each set of samples, to reduce the instrumental error, a calibration with Ag standard solutions, respectively at 2, 5, 10 and 15 ppm (parts per million) was performed.

2.2 Product analysis and quantification

Several types of reactions were performed throughout this project. Therefore, a range of analytic techniques was employed to perform quantitative analysis of the reagent and (by)products present into a reaction mixture at a given time, in order to perform kinetic and mechanistic studies of the systems under study.
A summary of the theory behind every analytical technique is provided in this section, as well as specific details of the quantitative analysis procedure employed.

2.2.1 ^{1}H and ^{19}F-NMR Spectroscopy

Nuclear magnetic resonance spectroscopy is a very useful technique for the identification and characterisation of organic compounds in solution. The basics of NMR Spectroscopy have already been described in section 2.1.4. However, liquid samples do not require any spinning as line-broadening effects, often observed for solid samples, do not occur for liquids, due to the rapid molecular motions in solution.

For nuclei such as ^{1}H and ^{19}F, NMR spectroscopy can also be employed as an analytical method for the quantification of organic molecules *via* addition of internal standards into the reaction solution. In fact, for these nuclei, which are characterised by fast nuclear relaxation, the magnitude of a signal is directly related to the number of molecules of that species in solution, multiplied by the number of protons (or fluorine atoms for ^{19}F) contributing to that signal. Therefore, by adding a known amount of standard, such as α,α,α-trifluorotoluene for ^{19}F NMR (δ=-63.72 ppm, 3 F), is possible to calculate the amount of the desired compound integrating the desired peak and the one of the standard, both of them opportunely divided by the number of protons (or fluorine atoms) contributing to the signals. In this study, quantitative ^{19}F NMR analysis was performed to quantify the fluorinated products obtained during decarboxylative

fluorination of several substrates, different from 2,2-dimethylglutaric acid (see Chapter 3 and Chapter 4 for more details). For each reaction, to analyse the amount of fluorinated product at a given time (t > 10 min), a standard solution of α,α,α-trifluorotoluene in acetone (typically 4 ml solution, 1.15 μl (α,α,α-trifluorotoluene) ml⁻¹ (acetone)) was added to the reaction mixture. The resulting mixture was subsequently stirred and a portion of the solution was withdrawn, centrifuged to remove the solid catalyst, hence terminating the reaction, and placed into an NMR tube. The corresponding moles of fluorinated product in solution were subsequently calculated via integration using equation 2.10:

$$\overline{}\quad\overline{}$$

<div align="right">**Equation 2.10**</div>

Where: a = number of fluorine atoms contributing to the signal of the product (typically one for monofluorination product)
b = number of fluorine atoms contributing to the signal of the standard (*b* = 3 for α,α,α-trifluorotoluene)
$n_{product}$ = moles of the product present into the NMR tube
$n_{standard}$ = moles of the standard added into the NMR tube
$A_{product}$ = area integrated on the signal of the product
$A_{standard}$ = area integrated on the signal of the standard (δ=-63.72 ppm for α,α,α-trifluorotoluene)

Notably, integration was recorded on ^{19}F NMR spectra with ^{1}H decoupling, to allow better integration of the signals. An illustrative spectrum with integration is shown below in Figure 2.14:
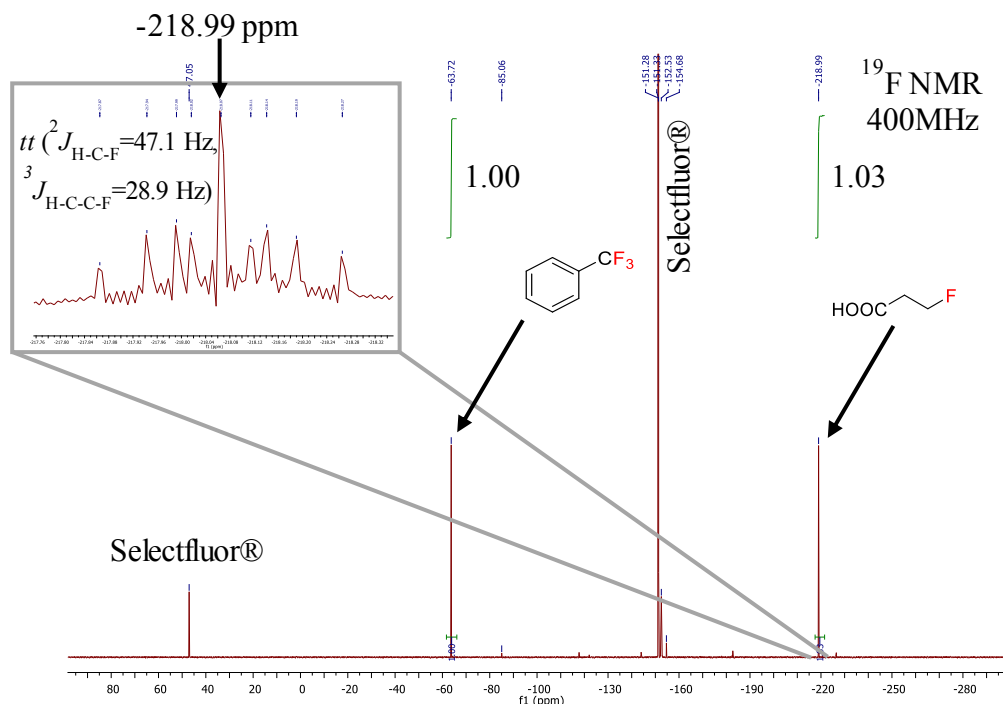
**Figure 2.14:** Crude ^{19}F NMR spectra with ^{1}H decoupling for succinic acid, (COOH)-(CH2)2-COOH decarboxylative fluorination. The top left insert represents the corresponding ^{19}F NMR spectra (in the region -218 -220 ppm) without ^{1}H decoupling to demonstrate the identity of the signal at -218.99 ppm related to the monofluorinated product obtained by decarboxylative fluorination of succinic acid. In fact, whilst the signal at -218.99 ppm is a singlet in the decoupled spectra, this signal spits into a triple triplet (*tt*) in the spectrum without ^{1}H decoupling, due to the coupling with the protons on the Cα and Cβ. Notably, $^2J_{H-C-F}$=47.1 Hz and $^3J_{H-C-C-F}$=28.9 Hz are observed due to the coupling with the two geminal protons and the two vicinal protons, respectively.

An important effect observed for fluorinated molecules is the heterocoupling [1]H-^{19}F, very useful for the identification and characterisation of fluorinated compounds. In fact, the nuclear spin ½ and high natural abundance of ^{19}F, results in strong [1]H-^{19}F couplings, which can be observed up to three bonds away. Therefore, by performing experiments with and without coupling, strong modifications to both ^{1}H and ^{19}F NMR spectra can occur.[20]

In this study ^{1}H NMR experiments both with, and without, ^{19}F coupling were performed to identify the nature of (by)products observed during the screening of different substrates. An example of the effect of fluorine coupling in ^{1}H NMR is given by the crude ^{1}H NMR spectra recorded for the benzylic fluorination of ethylbenzene (Figure 2.16). As expected no modification was observed in the shape of the triplet at 1.55 ppm related to the protons in β to the phenyl group (evidenced in blue in the following

scheme) of the reagent (ethyl benzene, **1a**). However, the same protons (highlighted in blue in Figure 2.15) present into the fluorinated product, 1-fluoro-1-phenylethane **1b**, experienced coupling with the fluorine in benzylic position. This coupling resulted into a double doublet observed at δ=1.98 ppm with two different coupling constants: J_1=24.6 Hz due to the coupling with the fluorine $(^3J_{\text{H-C-C-F}})$, and J_2=6.4 Hz due to the coupling with the benzylic proton, highlighted in red in Figure 2.15. As expected, applying ^{19}F decoupling on the ^{1}H NMR spectrum, the double doublet previously observed in the ^{1}H NMR not decoupled spectrum, converged into a single doublet (blue line, Figure 2.16), due to the loss of coupling with the fluorine.
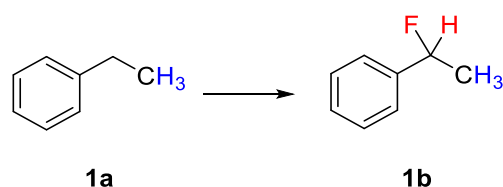
**Figure 2.15:** Schematic for ethylbenzene (**1a**) fluorination in 1-fluoro-1-phenylhetane (**1b**).
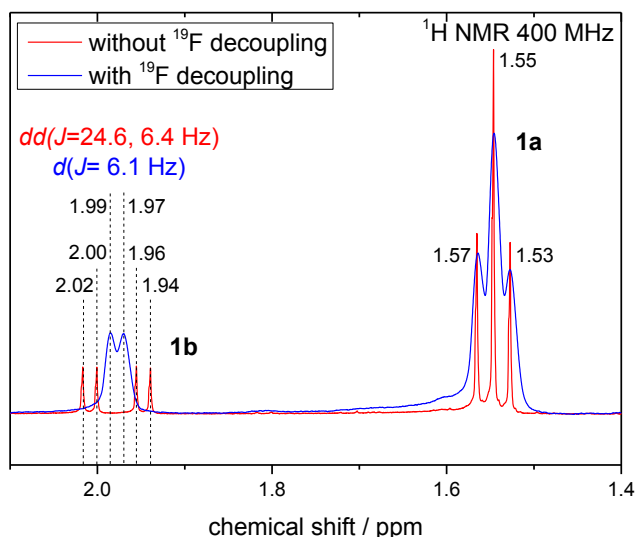
Figure 2.16: ^{1}H NMR with (blue line) line and without (red line) ^{19}F decoupling for a typical benzylic fluorination reaction in D_2O and $(CD_3)_2CO$. (*dd* = double doublet, *d* = doublet).

Analogous to the decoupling effect observed in ^{1}H NMR spectra, ^{19}F NMR can also be recorded with and without ^{1}H coupling, in order to aid the identification of reaction products and by-products. An example of splitting observed for ^{19}F NMR with and

without ^{1}H decoupling is reported in Figure 2.17, showing the pure product obtained by decarboxylative fluorination of 2,2-dimethylglutaric acid.
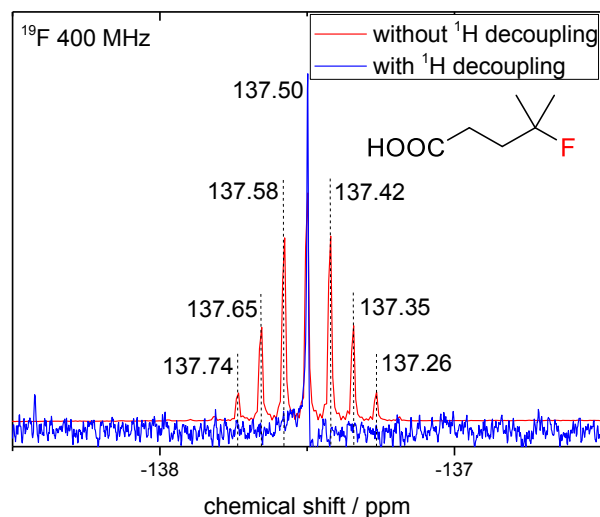
Figure 2.17: ^{19}F NMR spectra in H₂O/acetone of 4-fluoro-4-methylpentanoic acid with (blue line) and without (red line) ^{1}H decoupling.

^{19}F spectra were run on a JEOL Eclipse (+) 300 MHz NMR spectrometer equipped with a 5 mm autotunable BBO probe and on a 400 MHz Bruker UltraShield™ using α,α,α-trifluorotoluene as reference (δ=-63.72 ppm). ^{1}H of pure 4-fluoro-4-methylpentanoic acid was run on a 400 MHz Bruker UltraShield™ spectrometer using TMS as reference (δ=0 ppm).

2.2.2 High Performance Liquid Chromatography

High performance liquid chromatography (HPLC) is a useful technique to qualitatively and quantitatively analyse the different component of a reaction mixture *via* chromatography. In liquid chromatography, the separation of the analytes carried by a liquid mobile phase, known as the eluent, depends from their interactions with the stationary phase (column). The length of time between the injection of a sample and the elution of a particular analytes is referred as retention time; the stronger the interaction between analyte-stationary phase, the longer the retention time for that analyte will be.[21] By comparing the retention time observed during analysis to those observed for known standards, it is possible to identify the species present in a solution (*e.g.* crude reaction

mixture). Given that the area of a signal is proportional to the concentration of the species responsible for that signal, quantification of the individual product concentrations can also be achieved.
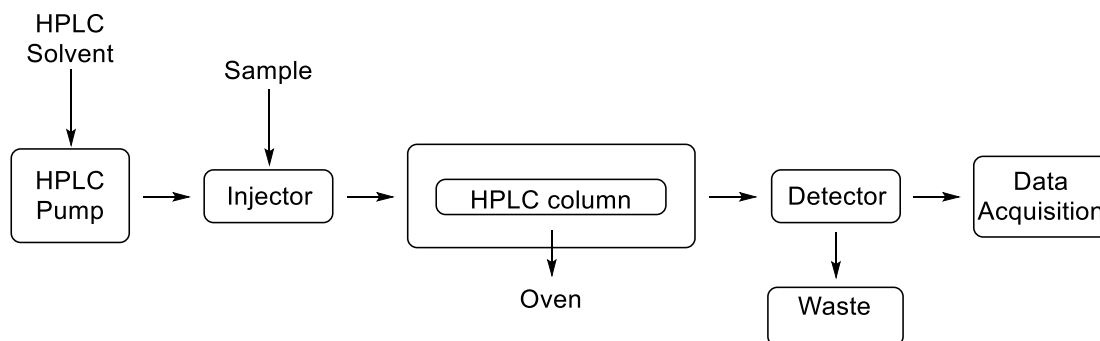
Figure 2.18: Schematic of the HPLC setup used throughout the project.

HPLC was employed to analyse various reaction mixtures to identify and quantify products, and gain important kinetic information. Considering the acid nature of the substrates and the acidity of the reaction mixture, a column specifically designed for organic acids, a MetaCarb 87H 250 x 4.6 mm was used to analyse the model reagent 2,2-dimethylglutaric acid (**2a**) and the product 4-fluoro-4-methylpentanoic acid (**2b**). Samples were analysed using an Agilent 1220 Infinity HPLC equipped with an autosampler, an oven designed to heat the column during the analysis (set at 60°C) and a variable wavelength UV-VIS (VWD) detector set at 210 nm. The analysis was carried out using an aqueous solution of phosphoric acid (0.1 % wt.) in ultrapure HPLC-water as eluent with a flow of 0.400 mL/min.
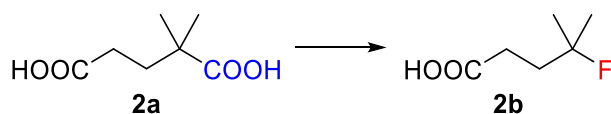
Figure 2.19: Schematic for 2,2-dimethylglutaric acid (**2a**) decarboxylative fluorination to give 4-fluoro-4-methylpentanoic acid (**2b**).

The calibration for the reagent, 2,2-dimethylglutaric acid (**2a**) was carried out with the commercial chemical from Sigma Aldrich, and succinic acid was employed as external standard. To obtain a calibration curve for the fluorinated product, 4-fluoro-4-methylpentanoic acid (**2b**)), which was not commercially available, the pure compound was isolated via column chromatography. Silica gel was used as stationary phase, and

first hexane, followed by mixture of hexane/ethyl acetate was used as eluent. The ratio of hexane/ethyl acetate was constantly increased until hexane/ethyl acetate = 2/1 was achieved. At the end of the chromatography pure ethyl acetate was used to elute all the products eventually retained on the column. The single fractions were examined by both ^{1}H and ^{19}F NMR and pure 4-fluoro-4-methylpentanoic acid (**2b**) was isolated, allowing for an HPLC calibration of the pure product against the succinic acid standard.

Notably, calibration equations were obtained plotting the ratios between the concentration of the desired compound and the concentration of the standard ($C_{(compounds)}/C_{(standard)}$) as a function of the ratios amongst the area values ($A_{(compound)}/A_{(standard)}$), given below by Equation 2.11:

$$C_{(compounds)}/C_{(standard)} = CF * A_{(compound)}/A_{(standard)}$$

Equation 2.11

Where: CF= calibration factor

The accuracy of the calibration is reported with R^2 values, representing the error related to the fitting of the several points fitted with a line; more this value is similar to 1, more accurate is the fitting. These values are reported in Table 2.1 and the calibration curves are shown in Figures 2.20 and 2.21.

|	Retention Time /min	Calibration equation	R^2
2,2 –Dimethylglutaric acid (1a)	6.704	y=0.5284x	0.9987
4-Fluoro-4-methylpentanoic acid (1b)	9.307	y=4.7378x	0.9983
Succinic acid (2)	5.108	external standard	

Table 2.1: Calibration results for the reactants involved in 2,2–dimethylglutaric acid (**2a**) decarboxylative fluorination to give 4-fluoro-4-methylpentanoic acid (**2b**).
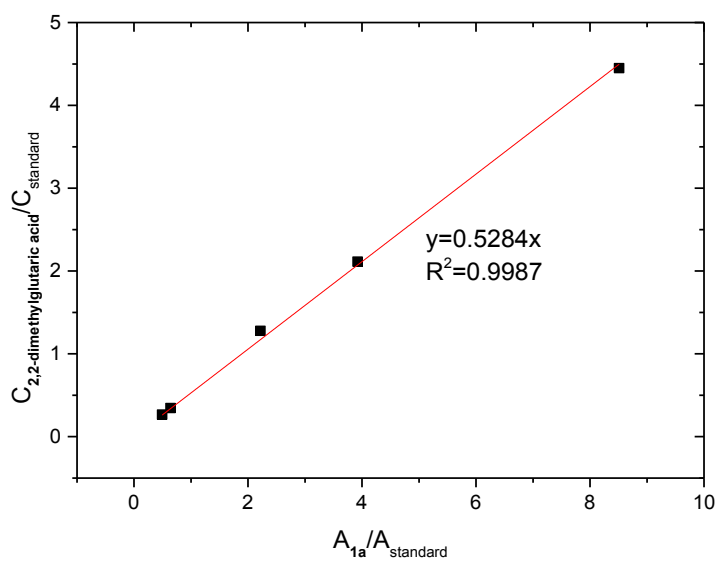
Figure 2.20: Calibration line for 2,2–dimethylglutaric acid (**2a**) performed with the HPLC using succinic acid as external standard.
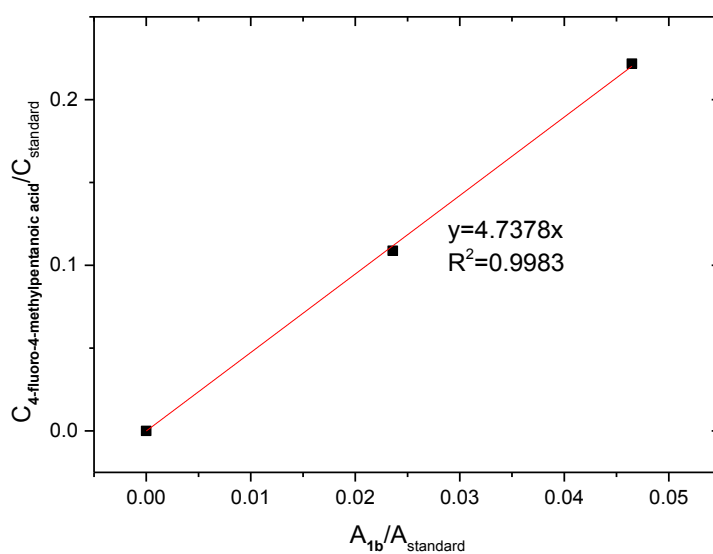
Figure 2.21: Calibration line for 4-fluoro-4-methylpentanoic acid (**2b**) performed with the HPLC using succinic acid as external standard.
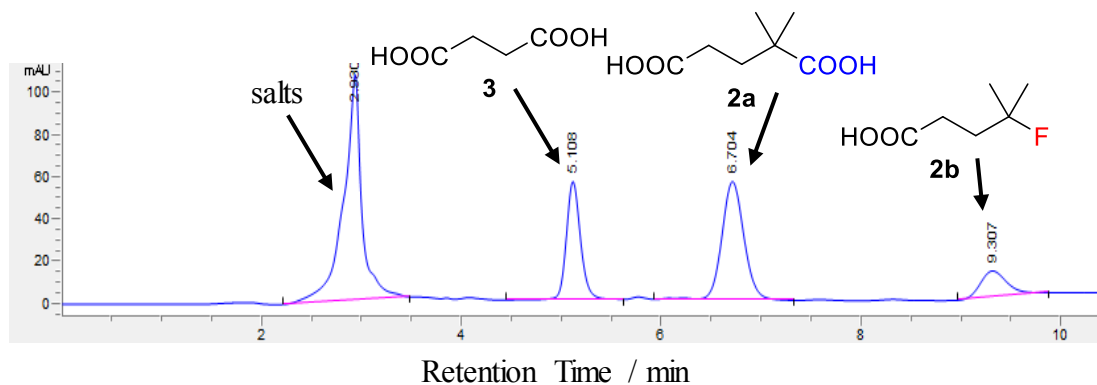
Figure 2.22: HPLC chromatogram for a typical reaction. The observed signals at 5.1, 6.7 and 9.3 min are respectively: succinic acid (**3**), 2,2–dimethylglutaric acid (**2a**) and 4-fluoro-4-methylpentanoic acid (**2b**).

To verify the potential formation of other products, ^{19}F NMR experiments were performed and no other by-product was observed during the reaction time. However, the selectivity (moles of product/initial moles of reagent) of the process was constantly calculated *via* HPLC (using the calibration displayed in Table 2.1), to monitor the formation of by-products eventually indicated by a drop of selectivity.

Every sample was prepared by withdrawing around 250 µl of reaction mixture, subsequently centrifuged to separate the solid catalyst from the reaction solution. 100 µl of reaction solution were then withdrawn and mixed with 500 µl of an aqueous solution of succinic acid (0.6 mM).

2.2.3 Gas Chromatography

Gas chromatography (GC) is a useful analytical technique widely employed to separate and detect different organic molecules present in a mixture (typically crude reactions) through chromatography using gaseous eluents.[22] The basic principle in chromatography, responsible for the separation of the different components of a mixture, is the different interaction between the analytes and a "stationary phase", the column. Unlike HPLC (Section 2.2.2), the application of gas chromatography is restricted only to molecules which possess relatively low boiling point and sufficient thermal stability. In fact, the analyte has to exist in gas phase without decomposing at the temperatures required for the run.
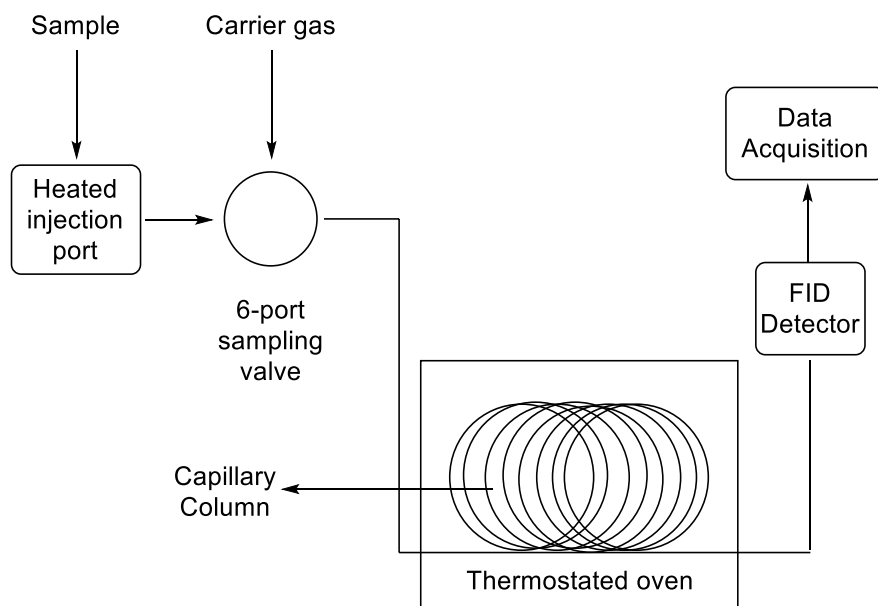
Figure 2.23: Schematic of the gas chromatography setup used throughout the project.

During a typical GC analysis, the sample is first injected into a heated injection port, where the analyte is vaporised by the high temperature of the port, and transported by the mobile phase, an inert gas (typically helium) through the column. GC instruments that are generally found in the laboratories are typically equipped with capillary columns: thin fused-silica capillaries, generally 10 - 100 meters in length and 250 μm of inner diameter, with the stationary phase coated on the inner surface.

Depending from the polarity of the column and the polarity of the different components of the analysing mixtures, the different analytes interact differently with the column *via* H-bonding or dipole-dipole interactions and, depending from the strength of these interactions the analytes are retained for a different amount of time. The length of time required for elution of a given analyte is denoted as retention time. Throughout the analysis, the oven containing the column can also be heated according to a specific heating program, tuning the separation of the different analytes.

The detector employed for this project was a Flame Ionisation Detector, (FID), suitable for the study of products with high amount of carbons with low oxidation. In fact, in the FID the molecules are oxidised with a flame, giving fragmented ions detected through two charged plates with opposite charge. The number of ions detected per time, known as retention time, gives the chromatogram plot. Qualitative analysis via GC is, hence, possible, by simply comparing the retention time of the different peaks present

in the chromatogram with the retention time of the corresponding commercial compounds. Also, considering that the area of the peak observed in the chromatogram for a given compound is directly proportional to the number of the molecules responsible for the given signal, quantification can also be achieved.

In this study, GC was employed to analyse the reaction mixtures of two different reactions: benzylic fluorination of ethylbenzene, and direct cyclooctane fluorination. For both reactions, reagents and by-products were calibrated by injecting known amounts of the corresponding commercial chemicals with a known amount of the analytical standards; biphenyl for ethylbenzene fluorination, and α,α,α-trifluorotoluene for cyclooctane fluorination. The results of these calibrations are given below in Table 2.2 and Table 2.3 for ethylbenzene and cyclooctane reactions respectively. The calibration curves of ethylbenzene, cyclooctane and fluorocyclooctane are shown in Figures 2.24, 2.25 and 2.26 respectively:

Benzylic fluorination	*Retention Time /min*	*Equation*	*R^2*
Ethylbenzene	8.61	y=1.540x	0.9937
1-Fluoro-1-phenylethane	10.18	y=1.540x	N./A.
1-Phenylethanol	13.45	y=1.5051x	0.9990
Acetophenone	12.69	y=1.6126x	0.9998
Styrene	9.88	y=1.4405x	0.9995
Biphenyl	14.83	external standard	

Table 2.2: Calibration results for the reactants involved in ethylbenzene (**1a**) fluorination to give 1-fluoro-1-phenylethane (**1b**) *via* GC analysis using biphenyl as external standard.

Due to the unavailability of pure 1-fluoro-1-phenylethane, the retention time of the product was identified by GC-MS. Subsequently, preliminary NMR and GC quantitative analysis revealed that using the same calibration factor of the reagent, 1.54, for the GC analysis, yielded values within the 5 % of difference amongst the values calculated by GC and NMR. As such, a calibration factor of 1.54 was used to analyse 1-fluoro-1-phenylethane *via* GC analysis. Notably, this approximation was possible only because an FID was used as detector. In fact, FID response for a given compound is related to the number of carbons with low oxidation, present into the compound. Therefore, as the number of carbons is exactly the same for ethylbenzene and 1-fluoro-

1phenylethane, with only one fluorine present into the product, similar response factors were hypothesised for both compounds.
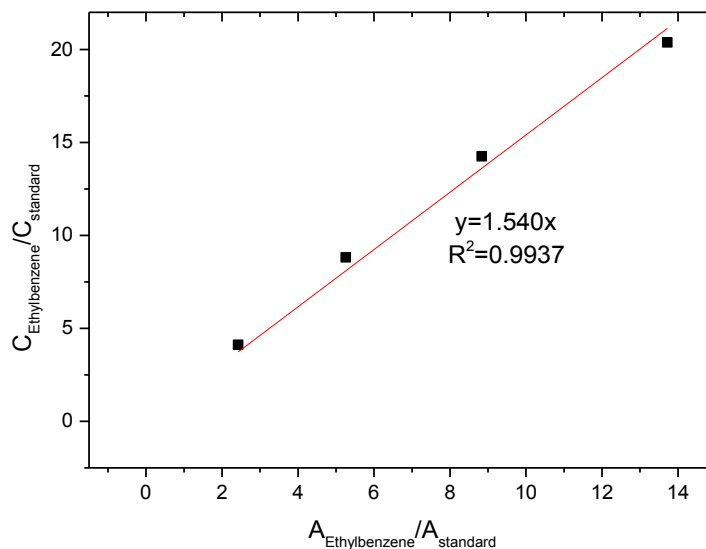

Figure 2.24: Calibration line for ethylbenzene (**1a**) performed with the GC using biphenyl as external standard.

During a typical reaction of ethylbenzene (**1a**) fluorination, samples were regularly withdrawn, centrifuged and diluted four times with a standard solution biphenyl 0.05 M in ethanol. Samples were then filtered again to remove the precipitated Selectfluor® using a syringe microfilter, and transferred in GC vials to be injected in Agilent technologies 7890B GC system equipped with a GC sampler 80 and a Varian capillary column CP-WAX 52-CB (25m x 0.53 mm x 2 µm, #CP7658).

Cyclooctane fluorination	Retention Time /min	Equation	R^2
Cyclooctane	3.56	y=0.8210x	0.9994
Fluorocyclooctane	4.74	y=0.7827x	0.9980
Cyclooctanol	6.98	y=0.8996x	0.9974
Cyclooctanone	6.57	y=0.7036x	0.9976
Cis-cyclooctene	3.27	y=0.7600x	0.9968
Cyclooctene oxide	6.37	y=0.7686x	0.9972
α,α,α-Trifluorotoluene	1.44	Internal standard	

Table 2.3: Calibration results for the reactants involved in cyclooctane fluorination to give fluorocyclooctane *via* GC analysis using α,α,α-trifluorotoluene as internal standard.

Due to the unavailability of pure F-cyclooctane, the retention time of the product was identified by GC-MS. Subsequently, GC-FID analysis and ^{19}F NMR analysis allowed quantification.
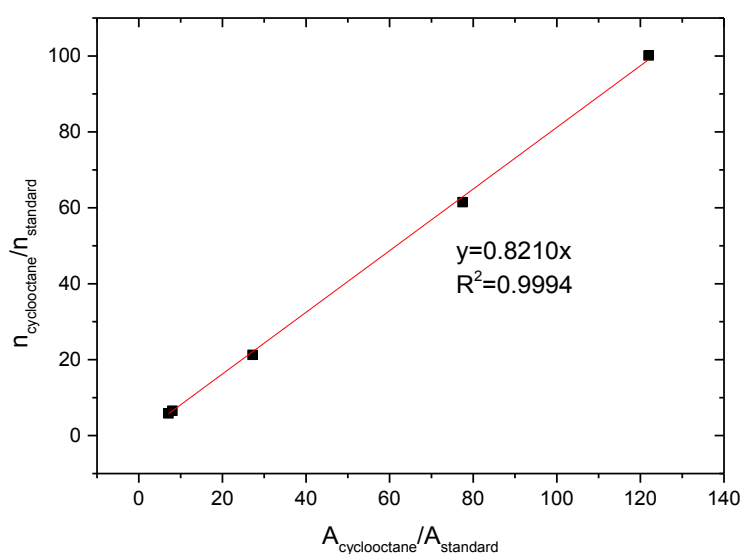
Figure 2.25: Calibration line for cyclooctane performed with the GC using α,α,α-trifluorotoluene as internal standard.
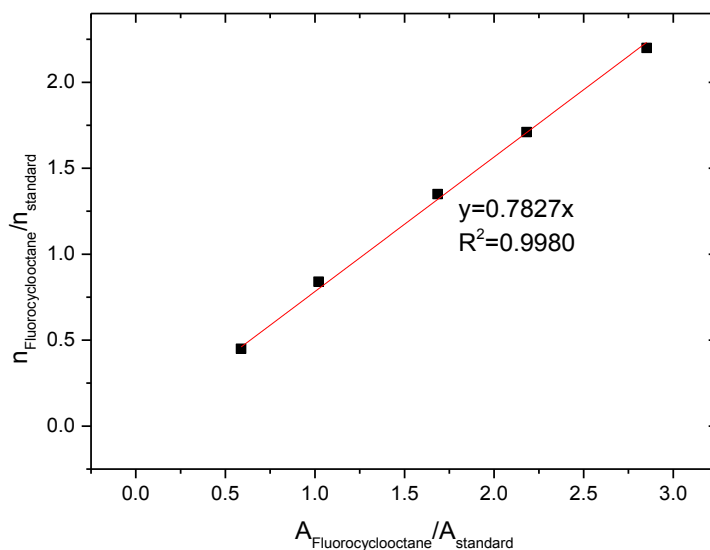
Figure 2.26: Calibration line for fluorocyclooctane performed with the GC using α,α,α-trifluorotoluene as internal standard. The moles of fluorocyclooctane were determined recording ^{19}F NMR experiments for each of the samples (withdrawn at different time over a real cyclooctane fluorination reaction) and integrating the peak of α,α,α-trifluorotoluene (divided by 3, considering 3F contributing to the same peak at δ=-63.72 ppm) and fluorocyclooctane (1F, δ=-159 ppm). The corresponding GC signal for fluorocyclootane at retention time 4.74 min was identified injecting the samples in a GC-MS using the same type of column.

During a typical reaction of cyclooctane fluorination, samples were regularly withdrawn, filtered through a small pad of silica gel and diluted in acetonitrile before injecting them into an Agilent technologies 7820A GC System equipped with an Agilent column HP-5 (30m x 320 μm x 0.25 μm, Agilent 19091J-413). Notably, for cyclooctane fluorinations, 20 μL of α,α,α-trifluorotoluene were used as internal standard for each reaction.

2.3 References

[1] J. W. Niemantsverdriet, *Spectroscopy in Catalysis*, Wiley-VCH, Weinheim, 2007.

[2] W. L. Bragg, *Proc. R. Soc. Lond. A.*, 1914, **89** (613), 468-489.

[3] K. Sakurai, M. Mizusawa, *Anal. Chem.*, 2010, **82** (9), 3519–3522.

[4] P. Atkins J. de Paula. *Atkins' Physical Chemistry for the Life Sciences*. New York: Oxford University Press, 2006.

[5] D. C. Harris, M. D. Bertolucci, *Symmetry and Spectroscopy: an Introduction to Vibrational and Electronic Spectroscopy*. New York: Dover Publications, 1989.

[6] M. A. Henderson, J. M. White, H. Uetsuka, H. Onishi, *J. Am. Chem. Soc.* 2003, **125**, 14974-14975.

[7] W. Paudler, *Nuclear Magnetic Resonance.* Boston: Allyn and Bacon Chemistry Series, 1974.

[8] E. O. Stejskal, J. D. Memory, *High resolution NMR in the Solid State*, 1994.

[9] W. Li, M. Body, C. Legein, D. Dambournet, *J. Sol. State Chem.*, 2017, **246**, 113-118.

[10] W. Li, M. Body, C. Legein, O. J. Borkiewicz, D. Dambournet, *Inorg. Chem.* 2016, **55**, 7182−7187.

[11] W. Li, M. Body, C. Legein, D. Dambournet, *Cryst. Growth Des.* 2016, **16**, 5441−5447.

[12] D. W. Turner, M. I. Al Jobory, *J. Chem. Phys.* 1962, **37**, 3007-3008.

[13] A. M. Ferraria, A. P. Carapeto, A. M. Botelho do Rego, *Vacuum*, 2012, **86** (12), 1988-1991.

[14] G. B. Hoflund, Z. F. Hazos, G. N. Salaita, *Phys. Rev. B*, 2000, **62** (16), 11126-11133.

[15] J. F. Weaver, G. B. Hoflund, *J. Phys. Chem.*, 1994, **98**, 8519-8524.

[16] R. A. Schoonheydt, *Chem. Soc. Rev.* 2010, **39**, 5051-5066.

[17] K. B. Mogensen, K. Kneipp, *J. Phys. Chem. C*, 2014, **118** (48), 28075−28083.

[18] J. L. Falconer, J. A. Schwarz, *Catalysis Review,* 1983, **25**, 141-227.

[19] C. Harris, *Quantitative chemical analysis,* 7th ed., W.H. Freeman, 2005.

[20] W. R. Dolbier, *Guide to Fluorine NMR for Organic Chemists*, 2nd ed., Wiley, 2016.

[21] L. R. Snyder, J. J. Kirkland, J. W. Dolan, *Introduction to Modern Liquid Chromatography,* 3rd Ed., Wiley, 2010.

[22] W. Jennings, *Analytical Gas Chromatography*, Elsevier, 1987.

# *Catalytic Formation of C(sp³)-F Bonds via Decarboxylative Fluorination*

3

3.1 Introduction

In recent years, fluorination reactions, particularly those focusing on C(sp³)-F formations, have gained increased attention due to the wide range of applications found by fluorinated compounds. Indeed, fluorinated compounds are widely employed in a large number of industrial fields as agrochemicals, pharmaceuticals and materials.[1-5] Also, ^{18}F compounds find wide application as tracers for Positron Emission Tomography.[6-8] Nevertheless, whilst there is a high demand for fluorine containing compounds, the synthesis of fluorinated molecules is a difficult task, and, even though several breakthroughs have been achieved, the synthesis of C(sp³)-F bonds *via* catalytic fluorination remains a great challenge.[9-15] Indeed, as reported in Chapter 1, following discovery of safer and easy to handle fluorinating reagents such as F-TEDA (Selectfluor®), NFSI or DAST,[1] many reports have focused on the development of new methodologies to perform fluorination reactions. Amongst them, several recent studies have demonstrated that transition metals such as iron, copper, silver and palladium can react with these fluorinating reagents (*e.g.* Selectfluor® and NFSI), to yield new C(sp³)-F and C(sp²)-F bonds.[16-22] Nevertheless, a remarkable number of these methods require stoichiometric (*i.e.* 100 mol. %) metal loadings, and the development of catalytic reactions possessing high levels of activity remains a major challenge. Moreover, robust and stable heterogeneous catalysts, preferred for several industrial reasons, for selective catalytic fluorination reactions are yet to be reported. The absence of heterogeneous catalysts for selective fluorination reactions, such as selective C(sp³)-F bond formation, is likely due to the challenging conditions generally employed for this type of reaction. Indeed, highly acidic reaction conditions often employed in these processes, representing a challenge for the stability of catalytic materials; the reaction media can, in fact, easily induce restructuring, leaching and thus, deactivation, of solid catalysts.

Nevertheless, despite such challenging conditions, recent reports have shown that $C(sp^3)$-F bond formation can be achieved by homogeneous catalysis through two different strategies: i) from pre-activated compounds, such as carboxylic acids, and ii) *via* direct $C(sp^3)$-H fluorination. As reported in Chapter 1, amongst the different methods to form $C(sp^3)$-F bonds, decarboxylative fluorination of aliphatic carboxylic acids is one of the most explored routes, mainly due to the wide range of readily available, non-toxic substrates. Moreover, the employment of pre-activated substrates implies that milder fluorination conditions are required. Therefore, decarboxylative fluorination has been identified as a suitable model system to begin to investigate the catalytic performance and stability of heterogeneous catalysts for selective $C(sp^3)$-F bond formation.

As reported in Chapter 1, amongst the studies reported to date within the literature, two different strategies for decarboxylative fluorination emerge as the most exploited ones: i) silver mediated decarboxylative fluorination,[23-25] and ii) photocatalytic decarboxylative fluorination.[26] Also, a noteworthy example of decarboxylative fluorination for the synthesis of targeted $C(sp^3)$-^{18}F bond has been reported by Groves group where a Mn-porphyrin, (TMP)Mn(III)Cl (see Chapter 1 for further discussion) was employed. Amongst these strategies, Ag mediated decarboxylative fluorinations catalysed by homogeneous $AgNO_3$, represents a powerful way to selectively synthesise new $C(sp^3)$-F bonds from readily available substrates under mild reaction conditions, without the requirement for additional light sources (Figure 3.1). For such reasons, Ag mediated decarboxylative fluorinations have been identified as a suitable system for the design of robust and efficient heterogeneous catalysts for the synthesis of new $C(sp^3)$-F bonds. Indeed, despite the potential of this process, active, stable and reusable heterogeneous catalysts able to achieve selective $C(sp^3)$-F bond formation with the new and safer electrophilic/radical fluorine sources (such as Selectfluor® and NFSI) are yet to be successfully developed. Moreover, catalyst activity remains generally low, with typical turnover numbers being below 5 even after extended periods *i.e.* 24 h. Accordingly, the development of a highly active, stable and truly heterogeneous catalyst for this process is the focus of this chapter. However, it should be added that although milder reaction conditions are thought to be required for Ag mediated decarboxylative reactions, the system under study still represents a formidable

challenge from a catalyst stability perspective. This is due to the presence of: i) various amounts of carboxylic groups, ii) fluorine sources, and iii) HF (as possible reaction by-product).[27] Each of these species are reported to cause extensive reorganisation, leaching and thus, permanent deactivation, of solid catalysts.[28-30]

$$R-COOH \xrightarrow[\text{Selectfluor®}]{\substack{AgNO_3 \\ (20\ mol.\%)}} R-F$$
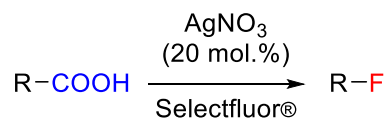
Figure 3.1: Decarboxylative fluorination of aliphatic carboxylic acids to yield new $C(sp^3)$-F bonds.

3.2 Experimental

Although spectroscopic and analytical methods are described in Chapter 2, experimental details of the catalytic reactions presented in this chapter are described herein.

3.2.1 Materials

The following materials were used as received without further purification, unless otherwise stated:

- Titanium oxide, TiO_2 (Degussa, P25, 99.5% trace metal basis, 20 – 30 nm particle size)
- Water, H_2O (HPLC grade, Sigma Aldrich)
- Silver (I) nitrate, $AgNO_3$ (*99.9999%* trace metals basis, Sigma Aldrich)
- Silver (I) oxide, Ag_2O (≥*99.99%* trace metals basis, Sigma Aldrich)
- Silver (I, III) oxide, Ag_2O_2 (Ag_xO, predominantly Ag_2O_2, Sigma Aldrich)
- Poly(vinyl alcohol), PVA (*99%*, Sigma Aldrich)
- Sodium borohydride, $NaBH_4$ (granular, *99.99%* trace metals basis, Sigma Aldrich)
- Selectfluor® fluorinating reagent, F-TEDA (>*95%* in F^+ active, Sigma Aldrich)
- Potassium carbonate, K_2CO_3 (*99.995%* trace metals basis, Sigma Aldrich)
- 2,2-dimethylglutaric acid, DMGA, $HOOCCH_2CH_2C(CH_3)_2COOH$ (≥*98%*, Sigma Aldrich)

- Succinic acid, HOOCCH$_2$CH$_2$COOH (BioXtra, ≥*99.0%*, Sigma Aldrich)

- Pivalic acid, (CH$_3$)$_3$CCO$_2$H (*99%*, Sigma Aldrich)

- 2,2-dimethylvaleric acid, DMVA, CH$_3$CH$_2$CH$_2$C(CH$_3$)$_2$COOH (≥*97.0%*, Sigma Aldrich)

- 2,2-dimethyl-3-phenylpropanoic acid, C$_6$H$_5$CH$_2$C(CH$_3$)$_2$COOH (*95.0 %*, Fluorochem Ltd)

- α,α,α-trifluorotoluene, C$_6$H$_5$CF$_3$ (anhydrous, ≥*99%*, Sigma Aldrich)

- Acetone, (CH$_3$)$_2$CO (Reagent grade, Fisher Scientific)

3.2.2 Definitions

Turnover number (TON) = Moles (product formed)/Moles (metal)

Conversion (*X*) = Moles (substrate consumed)/Moles (initial substrate) × 100

Yield (*Y*) = Moles (product produced)/Moles (initial substrate) × 100

Selectivity (*S*) = Yield/Conversion × 100

3.2.3 Experimental procedures

Details for catalyst preparations and kinetic studies for all the catalysts and reactions presented in this chapter are described below.

3.2.3.1 Synthesis of 1% Ag/TiO$_2$ via sol immobilisation (1Ag/TiO$_2$(SI))

To prepare Ag supported on TiO$_2$ *via* sol immobilization, AgNO$_3$ (0.185 mmol, 20 mg of Ag) was dissolved in 800 mL of deionised water. Under vigorous stirring, 1.3 mL of an aqueous poly(vinyl alcohol), PVA, solution (1 g/10 mL) and 9.26 mL of an aqueous sodium borohydrate, NaBH$_4$, solution (37.8 mg/10 mL) were added to solution, which suddenly became coloured, turning yellow. After 30 minutes, 990 mg of TiO$_2$ was added to the yellow solution, which was then acidified with a few drops of sulphuric acid to achieve a pH of 1. After 2 hours, the solid was filtered and washed with 2 L of H$_2$O and dried at 110 °C for 16 hours. Then, the purple catalyst obtained was ground in a pestle and mortar and calcined at various temperatures, at a ramp rate of 5 (°C min^{-1}) for 3 hours in static air, to oxidise the metallic Ag, resulting in formation of a white powder.

3.2.3.2 Synthesis of physical mixture Ag$_2$O/TiO$_2$ (1Ag$_2$O/TiO$_{2(PM)}$)

Physical mixtures of Ag$_2$O/TiO$_2$ were prepared by grinding Ag$_2$O (0.185 mmol, 20 mg of Ag) and 1.980 g of TiO$_2$ in a mortar for 20 min by hand.

3.2.3.3 Mechanochemical mixture Ag$_2$O/TiO$_2$ (1Ag$_2$O/TiO$_{2(MM)}$)

Mechanochemical mixtures of Ag$_2$O/TiO$_2$ were prepared mixing 21.5 mg of Ag$_2$O (0.185 mmol, 20 mg of Ag) with 1.980 g of TiO$_2$ in a Retsch Ball Mill model MM 400 for 20 min with various frequency (3-30 Hz), using stainless steel 25 mL jars and 10 mm stainless steel balls.

3.2.3.4 General procedure for fluorination reactions

The decarboxylative fluorination of various carboxylic acids was performed at 25 °C using a single neck 10 mL round bottom flask filled with 0.4 mmol of Selectfluor®, 0.0093 mmol of Ag from various Ag-containing catalysts and 0.23 mmol of potassium carbonate, K$_2$CO$_3$. For all reactions, N$_2$ was fluxed into the flask for 5 min, and 4 mL of an aqueous solution of the carboxylic acid 0.05 M was then added into the flask with a syringe. To perform the kinetic studies when 2,2-dimethylglutaric acid (**1a**) was employed as substrate, during the reaction, samples were regularly withdrawn using a syringe, filtered and analysed *via* HPLC, Agilent 1220 Infinity LC System, using a MetaCarb 87H column 250 x 4.6 mm. An aqueous solution of phosphoric acid 0.1 M was used as mobile phase, and succinic acid was used as external standard. The concentrations of 2,2-dimethylglutaric acid and 4-fluoro-4-methylpentanoic acid were calculated by HPLC analysis (see Chapter 2 for further details). When other substrates were used, to measure the product yield, 4 mL of a standard solution of α,α,α-trifluorotoluene in (CH$_3$)$_2$CO was added to the reaction mixture, the sample was centrifuged to remove the solid catalyst and ^{19}F NMR spectra of the solution were obtained. Kinetics for pivalic acid were determined *via* HPLC analysis, due to the high product volatility.

3.2.3.5 Leaching studies

To measure the amount of metal leached from the catalyst into the reaction solution, aliquots of the reaction mixture were withdrawn by a syringe PTFE micropore syringe filter. The filtered solutions were then diluted by a factor of four with water, and were subsequently analysed *via* Microwave Plasma – Atomic Emission Spectroscopy (MP-AES). Calibration details are provided in Chapter 2.

3.2.3.6 Hot filtration experiments

To investigate the potential catalytic activity of metals leached into the reaction solution, hot filtration experiments were performed. These were carried out by removing the solid catalyst from the reaction mixture during the reaction, according to the following procedure:

During the first part of the hot filtration experiment, a classic reaction with the solid catalyst, as described in 3.2.3.4, was initiated. After a given amount of time (typically ≤ 10 min of reaction), the reaction mixture was withdrawn and the solid catalyst was removed with a PTFE syringe microfilter. The filtered reaction mixture was then added into another flask equipped with a magnetic stirrer, previously filled with N_2, and the reaction continued, this time in the absence of the solid catalyst. After an appropriate length of time, the reaction solution was then analysed again to determine any differences in substrate conversion or product yield in the absence of the solid catalyst.

3.2.3.7 Reusability experiments

To study the reusability of the catalyst, the solid catalyst was recovered and reused according to the following procedure:

First, fresh catalyst (100 mg) was used under standard reaction conditions, as described in 3.2.3.4. After completion of the reaction, the solid was separated from the reaction mixture *via* filtration, and washed with de-ionised water. The used catalyst was then dried in an oven at 70 °C for 2 hours. Subsequently, a small portion of the dried solid was tested for catalytic activity under standard reaction conditions (opportunely scaling down all the reagents and solvent to keep reagent/catalyst ratio constant). The large

mass of catalyst was then treated again under standard reaction conditions, and the process repeated until a sufficient number of catalytic cycles were obtained.

3.2.3.8 Catalyst characterisation and analytical details

Powder XRD (pXRD), XPS, UV-Vis, TPDRO, MP-AES, ^{19}F NMR and HPLC were all employed to study the decarboxylative fluorination with heterogeneous Ag catalysts. Experimental details for each of these methods are fully described in Chapter 2. NMR spectra of products and GC calibration lines for (by)products are reported in Chapter 8.

3.3 Results and discussion

3.3.1 Catalytic performances of Ag supported nanoparticles compared with the homogeneous system (AgNO₃)

As described in Chapter 1, decarboxylative fluorination is an efficient way to form $C(sp^3)$-F bonds, converting pre-activated substrates into the desired R-F products. Amongst these reports, homogeneous salts of Ag (*e.g.* AgNO₃) have exhibited optimal levels of performances. Accordingly, the performance of a range of solid Ag-containing materials was explored. Ag supported nanoparticles on titanium dioxide (TiO₂) was identified as being a suitable catalyst for decarboxylative fluorination. Firstly, 1 wt. % Ag nanoparticles supported on TiO₂ were prepared *via* sol immobilisation[31] (henceforth denoted 1AgTiO₂(SI)), and subjected to an heat treatment procedure (calcination in static air at 350°C) in order to oxidise the reduced Ag(0) present on the catalyst after sol immobilisation preparation to Ag (I), reported to be active in the homogeneous AgNO₃ salt. Preliminary kinetic studies were performed with 2,2-dimethylglutaric acid (DMGA, (**1a**)), a useful model substrate possessing both a primary and a tertiary carboxylic group (Figure 3.2). The initial conditions for these experiments were adapted from the optimal conditions reported by Yin *et al.*[24] for AgNO₃, albeit a base, potassium carbonate (K₂CO₃), was also added to the reaction mixture to minimise the acidity of the solution.
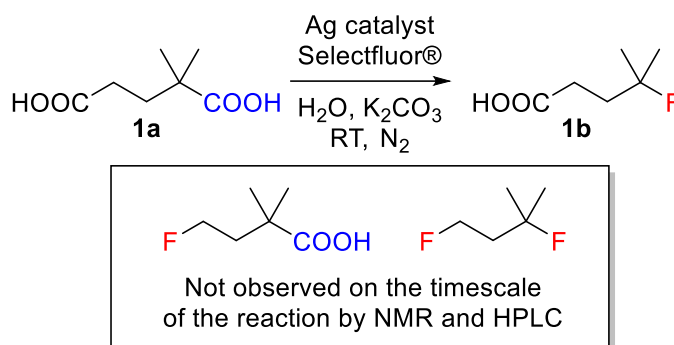
Figure 3.2: Decarboxylative fluorination of DMGA (**1a**) to yield 4-fluoro-4-methylpentanoic acid, (4F4MPA) (**1b**) with Selectfluor® as fluorine donor. Reaction conditions generally used: 0.2 mmol of DMGA (**1a**), 0.4 mmol of Selectfluor®, various amount of Ag from various sources, 4 mL H_2O, 0.2 mmol K_2CO_3, N_2 atmosphere, 25 °C.

Under conditions optimized from homogeneous $AgNO_3$ studies (20 mol. % Ag, 1.0 equivalent K_2CO_3, 25 °C), higher levels of activity were observed with the heterogeneous catalyst calcined at 350 °C (Figure 3.3). 72% of 4-fluoro-4-methylpentanoic acid (4F4MPA, **1b**) was detected after 10 minutes of reaction. It is worth noting that the only product observed over the timescale of the reaction by both NMR and HPLC was 4F4MPA (**1b**), with a selectivity >95 %. The high selectivity towards 4F4MPA (**1b**) confirms the greater reactivity of the tertiary carboxylic group, in accordance with previous studies.[23-25]
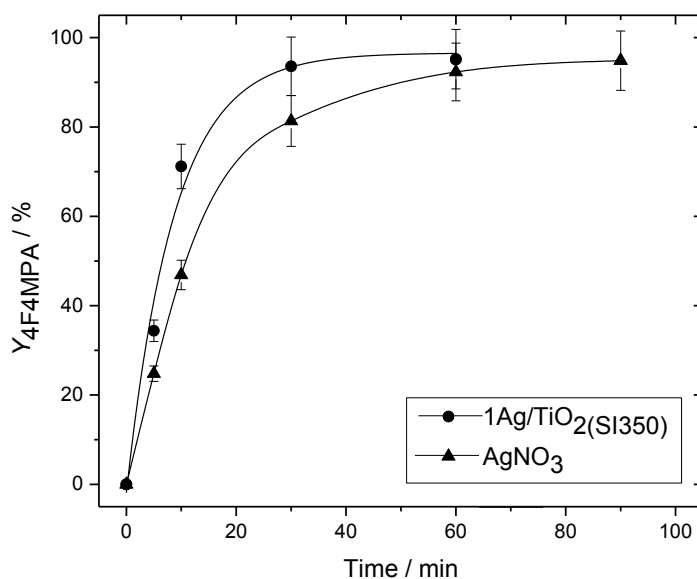
Figure 3.3: Yield of 4F4MPA (**1b**) with time over (circles) 1Ag/TiO2(SI350) and (triangles) AgNO3. Reaction conditions: 0.2 mmol of DMGA (**1a**), 0.4 mmol of Selectfluor®, 0.04 mmol of Ag, 4 mL H2O, 0.2 mmol K2CO3, N2 atmosphere, 25 °C.

To ensure that the reaction operates under a true kinetic regime, *i.e.* to ensure that no mass transport limitation affect the reaction, initial reaction rates, calculated as moles of substrate converted per unit time, were measured at a range of catalyst loadings. Catalyst loadings between 50 and 450 mg, corresponding to 2.3 to 20 mol. % of Ag, relative to the substrate, respectively, were used for these studies. Whilst the system exhibited good kinetic behaviour between 0 - 200 mg loading of 1% Ag/TiO2 prepared via sol immobilisation and calcined at 350 °C (1Ag/TiO2(SI350)) (Figure 3.4) the rate deviated from a linear behaviour above this loading. This indicates that transport limitations are present at the highest catalyst loadings. Accordingly, all further studies were performed with 100 mg of 1Ag/TiO2(SI350), corresponding to 4.64 mol. % Ag, relative to DMGA (**1a**), which represents the best compromise between intrinsic activity and overall performance.
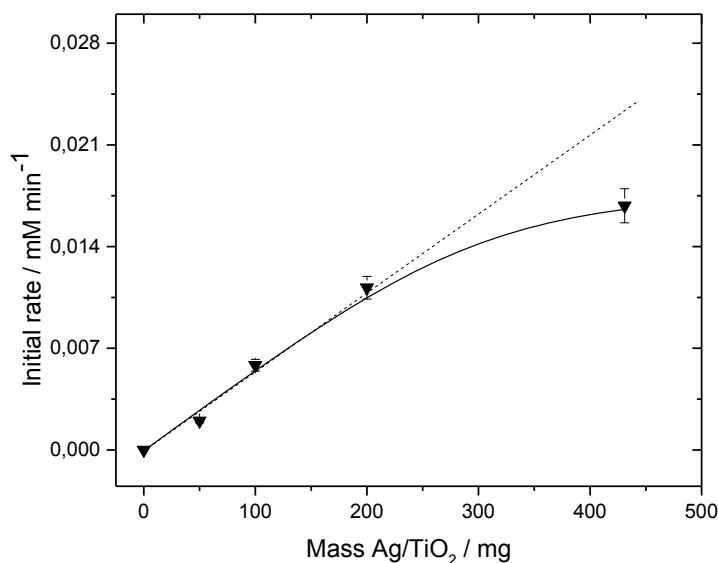
Figure 3.4: Initial rate with different amounts of 1Ag/TiO$_{2(SI350)}$. Reaction conditions: 0.2 mmol of DMGA (**1a**), 0.4 mmol of Selectfluor®, various amount of 1Ag/TiO$_{2(SI350)}$, 4 mL H$_2$O, 0.2 mmol K$_2$CO$_3$, N$_2$ atmosphere, 25 °C.

3.3.2 Stability experiments

As briefly reported in the introduction (3.1), the design of heterogeneous catalysts for fluorination reactions is particularly challenging, mainly due to the highly acidic reaction conditions and the potential presence of traces of hydrofluoric acid (HF), likely to be generated *in situ* by the fluorinating reagent, in the reaction mixture. Such conditions can promote metal leaching and decomposition of the heterogeneous catalyst could be expected. As such, thorough stability studies on 1Ag/TiO$_{2(SI350)}$ were performed. First, an investigation of catalyst stability over reaction time was performed, measuring the amount of active metal (Ag) leached from the catalyst surface into the solution at different reaction times (Figure 3.5). Notably, from an early stage (t ≤ 5 min) of reaction, high amounts of Ag were found in solution, indicating that 11.5% of the Ag previously supported on TiO$_2$ was leached into the solution. Clearly, the leaching of such high quantities of Ag is undesirable from an intensification perspective.
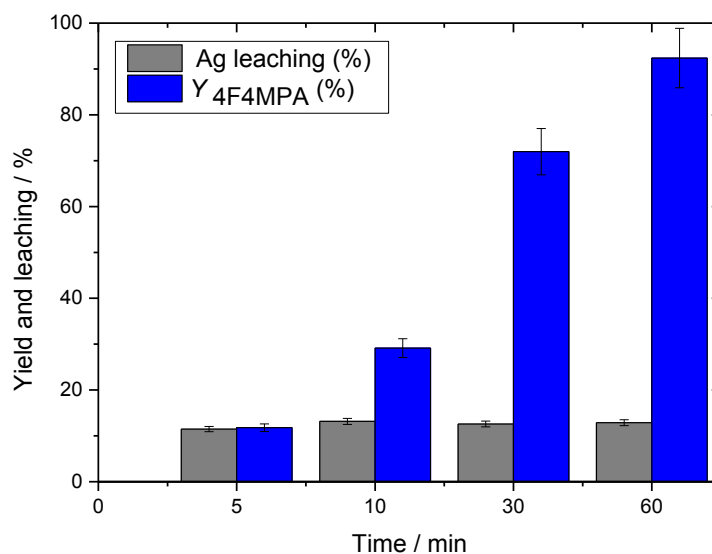
Figure 3.5: Ag leaching (grey bars) and yield of 4F4MPA (**1b**) (blue bars) with time over 1Ag/TiO$_{2(SI350)}$. Reaction conditions: 0.2 mmol of DMGA (**1a**), 0.4 mmol of Selectfluor®, 100 mg of 1Ag/TiO$_{2(SI350)}$ (0.0093 mmol of Ag), 4 mL H$_2$O, 0.2 mmol K$_2$CO$_3$, N$_2$ atmosphere, 25 °C.

3.3.3 Effect of heat treatment

In a first attempt to optimise catalyst stability, the effect of heat treatment on the material was investigated. It is well known that the temperature of catalyst heat treatment can strongly modify metal-support interactions, potentially affecting the stability of the catalyst. Therefore, to optimise the catalyst preparation, an investigation of the stability of 1Ag/TiO$_{2(SI)}$ prior to, and following calcination at different temperatures up to 400 °C, was performed. As shown in Figure 3.6, whilst the highest levels of catalytic performance were observed for the uncalcined material, the lowest levels of stability, *i.e.* highest metal leaching, were also observed. Similar activity was observed for the catalysts calcined between a range of 100 - 400 °C. Despite possessing somewhat lower activity, an increase of stability was obtained by subjecting the materials to calcination at temperatures greater than 200 °C. The catalyst that displayed the best compromise between stability and activity was 1% Ag/TiO$_2$ calcined at 350°C, this catalyst was therefore chosen to further study the effect of the concentration of base.
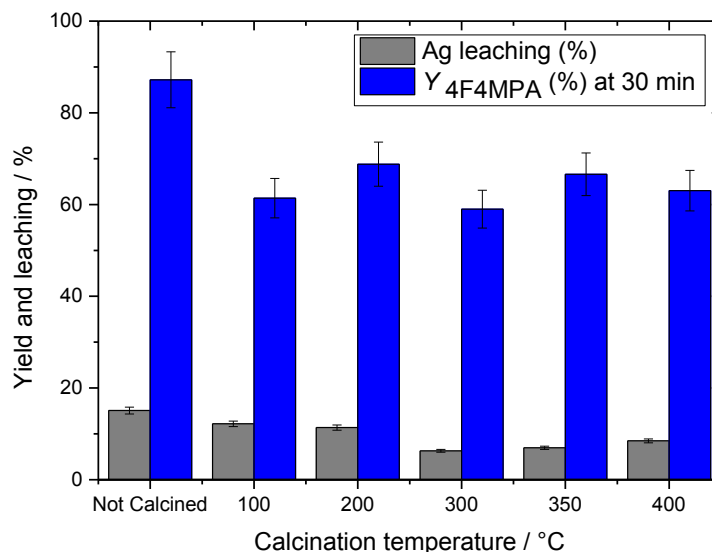
Figure 3.6: Ag leaching (grey bars) at 10 min and yield of 4F4MPA (**1b**) (blue bars) over 1Ag/TiO$_{2(SI350)}$ at 30 min. Reaction conditions: 0.2 mmol of DMGA (**1a**), 0.4 mmol of Selectfluor®, 100 mg of 1Ag/TiO$_{2(SI)}$ calcined at different temperatures (0.0093 mmol of Ag), 4 mL H$_2$O, 0.2 mmol K$_2$CO$_3$, N$_2$ atmosphere, 25 °C.

3.3.4 Effect of base loading

To further optimise the stability of the catalyst, an investigation of the effect of base loading was performed. The addition of a mild base such as, K$_2$CO$_3$ to the reaction mixture could, potentially, strongly affect the stability of the catalyst. This is achieved by potentially reducing the acidity of the reaction mixture and limiting the formation of trace amounts of HF, already described as potential cause of metal leaching. For these reasons, the impact of the loading of base (0 - 2 equivalents) on the stability and catalytic performance of 1Ag/TiO$_{2(SI350)}$ was investigated (Figure 3.7).
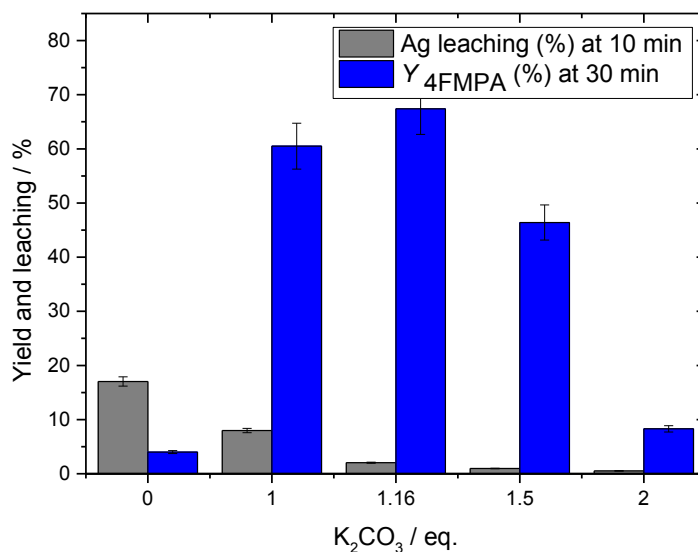
Figure 3.7: Ag leaching (grey bars) at 10min and 4F4MPA (**1b**) yield at 30 minutes with various K₂CO₃ loadings. Reaction conditions: 0.2 mmol of DMGA (**1a**), 0.4 mmol of Selectfluor®, 100 mg of 1Ag/TiO$_{2(SI350)}$ (0.0093 mmol of Ag), 4 mL H$_2$O, various amount of K$_2$CO$_3$ (equivalents respect to substrate), N$_2$ atmosphere, 25°C.

Interestingly, substantially lower activity was found in the absence of K$_2$CO$_3$, with less than 5% conversion detected after 30 minutes. In contrast, the highest catalytic activity was observed in a range 1 - 1.16 equivalents of base, with yields in the range 60 - 70% observed at these base loadings. This observation suggests that the base may play a key role in the reaction mechanism, potentially by deprotonation of the substrate and therefore facilitating its coordination to Ag, resulting in the formation of RCOO-Ag. Although slight excess of K$_2$CO$_3$ leads to an increase of catalytic activity, further increasing the amount of base to 1.5 and 2 equivalents leads to a decrease in activity, with 47 and 10% of yield detected, respectively. This negative effect observed for the two highest base loadings can potentially be due to a coordinating effect of the carbonate group, that might inhibit the formation of the intermediate species RCOO-Ag (see reaction mechanism in Section 1.3.1.1). As well as strongly affecting the catalytic performance of the catalyst, a dramatic effect on the stability of the material was observed by varying the base loading. In fact, whilst 17% of metal leaching was detected in the absence of K$_2$CO$_3$, only 2% of metal leaching was detected when 1.16 equivalents of K$_2$CO$_3$ were employed. Notably, metal leaching lower than 1%, within the instrumental error, was detected when higher amounts of K$_2$CO$_3$ were added to the

reaction mixture, dramatically increasing the stability of the catalyst. In view of this, 1.16 equivalents of K_2CO_3 was identified as the optimal amount of K_2CO_3, providing the best compromise in terms of catalytic activity and stability.

3.3.5 Elucidating homogeneous contributions: hot filtration experiment

To elucidate the impact of the low levels of leached Ag species under optimised reaction conditions, the effect of homogeneous Ag dissolved into solution on the overall reaction rate was investigated. To understand the homogeneous contribution to the reaction rate, a hot filtration experiment at the optimal base loading of 1.16 equivalents was performed (Figure 3.8). This was achieved by removing the solid catalyst from the reactor after 10 minutes of reaction, and subsequently monitoring the change in conversion and yield in the filtered solution. As shown in Figure 3.8, the removal of the solid catalyst from the reaction mixture clearly terminated the catalytic reaction, demonstrating catalysis to be truly heterogeneous, and confirming that eventual traces of Ag in solution did not contribute to the reaction rate. Notably, termination of the reaction also implies that Ag is acting as a true catalyst, and not solely a reaction initiator in the same manner as Cu(I) as observed by Pitts et al.[27] This experiment, therefore, demonstrates Ag-supported TiO_2 to be a truly heterogeneous catalyst for the formation of $C(sp^3)$–F bonds from already activated substrates *via* decarboxylative fluorination with electrophilic fluorine donors.
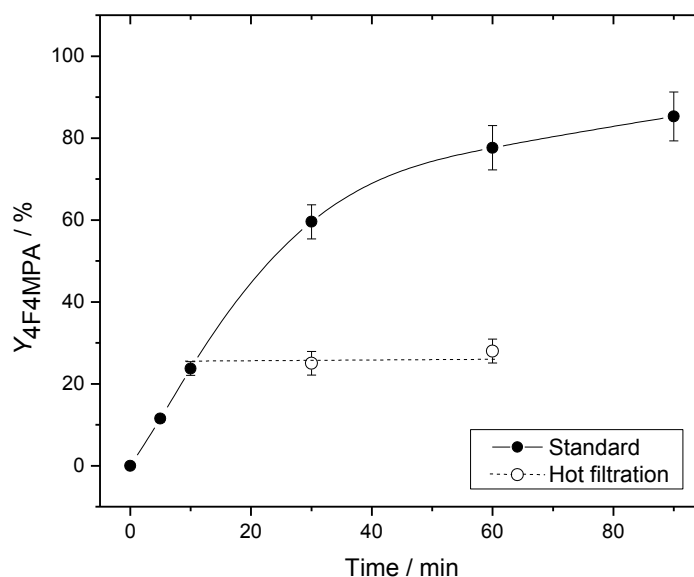
Figure 3.8: Solid line: Yield of 4F4MPA (**1b**) with time without filtering the catalyst. Dashed line, catalytic activity of the supernatant solution following filtration of the catalyst at 10 min. Reaction conditions: 0.2 mmol of DMGA (**1a**), 0.4 mmol of Selectfluor®, 100mg of 1Ag/TiO$_{2(SI350)}$ (0.0093 mmol of Ag), 4 mL H$_2$O, 0.23 mmol K$_2$CO$_3$, N$_2$ atmosphere, 25 °C.

3.3.6 Investigation of Ag(0) interactions with Selectfluor®

According to the work published by Yin *et al.*,[24] decarboxylative fluorination requires cationic Ag species for efficient catalysis to be observed.[23-25] However, sol immobilisation catalysts are known to contain a heterogeneous distribution of cationic and metallic species following heat treatment.[30,32] Thus, to understand the catalytic roles of Ag(0) and Ag(I), and hence providing indications for further catalyst design studies, the interaction between Selectfluor® and Ag(0) was investigated. Accordingly, a colloidal solution of Ag(0) was placed into a UV-Vis cuvette, and the Plasmon resonance[33] of Ag(0) at 400 nm was monitored *in situ* following addition of Selectfluor® and K$_2$CO$_3$ (Figure 3.10). This treatment resulted in the disappearance of the Plasmon peak in < 30 s. Clearly, any residual Ag(0) species in the solid catalysts are immediately oxidised upon interaction with Selectfluor®, and no metallic Ag is present under the reaction conditions.
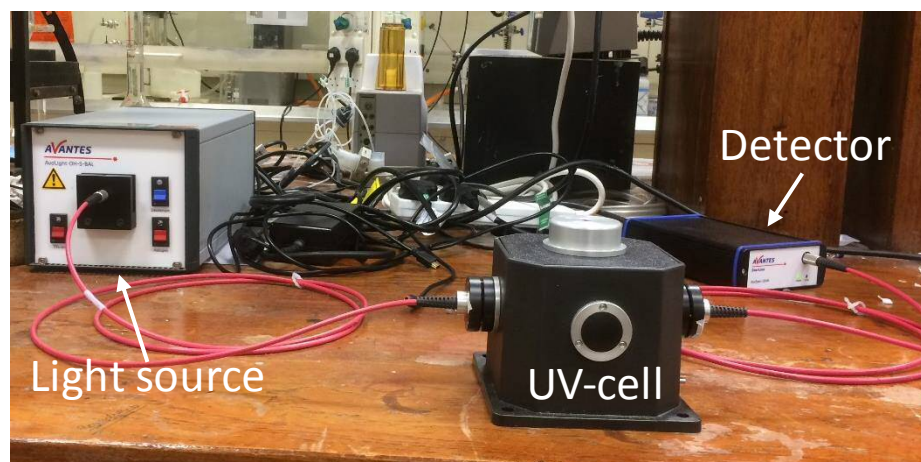
Figure 3.9: UV-Vis spectrometer setup, composed of: i) an AvaLight-DH-S-BAL (Avantes) light source, emitting effectively from 200 to 1000 nm with a power of 90W, connected to a computer able to record UV spectra *via* an *"Avantes"* software, ii) a UV cell containing the UV cuvette in which the analysing sample is placed, and iii) an AvaSpec-2048 (Avantes) detector.
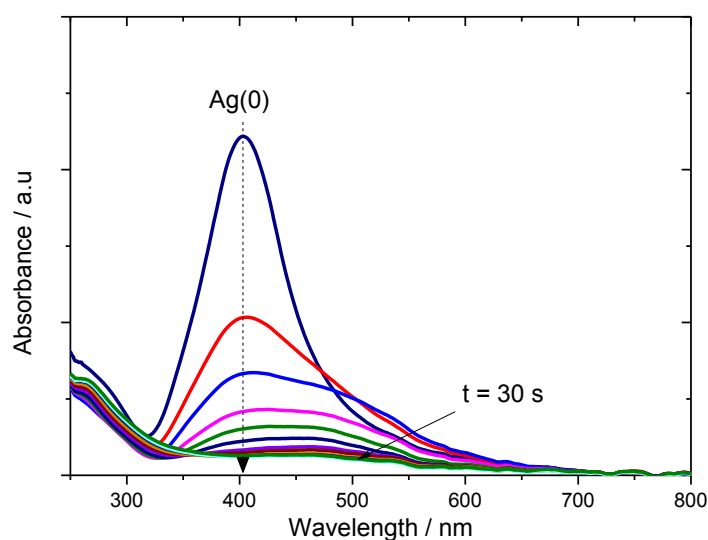
Figure 3.10: UV-Vis spectra of colloidal Ag(0) after addition of Selectfluor® and K_2CO_3.

Given that cationic Ag species are present during reaction, the preparation of materials directly containing Ag(I), and not Ag(0), was targeted. This would remove the requirement of a heat pre-treatment step, and also improve the process selectivity with respect to Selectfluor®. Both of which clearly improve the sustainability of the process. Mechanochemistry, whereby mechanical energy is employed to facilitate chemical processes, has recently received considerable attention as a sustainable and scalable

method of catalyst synthesis.[34-36] In addition, it allows metal oxides such as Ag_2O to be directly employed as solid precursors of the desired active phase.

3.3.7 Catalytic performances of physical mixtures of Ag_2O/TiO_2

In this context, physical mixtures of Ag_2O/TiO_2 were prepared by simple physical grinding of Ag_2O and TiO_2, ($1Ag_2O/TiO_{2(PM)}$), and employed to perform the decarboxylative fluorination. It was found that physically grinding mixtures of Ag_2O and TiO_2 in a pestle and mortar for 20 min led to a catalyst demonstrating almost identical behaviour to heat-treated $1Ag/TiO_{2(SI350)}$, despite the rapidity of the catalyst synthesis and the complete absence of high temperature heat treatments (Figure 3.11).
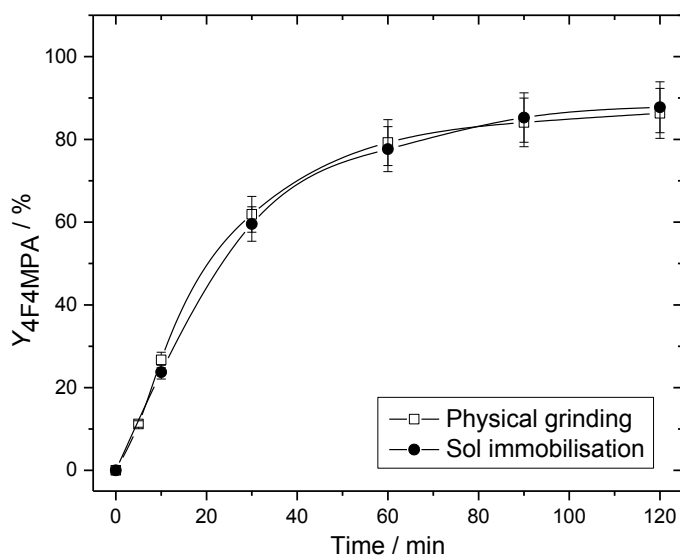
Figure 3.11: Yield of 4F4MPA (**1b**) against time for $1Ag_2O/TiO_{2(PM)}$ (hollow squares) and $1Ag/TiO_{2(SI350)}$ (black circles). Reaction conditions: 0.2 mmol of DMGA (**1a**), 0.4 mmol of Selectfluor®, 100 mg of catalyst (0.0093 mmol of Ag), 4 mL H_2O, 0.23 mmol K_2CO_3, N_2 atmosphere, 25 °C.

3.3.8 Catalytic performances of neat Ag_2O and segregated Ag_2O + TiO_2

To investigate the effect of the support (*i.e.* TiO_2) on the catalytic performances of the material, a control experiment was performed, by simply grinding Ag_2O alone, without the presence of a support, and then performing a reaction in the absence of TiO_2. As

expected, in these conditions, good levels of activity were exhibited by neat Ag_2O, with > 80% of 4F4MPA (**1b**) yield achieved in 1 hour of reaction (Figure 3.12), thus, indicating that the catalytic activity of $1Ag_2O/TiO_{2(PM)}$ and $1Ag_2O/TiO_{2(SI350)}$ arises from the Ag(I) species present on the catalytic surface. However, despite the high activity of Ag_2O, the unsupported oxide is highly unstable, and a high level of Ag leaching was found to occur (up to 17% Ag observed in solution). This result demonstrates that the addition of TiO_2 is essential to the stability of the catalytic material.

Following investigation of the catalytic ability of unsupported Ag_2O, the effect of the interactions between Ag_2O and TiO_2 (*i.e.* the effect of the physical grinding stage), was investigated. Thus, another control experiment, performed in the absence of the grinding stage was undertaken *i.e.* when Ag_2O and TiO_2 were placed into the reaction mixture without prior physical contact, here forth referred to as "segregated Ag_2O and TiO_2. It can be seen in Figure 3.12, that high levels of catalytic activity were exhibited, although extensive Ag leaching occurred, with 25% of Ag found in the reaction solution. This experiment clearly demonstrates that physical interaction between Ag_2O and TiO_2, prior to the reaction, is essential from a catalytic stability perspective. In fact, by simply physically grinding together Ag_2O and TiO_2, remarkably lower levels of leaching occurred, with 2% of metal leaching detected for $1Ag/TiO_{2(PM)}$.
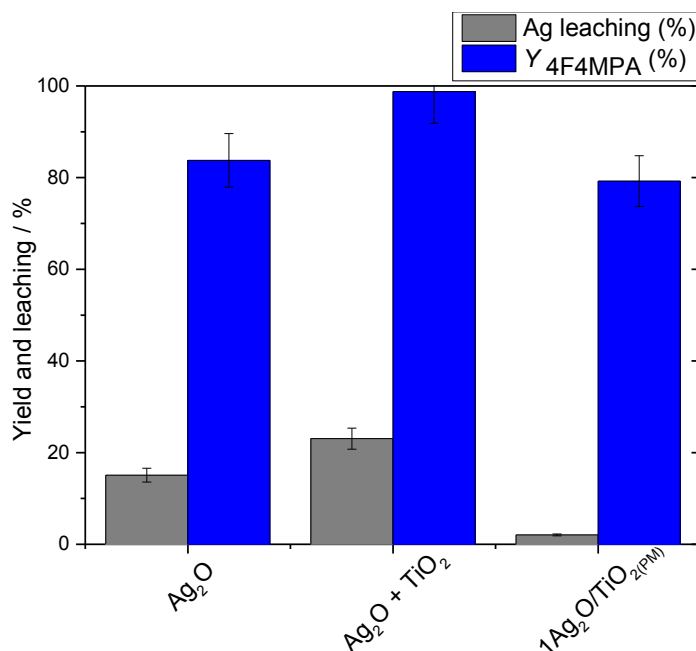
Figure 3.12: Ag leaching (grey bars) at 10 min and yield of 4F4MPA (**1b**) (blue bars) at 60 min over neat Ag_2O, not supported Ag_2O + TiO_2, and $1Ag_2O/TiO_{2(PM)}$. Reaction conditions: 0.2 mmol of DMGA (**1a**), 0.4 mmol of Selectfluor®, 0.0093 mmol of Ag from various sources, 4 mL H_2O, 0.23 mmol K_2CO_3, N_2 atmosphere, 25 °C.

Considering the high metal leaching values observed for unsupported Ag_2O, along with segregated Ag_2O and TiO_2, the homogeneous contribution to the reaction rate for these two materials was then studied *via* hot filtration experiments. Interestingly, and in contrast to $1Ag/TiO_{2(SI350)}$ (Figure 3.8), large homogeneous contributions to the reaction rate were observed (Figures 3.13 and 3.14). This further demonstrates that obtaining strong interaction between Ag_2O and TiO_2 is essential to have truly heterogeneous catalysis.

Homogeneous catalytic activity by Ag_2O for aryl silane and aryl stannate fluorination (*via* transmetallation) has been reported by the Ritter group.[37,38] In fact, in this work, it was proposed that the catalytic activity of Ag_2O arises from homogeneous Ag(I) leached into the solution, thus acting as a pure homogeneous catalyst. According to the reported procedure, Ag_2O can partially be restored (80%) following treatment of the reaction mixture with a basic NaOH solution.
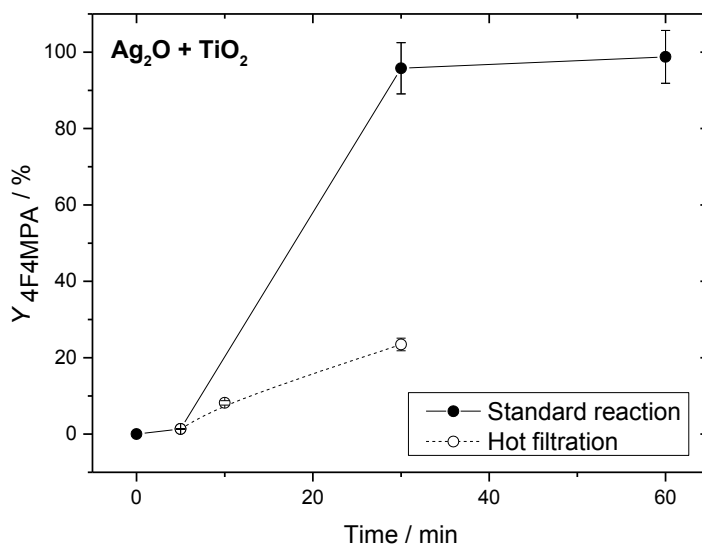
Figure 3.13: Hot filtration experiment using segregated Ag_2O + TiO_2 without milling. Reaction conditions: 0.2 mmol of DMGA (**1a**), 0.4 mmol of Selectfluor®, 100 mg of TiO_2, 0.0093 mmol of Ag, 4 mL H_2O, 0.23 mmol K_2CO_3, N_2 atmosphere, 25 °C.
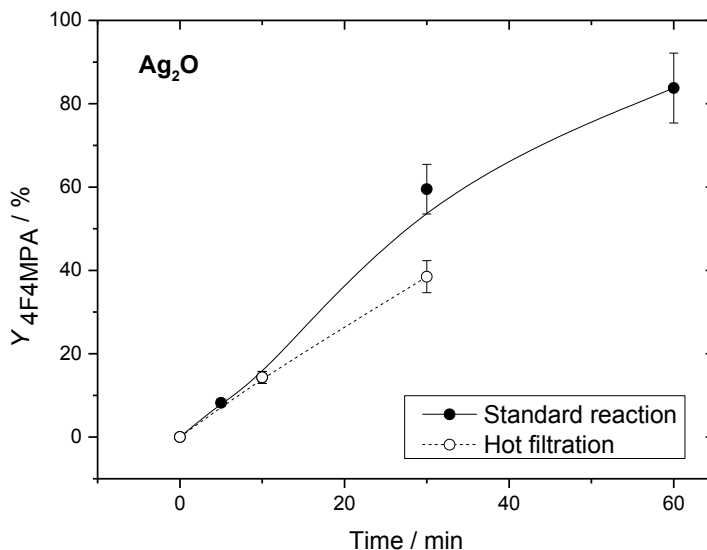
Figure 3.14: Hot filtration experiment using neat Ag_2O. Reaction conditions: 0.2 mmol of DMGA (**1a**), 0.4 mmol of Selectfluor®, 0.0093 mmol of Ag, 4 mL H_2O, 0.23 mmol K_2CO_3, N_2 atmosphere, 25 °C.

To further verify the effect of the physical grinding on the catalytic performance of the material, a hot filtration experiment was performed with $1Ag_2O/TiO_{2(PM)}$. As shown in Figure 3.15, following physical grinding of Ag_2O/TiO_2, a dramatic decrease of the

homogeneous contribution to the reaction rate was achieved, thus further demonstrating that interactions between Ag_2O/TiO_2 are essential to the stability of the material.
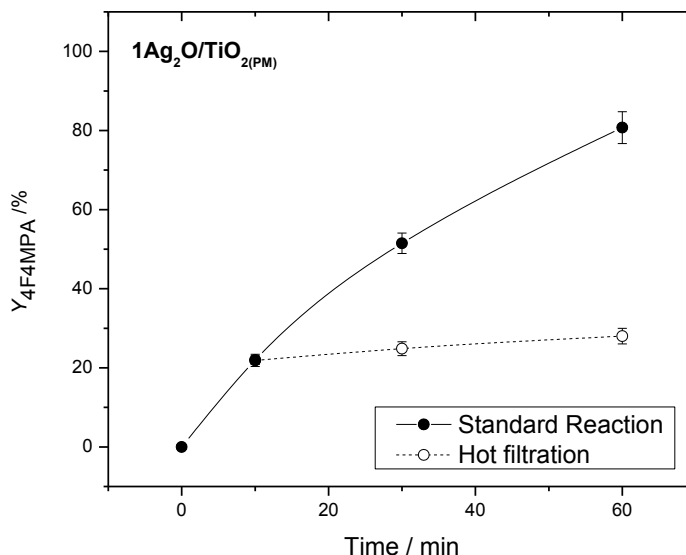
Figure 3.15: Solid line: Yield of 4F4MPA (**1b**) with time without filtering the catalyst. Dashed line, catalytic activity of the supernatant solution following filtration of the catalyst at 10 min. Reaction conditions: 0.2 mmol of **1a**, 0.4 mmol of Selectfluor®, 100 mg of $1Ag_2O/TiO_{2(PM)}$ (0.0093 mmol of Ag), 4 mL H_2O, 0.23 mmol K_2CO_3, N_2 atmosphere, 25 °C.

3.3.9 Reproducibility studies on physical mixture $1Ag_2O/TiO_{2(PM)}$

Despite of the stability demonstrated by $1Ag_2O/TiO_{2(PM)}$, simple mixing between Ag_2O and TiO_2 without heat treatment, may result in a non-homogeneous material, characterised by a heterogeneous distribution of Ag. Thus, to study the reproducibility of this catalyst, the same material ($1Ag_2O/TiO_{2(PM)}$) was prepared several times, and several batches of each material were tested under identical reaction conditions. As shown in Figure 3.16, relatively low reproducibility was found between, and within, the batches, with 4F4MPA (**1b**) yield values ranging from around 30 to 75 % for the same batch under otherwise identical reaction conditions. This indicates that physical mixing of Ag_2O/TiO_2, *via* physical grinding, leads to the preparation of a relatively heterogeneous material, characterised by poor levels of reproducibility.
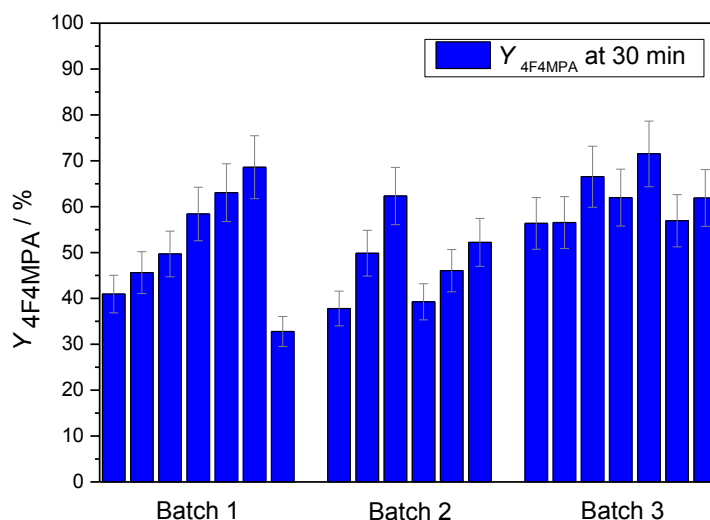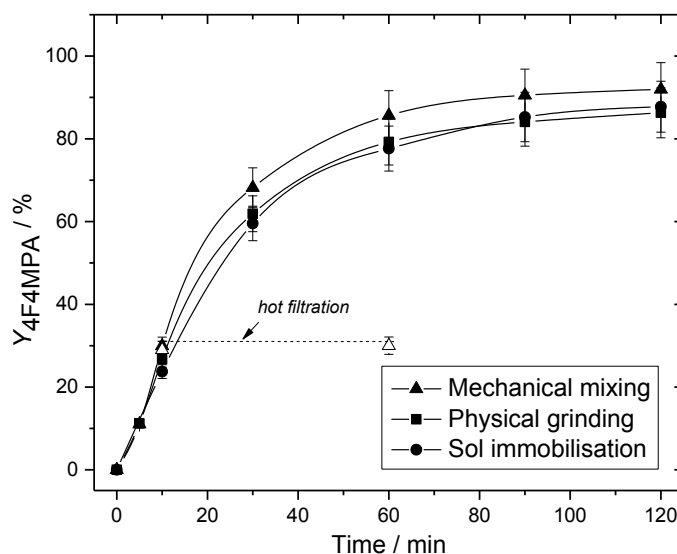
Figure 3.16: Activity and reproducibility of different batches of $1Ag_2O/TiO_{2(PM)}$. Reaction conditions: 0.2 mmol of DMGA (**1a**), 0.4 mmol of Selectfluor®, 100 mg of $1Ag_2O/TiO_{2(PM)}$ (0.0093 mmol of Ag), 4 mL H_2O, 0.23 mmol K_2CO_3, N_2 atmosphere, 30 °C.

## 3.3.10 Catalytic activity and stability of mechanochemical mixtures Ag_2O/TiO_2

In view of the poor reproducibility observed for $1Ag_2O/TiO_{2(PM)}$ and to allow for a greater control of the preparation conditions, alternative methods of mixing Ag_2O/TiO_2 were explored. As such, the optimal catalyst composition was re-made by mechanochemical mixing using a high frequency milling machine. Mixing Ag_2O and TiO_2 for 20 minutes at 15 Hz led to the formation of a catalyst ($1Ag_2O/TiO_{2(MM)}$) that was slightly more active than the sol immobilisation and physical grinding analogues. A hot filtration experiment was also performed for $1Ag_2O/TiO_{2(MM)}$ (dashed line in Figure 3.17), showing that catalysis was totally heterogeneous (Figure 3.17) for this material. Indeed, complete termination of reaction rate was observed after removal of the catalyst at 10 min, with the yield of 4F4MPA (**1b**) not increasing above 30% even after 60 min of reaction.

Figure 3.17: Yield of 4F4MPA (**1b**) against time for $1Ag_2O/TiO_{2(PM)}$ (black squares), $1Ag/TiO_{2(SI350)}$ (black circles) and $1Ag_2O/TiO_{2(MM)}$ (black triangles). Dashed line, catalytic activity of the supernatant solution following filtration of $1Ag_2O/TiO_{2(MM)}$ at 10 min. Reaction conditions: 0.2 mmol of DMGA (**1a**), 0.4 mmol of Selectfluor®, 0.0093 mmol of Ag from various sources, 4 mL H_2O, 0.23 mmol K_2CO_3, N_2 atmosphere, 25 °C.

Reproducibility experiments were subsequently performed on $1Ag_2O/TiO_{2(MM)}$, with different batches prepared and tested several times at identical reaction conditions (Figure 3.18). In this case, excellent reproducibility was observed between, and within, different batches, demonstrating that a good homogeneous dispersion of Ag on the surface support can be achieved *via* mechanochemical milling. Moreover, the material also exhibited good stability over extended periods of time (Figure 3.18), with less than 10% of its initial activity lost even after 6 months in storage.
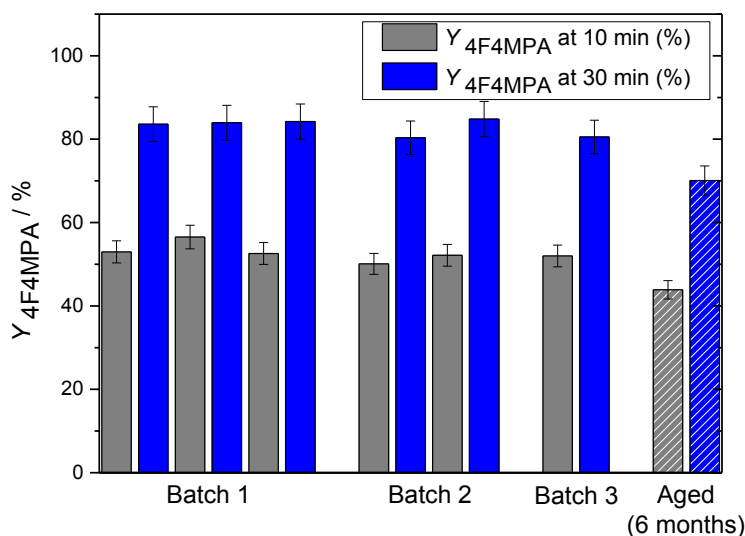
Figure 3.18: Activity and reproducibility of three different batches of 1Ag$_2$O/TiO$_{2(MM)}$. Grey bars conversion at 10 min, blue bars conversion at 30 min. White/grey and blue/grey bars correspond to the activity of 1Ag$_2$O/TiO$_{2(MM)}$ aged for 6 months. Reaction conditions: 0.2 mmol of DMGA (**1a**), 0.4 mmol of Selectfluor®, 100 mg of 1Ag$_2$O/TiO$_{2(MM)}$ (0.0093 mmol of Ag), 4 mL H$_2$O, 0.23 mmol K$_2$CO$_3$, N$_2$ atmosphere, 30°C.

The results obtained from the employment of the high frequency milling machine are promising. Indeed, preparing an effective and reproducible catalyst directly from Ag$_2$O so rapidly, without the presence of solvents or other additives, and in readily available experimental apparatus, presents many synthetic advantages over other catalyst preparation methodologies such as sol immobilisation (Figure 3.19).
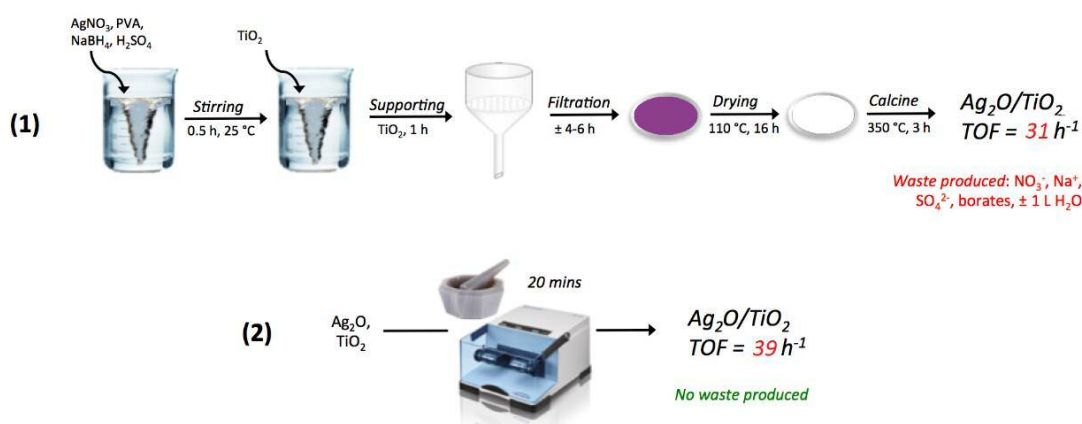
Figure 3.19: Advantages of catalyst preparation *via* mechanochemical mixing over "wet" preparation methodologies *e.g.* sol immobilisation.

To further optimise the preparation of $1Ag_2O/TiO_{2(MM)}$, a series of different milling frequencies, in a range 3-30 Hz, was explored (Figure 3.20). Interestingly, increasing the milling frequency results in a decrease in catalytic activity, with 4F4MPA (**1b**) yield values decreasing from 95% to around 10% over the frequency series. Nevertheless, while metal leaching values below the instrument detectability limits were detected by MP-AES analysis for $1Ag_2O/TiO_{2(MM)}$ milled at frequencies above 15 Hz (15 Hz, 22.5 and 30 Hz), leaching values of 6% and 5% were found for the two lowest frequencies (3 Hz and 7.5 Hz, respectively). This demonstrates that although low frequencies result in active materials, they do not provide suｆcient energy to result in strong metal-support interactions nor synthesise a truly heterogeneous catalyst. Accordingly, all further experiments were performed with $1Ag_2O/TiO_{2(MM)}$ milled at 15 Hz, which exhibited the best compromise of activity and stability.
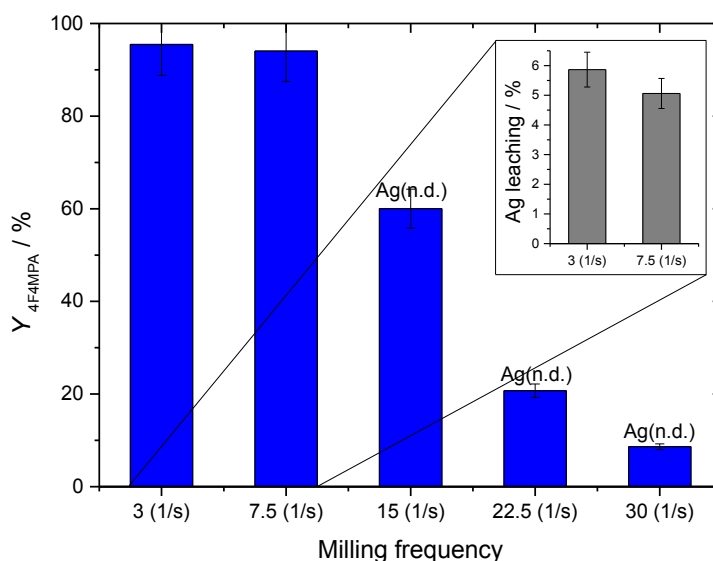

Figure 3.20: 4F4MPA (**1b**) yield (blue bars) at 30 min with 1% Ag_2O/TiO_2 milled at various frequencies. Inset on the top right: Ag leaching values at 10 min for 1% Ag_2O/TiO_2 milled at 3Hz and 7.5 Hz. Reaction conditions: 0.2 mmol of DMGA (**1a**), 0.4 mmol of Selectfluor®, 100 mg of catalyst, 4 mL H_2O, 0.23 mmol K_2CO_3, N_2 atmosphere, 25 °C.

3.3.11 Characterisation of materials

Clearly, major changes in terms of activity and stability of mechanochemically prepared Ag_2O/TiO_2 can be achieved by modifying the preparation protocol. Thus, to fully understand the effect of the different frequencies on the silver speciation and other

properties of the catalyst, detailed characterisation of the mechanochemically-prepared catalysts with Powder X-Ray Diffraction (pXRD), Temperature Programmed Reduction (TPR) and X-ray Photoelectron Spectroscopy (XPS) was performed.

XRD analysis (Figure 3.21) revealed that upon increasing the frequency from 3 to 30 Hz, the reflection at 32.7°, corresponding to Ag_2O, decreases in intensity, and a new reflection at 32.2°, characteristic of AgO, appears. As reported in literature, AgO is known to be a mixture of Ag(III) and Ag(I) oxides[39] and will therefore be denoted as Ag_2O_2. Interestingly, only a weak signal is observed for $1Ag_2O/TiO_{2(MM)}$ milled at 3 Hz, indicating that poor dispersion is likely prevalent at lower frequencies.
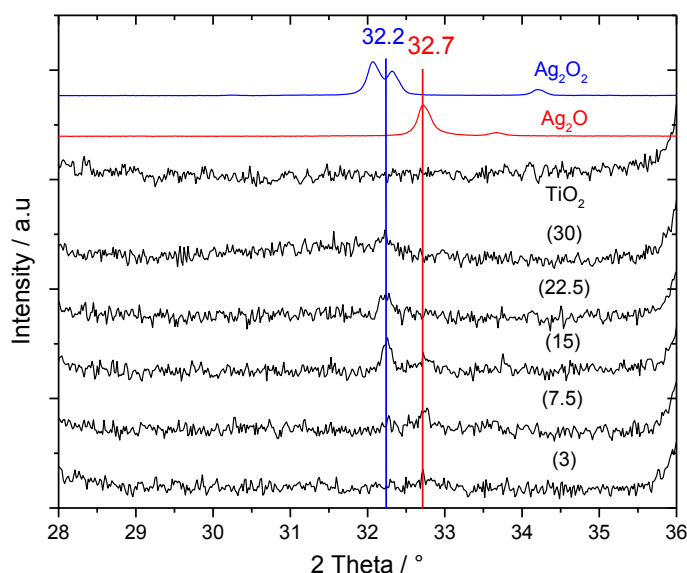
Figure 3.21: Powder X-Ray Diffraction (pXRD) pattern of $1Ag_2O/TiO_{2(MM)}$ prepared at di erent milling frequencies (3–30 Hz).

In agreement with the trend seen in the XRD patterns, the presence of multiple Ag species in the higher frequency materials was also observed *via* TPR analysis (Figure 3.22). The TPR profile of $1Ag_2O/TiO_{2(MM)}$ prepared at 3 Hz clearly shows only one intense reduction step at 240 °C, at temperatures higher than that found for unsupported Ag_2O (196 °C). This reduction peak was attributed to Ag_2O interacting with the support material resulting in a more challenging reduction process. Upon increasing the milling frequency from 3 Hz to 22.5 Hz, the reduction step at 240 °C gradually decreases, whilst a new reduction feature appears around 160 – 170 °C. This new feature overlaps well

with the temperature measured for unsupported Ag_2O_2. The presence of two features in these samples indicates the presence of two distinct Ag species in these materials, in good agreement to the XRD analysis. At the highest frequency, only Ag_2O_2 was observed, indicating full transformation of Ag_2O to Ag_2O_2.
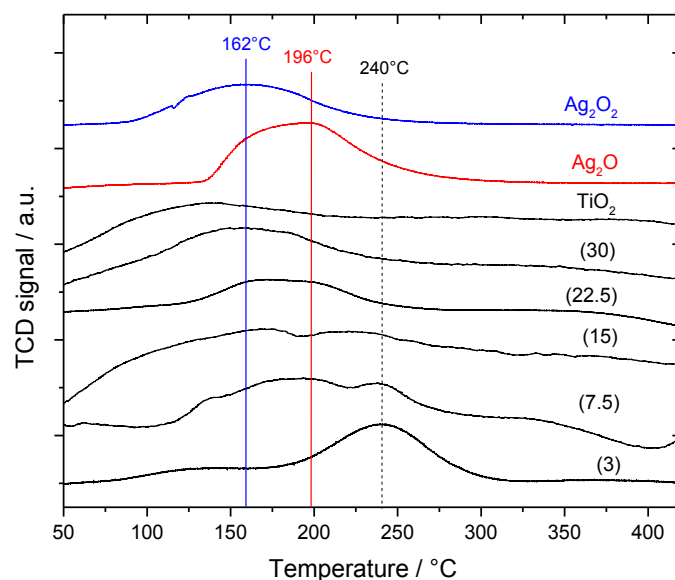
Figure 3.22: Temperature Programmed Reduction (TPR) profiles of $1Ag_2O/TiO_{2(MM)}$ prepared at di erent milling frequencies (3–30 Hz).

To further demonstrate the presence of multiple Ag species on the optimal material, prepared at 15 Hz, XPS analysis was also performed. Although several of the Ag signals overlap, XPS analysis also revealed the presence of multiple Ag species in $1Ag_2O/TiO_{2(MM)}$ milled at 15 Hz (Figure 3.23). The broad asymmetrical peak observed in Figure 3.23 was deconvoluted into two di erent components; firstly, a signal at 368.0 eV, overlapping well with the signal obtained for Ag_2O; secondly, a signal at lower binding energy (367 eV), assigned in the literature to Ag(III).[40-42] Notably, a reversed photoemission shift, with lower binding energy assigned to Ag(III) has previously been observed and reported in the literature, potentially arising from differences in lattice potentials.

Clearly, increasing the energy of the mechanochemical preparation by increasing the milling frequency results in the transformation of Ag_2O to Ag_2O_2, with a distribution of both oxides being observed at the optimal frequency (15 Hz).
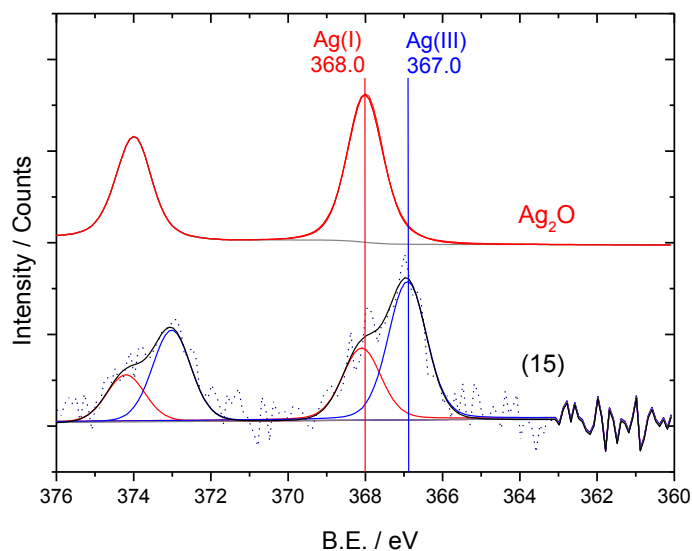
**Figure 3.23:** XPS analysis of standard Ag_2O and $1Ag_2O/TiO_2$(15Hz).

Notably, an increase in Ag_2O_2 formation at higher frequencies appears to correlate with decreased catalytic performance (*vide supra*). To verify that the loss in activity observed upon increasing the milling frequency from 3–15 Hz correlates to the partial conversion of Ag_2O into Ag_2O_2, $1Ag_2O_2/TiO_2$(MM) was prepared by milling Ag_2O_2 with TiO_2 at 15 Hz. To characterise the material, pXRD analysis of $1Ag_2O_2/TiO_2$(MM)) was performed, and, as expected, only one peak at 32.2 ° was observed (blue line in Figure 3.24), demonstrating that only Ag_2O_2 is present in this material.
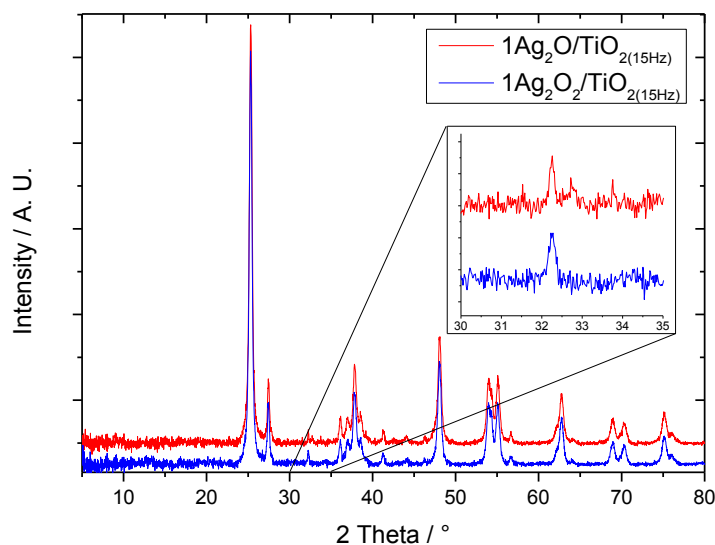
Figure 3.24: Powder X-Ray Diffraction (pXRD) pattern of 1Ag₂O₂/TiO$_{2(15Hz)}$ (blue line) and 1Ag₂O/TiO$_{2(15Hz)}$ (red line).

The catalytic performances of 1Ag₂O₂/TiO$_{2(15Hz)}$ were investigated and compared with those exhibited by the Ag$_2$O analogue. A loss of activity was observed for 1Ag₂O₂/TiO$_{2(MM)}$, in good agreement with the reaction mechanisms hypothesised in literature.[23-25] According to these studies, the key reaction step involves the oxidation of a Ag(I)-OOCR species by Selectfluor®. It is likely that Ag(III) (present as approximately 50% of the Ag content in Ag$_2$O$_2$) cannot be further oxidized, thus stopping the reaction cycle and acting as a trap. According to this, it would be expected that catalysts milled at the highest frequencies (22.5 and 30 Hz) should still display some levels of catalytic performance, given that Ag$_2$O$_2$ contains approximately 50% of Ag(I). The greater than expected decrease in activity for these materials may be due to potential modification of the crystal structure of the TiO$_2$ employed as support, during mechanochemical milling.
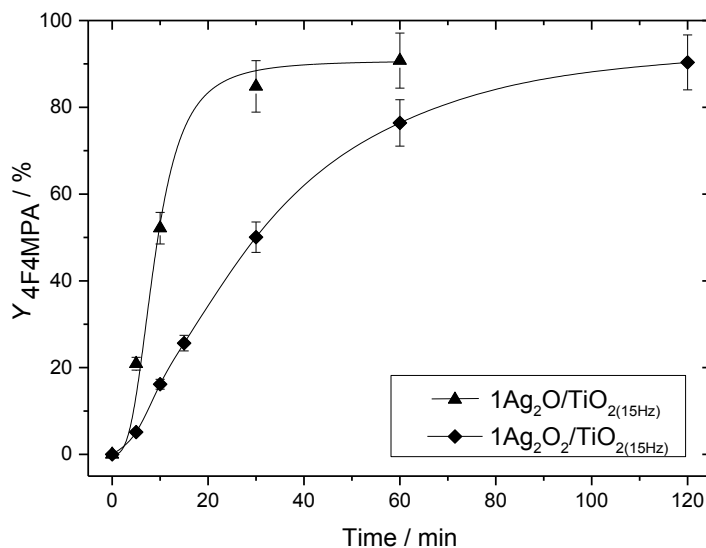
Figure 3.25: Yield of 4F4MPA (**1b**) against time over 1Ag₂O/TiO2(15Hz) (triangles), and 1Ag₂O₂/TiO2(15Hz) (rhombus). Reaction conditions: 0.2 mmol of DMGA (**1a**), 0.4 mmol of Selectfluor®, 100 mg of catalyst (0.0093 mmol of Ag), 4 mL H_2O, 0.23 mmol K_2CO_3, N_2 atmosphere, 30 °C.

Mechanochemical treatments can induce several modifications to the support, indeed, many properties of the material may be altered such as: surface area, crystallinity, and surface structure. Therefore, a more detailed characterisation was performed focusing on the support (TiO₂), *via* Brunauer-Emmett-Teller (BET) and pXRD analysis. Firstly, to analyse the effect of mechanochemical treatments on the surface area, BET analysis of the catalysts was performed, however, no statistically significant changes in the surface area of the catalysts were observed, with specific surface area in a range 55 – 65 m^2/g for all samples (see Appendix for further details of BET analysis). Secondly, the effect of mechanochemical treatments on the crystallinity of the support was investigated; pXRD pattern of the catalysts, 1Ag₂O/TiO2(MM), milled at the different frequencies (3 - 30 Hz) were obtained under identical conditions and compared with untreated, commercial TiO₂ (P25). As reported in Figure 3.26, following mechanochemical milling, both a decrease in peak intensity and broadening of peaks was observed, thus, suggesting that a decrease in crystallinity of TiO₂ occurs. Notably, increasing the milling frequency, a higher loss of crystallinity is observed. Additional data regarding the ratio between the two main phases present in TiO₂, anatase and rutile,

and their approximative crystallite sizes, calculated by employing the Scherrer equation, is reported in Appendix 8.1.
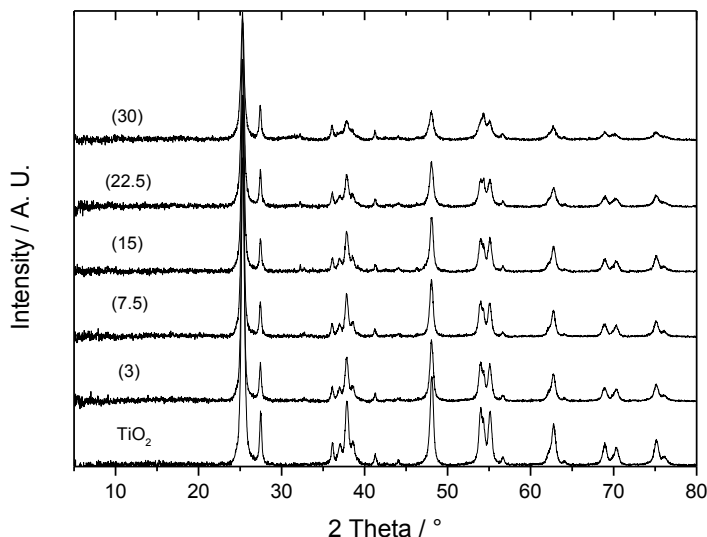
Figure 3.26: Full Powder X-Ray Diffraction (pXRD) pattern of 1Ag₂O/TiO₂(MM) prepared at di erent milling frequencies (3 – 30 Hz).

3.3.12 Versatility of the system

A key parameter for any $C(sp^3)$-F bond forming system is the ability to demonstrate versatility for a wide range of substrates. Accordingly, the general applicability of the heterogeneous catalytic system in terms of $C(sp^3)$-F bond formation was also investigated, using $1Ag_2O/TiO_2(MM)$ milled at 15 Hz as catalyst.

According to the reaction mechanism reported in the literature for Ag catalysed decarboxylative fluorination, the formation of alkyl radicals implies tertiary carboxylic groups to be more reactive than secondary and primary ones. In fact, the higher reactivity of tertiary carboxylic groups over more stable primary ones is demonstrated above when DMGA (**1a**), is used as substrate, as only 4F4MPA (**1b**) is detected under short reaction times. Therefore, to demonstrate the catalytic ability of $1Ag_2O/TiO_2(MM)$ to convert a variety of other substrates, even those with less reactive primary carboxylic groups, a number of other substrates were screened. In all cases, catalytic numbers of turnovers were observed within a short period of time (≤ 1 h). Even when stable primary acids, such as succinic acid (**3a**, Table 3.1 Entry 3) were employed as substrates,

turnover numbers of 4 were still found, demonstrating the catalyst to be able to catalyse substrates that are known to be more difficult to convert. To further demonstrate the system to be active also with other carboxylic acids that do not contain an additional functional group, pivalic acid (**2a**, Table 3.1 Entry 2) and 2,2-dimethyl-valeric acid (**4a**, Table 3.1 Entry 4) were also used as substrates. For both of these cases, catalytic numbers of turnovers were also observed.

Notably, a strong influence of K_2CO_3 loading on both activity and stability of the $1Ag_2O/TiO_{2(MM)}$ was found also for these substrates. In fact, the TON observed for pivalic acid (**2a**) and 2,2-dimethyl-valeric acid (**4a**) increased by greater than two when only 0.58 equivalents of K_2CO_3 were used (Table 3.1 Entries 2 and 4). Clearly, optimising the base to carboxylic acid ratio for each individual substrate is critical for obtaining the highest levels of catalytic performance. Considering the restricted amount of carboxylic acids fully soluble in neat water, substrates that are insoluble in neat water, such as 2,2-dimethyl-3-phenylpropanoic acid (**5a**), were also efficiently converted into the corresponding $C(sp^3)$-F fluorinated compounds (**5b**, Table 3.1 Entry 5). In this case, a water:acetone mixture (1:1) was employed as the solvent, and TONs comparable or better than the those obtained using $AgNO_3$ were observed.[23-25] Interestingly, when **5a** was used as substrate, traces of the corresponding fluorinated product with the fluorine in benzylic position (**5c**) were detected, indicating that benzylic fluorination can also occur under these conditions (for further discussion see Chapter 5).

Table 3.1: Screening of substrates

Entry	Substrate		Product		TON[a]
1	HOOC—...—COOH (gem-dimethyl diacid)	**1a**	HOOC—...—F	**1b**	17.8
					34.2[b]
2	(CH$_3$)$_3$C–COOH	**2a**	(CH$_3$)$_3$C–F	**2b**	9.6[c], 18.6[d]
3	HOOC–CH$_2$–CH$_2$–COOH	**3b**	HOOC–CH$_2$–CH$_2$–F	**3b**	4.0[e]
4	2,2-dimethylpentanoic acid	**4a**	2-fluoro-2-methylpentane	**4b**	3.25[c],
					6.47[c,d]
					(14.6[c,f]
5	2,2-dimethyl-3-phenylpropanoic acid	**5a**	(2-fluoro-2-methyl-1-phenylpropane)	**5b**	3.21[d, g]
			F–CH(Ph)–C(CH$_3$)$_2$–COOH	**5c**	Found in traces[d,g]

Yields calculated with ¹⁹F NMR using ，，-trifluorotoluene and HPLC analysis against authentic standards. Values in parentheses correspond to total TON including reuses. Reaction conditions: 0.2 mmol substrate, 0.4 mmol Selectfluor®, 100 mg 1Ag$_2$O/TiO$_{2(MM)}$, 4 mL H$_2$O, 0.23 mmol K$_2$CO$_3$, N$_2$, 30°C, 0.5 h. [a] TON calculated as "mol (product)/mol (Ag)" for entries 1, 3, 4 and 5, and as "mol (**2a** converted)/mol(Ag)" for entry 2. [b] after two catalytic cycles. [c] reaction time 1 h. [d] 0.115 mmol K$_2$CO$_3$. [e] 200 mg 1Ag$_2$O/TiO$_{2(MM)}$, 50 °C, 2 mL H$_2$O. [f] after five catalytic cycles. [g] 200 mg 1Ag/TiO$_{2(MM)}$, H$_2$O/(CH$_3$)$_2$CO (2mL/2mL), 60°C.

3.3.13 Reusability

A major advantage of a heterogeneous catalyst over a homogeneous analogue is the ease in which it can be recovered and reused. Accordingly, the reusability of 1Ag$_2$O/TiO$_{2(MM)}$ was explored with different substrates. First, a substrate possessing

only one functional group 2,2-dimethyl-valeric acid (DMVA) (**4a**) was used, to exclude any eventual effect of other functional groups (such as additional -COOH groups) on the reusability properties of the material. Also, to ensure that true kinetic comparisons were made, the activity of the catalyst in multiple cycles was examined at low conversion, so that the intrinsic activity and reusability of the catalyst could be correctly examined.[29]

To investigate the reusability properties of the catalyst, after each catalytic cycle the used catalyst was filtered, washed with de-ionised water, dried in an oven at 100°C for 1 hour and then re-used for the subsequent cycle. Notably, reaction conditions were appropriately scaled down according to the amount of recovered catalyst, in order to keep substrate/catalyst ratio constant. As can be seen in Figure 3.27, with DMVA (**4a**) as substrate, good levels of reusability were exhibited by $1Ag_2O/TiO_{2(MM)}$ even without any intermediate treatment being performed.
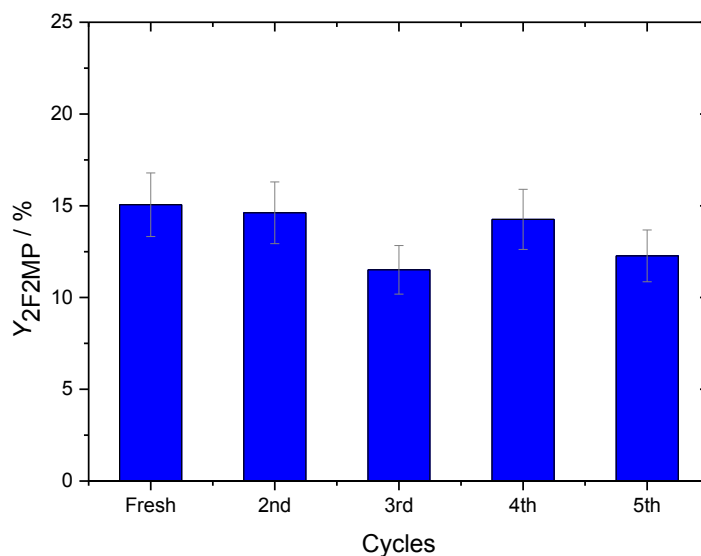
Figure 3.27: Reusability of $1Ag_2O/TiO_{2(MM)}$ at 30 °C with DMVA (**4a**) as substrate. No intermediate treatments were performed.

Substrates containing additional functional groups, such as DMGA (**1a**), unfortunately present a greater challenge. Indeed, in the absence of secondary treatments, a large drop in the catalytic activity of $1Ag_2O/TiO_{2(MM)}$ was observed during the second cycle for DMGA (**1a**) decarboyxlative fluorination (Figure 3.28); from 80% of yield to 10% for the first and the second catalytic cycle, respectively. Nevertheless, despite there being

an initial decrease in activity observed between the first two cycles, no further change in activity was detected between the second and the third catalytic cycles.
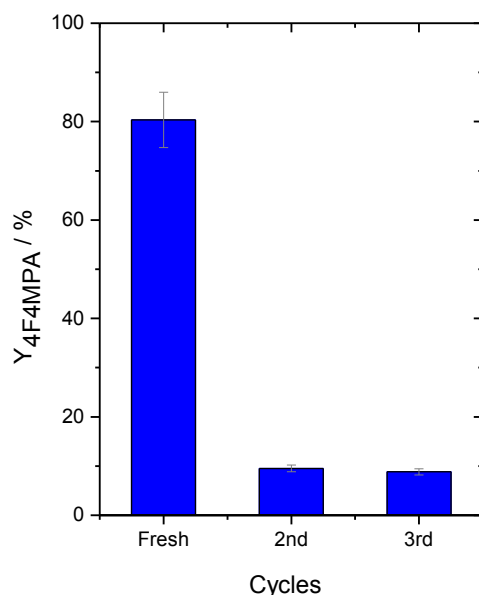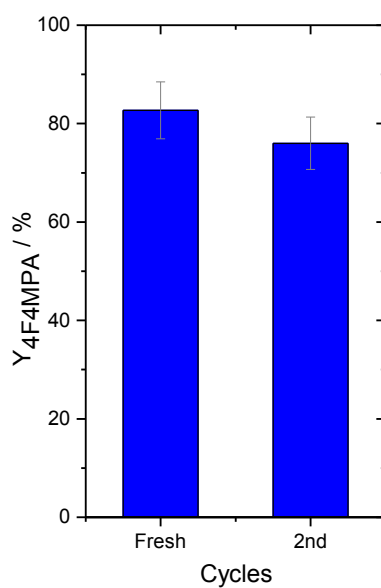

Figure 3.28: Reusability of 1Ag$_2$O/TiO$_{2(MM)}$ at 30 °C with DMGA (**1a**) as substrate. No intermediate treatments were performed.

In contrast, other substrates such as pivalic acid (**2a**), do not result in such decreased levels of performance upon reuse. This can tentatively be attributed to the high volatility of the product (12 °C), likely resulting in its evaporation out of the reaction vessel under typical reaction conditions. In light of this, it was hypothesised that full recovery of activity could be achieved even for difficult substrates, such as DMGA (**1a**), if a suitable regeneration strategy could be designed. As can be seen (Figure 3.29), washing the catalyst in a basic aqueous solution can indeed restore a substantial amount of initial activity. This further indicates that removing adsorbed species presents on the used catalyst is key towards achieving high levels of reusability. Indeed, it can be hypothesised that removal of residual carboxylic species by K$_2$CO$_3$ is responsible for improved reusability, as such species are well established poisons of metal-based catalysts.[28] It is therefore clear that the heterogeneous catalyst possesses promising stability characteristics for intensified operation. For DMVA (**4a**) and DMGA (**1a**),

TONs greater than an order of magnitude higher than previously reported were obtained after 5 and 2 cycles, respectively.
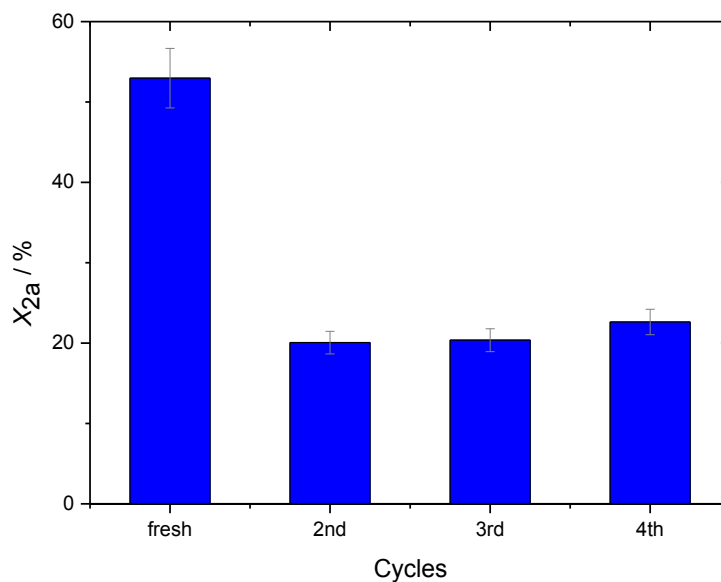

Figure 3.29: Reusability of 1Ag$_2$O/TiO$_{2(MM)}$ at 30 °C with pivalic acid (**2a**) as substrate. No intermediate treatments were performed.

Figure 3.30: Reusability of 1Ag$_2$O/TiO$_{2(MM)}$ at 30 °C with DMGA (**1a**) as substrate. The catalyst was washed in an aqueous K$_2$CO$_3$ solution (0.06 M) for 1 h between cycles.

3.3.14 Effect of heat treatment on 1Ag$_2$O/TiO$_{2(MM)}$

To further optimise the catalyst, and possibly further increase the metal-support interaction, the effect of heat treatments was also investigated on the best mechanochemical mixture catalyst, 1Ag$_2$O/TiO$_{2(MM)}$. Interestingly, following heat treatment in a temperature range 150-550 °C, a similar behaviour to the effect of increasing milling frequency was observed (Figure 3.31). Indeed, calcining the catalyst at higher temperatures resulted in a large drop of catalytic activity, with only 35% and 30% of 4F4MPA (**1b**) yield observed after relatively long reaction time (2 h) for the two catalysts calcined at the highest temperatures, 400 °C and 550 °C, respectively.
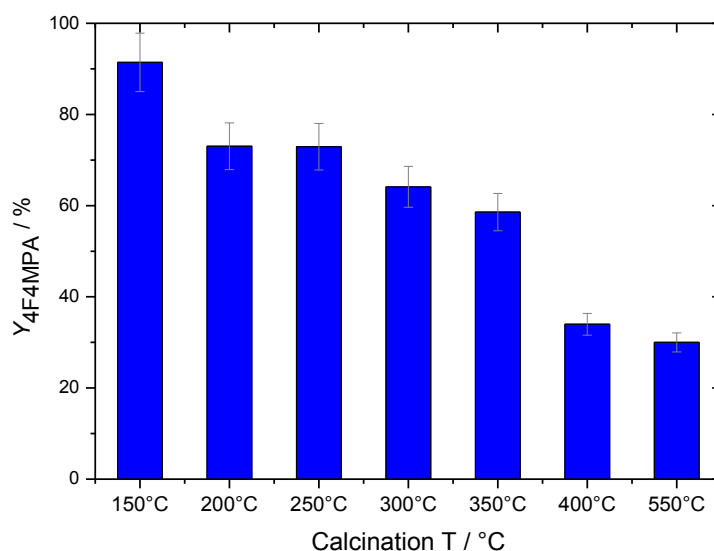

Figure 3.31: 4F4MPA (**1b**) yield (blue bars) at 120 min with 1% Ag$_2$O/TiO$_{2(15Hz)}$ calcined at various temperatures. Reaction conditions: 0.2 mmol of DMGA (**1a**), 0.4 mmol of Selectfluor®, 100 mg of catalyst, 4 mL H$_2$O, 0.23 mmol K$_2$CO$_3$, N$_2$ atmosphere, 25 °C.

To correlate the observed drop in activity following heat treatment with the eventual changing of Ag speciation, pXRD analysis was performed. Analogously to the trend observed increasing milling frequency (Figure 3.21), the reflection at 32.7°, characteristic of pure Ag (I) oxide disappeared after calcination, thus demonstrating that heat treatments can lead to similar modifications of Ag speciation reported for the increasing frequencies.
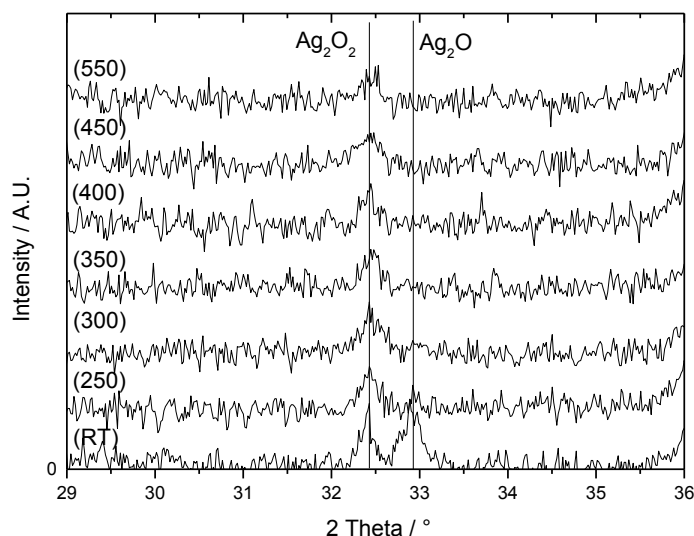
Figure 3.32: Full Powder X-Ray Diffraction (pXRD) pattern of 1Ag₂O/TiO₂₍₁₅Hz₎ calcined at di erent temperatures (RT–550 °C).

Interestingly, however, high photo-sensitivity was also observed for the catalysts calcined at temperatures >150 °C, which displayed a change in colour when exposed to light (Figure 3.33).
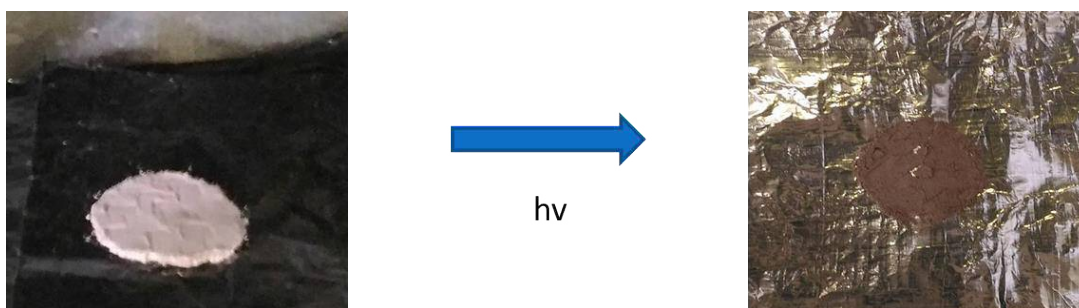
Figure 3.33: Changing in colour observed upon interaction of 1Ag₂O/TiO₂₍₁₅Hz₎ calcined at 550°C, with UV-Vis light. Conditions: 280-760 nm UV-VIS light source, 300 W, irradiation time 1 hour.

To investigate the effect of light on these catalysts, time on line UV-Vis analysis was performed on 1Ag₂O/TiO₂₍₁₅Hz₎ heat treated at 350°C. Notably, following irradiation, a new peak centred around 500 nm appeared in the spectrum (Figure 3.34).
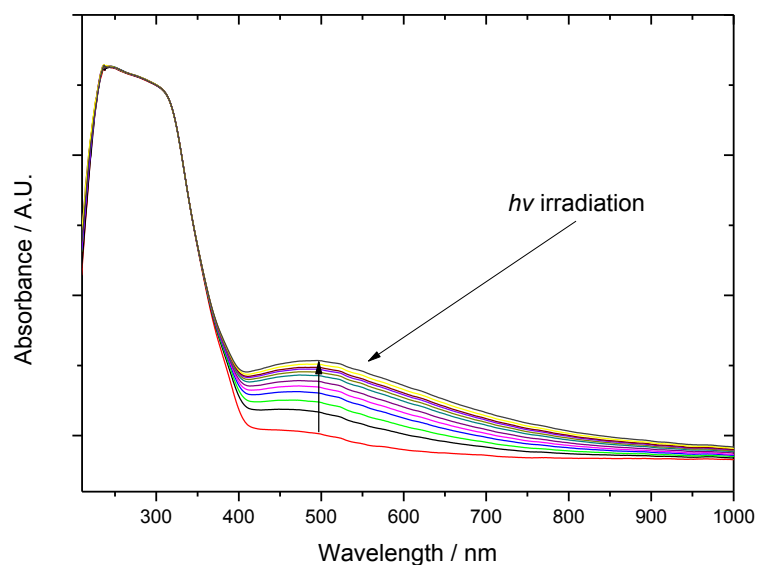
**Figure 3.34:** Time on line UV-vis analysis of 1Ag$_2$O/TiO$_{2(15Hz)}$ calcined at 350 °C. Conditions: 280-760 nm UV-VIS light source, 300 W.

To study the relationship between irradiation and temperature of the heat treatment, UV-Vis spectra of 1Ag$_2$O/TiO$_{2(15Hz)}$ previously heat treated in a range of temperatures (150 - 550 °C) were recorded following 1 hour of *hv* irradiation. As reported in Figure 3.35, no changes were observed for the uncalcined catalyst or the catalyst calcined at 150 °C, even though a new peak centred at around 500 nm appeared in all the other samples. This can potentially be ascribed to the formation of metallic silver particles, under the irradiation from the UV light potentially due to the formation of metallic silver.[43]
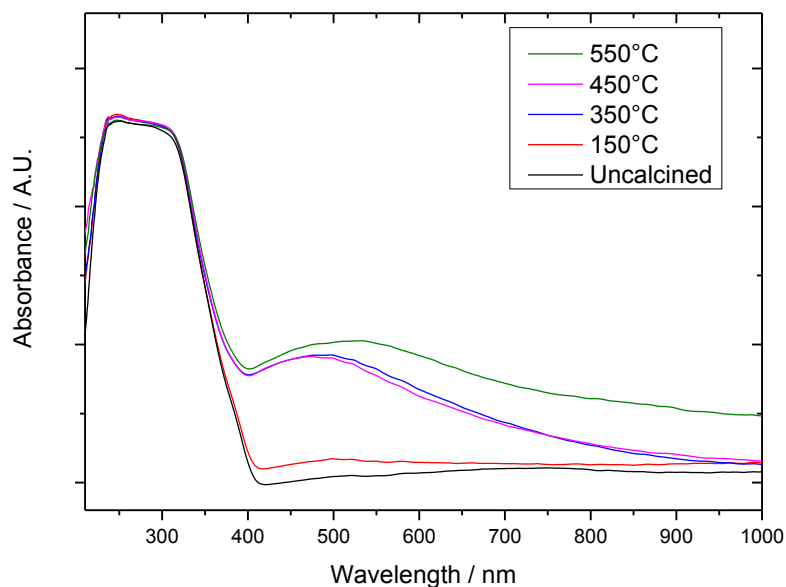
Figure 3.35: UV-VIS analysis of 1Ag$_2$O/TiO$_{2(15Hz)}$ calcined at different temperatures after 1h of irradiation. Conditions: 280-760 nm UV-VIS light source, 300 W.

Considering the photo-sensitivity exhibited from 1Ag$_2$O/TiO$_{2(MM)}$ calcined at the highest temperatures, the potential of these materials as photocatalysts was explored. First, the most promising catalyst with the greatest photosensitivity (1Ag$_2$O/TiO$_{2(MM)}$ calcined at 550 °C) was irradiated with a solar lamp at 300 Watt. The photo-reduced material was then employed to perform DMGA (**1a**) decarboxylative fluorination under photocatalytic conditions (*i.e* irradiating the reaction mixture with a solar light simulator). The results show a high catalytic activity: after only 10 minutes ~ 90% of 4F4MPA (**1b**) yields were reached both in nitrogen atmosphere and air, whilst less than 10% 4F4MPA (**1b**) yield was observed under the same reaction conditions albeit in the absence of catalyst, demonstrating the catalyst to be essential to the reaction. This result is highly promising, indeed, not only does the reaction proceed faster than under dark conditions (*vide supra*), but also high yields of 4F4MPA (**1b**) were obtained in open air.
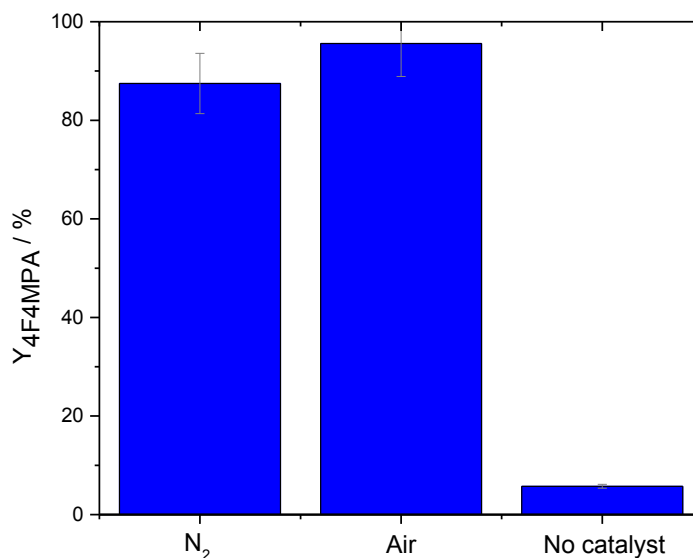
Figure 3.36: 4F4MPA (**1b**) yield at 10 min performed with Ag_2O/TiO_2 (15Hz calcined at 550 °C), using the photoreactor, UVA-UVB lamp at 300 Watt: i) in N_2 atmosphere, ii) in air, and iii) without catalyst. Reaction conditions: 0.2 mmol of DMGA (**1a**), 0.4 mmol of Selectfluor®, 100mg of catalyst (0.0093 mmol of Ag), 4 mL H_2O, 0.23 mmol K_2CO_3, 25 °C.

3.4 Conclusions

Mechanochemically prepared 1 wt. % Ag_2O/TiO_2 was found to be an e cient and reusable heterogeneous catalyst for the decarboxylative fluorination of various carboxylic acids in aqueous media at 25 °C. The mechanochemical mixture presents higher levels of catalytic activity than the state of the art homogeneous catalyst, $AgNO_3$, and is also easily recovered and reused over five successive catalytic cycles. Good general applicability of the catalytic system is also observed, with a variety of primary and tertiary carboxylic acid groups being selectively converted to the desired $C(sp^3)$–F products. Spectroscopic characterisation of the mechanochemically-prepared materials indicates that phase transformations between Ag_2O and Ag_2O_2 can occur, and the optimal milling frequency in terms of activity and stability was found to be 15 Hz.

Heat treatments on 1 wt. % Ag_2O/TiO_2 milled at 15 Hz not only resulted in a decreased catalytic activity, but also in higher levels of photo-sensitivity, when calcination at temperatures higher than 150°C are employed. DMGA (**1a**) decarboxylative fluorination was also performed under photocatalytic conditions and high activity

was observed with 1wt. % Ag$_2$O/TiO$_2$ milled at 15 Hz and subsequently calcined at 550 °C. The substantially improved activity observed under photocatalytic conditions is very promising. As such, a detailed investigation of the catalytic performances of both Ag-based TiO$_2$ and unmodified titanium oxide to perform photocatalytic decarboxylative fluorination is the focus of next chapter. Notably, due to the simultaneous presence of different Ag oxides on the catalytic materials, Ag$_2$O/TiO$_2$ mixtures prepared via mechanochemical milling, will be denoted as Ag$_x$O/TiO$_2$ in the subsequent chapters.

3.5 References

[1] K. Müller, C. Faeh, F. Diederich, *Science,* 2007, **317**, 1881-1886.

[2] D. O'Hagan, *Chem. Soc. Rev.* 2008, **37**, 308-319.

[3] T. Liang, C. N. Neumann, T. Ritter, *Angew. Chem. Int. Ed.* 2013, **52**, 8214-8264.

[4] S. Purser, P. R. Moore, S. Swallow, V. Gouverneur, *Chem. Soc. Rev.* 2008, **37**, 320-330.

[5] T. Ritter, *Nature,* 2010, **466**, 447-448.

[6] P. W. Miller, N. J. Long, R. Vilar, A.D. Gee, *Angew. Chem. Int. Ed.* 2008, **47**, 8998-9033.

[7] R. Littich, P. J. H. Scott, *Angew. Chem. Int. Ed.* 2012, **51**, 1106-1109.

[8] A. F. Brooks, J. J. Topczewski, N. Ichiishi, M. S. Sanford, P. J. H. Scott, *Chem. Sci.* 2014, **5**, 4545-4553.

[9] W. Liu, X. Huang, M. J. Cheng, R. J. Nielsen, W. A. Goddard III, J. T. Groves, *Science,* **2012**, 337, 1322-1325.

[10] M. P. Sibi, Y. Landais, *Angew. Chem. Int. Ed.* 2013, **52**, 3570-3572.

[11] T. Furuya, A. S. Kamlet, T. Ritter, *Nature,* 2011, **473**, 470-477.

[12] W. Liu, J. T. Groves, *Angew. Chem. Int. Ed.* 2013, **52**, 6024-6027.

[13] K. L. Hull, W. Q. Anani, M. S. Sanford, *J. Am. Chem. Soc.* 2006, **128**, 7134-7135.

[14] D. A. Watson, M. Su, G. Teverovskiy, Y. Zhang, J. Garcia-Fortanet, T. Kinzel, S. L. Buchwald, *Science* 2009, **325**, 1661-1664.

[15] A. J. Hickman, M. S. Sanford, *Nature,* 2012, **484**, 177-185.

[16] T. J. Barker, D. L. Boger, *J. Am. Chem. Soc.* 2012, **134**, 13588-13591.

[17] T. Furuya, H. M. Kaiser, T. Ritter, *Angew. Chem. Int. Ed.* 2008, **47**, 5993-5996.

[18] S. Bloom, C. R. Pitts, R. Woltornist, A. Griswold, M. G. Holl, T. Lectka, *Org. Lett.* 2013, **15**, 1722-1724.

[19] P. S. Fier, J. Luo, J. F. Hartwig, *J. Am. Chem. Soc.* 2013, **135**, 2552-2559.

[20] A. R. Mazzotti, M. G. Campbell, P. Tang, J. M. Murphy, T. Ritter, *J. Am. Chem. Soc.* 2013, **135**, 14012-14015.

[21] T. Furuya, A. E. Strom, T. Ritter, *J. Am. Chem. Soc.* 2009, **131**, 1662-1663.

[22] N. Ichiishi, A. F. Brooks, J. J. Topczewski, M. E. Rodnick, M. S. Sanford, P. J. H. Scott, *Org. Lett.* 2014, **16**, 3224–3227.

[23] X. Zhang, *Comput. Theor. Chem.* 2016, **1082**, 11-20.

[24] F. Yin, Z. Wang, Z. Li, C. Li, *J. Am. Chem. Soc.* 2012, **134**, 10401-10404.

[25] N. R. Patel, R. A. Flowers, *J. Org. Chem.* 2015, **80**, 5834-5841.

[26] J. A. Porras, I. N. Mills, W. J. Transue, and S. Bernhard, *J. Am. Chem. Soc.*, 2016, **138** (30), 9460.

[27] C. R. Pitts, S. Bloom, R. Woltornist, D. J. Auvenshine, L. R. Ryzhkov, M. A. Siegler, T. Leckta, *J. Am. Chem. Soc.* 2014, **136**, 9780-9791.

[28] S. Biella, L. Prati, M. Rossi, *J. Catal.* 2002, **206**, 242-247.

[29] I. Sadaba, M. L. Granados, A. Riisager, E. Taarning, *Green. Chem.* 2015, **17**, 4133-4145.

[30] T. Mallat, A. Baiker, *Chem. Rev.* 2004, **104**, 3037-3058.

[31] J. Kennedy, J. Wilm, D. J. Morgan, M. Bowker, L. Lu, C. J. Kiely, P. P. Wells, N. Dimitratos, *Cat. Struct. Reac.* 2015, **1**, 35-43.

[32] R. C. Tiruvalam, J. C. Pritchard, N. Dimitratos, J. A. Lopez-Sanchez, J. K. Edwards, A. F. Carley, G. J. Hutchings, C. J. Kiely, *Faraday Discuss.* 2011, **152**, 63-86.

[33] V. Amendola, O. M. Bakr, F. Stellacci, *Plasmonics*, 2010, **5**, 85-97.

[34] C. Hammond, S. Conrad, I. Hermans, *Angew. Chem. Int. Ed.* 2012, **51**, 11736-11739.

[35] C. Hammond, D. Padovan, A. Al-Nayili, E. K. Gibson, P. P. Wells, N. Dimitratos, *ChemCatChem,* 2015, **7**, 3322-3331.

[36] C. Hammond, J. Straus, M. Righettoni, S. E. Pratsinis, I. Hermans, *ACS Catalysis* 2013, **3**, 321-327.

[37] P. Tang, T. Ritter, *Tetrahedron,* 2011, **67**, 4449-4454.

[38] P. Tang, T. Furuya, T. Ritter, *J. Am. Chem. Soc.* 2010, **132**, 12150-12154.

[39] D. Tudela, *J. Chem. Educ.*, 2008, **85**, 863-865.

[40] G. B. Hoflund, Z. F. Hazos and G. N. Salaita, *Phys. Rev. B*, 2000, **62**, 11126-11133.

[41] A. M. Ferraria, A. P. Carapeto and A. M. Botelho do Rego, *Vacuum*, 2012, **86**, 1988-1991.

[42] J. F. Weaver and G. B. Hoflund, *J. Phys. Chem*., 1994, **98**, 8519-8524.

[43] X. Wang, S. Li, H. Yu, J. Yu, S. Li *Chem. Eur. J.* 2011, **17**, 7777-7780.

Photocatalytic Decarboxylative Fluorination

4

4.1 Introduction

Amongst the most exploited routes to achieve $C(sp^3)$-F bonds from pre-activated substrates, photocatalysed decarboxylative fluorinations represents one of the most exploited routes. Indeed, recent studies have successfully demonstrated the possibility of using light to facilitate fluorination reactions, with Selectfluor® as fluorinating agent and homogeneous species as photocatalysts.[1-4] As discussed in Chapter 1, since 2012, several reports have been focussed on the development of photocatalysed decarboxylative fluorination methodologies. Noteworthy examples are: i) Ru complex photocatalysis reported by Rueda-Becerril *et al*,[1] ii) Ir complex photocatalysis reported by Ventre *et al*.,[2] and, iii) organic dyes photocatalysis reported by Wu *et al*.[3] Moreover, the Bernhard group, has recently reported the synthesis of an Ir complex highly active for both hydrogen generation and photocatalysed fluorination.[4] In contrast to classic decarboxylative fluorination, where TONs $\leq$ 5 were generally observed, TONs > 2 orders of magnitude, up to 1960 (with maximum TOF of 653) have been achieved for systems photocatalysed by Ru and Ir complexes. Indeed, lower TONs, up to 20, were achieved using organic dyes as catalysts. Notably, the formation of $C(sp^3)$-F bonds in such short time and with such high TONs is extremely desirable and is especially important for Positron Emission Tomography (PET) applications, where fast formation of $C(sp^3)$-^{18}F targeted bonds is required.

Therefore, as indicated by the high TONs/TOFs achieved by Ru and Ir complex photocatalysis, combining fluorination processes with photocatalysis (photo-fluorination) represents a powerful and sustainable method of performing fluorinations, and is one of the major breakthroughs achieved in the entire field. However, several major challenges have not yet been solved. For example, the reaction mechanisms that are predominant during such processes have not yet been clearly identified. Also, TONs higher than 20 have been achieved only with the employment of complexes of expensive metals (such as Ru and Ir), prepared *via*

complex synthetic procedures. Moreover, heterogeneous photocatalysts, preferred for industrial reasons, are yet to be employed to form $C(sp^3)$-F bonds using safer electrophilic/radical fluorine source *e.g.* Selectfluor®.

However, in Chapter 3 it has been demonstrated that the design of active and stable heterogeneous catalysts for selective fluorination reactions, especially focusing on selective $C(sp^3)$-F formation, can be achieved. Indeed, mechanochemical mixtures Ag_xO/TiO_2 were found to be active, stable and truly heterogeneous catalysts for decarboxylative fluorination reactions under typical reaction conditions (*i.e.* without the employment of light sources). It was also demonstrated in Chapter 3 that performing the same reaction under photocatalytic conditions, *i.e.* with the employment of a solar simulator light source, led to a dramatic increase in the activity of supported Ag heterogeneous catalysts.

Therefore, a detailed investigation into the photocatalytic performance of the system previously reported in Chapter 3, will be the focus of this chapter. Also, the catalytic performances of the supporting material alone, TiO_2, a non-toxic, stable and readily available well-known photocatalyst, will be investigated. Indeed, removal of the additional noble metal (Ag), from the catalyst, would represent a remarkable achievement for the sustainability and applicability of the system for several reasons, including: i) dramatic material cost reduction, and ii) removal of potential poisoning metals (potentially leached from the catalytic material) from the reaction solution. Moreover, spectroscopic studies in order to elucidate the reaction mechanism involved in photocatalytic decarboxylative fluorinations, will be reported in this chapter.

4.2 Experimental

Although spectroscopic and analytical methods are described in Chapter 2, experimental details of the catalytic reactions presented in this chapter are described in below. In addition, NMR spectra of products are reported in Chapter 8.

4.2.1 Materials

The following materials were used as received without further purification, unless otherwise stated:

- 3-Chloro-2,2-dimethylpropionic acid, $ClCH_2C(CH_3)_2COOH$ (*99 %*, Sigma Aldrich)

- Phenylacetic acid, $C_6H_5CH_2COOH$ (*99 %*, Sigma Aldrich)

- 1-Adamantane carboxylic acid, $C_{11}H_{16}O_2$ (*99 %*, Sigma Aldrich)

- Malonic acid, $CH_2(COOH)_2$ (*ReagentPlus®, 99 %*, Sigma Aldrich)

- Citric acid, $HOC(COOH)(CH_2COOH)_2$ (ACS reagent, *≥99.5%*, Sigma Aldrich)

- Titanium oxide, TiO_2 (Degussa, P25, *99.5%* trace metal basis, 20 – 30 nm particle size)

- Water, H_2O (HPLC grade, Sigma Aldrich)

- Silver (I) nitrate, $AgNO_3$ (*99.9999%* trace metals basis, Sigma Aldrich)

- Silver (I) oxide, Ag_2O (*≥99.99%* trace metals basis, Sigma Aldrich)

- Silver (I, III) oxide, Ag_2O_2 (Ag_xO, predominantly Ag_2O_2, Sigma Aldrich)

- Poly(vinyl alcohol), PVA (*99%*, Sigma Aldrich)

- Sodium borohydride, $NaBH_4$ (granular, *99.99%* trace metals basis, Sigma Aldrich)

- Selectfluor® fluorinating reagent, F-TEDA (*>95%* in F^+ active, Sigma Aldrich)

- Potassium carbonate, K_2CO_3 (*99.995%* trace metals basis, Sigma Aldrich)

- 2,2-dimethylglutaric acid, DMGA, $HOOCCH_2CH_2C(CH_3)_2COOH$ (*≥98%*, Sigma Aldrich)

- Succinic acid, $HOOCCH_2CH_2COOH$ (BioXtra, *≥99.0%*, Sigma Aldrich)

- Pivalic acid, $(CH_3)_3CCO_2H$ (*99%*, Sigma Aldrich)

- 2,2-dimethylvaleric acid, DMVA, $CH_3CH_2CH_2C(CH_3)_2COOH$ (*≥97.0%*, Sigma Aldrich)

- α,α,α-trifluorotoluene, $C_6H_5CF_3$ (anhydrous, *≥99%*, Sigma Aldrich)

- Acetone, $(CH_3)_2CO$ (Reagent grade, Fisher Scientific)

4.2.2 Definitions

Turnover number (TON) = Moles (product formed) / Moles (metal)

Turnover frequency (TOF) = (Moles (product formed) / Moles (metal)) / Time

Conversion (X) = Moles (substrate consumed) / Moles (initial substrate) $\times$ 100

Yield (Y) = Moles (product produced) / Moles (initial substrate) $\times$ 100

Selectivity (S) = Yield / Conversion $\times$ 100

4.2.3 Experimental procedures

Details for catalyst preparations and kinetic studies for all the catalysts and reactions presented in this chapter are described below.

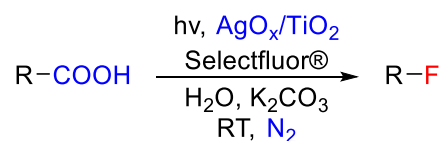## 4.2.3.1 General procedure for photocatalysed decarboxylative fluorination in open air in a photoreactor
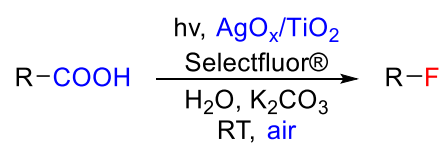
Figure 4.1: Reaction scheme for photocatalysed decarboxylative fluorination in open air.

Photocatalysed decarboxylative fluorinations were generally performed at room temperature using a single neck, 10 mL round bottom flask filled with 0.4 mmol of Selectfluor®, varying amounts of Ag$_x$O/TiO$_2$ (in a range 10-100 mg of Ag$_x$O/TiO$_2$; 0.00093-0.0093 mmol of Ag), and 0.23 mmol of K$_2$CO$_3$. An aqueous solution (4mL) of the carboxylic acid 0.05 M was then added to the flask, and subsequently placed into the photoreactor (PV cell testing solar simulator 16S-300-002, Solar light) and stirred at 700 rpm. Before turning on the power supply of the photoreactor, a small portion of the reaction mixture was withdrawn (t$_0$), and the reaction was initiated by irradiation.

To perform the kinetic studies when 2,2-dimethylglutaric acid (DMGA) (**1a**) was employed as substrate, samples were withdrawn during reaction at regular intervals, filtered and opportunely diluted with a stock solution of succinic acid. Each sample was prepared by adding 100 µL of reaction solution to 500 µL of an aqueous succinic

acid solution (0.6 mM). Samples were then analysed *via* HPLC, Agilent 1220 Infinity LC System, equipped with a MetaCarb 87H column 250 x 4.6 mm, with aqueous phosphoric acid (0.1 M) as mobile phase. The concentration of DMGA (**1a**) and 4-fluoro-4-methylpentanoic acid (4F4MPA) (**1b**) were obtained by previous HPLC calibration with the respective standards.

4.2.3.2 General procedure for photocatalysed decarboxylative fluorination in a photoreactor in N$_2$

$$\text{R-COOH} \xrightarrow[\substack{\text{H}_2\text{O, K}_2\text{CO}_3 \\ \text{RT, N}_2}]{\substack{\text{hv, AgO}_x/\text{TiO}_2 \\ \text{Selectfluor®}}} \text{R-F}$$
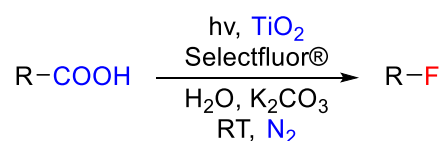
Figure 4.2: Reaction scheme for photocatalysed decarboxylative fluorination in nitrogen.

Inert atmosphere decarboxylative fluorination reactions were performed at room temperature using a single neck 10 mL round bottom flask filled with 0.4 mmol of Selectfluor®, varying amounts of Ag$_x$O/TiO$_2$ (in a range 10-100 mg of Ag$_x$O/TiO$_2$; 0.00093-0.0093 mmol of Ag), and 0.23 mmol of K$_2$CO$_3$. For all reactions, N$_2$ was fluxed into the flask for 5 min, and an aqueous solution (4 mL) of the carboxylic acid (0.05 M) was added into the flask with a syringe. The flask was then placed into the photoreactor (PV cell testing solar simulator 16S-300-002, Solar light) and the reaction was initiated switching on mechanical stirring (700 rpm) and the photoreactor (irradiating the solution).

To perform kinetic studies when DMGA (**1a**) was employed as substrate, during the reaction, samples were regularly withdrawn using a syringe, filtered and opportunely diluted with a stock solution of succinic acid. Each sample was prepared by adding 100 µL of reaction solution to 500 µL of an aqueous succinic acid solution (0.6 mM). Samples were analysed *via* HPLC, Agilent 1220 Infinity LC System, equipped with a MetaCarb 87H column 250 x 4.6 mm, with aqueous phosphoric acid (0.1 M) as mobile phase and succinic acid as external standard. The concentration of DMGA (**1a**) and 4F4MPA (**1b**) were obtained by previous HPLC calibration with the respective standards.

4.2.3.3 General procedure for photocatalysed decarboxylative fluorination with TiO₂ (P25) in N₂

$$R-COOH \xrightarrow[\substack{H_2O, K_2CO_3 \\ RT, N_2}]{\substack{h\nu, TiO_2 \\ Selectfluor®}} R-F$$

Figure 4.3: Reaction scheme for TiO₂ photocatalysed decarboxylative fluorination under nitrogen atmosphere.

TiO₂(P25)-catalysed photocatalytic decarboxylative fluorination under N₂ atmosphere were performed according to the general procedure described in Section 4.2.3.2, albeit with commercial TiO₂ (P25) as catalyst (1.0 mg, 0.0125 mmol).

When substrate **3-9a** (see Table 4.1) were used; to measure the product yield, 4 mL of a standard solution of α,α,α-trifluorotoluene in $(CH_3)_2CO$ was added to the reaction mixture. The sample was centrifuged to remove the solid catalyst, and ^{19}F NMR spectra of the solution was obtained. Kinetics for pivalic acid (**2a**) were determined measuring pivalic acid (**2a**) conversion *via* HPLC analysis, due to the high product volatility.

4.2.3.4 General procedure for photocatalysed decarboxylative fluorination with TiO₂ (P25) in N₂ with monochromatic 365 nm light source

The reaction was performed according to the procedure described in Section 4.2.3.3 of this Chapter (*vide supra*), albeit constantly irradiating the reaction flask with a monochromatic 365 nm light source (Labino® Torch Light UVG2 Spotlight).

4.2.3.5 Hot filtration experiments

To investigate the potential catalytic activity of active metals leached into the reaction solution, hot filtration experiments were performed. These were carried out by removing the solid catalyst from the reaction mixture during the reaction, according to the following procedure:

During the first part of the hot filtration experiment, a classic reaction with the solid catalyst, as described in Section 4.2.3.3 of this Chapter (*vide supra*), was initiated. After a given amount of time (typically ≤ 10 min of reaction), the reaction mixture was withdrawn and the solid catalyst was removed with a PTFE syringe microfilter. The filtered reaction mixture was then added into another flask equipped with a magnetic stirrer, previously filled with N_2, and the reaction continued, this time in the absence of the solid catalyst. After the appropriate length of time, the reaction solution was then analysed again to determine any differences in substrate conversion or product yield in the absence of the solid catalyst.

4.2.3.6 Reusability experiments

In order to investigate reusability, the solid catalyst was recovered and reused according to the following procedure:

Firstly, fresh catalyst (100 mg) was used under standard reaction conditions, as described in Section 4.2.3.3 of this Chapter. After completion of the reaction, the solid was separated from the reaction mixture *via* filtration, and washed with water. The used catalyst was then dried in an oven at 70 °C for 2 hours. Subsequently, a small portion of the dried solid was tested for catalytic activity under standard reaction conditions (opportunely scaling down all the reagents and solvent to keep reagent/catalyst ratio constant). The large mass of catalyst was then treated again under standard reaction conditions, and the process repeated until a sufficient number of catalytic cycles were obtained.

4.2.3.7 DRIFT experiments

Diffuse Reflectance Infra-red Fourier Transform (DRIFT) spectroscopy was performed using a Harrick praying mantis cell. All spectra were recorded on a Bruker Tensor spectrometer over a range of 4000–650 cm^{-1} at a resolution of 4 cm^{-1}. TiO_2-pivalic acid $(CH_3)_3CCOOH)$ interactions were measured on TiO_2, previously dehydrated in the following conditions: 150°C, 2h under flowing N_2, 20 mL min^{-1}). Following the pre-treatment, the cell was cooled at 30°C and a spectrum was recorded. Pivalic acid was adsorbed on the catalyst surface as follows: pivalic acid

was placed into a bubbler connected to the gas line flowing through the DRIFT cell and heated to 130°C. Nitrogen was then fluxed (40 mL min^{-1}) into the bubbler, and the nebulised pivalic acid carried through the DRIFT cell (30°C), adsorbing on TiO$_2$ surface. After 30 min of dosing, the nitrogen flow containing pivalic acid was stopped, and a spectrum was recorded. The chamber was then evacuated under dynamic vacuum (approximately 10^{-4} mbar) followed by heating of the cell up to 600 °C. Spectra were then respectively recorded at 30, 50, 100, 300, 450, 550 and 600°C.

4.2.3.8 DRIFT experiments under UV light irradiation (UV torch at 365 nm)

To study the effect of monochromatic UV light irradiation on the intermediate species formed upon interaction between TiO$_2$ and pivalic acid, a DRIFT experiment was carried out following the protocol described in Section 4.2.3.7 of this Chapter, but, instead of heating the cell up to 600 °C, the cell was maintained at 30 °C and a monochromatic UV light with 365 nm was irradiated through the window of the cell directly onto the sample. A Labino® Torch Light UVG2 Spotlight was employed to irradiate the cell for 2 hours.

Notably, a "blank" test to establish the stability of the intermediate species formed upon interaction between TiO$_2$ and pivalic acid, was performed by repeating this experiment but without irradiation of the sample with the UV light.

4.2.3.9 Catalyst characterisation and analytical details

Powder, XPS, MAS NMR, ^{19}F NMR and HPLC were all employed to study the photo-decarboxylative fluorination with heterogeneous Ag catalysts and with TiO$_2$. Experimental details for each of these methods are fully described in Chapter 2. NMR Spectra of products are reported in Chapter 8.

4.3 Results and discussion

4.3.1 Photocatalysed decarboxylative fluorination with Ag_xO/TiO_2

As reported in Chapter 3, 1% Ag-containing mechanochemical mixtures between Ag_2O and TiO_2 milled at 15 Hz, $1Ag_2O/TiO_{2(15Hz)}$, was found to become sensitive to light following heat treatment at temperatures > 150 °C. Since $1Ag_2O/TiO_{2(15Hz)}$ was found to become light sensitive after calcination, a variety of heat treatments were explored to optimise its light sensitivity, the range of calcination temperatures used was 150 - 550 °C (see Chapter 3 for further information). Amongst the different materials, $1Ag_2O/TiO_{2(15Hz)}$ calcined at 550 °C ($1Ag_2O/TiO_{2(15Hz,550)}$) was identified as the most light sensitive material. $1Ag_2O/TiO_{2(15Hz,550)}$ was also found to be an active catalyst for 2,2-dimethylglutaric acid (DMGA, **1a**) decarboxylative fluorination under light irradiation (see Chapter 3 for further information); with yields > 90% of 4-fluoro-4-methylpentanoic acid (4F4MPA, **1b**) detected after 10 minutes of reaction in open air.

To investigate the influence of the heat treatment on the photocatalytic performance of $1Ag_2O/TiO_{2(15Hz)}$, both the uncalcined catalyst and the catalyst calcined at 550 °C, were tested under the same reaction conditions, *i.e.* irradiating the reaction mixture with a full spectrum solar light simulator lamp at 300 W.
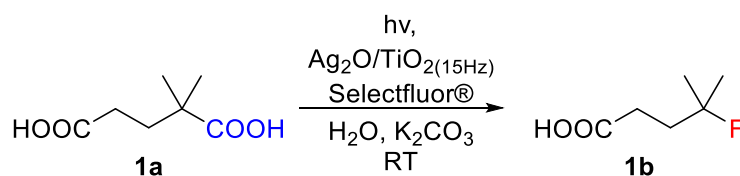
Figure 4.4: Decarboxylative fluorination of DMGA (**1a**) to yield 4F4MPA (**1b**) with Selectfluor® as fluorine donor.
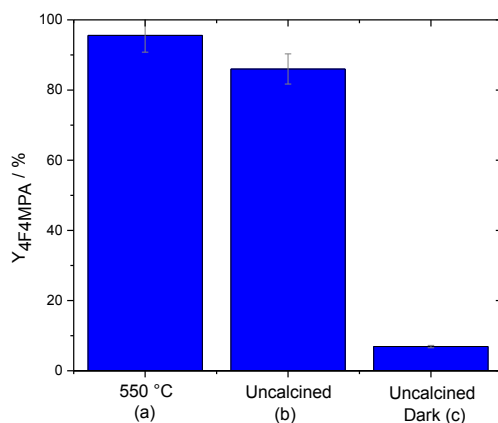
Figure 4.5: yield of 4F4MPA (**1b**) at 10 min performed with: a) $1Ag_2O/TiO_{2(15Hz)}$ calcined at 550 °C, and uncalcined $1Ag_2O/TiO_{2(15Hz)}$ b) under light irradiation and c) in dark conditions. Reaction conditions: 0.2 mmol of DMGA (**1a**), 0.4 mmol of Selectfluor®, 100 mg of catalyst (0.0093 mmol of Ag), 4 mL H_2O, 0.23 mmol K_2CO_3, 25 °C, open air. Full spectrum solar light simulator lamp at 300 W was used to irradiate the reaction mixture.

As can be seen in Figure 4.5, both materials, calcined and uncalcined, show good activity for photocatalytic DMGA (**1a**) decarboxylative fluorination. Indeed, over 85% yield of 4F4MPA (**1b**) was obtained after 10 min of reaction in open air; 95 % and 86 % of yield detected for $1Ag_2O/TiO_{2(15Hz,550)}$ and $1Ag_2O/TiO_{2(15Hz)}$, respectively.

Considering the excellent catalytic performances displayed also by uncalcined $1Ag_2O/TiO_{2(15Hz)}$, thus demonstrating that heat treatments of the material are not essential to the enhanced activity observed under light irradiation (going from dark to light conditions), the following experiments will therefore focus on the investigation of the catalytic performances of the uncalcined catalysts under light irradiation. In fact, the removal of additional, energy consuming heat treatments during the synthesis of a heterogeneous catalyst makes it more suitable for eventual industrial applications.

Notably, to ensure the enhancement of activity can be attributed to the effect of light irradiation, a control experiment in the absence of light (*i.e.* under dark conditions) was also performed, using the uncalcined material, $1Ag_2O/TiO_{2(15Hz)}$. Under these conditions (Figure 4.5), poor activity was observed with only 7% yield of 4F4MPA (**1b**) detected. The dramatic drop in activity observed under dark conditions (*i.e.* in the absence of light) further confirms that light irradiation is essential for the increased

catalytic activity that has been observed. This effect could potentially be due to the interactions between the light and the Ag species present on the catalyst surface. In fact, light irradiation can promote changes of the oxidation state of Ag, affecting the rate of the reaction.

Therefore, in order to investigate the interactions between light and Ag, before optimising reaction conditions, the activity of pure Ag (I) oxide and pure Ag (I, III) oxide, present in some extent in $1Ag_2O/TiO_{2(15Hz)}$ (*vide supra*, Chapter 3), was investigated. Notably, the same number of moles of Ag (0.0093 mmol) used in the previous experiments were employed to correctly compare the activity of supported and unsupported Ag.
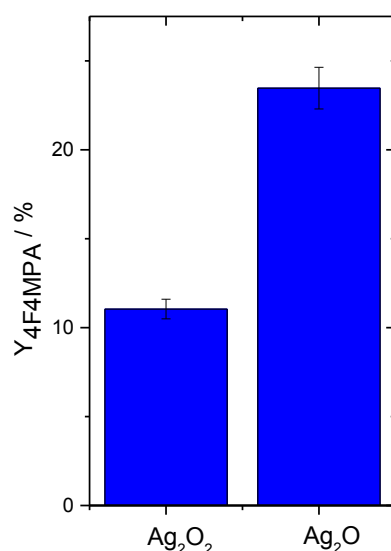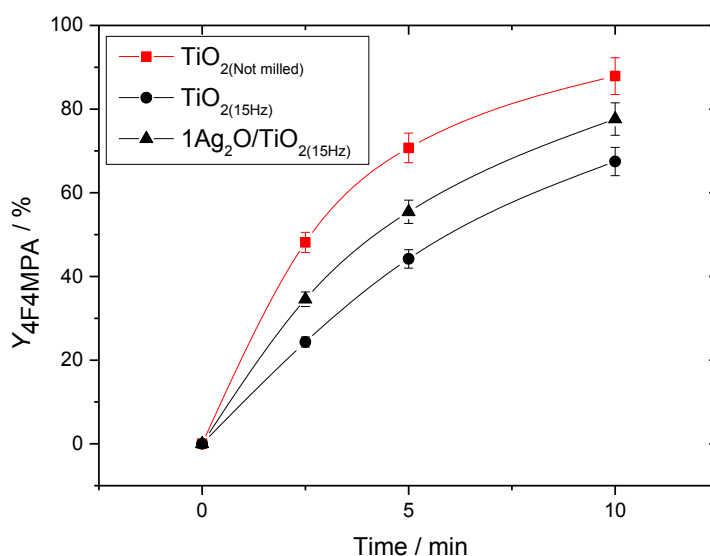

Figure 4.6: Yield of 4F4MPA (**1b**) at 10 min performed with unsupported Ag_2O_2 and Ag_2O. Reaction conditions: 0.2 mmol of DMGA (**1a**), 0.4 mmol of Selectfluor®, 0.0093 mmol of Ag, 4 mL H_2O, 0.23 mmol K_2CO_3, 25 °C, open air. Full spectrum solar light simulator lamp at 300 W was used to irradiate the reaction mixture.

Interestingly, unsupported and uncalcined Ag (I) and Ag (I, III) oxides exhibited much lower activity than $1Ag_2O/TiO_{2(15Hz)}$, with only 11% and 23% yield values observed for Ag_2O_2 and Ag_2O respectively, thus suggesting a potential catalytic activity of TiO_2. Also, the yield of 4F4MPA (**1b**), observed for Ag(I) oxide, twice that of the yield observed for Ag (I, III) oxide, clearly indicates that Ag(III), present at

50% in Ag_2O_2, does not exhibit any catalytic activity, in good agreement with the results observed in Chapter 3 (*vide supra*).

Considering the low activity observed for unsupported Ag_xO, and that TiO_2 is well-known to be an active semiconductor for photocatalysis, the activity of not-doped titanium oxide to photocatalyse decarboxylative fluorination reactions was investigated. Notably, to properly compare the catalytic activity of the catalysts, both in the presence and absence of Ag, all reactions were performed at the same mass charge of catalyst. The mass charge was scaled down from 100 mg to 10 mg of catalyst, to ensure that kinetic trends could be observed. First, pure TiO_2 was mechanically milled at 15 Hz ($TiO_{2(15Hz)}$), then $TiO_{2(15Hz)}$ and untreated TiO_2 were employed for DMGA (**1a**) decarboxylative photo-fluorination (Figure 4.7).

Figure 4.7: Yield of 4F4MPA (**1b**) at 10 min performed with various catalysts. Reaction conditions: 0.2 mmol of DMGA (**1a**), 0.4 mmol of Selectfluor®, 10 mg of catalyst, 4 mL H_2O, 0.23 mmol K_2CO_3, 25 °C, open air. Full spectrum solar light simulator lamp at 300 W was used to irradiate the reaction mixture.

Although doping TiO_2 with Ag led to a slight increase in the catalytic performance when compared with pure TiO_2 milled at 15 Hz (around 67% and 77% of 4F4MPA yields for $TiO_{2(15HZ)}$ and $1Ag_2O/TiO_{2(15Hz)}$, respectively) both milled materials are less active than commercially available, unmilled TiO_2 (red squares, Figure 4.7). This clearly demonstrates that it is TiO_2, and not Ag, that is responsible for the high levels

of activity observed under photocatalytic conditions. Interestingly, a decreasing of catalytic activity was observed by milling pure TiO_2 at 15 Hz, with 4F4MPA (**1b**) yield decreasing from 88% to 77%. This could be due to: i) a partial loss in crystallinity, as observed by Powder X-Ray Diffraction (pXRD) measurements in Chapter 3, and ii) possible increases in crystallite size during the treatment.

The ability to achieve high yields in short reaction time, employing simple commercially available titanium oxide (P25) without further treatments and without any additional metal, is indeed promising from an industrial perspective. Hence, a thorough investigation into the catalytic performances and reaction mechanisms of TiO_2-photocatalysed decarboxylative fluorination was further performed.

4.3.2 Photocatalysed decarboxylative fluorination with commercially available TiO₂ (P25)

Following the observation that high activity was exhibited by commercially available TiO_2 (P25) (Figure 4.7), the optimisation of the system and a thorough investigation of the catalytic properties of TiO_2 (P25) for decarboxylative fluorination of aliphatic carboxylic acids under photo-fluorination conditions were required. Also in this case, DMGA (**1a**) was used as model substrate due to its high solubility in water, and a full spectrum solar light simulator lamp at 300 W (Figure 4.8) and/or a monochromatic LED torch at 365nm wavelength were employed to irradiate the reaction mixture.
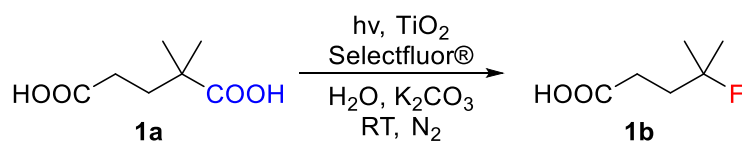

Figure 4.8: Decarboxylative fluorination of DMGA (**1a**) to yield 4F4MPA (**1b**) with Selectfluor® as fluorine donor.

Analogous to the results observed in Chapter 3 for Ag_xO/TiO_2, under these conditions, selective mono-fluorination of DMGA (**1a**) to 4F4MPA (**1b**) as reaction product was observed in the first 10 minutes of reaction, in line with the radical-based mechanism reported for this reaction, in which it is postulated that tertiary positions exhibit greater activity than primary and secondary ones. High reaction rates were observed, with around 80% of 4F4MPA (**1b**) yield values reached after only 5

minutes of reaction, yielding a preliminary turnover frequency (TOF) of 242, when a metal/substrate ratio of 6.25 mol % was employed (Figure 4.9).

4.3.2.1 Blank reactions/control experiments

Prior to optimising the system, several control reactions, were performed, in the absence of: i) K_2CO_3, ii) TiO_2 and iii) Selectfluor® (Figure 4.9), in order to investigate the behavior of the system in the absence of one of the different components.
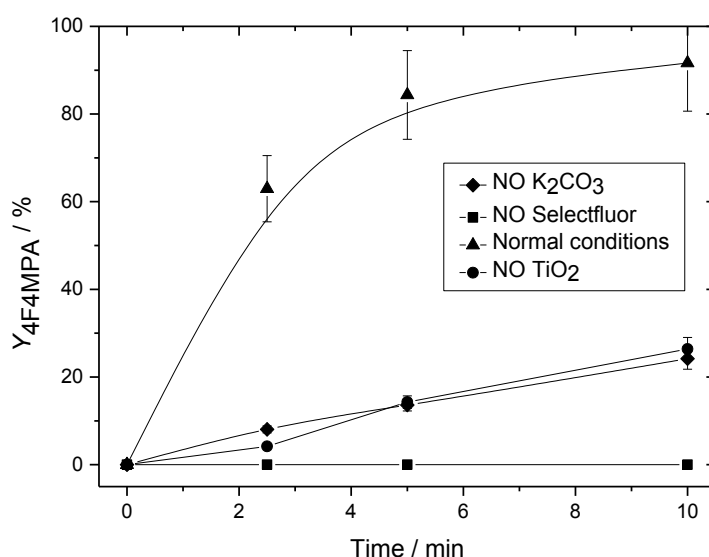
Figure 4.9: Yield of 4F4MPA (**1b**) with time over TiO_2(P25), irradiating with solar light simulator lamp at 300 W. Reaction conditions: 0.2 mmol of DMGA (**1a**), 0.4 mmol of Selectfluor®, 0.0125 mmol TiO_2, 4 mL H_2O, 0.23 mmol K_2CO_3, N_2 atmosphere, 25 °C

Interestingly, no 4F4MPA yield was observed in the absence of the fluorinating agent. However, some level of performance is observed with Selectfluor® alone *i.e.* in the absence of TiO_2, although at a much lower rate compared to the catalytic system, with only 30% of 4F4MPA (**1b**) yield observed after 10 minutes of reaction. Notably, similar kinetic behavior to that observed in the absence of TiO_2, was also demonstrated when TiO_2 and Selectfluor® were used in the absence of base, K_2CO_3, thus suggesting a key role is played by K_2CO_3 upon TiO_2 activation. In fact, K_2CO_3 can affect the reaction rate in two different ways: i) increasing the recombination time of the electron/hole (e^-/h^+) pairs generated into TiO_2, and ii) favoring the adsorption of

the substrate (in its carboxylate form) on TiO_2 surface. Notably, 4F4MPA (**1b**) selectivity greater than 95 % was observed in each experiment.

Experiments performed in the absence of the light source, were also performed and no substrate conversion was observed, demonstrating that light irradiation is essential for the reaction to happen under these reaction conditions.

Accordingly, the following conclusions can be made: i) Selectfluor® is essential for activity to be observed, ii) low levels of activity are demonstrated by the Selectfluor® alone, suggesting that the presence of a secondary non-catalytic reaction pathway is present to a small extent, iii) K_2CO_3 is essential for the catalytic activity of TiO_2 to be observed.

4.3.2.2 Effect of K_2CO_3

To further study the effect of base, a number of kinetic experiments at different base loadings was performed in a range $0 - 2.3$ equivalents (ratio K_2CO_3:DMGA (**1b**) in a range $0 - 2.3$).
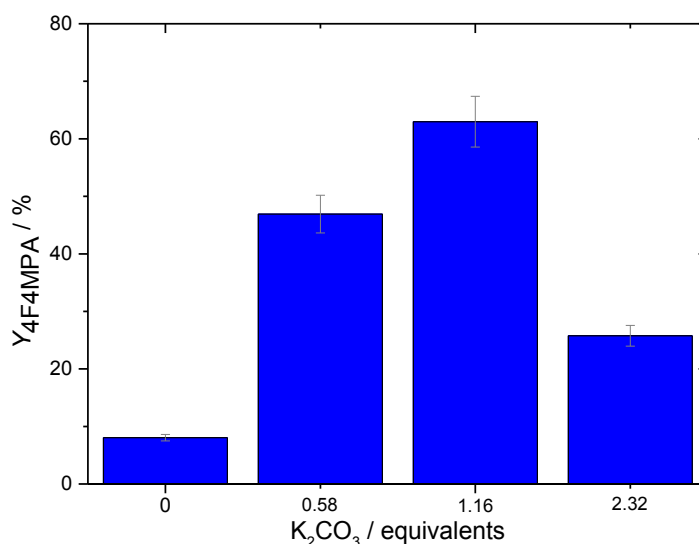
Figure 4.10: Yield of 4F4MPA (**1b**) at 2.5 min with varying amount of K_2CO_3, over TiO_2 (P25) with solar light simulator at 300 W. Reaction conditions: 0.2 mmol DMGA (**1a**), 0.4 mmol of Selectfluor®, 0.0125 mmol TiO_2, 4 mL H_2O, various amount of K_2CO_3, N_2 atmosphere, 25 °C.

As expected, a large drop in the catalytic activity was observed when performing the reaction in the absence of K_2CO_3, with only 8 % yield of 4F4MPA (**1b**) detected at 2.5 minutes, against 47 % and 63 % yields obtained for 0.58 and 1.16 K_2CO_3 equivalents, respectively. However, despite the increasing activity observed for 0.58 and 1.16 equivalents, a decrease in the catalytic activity was observed following addition of 2.32 equivalents of K_2CO_3, following a similar trend to that previously reported in Chapter 3.

Clearly, K_2CO_3 has an impact on the reaction rate. As briefly reported before, this can be thought to be due to two different effects; i) stabilisation of electron/hole pairs in TiO_2, and ii) deprotonation of the substrates, favoring the formation of eventual TiO_2-carboxylate intermediate species. The role of K_2CO_3 on the reaction mechanism is discussed further in this Chapter.

4.3.2.3 Hot filtration experiment

To further optimise the reaction conditions, a number of experiments at different substrate to metal ratios were performed. Impressively, high catalytic activity was still observed even at a Ti loading of 1.25 mol %, which represents a four-fold decrease in catalyst concentration. Indeed, despite the four-fold decrease in catalyst concentration, the quantity of substrate converted decreased by less than 10 %. The non-linear decrease in rate with catalyst loading strongly indicates that some transport limitations may still be present, and hence, the true activity of the catalyst may still be underestimated (see Chapter 7 for further discussion). However, even with this limitation, a TOF of 1113 h^{-1} is obtained after 2.5 minutes of reaction, which is approximately twice that of any other TOF reported for this process to date.

To ensure that the reaction is truly heterogeneously catalysed, a hot filtration test was also performed. As can be seen, filtering the reaction mixture and thereby removing the solid catalyst at 2.5 minutes, correlating to approximately 50 % yield, totally terminates the reaction, clearly demonstrating catalysis to be heterogeneous. In addition to showing catalysis to be fully heterogeneous, termination of the reaction by removal of the catalyst also excludes the possibility that TiO_2 simply acts as a free radical initiator to an otherwise homogeneous free radical chain mechanism.
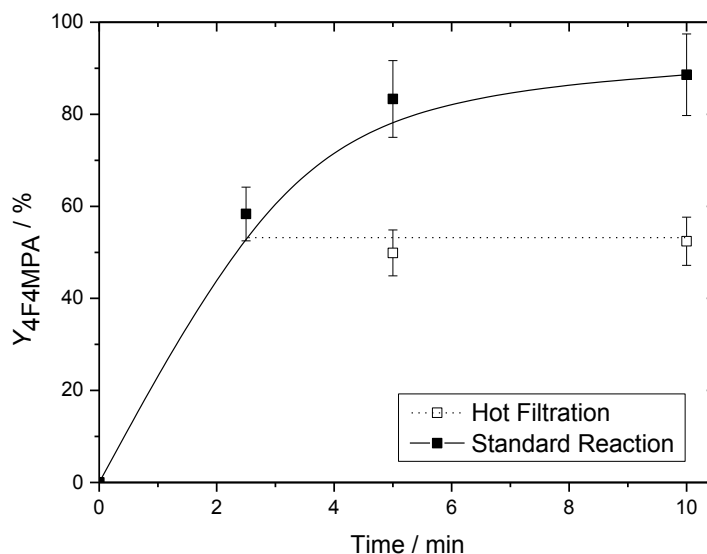
Figure 4.11 Solid line: yield of 4F4MPA (**1b**) with time without filtering the catalyst. Dashed line, catalytic activity of the supernatant solution following filtration of the catalyst at 2.5 min. Reaction conditions 1.0 mmol of DMGA (**1a**), 2.0 mmol of Selectfluor®, 0.0125 mmol TiO_2, 10 mL H_2O, 1.16 mmol K_2CO_3, N_2 atmosphere, 25 °C. Solar light simulator at 300 W was used to irradiate the reaction mixture.

4.3.2.4 Effect of the light irradiation

To verify the necessity of continuous irradiation of the reaction vessel for the entirety of the reaction and to confirm the photocatalytic-type mechanism, a light/dark experiment was performed, by periodically switching the lamp on and off throughout the reaction. As shown in Figure 4.12, carrying out the reaction under the dark (UV lamp OFF, illustrated by the grey bars in Figure 4.12) the reaction completely stopped, and no further DMGA (**1a**) conversion and 4F4MPA (**1b**) yield was detected under dark conditions. This clearly indicates that continuous irradiation is required, excluding the role of light as radical initiator for a homogeneous free radical chain mechanism. The activity observed in the presence of light is, in fact, thought to be due to the constant generation of hole/electron pairs in TiO_2, involved into the reaction mechanism.
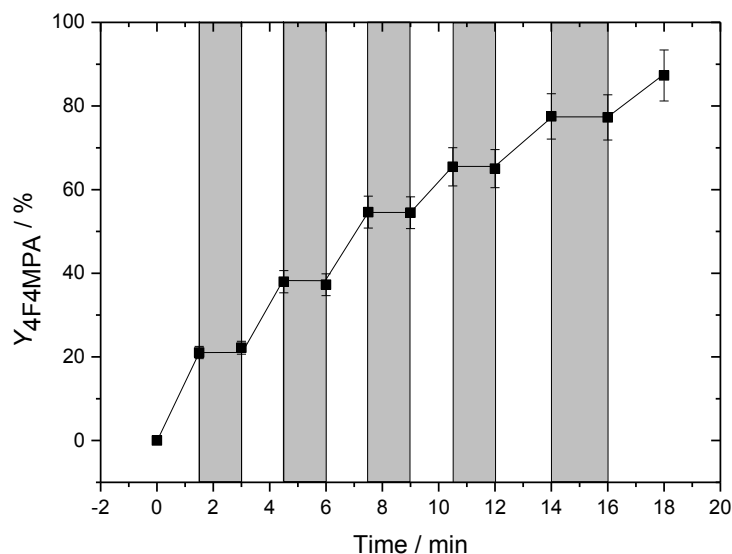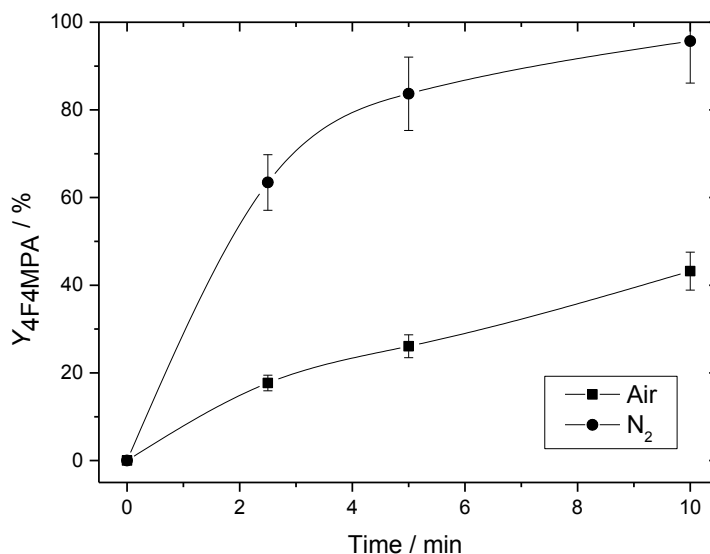
Figure 4.12: Yield of 4F4MPA (**1b**) with time over TiO_2 with light and (grey area) in dark conditions. Reaction conditions: 1.0 mmol of DMGA (**1a**), 2.0 mmol of Selectfluor®, 0.0125 mmol TiO_2, 10 mL H_2O, 1.16 mmol K_2CO_3, N_2 atmosphere, 25 °C. Solar light simulator at 300 W was used to irradiate the reaction mixture.

Although a homogeneous free radical chain reaction does not operate following potential initiation by the catalyst, the decarboxylative reaction has been shown to proceed *via* single electron transfer (SET) process.[5] To further verify the potential role of SET during the reaction, the impact of oxygen was evaluated. In fact, O_2 is a well-known radical trap, as it is able to readily react with carbon-based radicals, R•, due to its triplet ground state, resulting into the formation of a peroxo-radical species, RO_2•.

4.3.2.5 Effect of O_2

Accordingly, an additional reaction was performed in air instead of N_2, using 1.25 mol% of Ti. Although a drop in catalytic activity was observed when the reaction was performed in open air, around 40% of yield was still detected after 10 minutes of reaction. A blank test, without TiO_2, was then performed in air and negligible DMGA (**1a**) conversion values were observed, demonstrating that TiO_2 is necessary for the reaction to occur in air. The large decrease of activity observed in the presence of O_2, a well-known radical scavenger, provides evidence that radical intermediates are thought to be involved in the reaction mechanism.
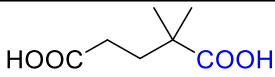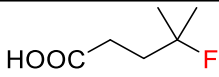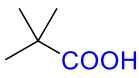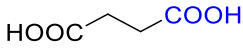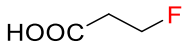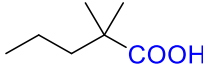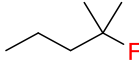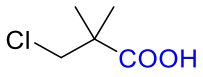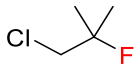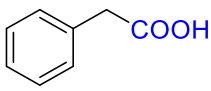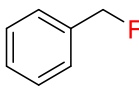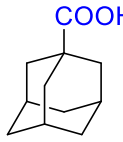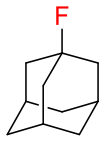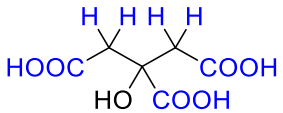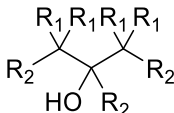
Figure 4.13: Yield of 4F4MPA (**1b**) with time over TiO$_2$ under N$_2$ atmosphere (black circles) and in air (black squares). Reaction conditions: 0.2 mmol of DMGA (**1a**), 0.4 mmol of Selectfluor®, 0.0125 mmol TiO$_2$, 4 mL H$_2$O, 0.23 mmol of K$_2$CO$_3$, 25 °C. Solar light simulator lamp at 300 W was used to irradiate the reaction mixture.

To elucidate the energy of light that is thought to be required to activate the catalytic material, various monochromatic light sources were investigated. Given TiO$_2$ possesses a well-known energy band gap of 3.2 eV, wavelengths with higher energy than 387 nm ($\lambda \leq 387$ nm) are required (see Chapter 1). Therefore, a reaction was performed substituting the solar light simulator with a forensic LED torch with a monochromatic wavelength of 365 nm and identical reaction rates were observed. Therefore, demonstrating that instead of using a broader range of wavelengths, monochromatic irradiation with a 365 nm wavelength has sufficient energy to overcome the TiO$_2$ energy band gap (3.2 eV for anatase and 3.0 eV for rutile), activating the catalytic material. Henceforth, monochromatic 365 nm wavelength was employed as irradiation source for all following experiments.
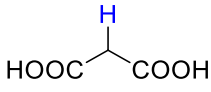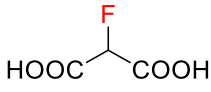
4.3.2.6 Versatility of the process

A key target for a C(sp^3)-F bond forming catalyst is the ability to demonstrate activity towards a wide range of substrates. Accordingly, the general applicability of TiO$_2$ to photocatalyse decarboxylative fluorination of carboxylic acids was then demonstrated using a series of different carboxylic acids (Table 4.1).

Table 4.1: General applicability of TiO₂ for the photocatalytic fluorination of various carboxylic acids.

Entry	Substrate		Product		Yield / %[a]	Time / min
1	HOOC, COOH	**1a**	HOOC, F	**1b**	92, 35 [b]	10
2	COOH	**2a**	F	**2b**	94[c]	10
3	HOOC, COOH	**3a**	HOOC, F	**3b**	48	30
4	COOH	**4a**	F	**4b**	42[d]	10
5	Cl, COOH	**5a**	Cl, F	**5b**	22[d], 46[d]	10, 30
6	COOH	**6a**	F	**6b**	17[d]	60
7	COOH	**7a**	F	**7b**	22[d]	10
8	H, HOOC, COOH	**8a**	F, HOOC, COOH	**8b**	21	30
9	H H H, HOOC, COOH, HO COOH	**9a**	$R_1 R_1 R_1 R_1$, R_2, R_2, HO R_2, R_1= H, F, R_2=COOH, F		Mixture of products	10

[a] Yields calculated as "mol (product)/mol (initial substrate moles)" for entries 1, 3, 4 and 5, and as "mol (**2a** converted)/mol(initial **2a** moles)" for entry 2 due to high product volatility (12.1 °C). [b] 2 mL H₂O and 2 mL of (CH₃)₂CO as solvent. [c] 0.115 mmol K₂CO₃. [d] 5 mL H₂O, 5 mL (CH₃)₂CO, 0.115 mmol K₂CO₃. Yields calculated with ¹⁹F NMR using α,α,α-trifluorotoluene and HPLC analysis against authentic standards. Values in parentheses correspond to yields. Reaction conditions: 0.2 mmol substrate, 0.4 mmol Selectfluor®, 0.0125 mmol TiO₂, 4 mL H₂O, 0.23 mmol of K₂CO₃, 25 °C, 10 min. Forensic monochromatic LED torch at 365 nm wavelength was used to irradiate the reaction mixture.

Firstly, the capability of TiO_2 to fluorinate more stable, primary -COOH groups was investigated, using succinic acid (**3a**) as substrate. Interestingly after 30 min, 48% of the mono-fluorinated product was observed. Hence, although proceeding with a lower reaction rate, TiO_2 is able to photo-fluorinate more stable primary carboxylic groups. Considering the restricted amount of H_2O soluble substrates, a $H_2O/(CH_3)_2CO$ (v/v 1:1) mixture was then used as solvent to investigate the catalytic activity of TiO_2 for the fluorination of a broader range of carboxylic acids, including substrates possessing aromatic groups (entry 4-7 Table 4.1). Although lower activity was observed replacing neat H_2O with a $H_2O/(CH_3)_2CO$ (v/v 1:1) solution, entry 1 Table 4.1 (from 92 to 35 % yield of 4F4MPA, (**1b**)), TiO_2 still exhibited good activity for the fluorination of substrates that are insoluble in neat H_2O, such as adamantane carboxylic acid. Indeed, with the new reaction conditions, 42% of **4b** yield after 10 min was observed with 2,2-dimethylvaleric acid (DMVA, **4a**), another tertiary carboxylic acid that does not possess any other functional group, whilst lower activity was observed for 3-chloro-2,2-dimethylpropionic acid (**5a**) possessing a chlorine on the C atom in β position to the carboxylic group. To investigate the effect of the dimension of the substrate on reaction rate, a hindered substrate, 1-adamantane carboxylic acid (**7a**) was tested. Although lower activity was observed with this substrate, relative to those less hindered substrates (such as DMGA (**1a**) and DMVA (**4a**)), 22 % yield of 1-fluoro-adamantane (**7b**) was reached in only 10 min, thus indicating that TiO_2 can successfully activate even larger and more sterically-hindered carboxylic groups. To investigate the capability of TiO_2 to activate H_2O insoluble primary carboxylic groups, phenylacetic acid (**6a**) was employed as substrate and 17 % of product yield was achieved in one hour. Control experiments without TiO_2 in $H_2O/(CH_3)_2CO$ (v/v 1:1) solution were performed and no activity was observed.

Analogous to the observations in Chapter 3 for 2,2-dimethyl-3-phenylpropionic acid, it was also found that specific substrates were able to activate C-H bonds giving direct $C(sp^3)$-H fluorination. Indeed, using pluri-carboxylic acids with additional carboxylic groups in β or γ positions, $C(sp^3)$-H fluorination occurred: malonic acid (**8a**) and citric acid (**9a**), entry 8 and 9 Table 4.1.

Unexpectedly, when malonic acid (**8a**) was employed as substrate, the product of classic decarboxylative fluorination (resonating at -219 ppm) was not observed in the ^{19}F NMR spectrum of the crude reaction mixture, even though 30 % of the initial malonic acid (**8a**) was converted during the reaction. However, different peaks resonating around -180 ppm were observed. The presence of these additional resonances suggests that secondary fluorine atoms are present, potentially due to $C(sp^3)$-H fluorination on the α carbon of malonic acid (**8a**). To further verify the identity of these signals, ^{19}F NMR spectra were recorded with, and without, ^1H decoupling. As observed in the top right inset in Figure 4.14, under decoupled conditions one of the singlets splits into a doublet (expanded in Figure 4.15) with a coupling constant of $J = 56$ Hz. This is in good agreement with the range of coupling constants typically observed for geminal ^1H-^{19}F coupling ($^2J_{H-C-F} = 40$-60 Hz), further indicating the formation of 2-fluoro-propanedioic acid (**8b**) as product. This is potentially due to the activation of the $C(sp^3)$-H bond generated by the presence of the two carboxylic groups -COOH substituents on the central carbon.
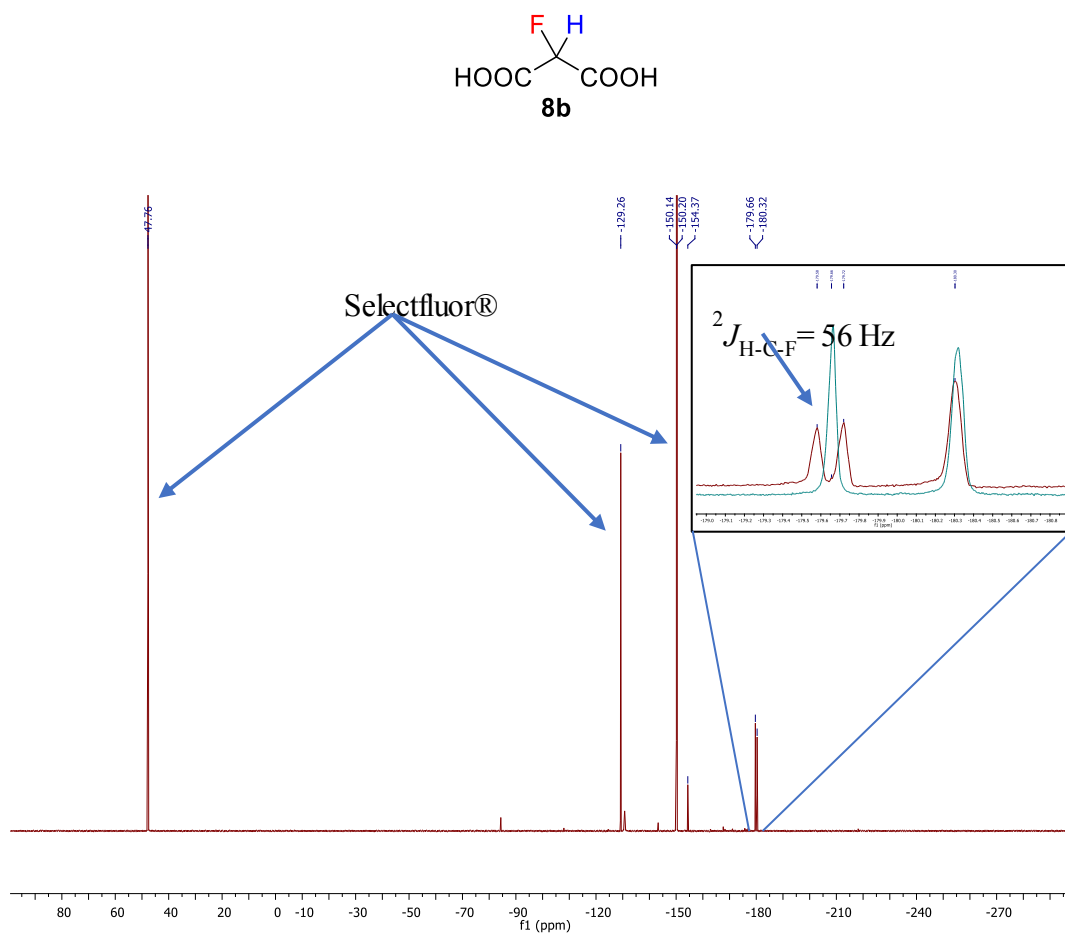
Figure 4.14: ^{19}F NMR spectrum of crude reaction mixture obtained following malonic acid (**8a**) fluorination. Top right inset: ^{19}F NMR with (blue line) and without (red line) ^{1}H decoupling in the region -179 -181 ppm. Reaction conditions: 0.2 mmol of malonic acid (**8a**), 0.4 mmol Selectfluor®, 0.0125 mmol TiO_2, 2 mL H_2O, 0.23 mmol of K_2CO_3, 25 °C, 30 min. Forensic monochromatic LED torch at 365nm wavelength was used to irradiate the reaction mixture.
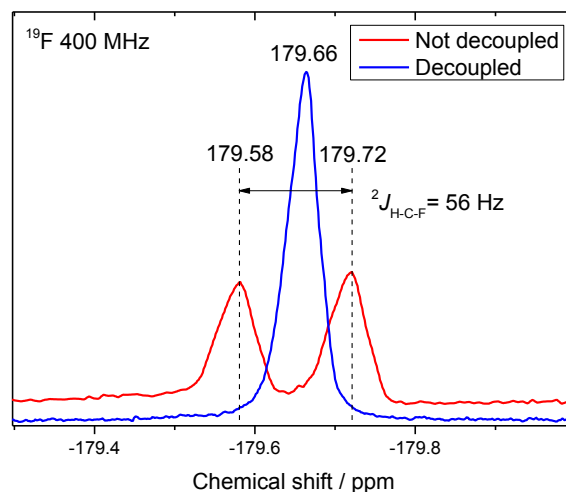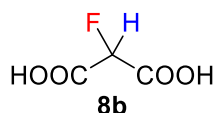
Figure 4.15: ^{19}F NMR spectrum (-179 -180 ppm) of crude reaction for malonic acid (**8a**) fluorination. Top right inset: ^{19}F NMR with (blue line) and without (red line) ^{1}H decoupling in the region -179 -181 ppm. Reaction conditions: Reaction conditions: 0.2 mmol of malonic acid (**8a**), 0.4 mmol Selectfluor®, 0.0125 mmol TiO_2, 2 mL H_2O, 0.23 mmol of K_2CO_3, 25 °C, 30 min. Forensic monochromatic LED torch at 365nm wavelength was used to irradiate the reaction mixture.

When citric acid, a tri-carboxylic acid with vicinal carboxylic groups (**9a**), was used as substrate, a mixture of byproducts was observed. In fact, under these conditions, competition between $C(sp^3)$-H fluorination and decarboxylative fluorination was observed: ^{19}F NMR spectrum of crude reaction mixture (Figure 4.16) shows a consistent number of signals in the region -185 -200 ppm, typically related to R_2CHF resonance, further demonstrated by modifications of the signals when proton decoupling was applied.

The observation of reaction products arising from direct $C(sp^3)$-H fluorination is highly interesting, suggesting that despite decarboxylative fluorination being the preferred fluorination route, direct C-H fluorination on specific substrates can be achieved under these conditions. Along with the similar observations made in Chapter

3, these findings further indicate that heterogeneous catalysts can potentially be employed also for highly challenging C(sp^3)-H fluorination.

Figure 4.16: ^{19}F NMR spectrum of crude reaction for citric acid (**9a**) fluorination. Reaction conditions: 0.2 mmol of citric acid (**9a**), 0.4 mmol Selectfluor®, 0.0125 mmol TiO$_2$, 4 mL H$_2$O, 0.34 mmol of K$_2$CO$_3$, 25 °C, 10 min. Forensic monochromatic LED torch at 365nm wavelength was used to irradiate the reaction mixture.
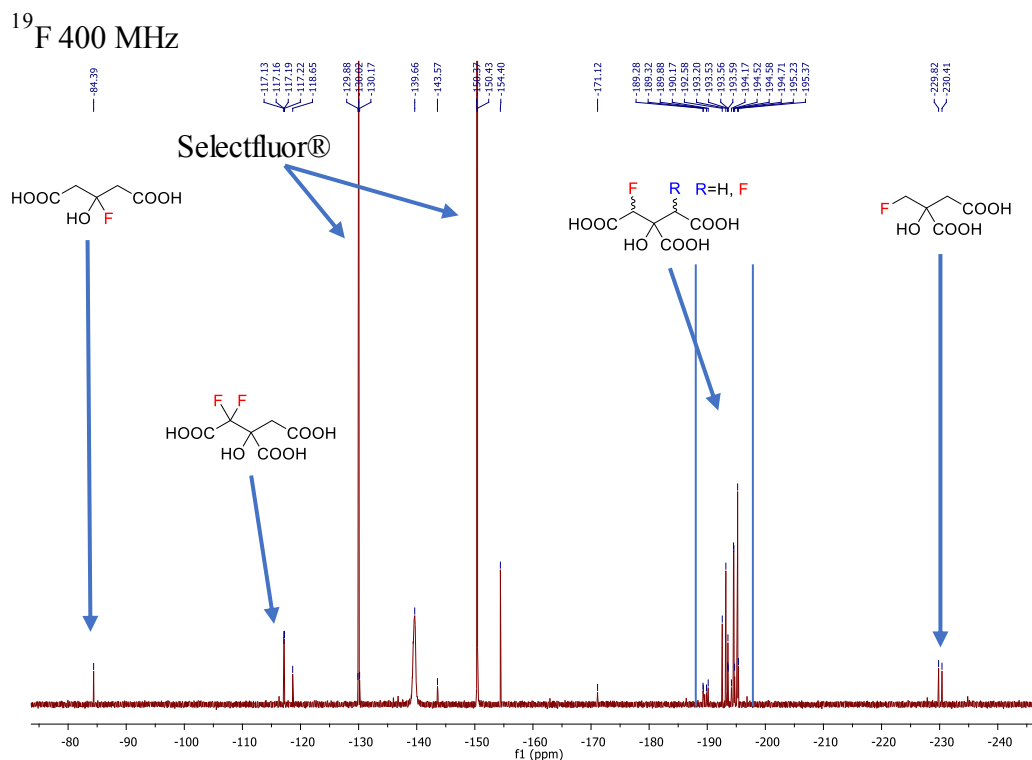
4.3.2.7 Reusability

As already reported in Chapter 3, one of the major advantages of heterogeneous catalysts over their homogeneous analogues is the ease in which they can be recovered and reused. This would lead to remarkable increases in overall process sustainability as well as facilitating product purification steps, thus decreasing industrial implementational cost. After demonstrating the versatility of TiO$_2$ as heterogeneous photocatalyst for decarboxylative fluorination of different carboxylic acids, reusability properties of TiO$_2$, were also investigated, using DMGA (**1a**) as substrate and neat water as reaction solvent.
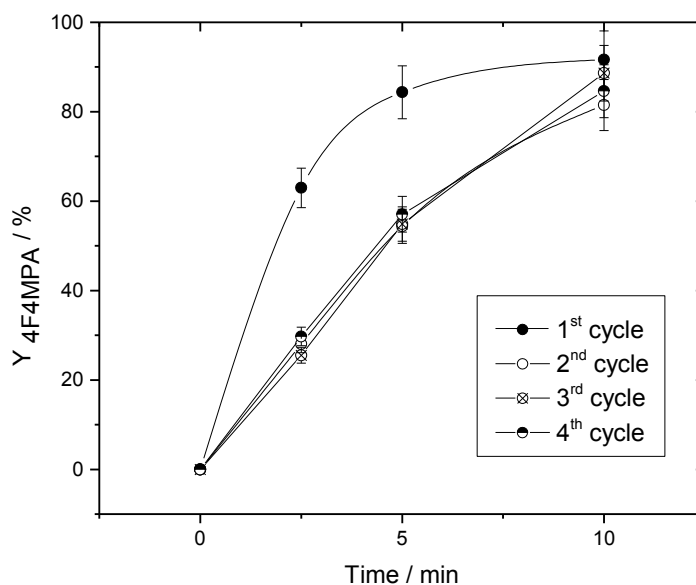
Figure 4.17: Reusability of TiO$_2$ for photocatalysed DMGA (**1a**) decarboxylative fluorination. No intermediate treatments were performed between catalyst recycles. Reaction conditions: 0.2 mmol of DMGA (**1a**), 0.4 mmol of Selectfluor®, 0.0125 mmol TiO$_2$, 4 mL H$_2$O, 0.23 mmol of K$_2$CO$_3$, 25 °C. Forensic monochromatic LED torch at 365nm wavelength was used to irradiate the reaction mixture.

Although there is a decrease in reaction rate following the first reuse of TiO$_2$, no further decrease in performance was observed for the following catalytic cycles (*i. e.* same kinetic rates were observed for 2nd, 3rd and 4th cycles). Notably, the same final yield values (80-90 % yield of 4F4MPA (**1b**)) were also achieved after 10 minutes reaction in every catalytic cycle, for both fresh and used catalyst. The ability of the catalyst to be reused, without loss in activity, even without periodic regeneration treatments, is desirable and indicates the material possesses potential for continuous operation.

4.3.3 Mechanistic studies of photocatalysed decarboxylative fluorination with commercially available TiO$_2$ (P25)

Several possible chemical reactions can occur during photo-fluorination. Accordingly, obtaining a detailed understanding of the reaction mechanism(s) is challenging. Indeed, from the literature a number of possible reaction mechanisms can be proposed, ranging from SET processes between carboxylate groups bound on TiO$_2$,[5,6]

to the formation of catalytically active Ti-F intermediates potentially formed *in situ*.[7-9] To elucidate the potential mechanism, and hence identify a detailed reaction network, a variety of spectroscopic experiments were thus performed.

Firstly, in order to investigate substrate/catalyst interactions, Diffuse Reflectance Infrared Fourier-Transform Spectroscopic (DRIFT) analysis was performed, by adsorbing the carboxylic acid on TiO_2 surface and irradiating the sample with a monochromatic light of wavelength 365 nm. Since the substrate needs to be nebulised for DRIFT experiments, pivalic acid (**2a**) was chosen as the most suitable substrate because of his higher volatility (melting point 35.5 °C, boiling point 163.8 °C). Pivalic acid (**2a**) was nebulised into a gas bubbler under N_2 flow at 120 °C and fluxed into the cell DRIFT cell containing the catalyst.

To establish the nature of the interaction between the substrate and TiO_2, firstly in the absence of light, an experiment was performed whereby pivalic acid was adsorbed onto TiO_2 surface at 30 °C and subsequently heating the DRIFT cell up to 600 °C. As shown in Figure 4.18, after interaction with pivalic acid, new features appear in the IR spectrum (blue line Figure 4.18); a group of bands in the region 3000 - 2850 cm^{-1}, characteristic of aliphatic C-H stretching, and other signals with wavenumbers in the region of 1700 - 1100 cm^{-1} appear. Interestingly, although the new C-H stretching bands correspond well to the ones of free pivalic acid (red line in Figure 4.18), the key signal at 1692 cm^{-1} characteristic of the COOH group (red line Figure 4.18), is present in only a negligible amount. This demonstrates that only a small percentage of pivalic acid in its free acid form adsorbs on the catalyst surface. Moreover, new intense peaks appear in the region 1600 - 1100 cm^{-1}. These have previously been assigned to the deprotonated form of pivalic acid, $(CH_3)_3CCOO^-$.[10-12] Whilst the small feature at 1692 cm^{-1} disappears above 50 °C indicating physisorbed pivalic acid (in its acid form), both peaks at 1600 - 1100 cm^{-1} and the C-H stretching features at 3000 - 2850 cm^{-1} are more stable during heat treatment. Indeed, all these peaks are still clearly visible at 300 - 450 °C, temperatures much higher than the boiling point of pivalic acid (163.8 °C). Therefore, all the new features observed upon interaction between substrate/TiO_2 can be assigned to a chemisorbed $(CH_3)_3CCOO^-$ species. This indicates

the formation of a strongly coordinated RCOO-TiO₂ intermediate (intermediate **A** in Figure 4.28) upon interaction between TiO₂ and the substrate.
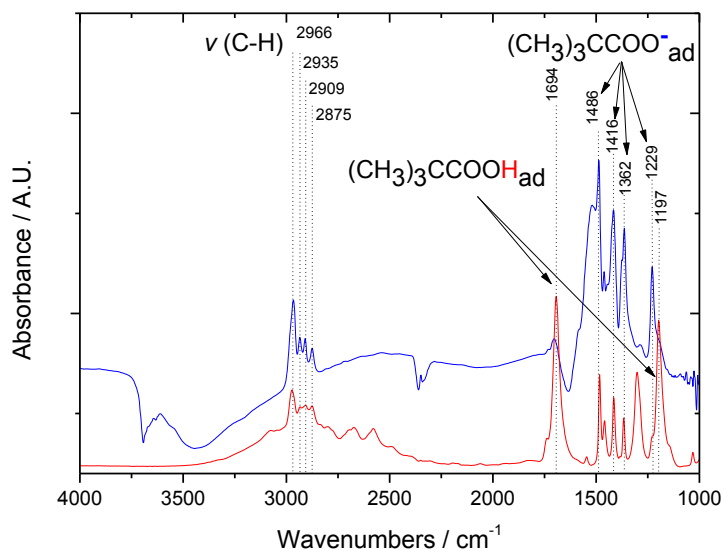
Figure 4.18: DRIFT spectra of (red line) pivalic acid (**2a**) and (blue line) TiO₂ after adsorption of pivalic acid (**2a**) at 30 °C.
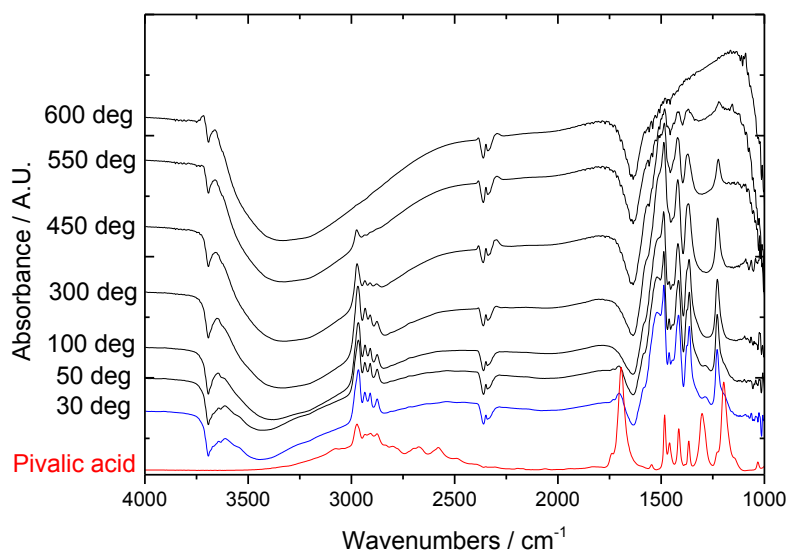
Figure 4.19: DRIFT spectra of (red line) pivalic acid (**2a**), and (blue line) TiO₂ after adsorption of pivalic acid (**2a**) at 30 °C and between 50 and 600 °C (dark lines).

To evaluate the role of light during the reaction, the DRIFT cell filled with TiO_2-bound carboxylate species was then irradiated with a monochromatic UV light of 365 nm wavelength for 2 hours, and the IR spectral changes were constantly recorded all throughout (Figures 4.20 and 4.21). As expected, a constant decrease of all the features related to the $(CH_3)_3CCOO^-$ species ($3000 - 2850 cm^{-1}$ and $1600 - 1250 cm^{-1}$) was observed, whilst no new features were observed in the full spectra. This clearly indicates that pivalate decomposition occurs during the entire irradiation period. Loss of the pivalate under these conditions likely results from its decomposition from R-COO^- into $R^{\bullet}$ and CO_2, as reported by Onishi and Manley.[5,6]
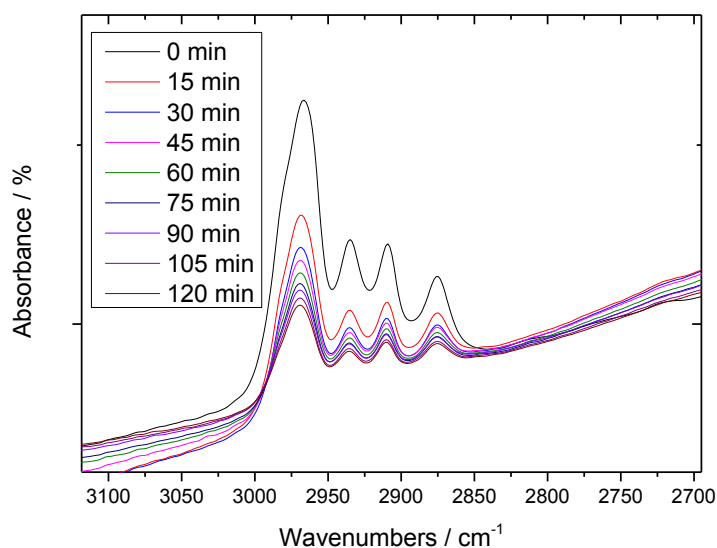
Figure 4.20: DRIFT spectra of TiO_2-bound pivalate species, during irradiation with a monochromatic UV light of 365 nm. Region $3125 - 2700 cm^{-1}$.
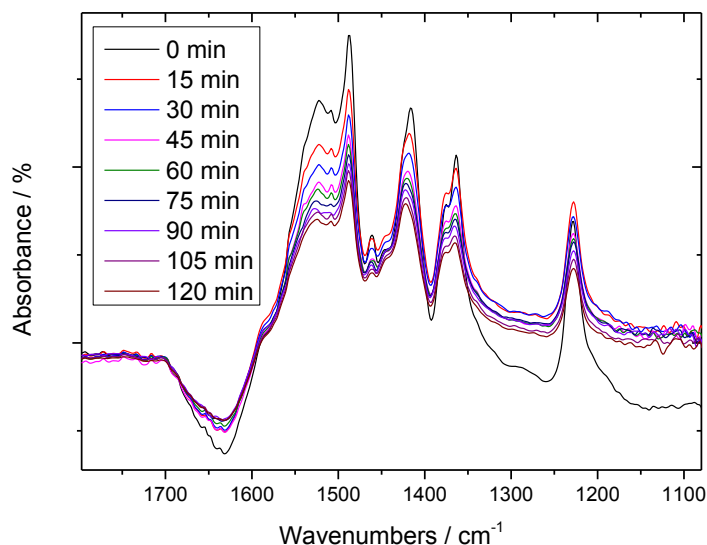
Figure 4.21: DRIFT spectra of TiO$_2$-bound pivalate species, during irradiation with a monochromatic UV light of 365 nm. Region 1800 - 1100 cm^{-1}.

Considering the presence of fluorine in the product, and the radical based nature of the mechanism, it is important to verify the origin of the incorporated F atom. Indeed, it is possible that Selectfluor® simply reacts through SET with the alkyl radical, or is incorporated *via* a metal-F species, potentially formed *in-situ*. Indeed, as already reported in literature, the presence of fluorine in the reaction medium can lead to surface modification of TiO$_2$ resulting in fluorinated species such as TiOF$_2$,[7-9] that can affect the catalytic properties of the material and potentially act as fluorinating agent. To confirm the potential involvement of Ti-F species in the reaction mechanism and to study the possible modification on TiO$_2$ surface, X-ray photoelectron spectroscopy (XPS) was performed.

To study the effect of several parameters (such as *hv* irradiation or the presence of base) on the formation of Ti-F species, different samples were prepared following TiO$_2$ treatments under standard reaction conditions but respectively in the absence of light or base and/or substrate. In each case the catalytic material was recovered *via* filtration, washed with deionised water and dried in an oven at 70°C for 1 - 2 hours.

In all the analysed samples, residual amounts of fluorine (0.4 - 1.6 wt. %) were found on the catalyst surface (Table 4.2) and the same fluorine species with binding energy

of 684.6 eV was detected (Figure 4.22). There are several contrasting opinions of the origin of this peak, with $TiOF_2$, and simple fluoride anions bound to TiO_2 having been suggested. However, in light of the washing procedure performed after reaction, it is unlikely that simple fluoride anions can remain strongly bound to the catalyst, and hence, Ti-F type species are thought to be likely to be responsible for this signal. Interestingly, a much lower amount of fluorine was found on the TiO_2 surface after dark reaction, *i.e.* under standard reaction condition but in the absence of light (entry 2 Table 4.2). This suggests a promoting effect of light irradiation on the binding mechanism between fluorine and TiO_2. Likely, F-TiO_2 surface binding is promoted by the formation of the electron/holes charge carriers in TiO_2. Notably, negligible amounts of nitrogen (0 - 0.3 atom %, see Chapter 8) were found on the analysed samples, thus suggesting that the fluorine species is not to be attributed to intact Selectfluor® molecules eventually adsorbed on TiO_2.

Table 4.2: XPS analysis. Reaction conditions: 0.2 mmol **1a**, 0.4 mmol Selectfluor®, 0.0125 mmol TiO_2, 4 mL H_2O, 0.23 mmol of K_2CO_3, 25 °C, 10 min. Forensic monochromatic LED torch at 365 nm wavelength was used to irradiate the reaction mixture.

Entry		Fluorine / atomic %	Fluorine / weight %
1	[a]	1.52	1.11
2	[b]	0.51	0.38
3	[c]	2.12	1.56
4	[d]	1.69	1.24

[a] Used TiO_2 post-reaction; [b] Used TiO_2 post-reaction under standard condition but in the absence of light; [c] Used TiO_2 post-reaction under standard condition but in the absence of the substrate and [d] Used TiO_2 post-reaction under standard condition but in the absence of both substrate and base (K_2CO_3).

To establish the nature of this fluorinated species, and further exclude the presence of simple fluoride anions F- adsorbed on TiO_2, [19]F Magic-Angle Spinning (MAS) NMR analysis was performed.
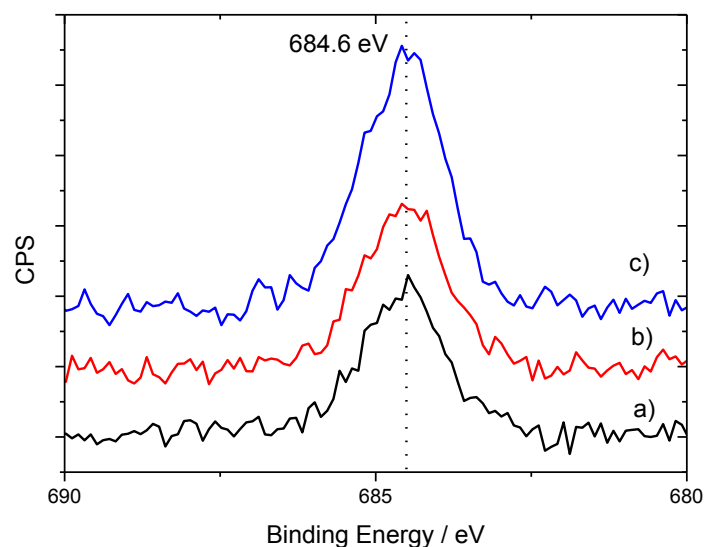
Figure 4.22: Fluorine 1s X-ray Photoelectron Spectroscopy (XPS) analysis of: a) used TiO_2 post-reaction (black line), b) TiO_2 recovered post-reaction using standard reaction conditions but in the absence of both substrate and base (red line) and c) TiO_2 recovered post-reaction using standard reaction conditions but in the absence of substrate (blue line). Standard reaction conditions: 0.2 mmol of DMGA (**1a**), 0.4 mmol Selectfluor®, 0.0125 mmol TiO_2, 4 mL H_2O, 0.23 mmol of K_2CO_3, 25 °C, 10 min.
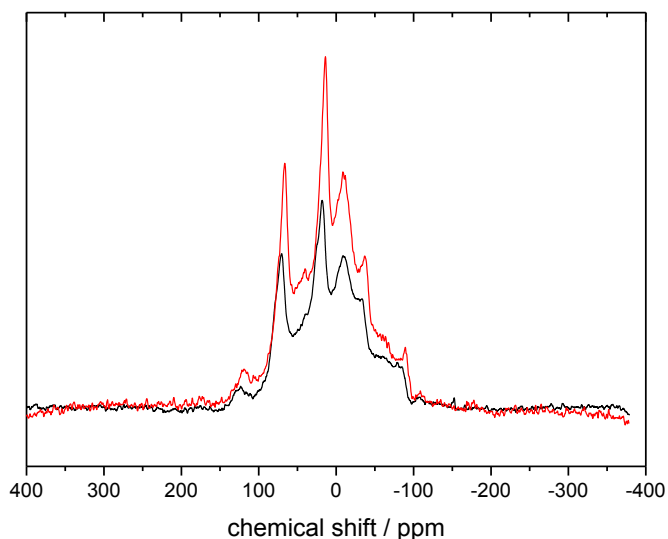
Figure 4.23: Magic-Angle Spinning ^{19}F NMR spectra of used TiO_2 (red line) and TiO_2 treated under standard reaction conditions but in the absence of the substrate (black line). Reaction conditions: 0.2 mmol of DMGA (**1a**) (red line), no substrate (blue line), 0.4 mmol Selectfluor®, 0.0125 mmol TiO_2, 4 mL H_2O, 0.23 mmol of K_2CO_3, 25 °C, 10 min.

As evidenced in the MAS NMR spectrum, all peaks are present in the range of chemical shifts from -100 - 150 ppm, further suggesting the presence of covalent bonds Ti-F. To further investigate the nature of the F-Ti species, the spectrum observed for the used TiO_2 post-reaction (red spectrum in Figure 4.23) was deconvoluted in 3 different main components, at chemical shift values 20, 12 and -9 ppm. Whilst the values 20 and 12 ppm are in good agreement with values reported in literature for Ti-F-Ti species, verifying the formation of Ti-F covalent bonds,[13] the nature of the species with resonance values lower than 0 ppm is still slightly unclear. This may potentially be attributed to the presence of vacancies (Ti_2- -F) as reported by Dambournet.[14-15]
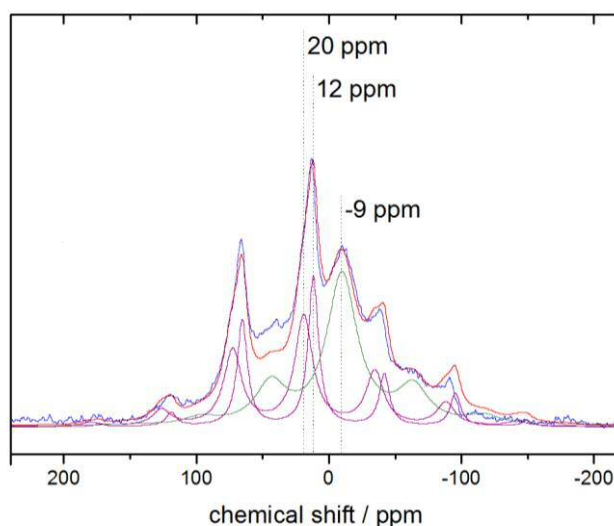
Figure 4.24: Deconvolution of Magic-Angle Spinning ^{19}F NMR spectra of used TiO_2, post-reaction. Reaction conditions: 0.2 mmol of DMGA (**1a**), 0.4 mmol Selectfluor®, 0.0125 mmol TiO_2, 4 mL H_2O, 0.23 mmol of K_2CO_3, 25 °C, 10 min.

According to the spectroscopic data observed so far, a possible route for the formation of the covalent Ti-F bonds observed after reaction can be proposed as follows: photo-activation of TiO_2 with the subsequent formation of Ti^{3+} sites followed by a single electron transfer (SET) between the Selectfluor® and the electron rich Ti^{3+} site, yielding to a radical Selectfuor® species and the Ti-F bond. This mechanism is in analogy with SET mechanism already described (Chapter 1) occurring between Selectfluor® and alkyl radical species.
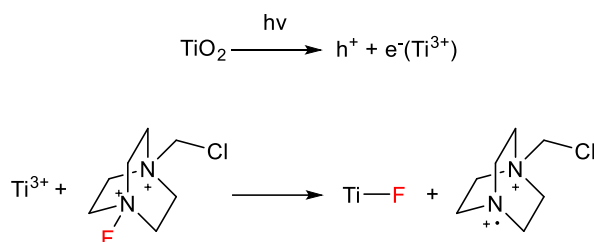
Figure 4.25: Proposed mechanism for the fluorination of TiO$_2$ surface by Selectfluor® in the presence of light.

To investigate the catalytic activity of this fluorinated species, and identify whether its formation is essential for fluorine transfer to be observed, 200 mg of TiO$_2$ was irradiated under standard reaction conditions but in the absence of the substrate. The irradiated sample was found to contain 1.56 wt.% of F (Entry 3, Table 4.2), characterised by an XPS signal at the binding energy of 684.6 eV (blue line in Figure 4.22). The pre-treated sample, containing 0.16 mmol of F, was subsequently employed to perform DMGA (**1a**), decarboxylative fluorination in the absence of other fluorinating agents, *i.e.* Selectfluor®. Although the catalyst containing a sufficient amount of fluorine to permit reaction (0.16 mmol F in total, corresponding to a 1:0.82 DMGA:F ratio) no conversion of DMGA (**1a**) and no yields of 4F4MPA (**1b**) were detected under the standard photo-fluorination conditions over a period of 30 minutes. This fully excludes the possibility of fluorinated-TiO$_2$ species acting as the active fluorinating species, and indicates that the formation of such species is not related to the main catalytic cycle.
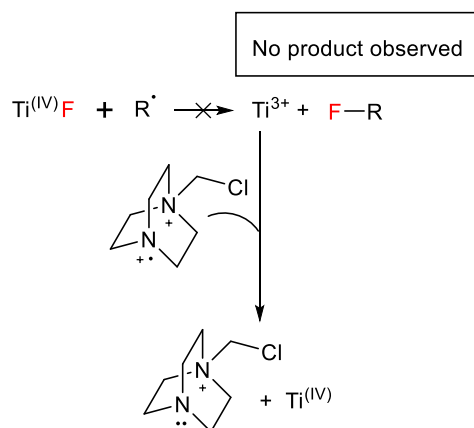
Figure 4.26: Hypothesised reaction mechanism involving Ti-F species as active fluorinating reagent.

Having ruled out the involvement of Ti-F species in the reaction mechanism, a proposed reaction mechanism for TiO_2 photocatalysed decarboxylative fluorination is reported in Figure 4.28. From DRIFT analysis, it is demonstrated that carboxylic acids bind to the TiO_2 surface in their carboxylate form, giving the intermediate **A** (Figure 4.28).[5,6] Simultaneously photoexcitation of TiO_2 with UV light, leads to the formation of electron - hole pairs. Such pairs are known to be stabilized by the presence of various electron donors, such as K_2CO_3. This may account for previous observations regarding the influence of K_2CO_3 concentration on reactivity. Indeed, as reported in Figure 4.10, TiO_2 does not exhibit any catalytic activity when K_2CO_3 is not present into the reaction mixture.

$$TiO_2 \rightarrow e^- + h^+$$
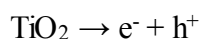
Figure 4.27: Reaction scheme for the formation of electron hole pairs catalysed by TiO_2 in the presence of UV light

The positive holes (h^+) so generated, can subsequently withdraw an electron from the chemisorbed carboxylate species according to the photo-Kolbe reaction,[16] *via* single electron transfer (SET) leading to the generation of a radical species, R-COO•. These radical species, can then decompose (*via* β-scission) to yield CO_2 and an alkyl radical species R•. Alternatively to β-scission, the R-COO• species can interact again with TiO_2 *via* another SET, reestablishing the R-COO⁻ species (intermediate **A**). This can explain why in the absence of Selectfluor®, no consistent yield is observed.

Moreover, the loss of a proton from the substrate could explain the necessity of K_2CO_3, that, may both accelerate the rate of this step, and improve the stability of the electron - hole pairs, which are evidently crucial for catalytic performance.

However, it is well known that Selectfluor® is able to functionalise such radical substrates through SET between unactivated Selectfluor®. Accordingly, it is possible to hypothesise that following decarboxylation, the alkyl radical species, R•, then reacts with Selectfluor® (present in excess) giving the desired R-F product and a radical Selectfluor® species (species **B** in Figure 4.28). This would also account for the negative role played by O_2 in the system, which is well-known to scavenge such alkyl radicals. It is further hypothesised that the radical Selectfluor® species subsequently traps the free e⁻ species formed by the photo-excitation of TiO_2, giving the more stable species **C**, analogous to the mechanism proposed by MacMillan group.[2]
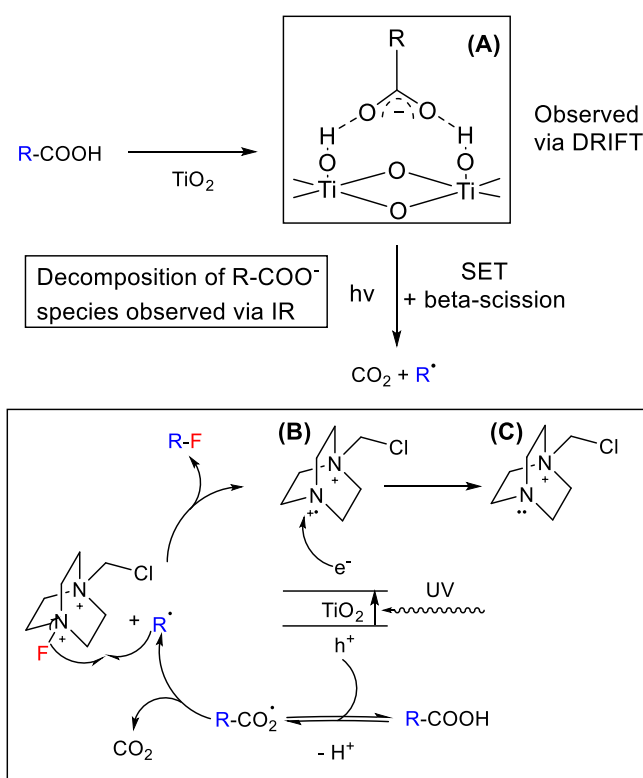
Figure 4.28: Proposed reaction mechanism for TiO_2 photocatalysed decarboxylative fluorination of aliphatic carboxylic acids.

In the absence of TiO$_2$, a slower, alternative pathway may take place, in which Selectfluor® is photoexcited by *hv* photons and radical fluorine species are free to diffuse into the reaction system. This competitive mechanism is further suggested by the lower conversion and yield values observed when the reaction is performed with Selectfluor® and base, in the absence of TiO$_2$ (Figure 4.9).

4.4 Conclusions

In this chapter, the catalytic performances of Ag$_x$O/TiO$_2$ and pure TiO$_2$ were investigated for the decarboxylative fluorination of aliphatic carboxylic acids under photo irradiation conditions. Although activity was observed for both materials, pure TiO$_2$ (unmilled *i.e.* untreated) exhibited the highest levels of catalytic activity. The finding that commercial TiO$_2$, a non-toxic, stable and readily available semiconductor, can be efficiently employed to perform selective decarboxylative fluorination of aliphatic carboxylic acids with Selectfluor® as fluorinating agent, under UV light irradiation, represents an important breakthrough for eventual industrial applications of fluorination process for selective C(sp^3)-F formation.

Further investigation of the catalytic performances of TiO$_2$ also demonstrate that catalytic amounts of TiO$_2$ (1.25 − 6 mol. % of Ti) can result in high levels of TONs and TOFs. In fact, TOF values up to 1113 h^{-1} were observed when using DMGA (**1a**) as substrate, almost twice that of the highest TOF reported by the best homogeneous catalyst found in literature for this reaction,[4] even though some transport limitations may result in an underestimation of the true rate of TiO$_2$. Moreover, the employment of water as solvent, the absence of additional metal into the reaction solution (e.g. Ag), and the facile recovery of TiO$_2$ (efficiently reused up to 4 times), dramatically increases the sustainability of this method over the previous ones.

Spectroscopic studies, including DRIFT, XPS and MAS NMR analysis are also reported in this Chapter, allowing for a better understanding of the reaction mechanism (Figure 4.28).

Both this Chapter and Chapter 3, hence, demonstrate that heterogeneous catalysts are suitable for the selective generation of new C(sp^3)-F bonds. However, despite the

potential of this discovery for industrial applications, in both Chapters pre-functionalised substrates (carboxylic acids) were employed. As previously described in Chapter 1, direct $C(sp^3)$-H fluorinations represent an alternative and more elegant route for the formation of new $C(sp^3)$-F bonds. However, the strong nature of $C(sp^3)$-H bonds makes the activation of these bonds more challenging and harsher reaction conditions are typically required. Thus, the development of heterogenous catalysts for these systems is challenging and despite the high demand for selective fluorinated compounds, industrial processes employing heterogeneous catalysts are yet to be developed.

It is notable, however, for both systems tested in Chapter 3 and Chapter 4, that various by-products indicative of $C(sp^3)$-H functionalisation were observed. For example, when malonic acid and citric acid were employed as substrates, competition between direct $C(sp^3)$-H fluorination and decarboxylative fluorination was demonstrated. The observation of direct C-H fluorination in the aforementioned conditions (both thermal- and photo-catalysed) in heterogeneous catalytic conditions is indeed promising, suggesting that the catalysts reported in Chapter 3 and Chapter 4 could potentially be employed also for direct $C(sp^3)$-H fluorination. Therefore, an investigation of the catalytic performances of heterogeneous catalysts to perform direct $C(sp^3)$-H fluorination employing substrates without carboxylic groups (*i.e.* removing the competition with the decarboxylative fluorination route) will be the focus of Chapter 5.

4.5 References

[1] M. Rueda-Becerril, O. Mahé, M. Drouin, M. B. Majewski, J. G. West, M. O. Wolf, G. M. Sammis, J.-F. Paquin, *J. Am. Chem. Soc.*, 2014, **136** (6), 2637–2641.

[2] S. Ventre, F. R. Petronijevic, D. W. C. MacMillan, *J. Am. Chem. Soc.*, 2015, **137** (17), 5654-5657.

[3] X. Wu, C. Meng, X. Yuan, X. Jia, X. Qian, J. Ye *Chem. Commun.*, 2015, **51**, 11864-11867.

[4] J. A. Porras, I. N. Mills, W. J. Transue, S. Bernhard, *J. Am. Chem. Soc.*, 2016, **138** (30), 9460-9472.

[5] M. A. Henderson, J. M. White, H. Uetsuka, H. Onishi, *J. Am. Chem. Soc.* 2003, **125**, 14974-14975.

[6] D. W. Manley, R. T. McBurney, P. Miller, J. C. Walton, *J. Org. Chem.* 2014, **79**, 1386-1398.

[7] H. Sun, S. Wang, H. M. Ang, M. O. Tadé, Q. Li, *Chem. Eng. J.*, 2010, **162**, 437-447.

[8] J. H. Moss, G. D. Parfitt, A. Wright, *Colloid Polym. Sci.*, 1978, **256**, 1121-1130.

[9] C. Shifu, Y. Yunguang, L. Wei, *J. Hazard. Mater.*, 2011, **186**, 1560-1567.

[10] B. Wen, Y. Li, C. Chen, W. Ma, J. Zhao, *Chem. Eur. J.*, 2010, **16**, 11859-11866.

[11] M. J. Backes, A. C. Lukaski, D. S. Muggli, *Appl. Catal. B Environmental*, 2005, **61**, 21–35.

[12] E. Szabó-Bárdos, B. Baja, E. Horváth, A. Horváth, *J. Photochem. Photobiol. A Chem.* 2010, **213**, 37–45.

[13] W. Li, M. Body, C. Legein, D. Dambournet, *J. Sol. State Chem.*, 2017, **246**, 113-118.

[14] W. Li, M. Body, C. Legein, O. J. Borkiewicz, D. Dambournet, *Inorg. Chem.* 2016, **55**, 7182−7187.

[15] W. Li, M. Body, C. Legein, D. Dambournet, *Cryst. Growth Des.* 2016, **16**, 5441−5447.

[16] S. Sato, *J. Phys. Chem.* 1983, **87** (18), 3531-3537.

Direct C(sp³)-H Fluorination:

Benzylic Fluorination

5

5.1 Introduction

Direct C(sp³)-H fluorination represents one of the biggest challenges within the field of fluorination. Mainly, this is due to the inert nature of the substrates that generally demands the use of harsh reaction conditions. Amongst various species suitable for direct C(sp³)-H fluorination, substrates possessing more reactive benzylic[1-5] and allylic[6] C(sp³)-H bonds represent good target molecules, particular due to their prevalence in biologically relevant compounds.

In recent years, benzylic fluorination has gained increased attention. This is primarily due to the milder reaction conditions required to activate benzylic C(sp³)-H bonds over alkanes bonds. Also, the formation of benzyl fluorides is highly desirable in several fields of the chemical industry, such as the pharmaceutical industry, due to high number of drugs containing benzylic C(sp³)-F bonds.[7-9] Therefore, in addition to providing good target molecules themselves, benzylic substrates also represent a suitable model system for the investigation of the catalytic performances of heterogeneous catalysts to perform direct C(sp³)-H fluorination. Indeed, several reports present in the literature have already shown the potential of this system, proven to be a powerful tool for site-specific C(sp³)-F bond formation through the cleavage of C(sp³)-H bond.[10-12] Although no heterogeneous catalyst (which is generally preferred for industrial applications) has been reported to effectively catalyse benzylic fluorination, in the last decade many milestones have been achieved in the homogeneous field and a few thorough reviews have been published for both mono-[10-12] and di-[13] fluorination of benzylic compounds.

Among these studies, as reported in Chapter 1, different fluorination routes have been explored, including: i) electrophilic fluorination employing Selectfluor®, N-fluoropiridinium salts and NFSI as fluorinating sources,[1-5] ii) nucleophilic fluorination *via* nucleophilic F-donor such as triethylamine trihydrofluoride, TREAT·HF, and fluoride salts[14-16] and iii) radical fluorination with and without radical initiator such as persulfate, photosensitive compounds and the utilisation of light sources (*hv*).[17-19]

Unfortunately, when nucleophilic sources are employed for benzylic fluorination, using Mn complexes (or a Mn porphyrin), the formation of small amounts of oxidised by-products were reported, suggesting possible competition between fluorination and oxidation.[20] Moreover, whilst alternative approaches do not exhibit such competition, they are instead characterised by lower levels of selectivity and lower rates of reaction. Therefore, although some progress has been made in this field, several challenges still remain, including the development of a selective and stable heterogeneous catalyst for selective $C(sp^3)$-H direct fluorination.

In Chapter 3 and Chapter 4, heterogeneous catalysts, such as Ag_2O/TiO_2 and pure commercial titanium dioxide, TiO_2 (P25, Degussa), were found to be active for the selective fluorination of activated substrates (carboxylic acids). It is notable, however, that when these catalysts were employed for the decarboxylative fluorination of certain substrates, such as malonic acid (see Chapter 4) and 2,2-dimethyl-3-phenylpropionic acid (see Chapter 3), competition between decarboxylative fluorination and direct $C(sp^3)$-H fluorination was found to occur to some extent. The observation that the heterogeneous decarboxylative fluorination system can selectively mediate $C(sp^3)$-H fluorination clearly represents a breakthrough. Consequently, in this chapter the ability of these heterogeneous materials to effectively catalyse the direct fluorination of non-activated substrates is investigated. Given their importance as specific target molecules, in addition to their higher levels of reactivity relative to non-activated alkanes, a particular focus is placed on benzylic fluorination.

5.2 Experimental

Whilst spectroscopic and analytical methods are described in Chapter 2, experimental details of the catalytic reactions presented in this Chapter are described below:

5.2.1 Materials

The following materials were used as received without further purification, unless otherwise stated:

- Ethylbenzene, $C_6H_5C_2H_5$ (*99.8%*, ACROS Organics™, Fisher Scientific)

- Deuterated acetone, $(CD_3)_2CO$ (*99.9* atom % D, Sigma Aldrich)

- Deuterium oxide, D_2O (*99.9* atom % D, Sigma Aldrich

- Titanium oxide, TiO_2 (Degussa, P25, *99.5%* trace metal basis, 20 – 30 nm particle size)

- Water, H_2O (HPLC grade, Sigma Aldrich)

- Silver (I) nitrate, $AgNO_3$ (*99.9999%* trace metals basis, Sigma Aldrich)

- Silver (I) oxide, Ag_2O (≥*99.99%* trace metals basis, Sigma Aldrich)

- Silver (I, III) oxide, Ag_2O_2 (Ag_xO, predominantly Ag_2O_2, Sigma Aldrich)

- Poly(vinyl alcohol), PVA (*99%*, Sigma Aldrich)

- Sodium borohydride, $NaBH_4$ (granular, *99.99%* trace metals basis, Sigma Aldrich)

- Selectfluor® fluorinating reagent, F-TEDA (>*95%* in F^+ active, Sigma Aldrich)

- Potassium carbonate, K_2CO_3 (*99.995%* trace metals basis, Sigma Aldrich)

- 2,2-dimethyl-3-phenylpropanoic acid, $C_6H_5CH_2C(CH_3)_2COOH$ (*95.0 %*, Fluorochem Ltd)

- α,α,α-trifluorotoluene, $C_6H_5CF_3$ (anhydrous, ≥*99%*, Sigma Aldrich)

- Acetone, $(CH_3)_2CO$ (Reagent grade, Fisher Scientific)

5.2.2 Definitions

Turnover number (TON) = Moles (product formed)/Moles (metal)

Conversion (X) = Moles (substrate consumed)/Moles (initial substrate) $\times$ 100

Yield (Y) = Moles (product produced)/Moles (initial substrate) $\times$ 100

Selectivity (S) = Yield/Conversion $\times$ 100

5.2.3 Experimental procedures

Details for catalyst preparations and kinetic studies for all the catalysts and reactions presented in this chapter are described herein.

5.2.3.1 Ethylbenzene fluorination

Benzylic fluorination reactions were performed at 55 °C using a single neck 10 mL round bottom flask filled with 1.6 mmol of Selectfluor®, 0.0186 mmol of Ag from

various Ag-containing catalysts and 0.23 mmol of K_2CO_3. For all reactions, N_2 was fluxed into the flask for 5 min, and 4 mL of a solution of ethylbenzene dissolved in a solution $H_2O/(CH_3)_2CO$ (v/v 1:1) (4 mL, 0.05 M, 0.2 mmol) was added to the flask with a syringe. A sample was then withdrawn to calculate the starting concentration of the reagent and the flask was placed into the oil bath at 55 °C, constantly stirred at 700 rpm and the reaction was initiated. During a typical reaction of ethylbenzene fluorination, samples were regularly withdrawn, centrifuged, and 150 μL of the reaction solution was diluted in 500 μL of a standard biphenyl solution (0.05 M in ethanol). The samples were then filtered using a syringe microfilter and transferred into GC vials to be analysed *via* an Agilent technologies 7890B GC system equipped with a GC sampler 80 and a Varian capillary column CP-WAX 52-CB (25m x 0.53 mm x 2 μm, #CP7658). Samples were also regularly analysed *via* ^{19}F and ^{1}H NMR analysis, with and without ^{1}H and ^{19}F decoupling, respectively, to further quantify the amount of product formed (integrating both product and reagent signals respectively and observing the formation of eventual by-products).

5.2.3.2 Catalyst preparation for benzylic fluorinations

Ag nanoparticles supported on TiO_2 were prepared according to the sol-immobilisation method described in Chapter 3, whilst Ag_2O/TiO_2 mixtures prepared *via* mechanochemical mixing at 15 Hz, according to the preparation method described in detail in Chapter 3.

5.2.3.3 Catalyst characterisation and analytical details

^{19}F NMR and GC were employed to study the benzylic fluorination reaction using heterogeneous Ag catalysts. Experimental details for each of these methods is fully described in Chapter 2.

TEM was carried out using a JEOL 2100 with a LaB6 filament operating at 200 kV. Samples were prepared by dispersing the powder catalyst in ethanol and dropping the suspension onto a lacey carbon film over a 300 mesh copper grid.

5.3 Results and discussion

Benzylic fluorinations represent a good method to achieve selective $C(sp^3)$-F bond formation *via* direct $C(sp^3)$-H fluorination. As briefly reported in Chapter 3, when substrates bearing C-H benzylic bonds were employed for decarboxylative fluorination under standard reaction conditions with Ag_xO/TiO_2 catalysts, trace amounts of benzylic fluorinated product were observed (Chapter 3).
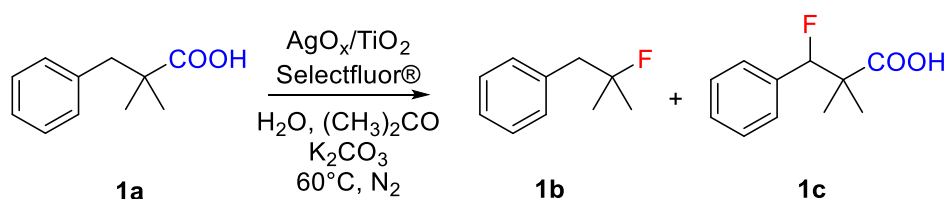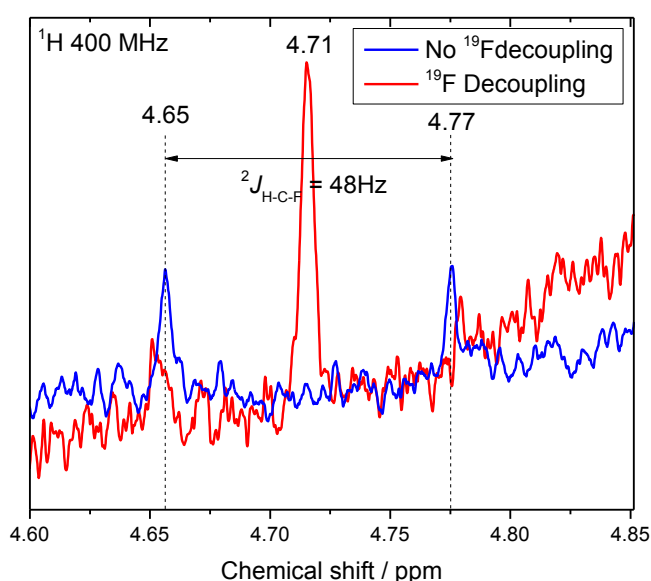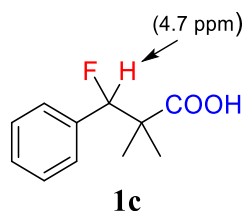

Figure 5.1: Decarboxylative fluorination of 2,2-dimethyl-3-phenylpropionic acid (**1a**) with Selectfluor® as fluorine donor. Reaction conditions: 0.2 mmol of 2,2-dimethyl-3-phenylpropionic acid (**1a**), 0.4 mmol of Selectfluor®, 200 mg $1Ag_2O/TiO_{2(MM)}$ (0.0186 mmol Ag), 2 mL H_2O, 2 mL $(CH_3)_2CO$, 0.115 mmol K_2CO_3, N_2, 60°C.

Interestingly, when 2,2-dimethyl-3-phenylpropionic acid (**1a**) was used as substrate, traces of the corresponding fluorinated product with the fluorine in benzylic position (**1c**) were detected. The presence of **1c** in the crude reaction mixture was demonstrated by comparing ^1H NMR spectra run respectively with and without ^{19}F decoupling (Figure 5.2). In fact, the nuclear spin value ½ related to ^{19}F, naturally abundant in fluorine, originates strong heterocoupling among the two nuclei, ^1H and ^{19}F. Therefore, without decoupling (blue line Figure 5.2), the benzylic proton exhibits a doublet at 4.71 ppm with coupling constant $J = 48$ Hz, in perfect agreement with the coupling constant value typically observed for geminal proton-fluorine coupling ($^2J_{H-C-F} = 48$ Hz). As expected, upon applying ^{19}F decoupling to the NMR experiment, the two signals at 4.65 and 4.77 ppm merged into a singlet centred at 4.71 ppm (red line Figure 5.2), confirming the presence of a fluorine in geminal position to the benzylic hydrogen (**1c**, Figure 5.2). The possibility to detect this product, even in trace amounts, is indeed promising, indicating that, although the presence of a more reactive group (*i.e.* -COOH), direct $C(sp^3)$-H fluorination can occur in these conditions. Hence, an investigation into the capability of this catalyst ($1Ag_2O/TiO_{2(15Hz)}$) to perform $C(sp^3)$-H fluorination via benzylic fluorination, in the absence of more reactive carboxylic

groups, will be performed and presented in the following section, using ethylbenzene as substrate.

Figure 5.2: ^{1}H NMR spectrum with (red line) and without (blue line) [19]F (region 4.6-4.85 ppm) of crude reaction for 2,2-dimethyl-3-phenylpropionic acid (**1a**) decarboxylative fluorination. Reaction conditions: 0.2 mmol of 2,2-dimethyl-3-phenylpropionic acid (**1a**), 0.4 mmol of Selectfluor®, 200 mg 1Ag$_2$O/TiO$_{2(MM)}$ (0.0186 mmol of Ag), 2 mL D$_2$O, 2 mL (CD$_3$)$_2$CO, 0.115 mmol K$_2$CO$_3$, N$_2$, 60°C.

5.3.1 Benzylic fluorination of ethylbenzene

In order to correctly investigate the catalytic performances of supported silver catalysts (Ag$_x$O/TiO$_2$) to activate benzylic positions, in the absence of the more favourable decarboxylative fluorination pathway, ethylbenzene was employed as substrate under optimised reaction conditions.
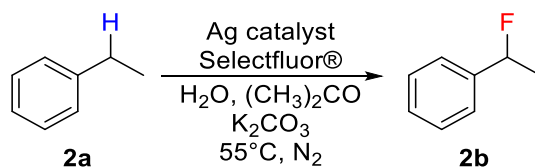
Figure 5.3: General scheme for benzylic fluorination of ethylbenzene (**2a**) to yield 1-fluoroethylbenzene (**2b**) with Ag-containing heterogeneous catalysts and Selectfluor® as fluorine donor. General reaction conditions: 0.2 mmol of ethylbenzene (**2a**), 1.6 mmol of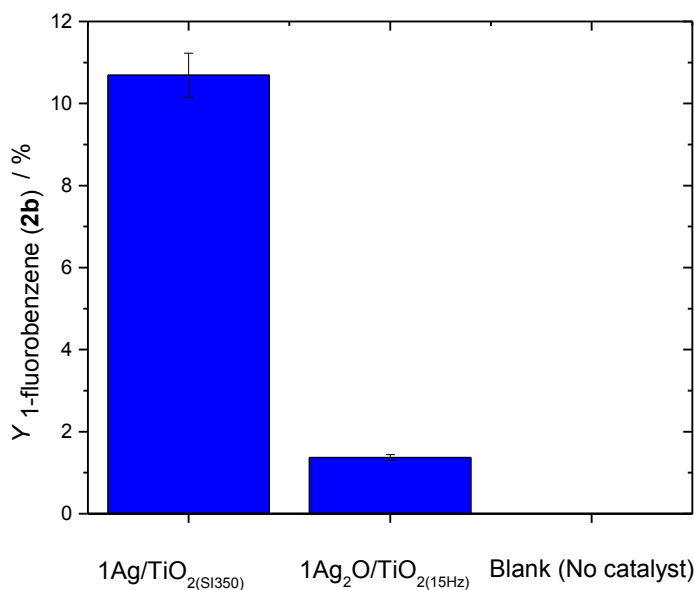 Selectfluor®, 200 mg $1Ag_2O/TiO_{2(MM)}$ (0.0186 mmol of Ag), 2 mL D_2O, 2 mL $(CD_3)_2CO$, 0.115 mmol K_2CO_3, N_2, 60°C.

In a preliminary analysis, two different types of Ag_xO/TiO_2 materials were prepared and employed for benzylic fluorination of a model substrate, ethylbenzene (**2a**). Following the results reported in Chapter 3, i) 1 wt. % Ag nanoparticles supported on titanium dioxide prepared *via* sol immobilisation, calcined at 350°C, $1Ag/TiO_{2(SI350)}$, and ii) (1 wt. % Ag) mechanochemical mixture Ag_2O/TiO_2 milled in a ball mill at a frequency of 15 Hz, $1Ag_2O/TiO_{2(15Hz)}$, were identified as the most suitable catalysts. In fact, despite different preparation procedures, these two catalysts exhibited similar catalytic properties for the decarboxylative fluorination of aliphatic carboxylic acids. However, whilst similar activity is reported for decarboxylative fluorination (Chapter 3), different catalytic performances of $1Ag_2O/TiO_{2(15Hz)}$ and $1Ag/TiO_{2(SI350)}$ may potentially be observed for benzylic fluorination reaction, due to the different preparation procedure of the two catalysts which leads to different Ag speciation and different particles size distribution in the resultant catalysts.

Figure 5.4: 1-Fluoroethylbenzene (**2b**) yield at 4 hours with: i) 1Ag/TiO2(SI350), ii) 1Ag2O/TiO2(15Hz), and iii) without solid catalyst. Reaction conditions: 0.2 mmol of ethylbenzene (**2a**), 1.6 mmol of Selectfluor®, 0.0186 mmol of Ag, 1 mL D2O, 3 mL (CD3)2CO, 0.115 mmol K2CO3, N2, 55°C.

As shown in Figure 5.4, Ag catalysts supported on TiO_2 are able to perform benzylic fluorination *via* direct C-(sp^3)-H fluorination. In fact, although at different extents, with both catalysts, 1-fluoroethylbenzene (**2b**) was observed in the post-reaction mixture, when analysed *via* GC-MS, ^{1}H and ^{19}F NMR. Notably, a control experiment without the catalyst was performed, to verify the catalytic activity of the material. Demonstrating solid catalyst to be essential to the reaction, no desired product was observed at all in the first hour of reaction, with no trace of 1-fluoroethylbenzene (**2b**) achieved after 4 hours, thus demonstrating that Selectfluor® alone is not enough to allow catalytic conversion of ethylbenzene (**2a**) into 1-fluoroethylbenzene (**2b**) and the catalyst is essential.

However, although similar activity was observed for both 1Ag/TiO$_{2(SI350)}$ and 1Ag$_2$O/TiO$_{2(15Hz)}$ for decarboxylative fluorination reactions (Chapter 3), different catalytic activities were observed for benzylic fluorination. The different behaviour exhibited by 1Ag/TiO$_{2(SI350)}$ and 1Ag$_2$O/TiO$_{2(15Hz)}$ may indicate that different reaction mechanisms are involved in benzylic fluorination and decarboxylative fluorination. Indeed, whilst 10.6 % yield of 1-fluoroethylbenzene were detected for 1Ag/TiO$_{2(SI350)}$,

only 1.4 % yield was observed using $1Ag_2O/TiO_{2(15Hz)}$. In the absence of advanced characterisation studies, definitive structure-activity relationships cannot be formed. However, several possible factors could account for this observation, such as particle size effects, changes to the speciation of Ag, crystallinity effects and different surface area. Indeed, preliminary analysis of $1Ag/TiO_{2(SI350)}$ and $1Ag_2O/TiO_{2(15Hz)}$ by Transmission Electron Microscopy (TEM) reveals there to be a substantial difference in the particle size of Ag by preparation method. TEM microscopy of $1Ag/TiO_{2(SI)}$, potentially reveals the presence of nanoparticles, in a range 1 - 10 nm (Figure 5.5). Notably, Ag oxides are challenging to observe *via* TEM, due to similar transmission with the support material (TiO_2). In fact, the presence of oxygen in Ag oxides greatly reduces the contrast between Ag oxides and TiO_2. However, good quality microscopy was observed with $1Ag/TiO_{2(SI)}$ uncalcined, due to the high amount of metallic Ag. Therefore, whilst preliminary microscopy can be only indicative of the size of the particles, high resolution techniques (*e.g.* Scanning Transmission Electron Microscopy, STEM) able to provide microscopy with higher contrast, are required for more detailed analysis. In contrast to $1Ag/TiO_{2(SI)}$, TEM analysis of $1Ag_2O/TiO_{2(15Hz)}$ revealed large Ag agglomerates, in a range $0.5 - 1$ μm, to be present on the catalyst (Figure 5.6).
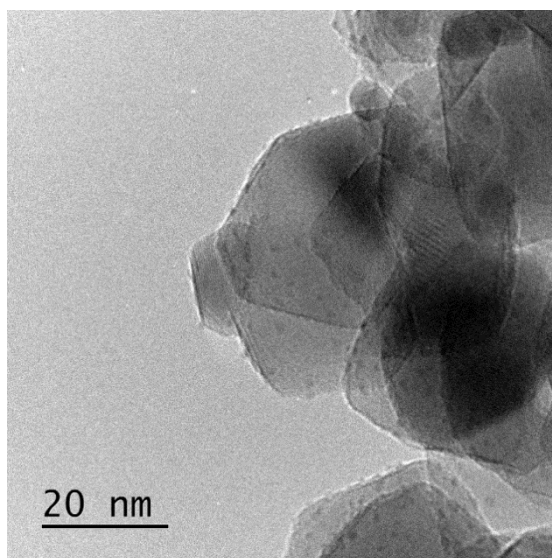
Figure 5.5: TEM image of 1Ag/TiO2(SI) uncalcined.
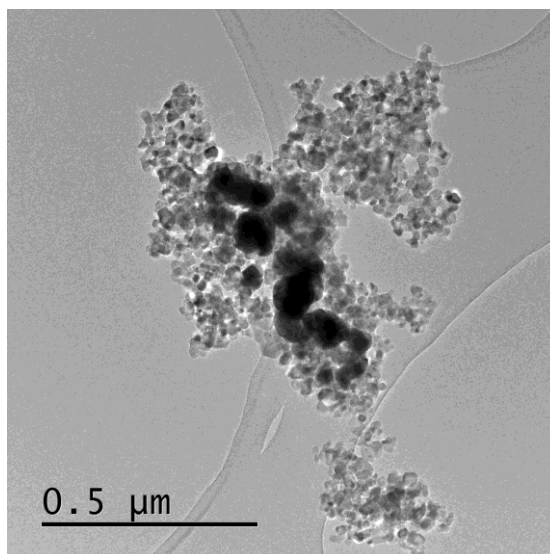
Figure 5.6: TEM image of 1Ag$_2$O/TiO$_{2(15Hz)}$.

Whilst Ag particles in a range of 0.5 - 1 μm are observed on Ag catalysts prepared using a ball mill, Ag nanoparticles in a range 1-10 are potentially formed (only evidenced on an uncalcined sample) using the sol immobilisation technique. The different Ag particle size observed for the two different preparation procedures, may, therefore, account for the difference in activity of the two catalysts for benzylic fluorination, however, further spectroscopic and/or microscopic studies would be required for more detailed analysis.

5.3.2 Time on line analysis of ethylbenzene fluorination

To better understand the performance of the system, in addition to gaining valuable information on the reaction mechanism, time on line analysis of the best catalyst 1Ag/TiO$_{2(SI350)}$ was performed.
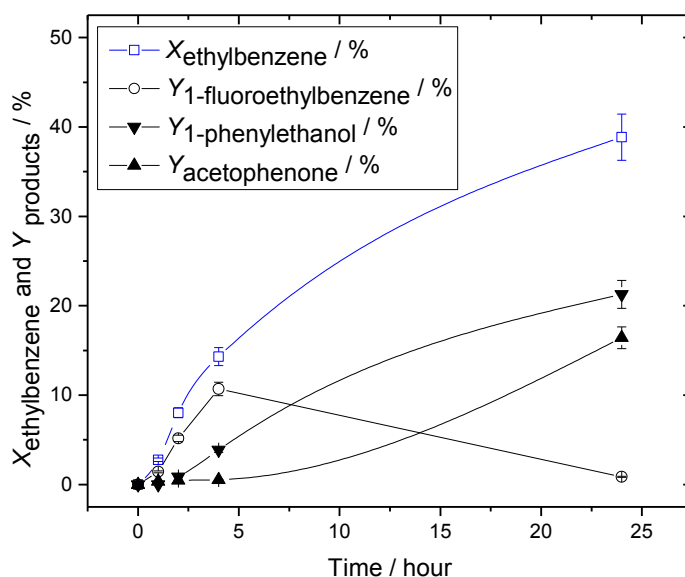
Figure 5.7: Conversion of ethylbenzene (**2a**) (blue line) and products yields (black lined) with time over 1Ag/TiO$_{2(SI350)}$. Reaction conditions: 0.2 mmol of ethylbenzene (**2a**), 1.6 mmol of Selectfluor®, 200 mg of 1Ag/TiO$_{2(SI350)}$ (0.0186 mmol of Ag), 1 mL D$_2$O, 3 mL (CD$_3$)$_2$CO, 0.115 mmol K$_2$CO$_3$, N$_2$, 55°C.

As shown in Figure 5.7, high selectivity towards the fluorinated product is observed in the first hours of reaction, with 14 % of ethylbenzene (**2a**) conversion and 11 % of 1-fluoroethylbnzene (**2b**) yield detected after 4 hours of reaction. Oxidised product, such as 1-phenylethanol and acetophenone were also observed, indicating the presence of a competitive oxidative pathway, leading to the formation of oxidised product. The formation of oxidised products could be due to several reasons, such as i) residual presence of O$_2$ in the reaction flask and in the solvents, ii) high oxidative potential of Selectfluor®, and iii) presence of H$_2$O, used as solvent. However, whilst small amounts of 1-phenylethanol (**2c**) and acetophenone (**2d**) were observed in the first hours of reaction, with ~ 70 % and 30 % selectivity for fluorinated product and oxidised products, respectively, completely different selectivity was detected after prolonged reaction time. In fact, whilst high selectivity was observed for both 1-phenylethanol (**2c**) and acetophenone (**2d**) at 24 hours, less than 1 % of yield of 1-fluoroethylbenzene (**2b**) was obtained, suggesting its instability in the reaction mixture.
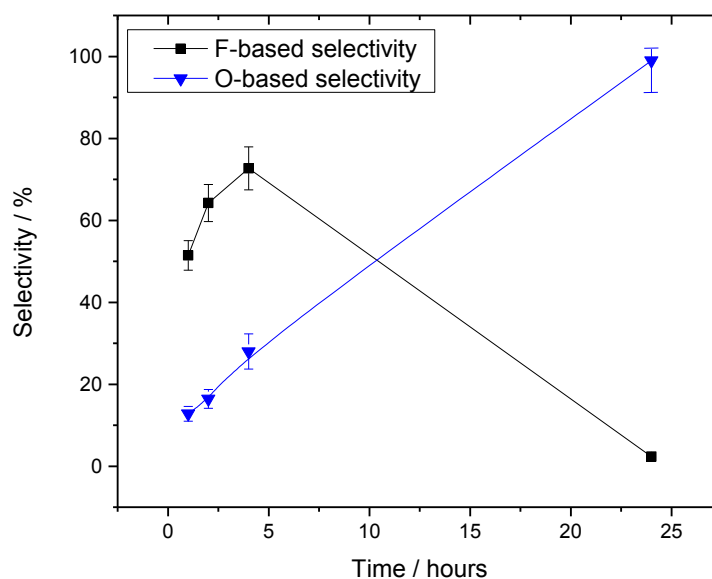
Figure 5.8: F-based selectivity (black squares) and O-based selectivity (blue triangles) with time.

The different product distribution detected over time, with high selectivity for the fluorinated product over short reaction time but high oxygen based selectivity (sum of selectivity for 1-phenylethanol (**2c**) and acetophenone (**2d**)) over extended reaction times, suggests that whilst the fluorination pathway is favoured up to 4 hours, the competitive oxidative pathway is favoured at 24 hours.

A representative scheme of competition between oxidation and fluorination is reported in Figure 5.9. Notably, the dashed arrow between 1-fluoroethylbenzene (**2b**) and the oxidised products (1-phenylethanol (**2c**) and acetophenone(**2d**)) indicates the potential conversion of 1-fluoroethylbenzene (**2b**) into 1-phenylethanol (**2c**) and acetophenone (**2d**), due to the instability of 1-fluoroethylbenzene (**2b**) in the reaction mixture.
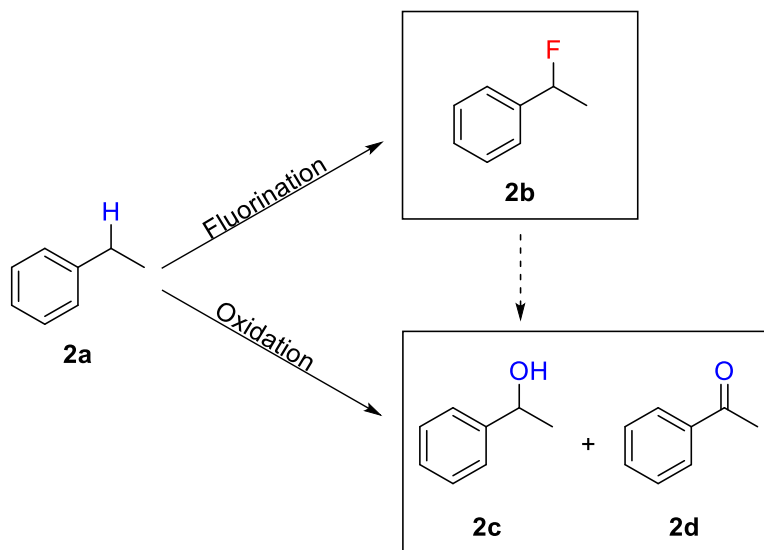
Figure 5.9: Schematic illustration of fluorination/oxidation competitivity. Dashed arrow represents possible decomposition of 1-fluoroethylbenzene (**2a**) to give 1-phenylethanol (**2c**) and subsequently acetophenone (**2d**).

The data reported in this section demonstrates that $1Ag/TiO_{2(SI350)}$ is able to activate benzylic $C(sp^3)$-H bonds yielding new $C(sp^3)$-F bonds. However, an oxidative competitive reaction pathway was also observed, favourable at long reaction time. A possible reason for the different selectivity detected over time, is due to the eventual consumption of active F^+ source, Selectfluor®.

5.3.3 Investigation of activity and selectivity of Selectfluor®

As briefly discussed in the previous section, the low fluorine selectivity observed after 4 hours of reaction could be due to the consumption of active Selectfluor®, i.e. consumption of the active F^+ source, highlighted in red in the following figure.
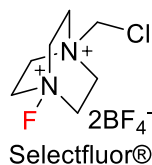
Selectfluor®

Figure 5.10: Chemical structure of Selectfluor® fluorinating agent.

In fact, as discussed in Chapter 1, homolytic cleavage of the N-F bond can occur under reaction conditions, thus releasing a Selectfluor® radical species (**3b**), capable of

withdrawing an electron from other species present in solution, thus making Selectfluor® radical species, a strong oxidant.
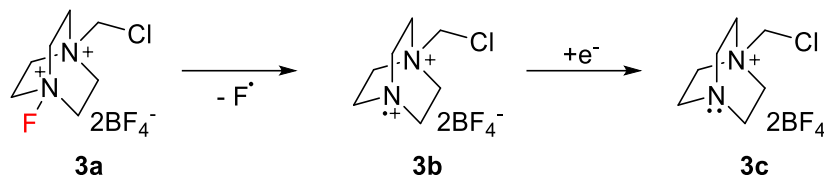
Figure 5.11: Possible mechanism for consumption of active Selectfluor® (**3a**).

Formation of Selectfluor® radical species (**3b**), as well as consumption of active fluorinated Selectfluor® (**3a**), could explain the increasing of selectivity for oxidised products (1-phenylethanol (**2c**) and acetophenone (**2d**)) as well as the dramatic drop in selectivity towards 1-fluoroethylbenzene (**2b**) upon increasing reaction times, previously observed.

Therefore, to investigate the activity and stability of Selectfluor®, a blank experiment was performed, under classic reaction conditions albeit in the absence of the $1Ag/TiO_{2(SI350)}$. During this experiment, GC and ^{19}F NMR analysis were both performed to: i) analyse and quantify reaction products produced in the absence of the catalyst, and ii) monitor the consumption of active fluorinated Selectfluor® (**3a**). The relative amount of **3a** present in the reaction mixture can, in fact, be measured by integration of the signal of the active $F^{\delta+}$ resonating at positive chemical shift (46.95 ppm) against the signal of α,α,α-trifluorotoluene, $C_6H_5CF_3$ (-63.72 ppm), used as internal standard, and BF_4^- present in Selectfluor (-151.11 ppm).

GC analysis of the reaction mixture revealed that, whilst 1-fluoroethylbenzene (**2b**) was not formed at all in the absence of solid catalyst ($1Ag/TiO_{2(SI350)}$), traces of 1-phenylethanol and acetophenone (yield ≤ 1 %) were observed after prolonged reaction timeframes, up to 24 hours. The formation of only trace amounts of oxidised products, indicates that the solid catalyst is essential for the synthesis of both fluorinated product and oxidised by-products. Thus, indicating that radical Selectfluor® species (**3b**) alone are not sufficient to oxidise ethylbenzene (**2a**) into 1-phenylethanol (**2c**) and acetophenone (**2d**).

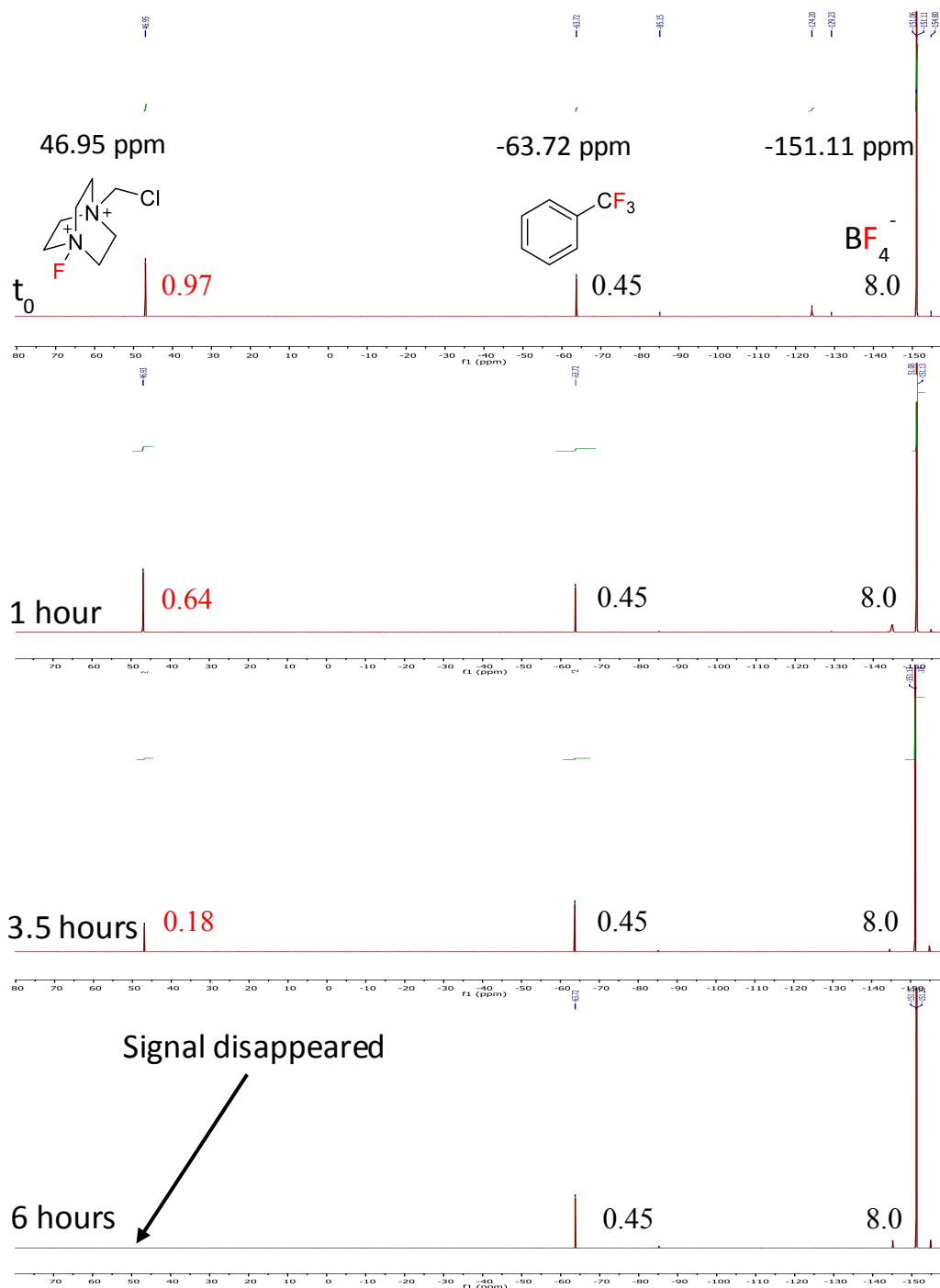To understand the stability of Selectfluor® (**3a**) in the reaction mixture, ^{19}F NMR spectra of the reaction mixture were recorded at different reaction times, up to 6 hours (Figure 5.12), particularly focusing on the signal of F$^{\delta+}$ resonating at a chemical shift of 46.95 ppm.

Figure 5.12: ^{19}F NMR spectra of benzylic fluorination at different time, up to 6 hours of reaction. Reaction conditions: 0.2 mmol of ethylbenzene (**2a**), 1.6 mmol of Selectfluor®, 1 mL H$_2$O, 3 mL (CH$_3$)$_2$CO, 0.115 mmol K$_2$CO$_3$, N$_2$, 55°C.

As shown in Figure 5.12, the signal of F $^{\delta+}$ at 46.95 ppm decreased with time, until totally disappearing following 6 hours of reaction. This demonstrates that, although 1-fluoroethylbenzene (**2b**) is not formed at all without solid catalyst, Selectfluor® (**3a**) is not fully stable in the reaction mixture, potentially undergoing homolytic cleavage of the N-F bond. Nevertheless, the continuous decreasing of active F$^{\delta+}$ sources, can explain the decreasing of F-based selectivity previously observed in Figure 5.8. In fact, the high selectivity for 1-fluoroethylbenzene (**2b**) observed in the first hours of reaction can be accountable to the high availability of active Selectfluor® species (**3a**). At the same time, the drop of selectivity observed after 4 hours of reaction can be due to the missing of active F$^+$ sources, demonstrated by the complete disappearance of the signal at 46.95 ppm in the ^{19}F NMR spectra.

In order to identify other fluorinated species formed upon decomposition of Selectfluor® (**3a**), more detailed GC-MS analysis of the reaction mixture was performed. During GC-MS analysis, fluoroacetone (**4**), a highly toxic compound, was found, indicating reaction between the co-solvent, $(CH_3)_2CO$, and Selectfluor® (**3a**).
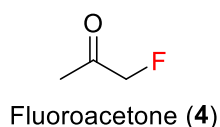
Fluoroacetone (**4**)

Figure 5.13: Chemical structure of fluoroacetone.

The presence of a very toxic compound (fatal if swallowed, inhaled and/or upon contact with skin) in the reaction mixture represents a large problem for the applicability of the system, due to safety issues. Thus, in order to have true feasibility of the system, several attempts to minimise/avoid the presence of fluoroacetone were performed.

5.3.4 Screening of alternative solvents

Following GC-MS analysis of the reaction mixture, fluoroacetone (**4**) was found in the reaction mixture, formed upon reaction of Selectfluor® with $(CH_3)_2CO$, needed as co-solvent to solubilise ethylbenzene (**2a**) in the reaction mixture. Therefore, to fully remove the presence of fluoroacetone (**4**) from the reaction mixture, improving the viability of the system, alternative co-solvents were explored in order to replace $(CH_3)_2CO$. Amongst them, tetrahydrofuran (THF) and acetonitrile (ACN) were found

as suitable co-solvents, able to dissolve ethylbenzene (**2a**) in the reaction mixture. However, when a THF/H$_2$O (v/v 1:1) mixture was used as solvent, no fluorinated product (1-fluoroethylbenzene (**2b**)) and no oxidised by-products (1-phenylethanol (**2c**) and acetophenone (**2d**)) were found in the reaction mixture, indicating that benzylic fluorination does not occur when using THF/H$_2$O (v/v 1:1) as solvent. In contrast, using ACN/H$_2$O (v/v 1:1) as solvent, a small amount of 1-fluoroethylbenzene (**2b**), up to 4 % of yield, was found in the first hour of reaction. Nevertheless, the reaction appears to cease after the first hour of reaction and no yield higher than 4 % was detected. The complete cessation of the reaction after 1 hour may be due to several reasons, including a possible negative effect of ACN on the catalytic performance of the catalyst, that may be deactivated/poisoned by the presence of ACN. Therefore, although THF and ACN were found suitable to solubilise ethylbenzene in the reaction mixture, a negative effect of the catalytic performance of 1Ag/TiO$_2$(SI350) was observed, potentially due to deactivation of the material in the different solvent.
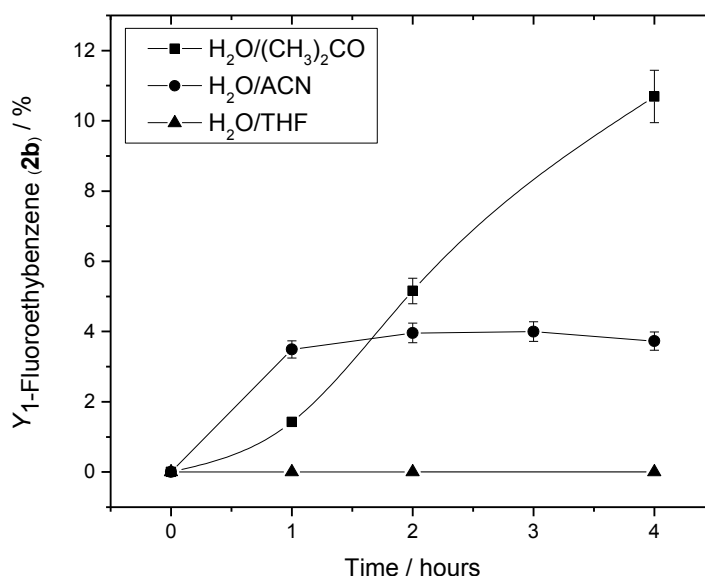
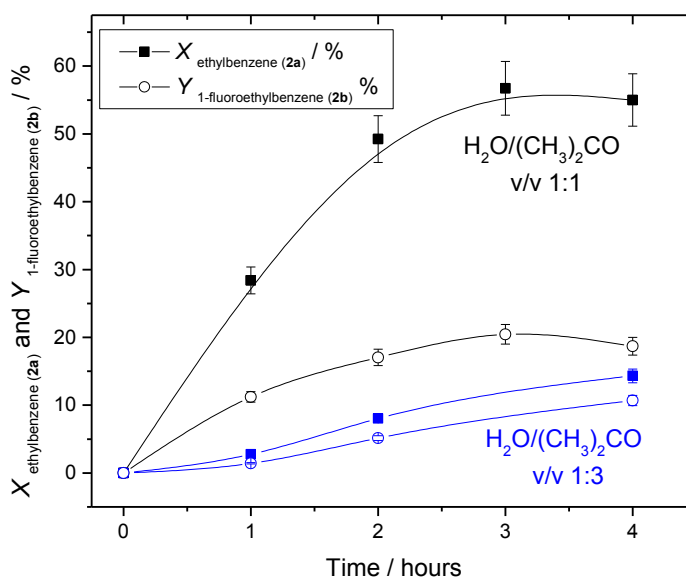**Figure 5.14:** Yield of 1-fuoroethylbenzene (**2b**) with time over 1Ag/TiO$_2$(SI350) with various solvent mixtures: i) H$_2$O/(CH$_3$)$_2$CO (v/v 1:3) (black squares), ii) H$_2$O/ACN (v/v 1:1) (black circles), and H$_2$O/THF (v/v 1:1) (black triangle). Reaction conditions: 0.2 mmol of ethylbenzene (**2a**), various amount of Selectfluor®, 0.0093 mmol of Ag, 4 mL of solvent, 0.115 mmol K$_2$CO$_3$, N$_2$, 55°C.

Because of the absence of a suitable solvent that can successfully replace (CH$_3$)$_2$CO, and therefore completely avoiding the generation of fluoroacetone (**4**), a different approach to reduce the presence of this toxic compound in the reaction mixture, was explored by decreasing the amount of (CH$_3$)$_2$CO and Selectfluor® emoployed to perform benzylic fluorination.

5.3.5 Effect of Selectfluor® concentration on activity and selectivity

As reported in the previous sections of this Chapter, the presence of fluoroacetone (**4**), formed upon interaction between Selectfluor® (**3a**) and (CH$_3$)$_2$CO, strongly affects the applicability of the system under study. In the previous section, a first attempt to find an alternative solvent was performed. However, unfortunately, no other solvent was found to be suitable to perform ethylbenzene fluorination with good activity and selectivity. Thus, instead of completely removing fluoroacetone (**4**) from the reaction mixture, another approach, in order to reduce the amount of fluoroacetone (**4**) generated in solution, was adopted by; i) decreasing the amount of (CH$_3$)$_2$CO and ii) using lower quantities of Selectfluor® (**3a**).

Firstly, the ratio H$_2$O/(CH$_3$)$_2$CO was adjusted to v/v 1:1 (instead of v/v 1:3), and an experiment was performed using typical amount (8 equivalents) of Selectfluor®. Notably, higher ratio H$_2$O/(CH$_3$)$_2$CO was unsuitable due to the low solubility of the substrate, ethylbenzene (**2a**), in neat H$_2$O.
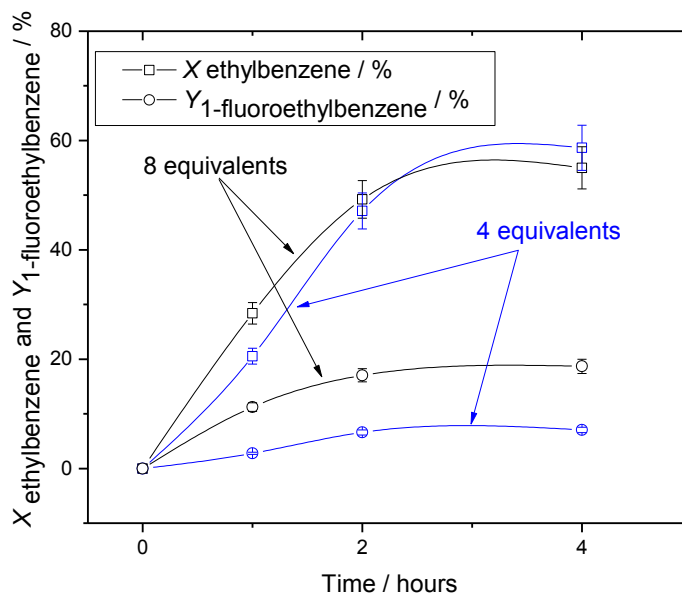
Figure 5.15 Conversion of ethylbenzene (**2a**) (hollow squares) and yield of 1-fuoroethylbenzene (**2b**) (hollow circles) with time over 1Ag/TiO$_{2(SI350)}$ with i) ratio H$_2$O/(CH$_3$)$_2$CO (v/v 1:1) (black symbols) and ii) ratio H$_2$O/(CH$_3$)$_2$CO (v/v 1:3) (blue symbols). Reaction conditions: 0.2 mmol of ethylbenzene (**2a**), 1.6 mmol of Selectfluor®, 200 mg of 1Ag/TiO$_{2(SI350)}$ (0.0186 mmol of Ag), 0.115 mmol K$_2$CO$_3$, N$_2$, 55°C.

Interestingly, upon increasing the relative ratio of H$_2$O/(CH$_3$)$_2$CO to (v/v 1:3) and using the amount of Selectfluor® typically employed for benzylic fluorination reactions (8 equivalents), 57% conversion of ethylbenzene (**2a**) and a 1-fluoroethylbenzene (**2b**) yield of 21% was achieved after 3 hours of reaction. However, under the same reaction conditions a drop in the yield of 1-fluoroethylbenzene (**2b**) was observed following the first hours of reactions, as already observed for H$_2$O/(CH$_3$)$_2$CO ratio (v/v 1:3) (Figure 5.15). Nevertheless, higher activity as exhibited from 1Ag/TiO$_{2(SI350)}$ using H$_2$O/(CH$_3$)$_2$CO ratio (v/v 1:3) was noted. The higher activity observed by the catalyst in the presence of lower amount of (CH$_3$)$_2$CO co-solvent can be due to several reasons, including; a negative effect (such as poisoning) of (CH$_3$)$_2$CO on the catalytic material (1Ag/TiO$_{2(SI350)}$). However, whilst a higher activity was demonstrated under the new conditions, lower 1-fluoroethylbenzene (**2b**) selectivity was also observed, potentially due to the higher amount of H$_2$O, which may favour oxidation reaction leading to higher amounts of oxidised by-products. Notably, despite decreasing the amount of (CH$_3$)$_2$CO, high amounts of fluoroacetone (**4**) were still observed upon analysis *via* GC-MS.

In another attempt to reduce the amount of fluoroacetone (**4**), another experiment was performed whereby the amount of Selectfluor® was halved (using $H_2O/(CH_3)_2CO$ ratio v/v 1:1).

Figure 5.16: Ethylbenzene (**2a**) conversion (hollow squares) of ethylbenzene (**2a**) and 1-fluoroethylbenzene (**2b**) yield (hollow circles) with time over $1Ag/TiO_{2(SI350)}$ with 4 equivalents (blue symbols) and 8 equivalents (black symbols) of Selectfluor®. Reaction conditions: 0.2 mmol of ethylbenzene (**2a**), various amount of Selectfluor®, 200 mg of $1Ag/TiO_{2(SI350)}$ (0.0186 mmol of Ag), 2 mL H_2O, 2 mL $(CH_3)_2CO$, 0.115 mmol K_2CO_3, N_2, 55°C.

As shown in Figures 5.16 and 5.17, upon halving the amount of Selectfluor® (**3a**), a significant decrease in the yield of 1-fluoroethylbenzene (**2b**) was observed, whilst similar activity was detected (*i.e.* similar ethylbenzene (**2a**) conversions), thus indicating similar reaction rate. However, a drop in selectivity was observed, highlighted in Figure 5.17, reporting the selectivity for 1-fluoroethylbenzene (**2b**) as a function of ethylbenzene (**2a**) conversion.
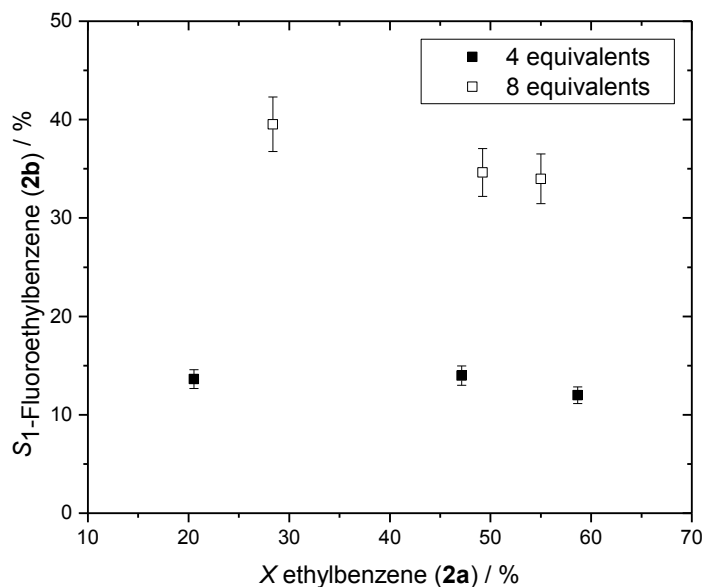
Figure 5.17: Selectivity for 1-fuoroethylbenzene (**2b**) over ethylbenzene (**2a**) conversion with 8 equivalents (hollow squares) and 4 equivalents (solid squares) of Selectfluor®. Reaction conditions: 0.2 mmol of ethylbenzene (**2a**), various amount of Selectfluor®, 200 mg of $1Ag/TiO_{2(SI350)}$ (0.0186 mmol of Ag), 2 mL H_2O, 2 mL $(CH_3)_2CO$, 0.115 mmol K_2CO_3, N_2, 55°C.

Despite achieving similar rates, a decrease in selectivity was observed, clearly demonstrating the need for high concentrations of Selectfluor®, similar activity rates observed with 4 and 8 equivalents of Selectfluor®, the large decrease of selectivity observed when 4 equivalents of Selectluor® were employed (from ~ 40 % ~ 14 %), albeit the high amount of Selectfluor® still present in the reaction mixture indicates that large excess of Selectfluor® is required to desirable product yields.

5.4 Conclusions

In this chapter, the catalytic performances of Ag-containing heterogeneous catalysts to perform direct $C(sp^3)$-H fluorination with electrophilic/radical F sources (*i.e.* Selectfluor®) was investigated, with a particular focus placed on benzylic fluorination reactions. Following the observations made in Chapter 3, where by-products fluorinated in benzylic positions were found when specific substrates (such as 2,2-dimethyl-3-phenylpropionic acid (**1a**)) were employed as substrates, two different types of Ag-containing material ($1Ag/TiO_{2(SI350)}$ and $1Ag_2O/TiO_{2(15Hz)}$) were tested for direct benzylic fluorination. However, whilst similar catalytic performances were observed

for decarboxylative fluorination (see Chapter 3), different performances were exhibited by $1Ag/TiO_{2(SI350)}$ and $1Ag_2O/TiO_{2(15Hz)}$, for benzylic fluorination, suggesting two different reaction pathways for the two reactions.

A deeper investigation of the catalytic performances of the best catalyst, $1Ag/TiO_{2(SI350)}$, was then performed. Unfortunately, whilst $1Ag/TiO_{2(SI350)}$ was shown to be active to some extent for benzylic fluorination reactions, several problems were identified. These include: i) a dramatic decrease in fluorination selectivity at extended reaction periods (> 4 hours); ii) competition between fluorination and oxidation pathways, with oxidised products, such as 1-phenylethanol and acetophenone being detected; iii) low stability of 1-fluoroethylbenzene, the primary product of the reaction; iv) requirements for large excesses of Selectfluor® (substrate/Selectfluor® ratio = 1/8); and v) the formation of highly toxic by-products, such as fluoroacetone. The poor atomy economy exhibited by this system, coupled with the other disadvantages described above, dramatically affect its applicability. Whilst experiments focused upon overcoming these disadvantages were performed, no suitable compromise between activity, atom economy and safety was identified. Nevertheless, the system still represents an interesting system from mechanistic perspective, and, considering the high demand for benzylic fluorides, may be worthy of future investigation (see Chapter 7).

Although this Chapter indicates that heterogeneous catalysts can perform challenging $C(sp^3)$-H direct fluorination, poor system viability has been observed. This can be largely attributed to the source of the fluorine donor (electrophilic/radical fluorine source, Selectfluor®). Consequently, the following chapter will focus on the investigation of a different type of system to achieve direct $C(sp^3)$-H fluorination, using a Mn porphyrin as catalyst, and avoiding the employment of electrophilic fluorine sources such as Selectfluor®.

5.5 References

[1] K. L. Hull, W. Q. Anani, M. S. Sanford, *J. Am. Chem. Soc.* 2006, **128**, 7134−7135.

[2] S. Bloom, C. R. Pitts, R. Woltornist, A. Griswold, M. G. Holl, T. Lectka, *Org. Lett.* 2013, **15**, 1722−1724.

[3] K. B. McMurtrey, J. M. Racowski, M. S. Sanford, *Org. Lett.* 2012, 14, 4094−4097.

[4] S. Bloom, C. R. Pitts, D. C. Miller, N. Haselton, M. G. Holl, E. Urheim, T. Lectka, *Angew. Chem. Int. Ed*. 2012, **51**, 10580 –10583.

[5] P. Xu, S. Guo, L. Wang, P. Tang, *Angew. Chem. Int. Ed*. 2014, **53**, 5955 –5958.

[6] M.-G. Braun, A. G. Doyle, *J. Am. Chem. Soc*., 2013, **135** (35), 12990–12993.

[7] K. Müller, C. Faeh, F. Diederich, *Science*, 2007, **317**, 1881-1886.

[8] W. K. Hagmann, *J. Med. Chem*., 2008, **51**, 4359-4369.

[9] S. Purser, P. R. Moore, S. Swallow, V. Gouverneur, *Chem. Soc. Rev*., 2008, **37**, 320–330.

[10] P. A. Champagne, J. Desroches, J. D. Hamel, M. Vandamme, J. F. Paquin, *Chem. Rev*., 2015, **115**, 9073–9174.

[11] T. Liang, C. N. Neumann, T. Ritter, *Angew. Chem. Int. Ed.,* 2013, **52**, 8214–8264.

[12] C. Hollingworth, V. Gouverneur, *Chem. Commun*., 2012, **48**, 2929-2942

[13] A. Koperniku, H. Liu, P. B. Hurley, *Eur. J. Org. Chem*., 2016, 871–886.

[14] W. Liu, J. T. Groves, *Angew. Chem., Int. Ed*. 2013, **52**, 6024−6027.

[15] W. Liu, X. Y. Huang, J. T. Groves, *Nat. Protoc*. 2013, **8**, 2348−2354.

[16] X. Huang, W. Liu, H. Ren, R. Neelamegam, J. M. Hooker, J. T. Groves, *J. Am. Chem. Soc.*, 2014, **136** (19), 6842–6845.

[17] J. B. Xia, C. Zhu, C. Chen, *J. Am. Chem. Soc.* 2013, **135**, 17494−17500.

[18] S. Bloom, M. McCann, T. Lectka, *Org. Lett*. 2014, **16**, 6338−6341

[19] D. Cantillo, O. de Frutos, J. A. Rincon, C. Mateos, C. O. Kappe, *J. Org. Chem*. 2014, **79**, 8486−8490.

[20] W. Liu, J. T. Groves, *Acc. Chem. Res.*, 2015, **48** (6), 1727–1735.

Direct C(sp³)-H Fluorination: Alkane Fluorination

6

6.1 Introduction

As reported in Chapter 1, direct $C(sp^3)$-H fluorination represents an ideal route for the synthesis of increased value fluorinated compounds. Nevertheless, although many goals have been recently achieved in this field using "activated" C-H bonds, such as benzylic fluorinations,[1-5] only a limited number of attempts have been made toward alkane direct fluorination, which represents an ideal and more elegant approach toward $C(sp^3)$-F formation. In fact, not only would this route provide higher atom efficiency, but it would also offer increased versatility due to the broad range of readily available substrates.

Whilst challenging to achieve, a few examples of direct alkane fluorination have been reported in the literature, demonstrating that such routes for the synthesis of $C(sp^3)$-F bonds are possible. Among all these reports (see Chapter 1 for further details), two different strategies can be identified: i) a biomimetic approach, involving an H-atom abstraction with high valent transition metals, and ii) radical mechanisms involving the use of radical initiators.

The first approach, reported by Groves in 2012,[6] indicates that biomimetic compounds, in particular Mn-porphyrins, can efficiently perform direct alkane fluorination in the presence of nucleophilic fluorine sources, such as AgF and TBAF. According to the mechanism suggested by Groves, the biomimetic catalyst, oxidised by an oxygen donor to yield high valent Mn(IV) and Mn(V), is able to abstract an H-atom (H-abstraction) from unactivated alkane substrates, forming alkyl radicals (R˙) species. These species then reportedly undergo a F-rebound-type mechanism. This reported mechanism is analogous to the O-rebound chemistry typically exhibited by biomimetic molecules, mimicking the enzymatic activity of the mono-oxygenase enzyme family (including Methane Mono-Oxygenase (MMO) and cytochrome P450)[7,8] but incorporating F atoms rather than oxygen, on the substrate. This system is highly interesting, especially considering such a mechanism for the formation of

C(sp^3)-F bonds does not occur in nature, unlike C(sp^3)-OH formation, which is well known to occur in biological systems under the most benign reaction conditions. However, considering that similar chemistry is involved in oxidation and fluorination reactions, side reactions that lead to the formation of oxidised products are likely to occur. Therefore, a good understanding of the rules that govern both these processes is essential to regulate the rate of both processes, ideally switching on only the fluorination or the oxidation route.

In contrast to the system reported by Groves, the second strategy reported to achieve direct alkane fluorination, involves the use of electrophilic/radical fluorine sources (such as Selectfluor® and NFSI). Noteworthy examples of this route are the photo-catalysed UO_2^{2+} based route reported by Ritter's group in 2016, and the light catalysed route employing a photosensitiser, such as 1,2,4,5-tetracyanobenzene, and 9-fluorenone/acetophenone.[9-11] Generally, the mechanism involved in photo-fluorination reactions is a radical chain process, with the catalyst (or photosensitiser) acting as a mere radical initiator.[12]

However, although the second strategy seems to be more promising, a preliminary investigation of electrophilic/radical mechanisms to achieve direct C(sp^3)-H fluorination was performed in Chapter 5, where it was found that systems involving the use of Selectfluor® as fluorinating agent are not viable for direct C(sp^3)-H fluorination. In fact, several major problems were found, such as: i) poor selectivity towards the desired fluorinated product at reaction time greater than 4 hours, ii) low stability of the fluorinated products, and iii) formation of highly toxic by-products (such as fluoroacetone). Therefore, in this chapter, a different approach to the synthesis of C(sp^3)-F bonds has been adopted, particularly focussing on a system involving nucleophilic fluorinating agents, using the fluorinating system developed by Groves as model system.[6]

Nevertheless, in order to develop an effective heterogeneous catalyst for C(sp^3)-H fluorination, capable of mimicking the activity of the homogeneous analogues, a good understanding and optimisation of the homogeneous system is essential. Therefore, a thorough study on the system developed by Groves' group is reported in this chapter, including studies on the reaction mechanism. Following kinetic and mechanistic analysis of the analogous homogeneous system, a preliminary attempt toward the

design of a heterogeneous catalyst, active for alkane fluorination reaction is also reported herein.

6.2 Experimental

Although spectroscopic and analytical methods are described in Chapter 2, experimental details of the catalytic reactions presented in this chapter are described below.

6.2.1 Materials

The following materials were used as received without further purification, unless otherwise stated.

- Tetramesitylporphyrin, $TMPH_2$ (Frontier Scientific, Inc)
- Dichloromethane, DCM (anhydrous, $\geq99.8\%$, contains 40-150 ppm amylene as stabilizer, Sigma Aldrich)
- Acetonitrile, ACN (anhydrous, 99.8%, Sigma Aldrich)
- Silver (I) fluoride, AgF ($\geq99.9\%$ trace metals basis, Sigma Aldrich)
- Tetrabutylammmonium fluoride trihydrate, TBAF ($\geq97.0\%$, Sigma Aldrich)
- Manganese (II) chloride tetrahydrate, $MnCl_2 \cdot 4H_2O$ ($\geq99.0\%$, BioUltra, Sigma Aldrich)
- (Diacetoxyiodo)benzene, $PhI(OAc)_2$ (98.0%, Sigma Aldrich)
- 3-Chloroperbenzoic acid, mCPBA ($\leq77.0\%$, Sigma Aldrich)
- Hydrogen peroxide, H_2O_2 (50 $wt\%$ solution in water, stabilized, ACROS Organics™, Fisher Scientific)
- Cyclooctane, C_8H_{16} ($\geq99.0\%$, Sigma Aldrich)
- N,N-Dimethylformamide, DMF ($\geq99.8\%$, ACS reagent, Sigma Aldrich)
- Alumina, Al_2O_3 (powder, ultra dry, Sigma Aldrich)
- Hexane, C_6H_{12} (97%, Acros Organics™, Fisher Scientific)
- Sodium sulphate, Na_2SO_4 (anhydrous $\geq99\%$, anhydrous, granular, free-flowing, Redi-Dri™, ACS reagent, Sigma Aldrich)
- Silica, SiO_2 (Aerocat®, Degussa)

- α,α,α-trifluorotoluene, $C_6H_5CF_3$ (anhydrous, ≥*99%*, Sigma Aldrich)
- Fluorocyclohexane, $C_6H_{11}F$ (*97%*, Alfa Aesar)

6.2.2 Definitions

Turnover number (TON) = Moles (product formed)/Moles (metal)

Turnover frequency (TOF) = (Moles (product formed)/Moles (metal))/Time

Conversion (X) = Moles (substrate consumed)/Moles (initial substrate) × 100

Yield (Y) = Moles (product produced)/Moles (initial substrate) × 100

Selectivity (S) = Yield/Conversion × 100

6.2.3 Experimental procedures

Details for catalyst preparations and kinetic studies for all the catalysts and reactions presented in this chapter are describe in this section.

6.2.3.1 Synthesis of (TMP)Mn(III)Cl

Tetramesitylporphyrin, $TMPH_2$ was purchased with high purity from Frontier Scientific, Inc. The coordination of the Mn to the desired porphyrin was performed according to literature procedures.[13,14]

Briefly, the procedure is as follows: $TMPH_2$ (0.187 mmol) and $MnCl_2 \cdot 4H_2O$ (0.752 mmol) were dissolved in DMF (23 mL) and stirred at reflux temperature (168 °C) for 6 hours. During the reaction, a change of colour from purple (due to $TMPH_2$) to dark green ((TMP)MnCl) occurred. The solvent was then removed *via* rotavapor.

The crude product was then purified and separated from unreacted $TMPH_2$ *via* chromatography over alumina using first a mixture of C_6H_{12}:DCM (v/v 1:1) then DCM, giving a black/dark green product.

6.2.3.2 Synthesis of (TMP)Mn(III)Cl supported on SiO₂, (TMP)Mn(III)Cl@SiO₂

(TMP)Mn(III)Cl@SiO_2 was prepared according to the method described in literature[15] (TMP)Mn(III)Cl (0.017 mmol) was dissolved in 20 mL of DCM and SiO_2 (430 mg) was added to the solution, subsequently stirred for 2 hours at 25 °C. The mixture was

then filtered and the solution analysed *via* UV-Vis, in order to quantify the (TMP)Mn(III)Cl loading on SiO$_2$. The solid catalyst was then dried under high vacuum for 2 hours.

6.2.3.3 Synthesis of PhIO

Iodosylbenzene (PhIO) was prepared according to the method reported in the literature.[16]

An aqueous sodium hydroxide solution $[NaOH]_{aq}$ = 1.88 M (81 mL) was added dropwise into an Erlenmeyer flask containing PhI(OAc)$_2$ (15 mmol), under vigorous stirring. Following the addition of the basic solution, the mixture was stirred for 3h and upon deacetylation, a colour change from white to yellow was observed. The yellow solid (PhIO) was then filtrated and washed with deionised water until the pH of the filtering solution became neutral. The recovered solid was then dried in open air and ground into a fine powder.

6.2.3.4 Cyclooctane fluorination

Nucleophilic alkane fluorination of cyclooctane was performed as follows.[6]

AgF (4.5 mmol), TMPMnCl (0.015 mmol) and TBAF·3H$_2$O (0.3 mmol) were added to a Schlenk flask and immediately purged with nitrogen. Then, 1.5 mL of anhydrous ACN, 0.5 mL of anhydrous DCM and cyclooctane (1.5 mmol) were added by syringe through a septum. α, α, α,-trifluorotoluene (0.16 mmol) was added as internal standard for both GC and NMR analysis. A small portion of solution was then withdrawn (t_0) for GC analysis and PhIO (1.5 mmol) was added. Finally, the flask was placed into an oil bath at 50 °C and the solution was stirred at 700 rpm, initiating the reaction. Various equivalents of oxidant were added, typically 2-3 equivalents, at a rate of one equivalent every 30 min.

Progress of the reaction was achieved by periodic sampling of the reaction. Samples were withdrawn, filtered and diluted with acetonitrile before being analysed *via* GC.

6.2.3.5 Catalyst characterisation and analytical details

UV-Vis and GC were employed to study cyclooctane fluorination. Experimental details for these methods are fully described in Chapter 2.

6.3 Results and discussion

As previously reported in Chapter 1, alkane fluorination catalysed by a Mn porphyrin (Mn(III) chloride 5,10,15,20-meso(tetramesityl)porphyrin, (TMP)MnCl), according to the system developed by Groves,[6] represents a good model system to investigate alkane $C(sp^3)$-H direct fluorination. However, despite the impact of this discovery, kinetic studies on this system, essential for its further optimisation, in addition to providing a benchmark against which screening of catalysts can be compared, are yet to be performed. Accordingly, kinetic and mechanistic studies of the system are required.

To perform kinetic studies on this model system, (TMP)Mn(III)Cl, as shown in Figure 6.1, was first prepared, according to the protocol reported in this Chapter (*vide supra*). Direct metallation of the commercial porphyrin, $TMPH_2$, was followed, which was subsequently prepared and purified through column chromatography.
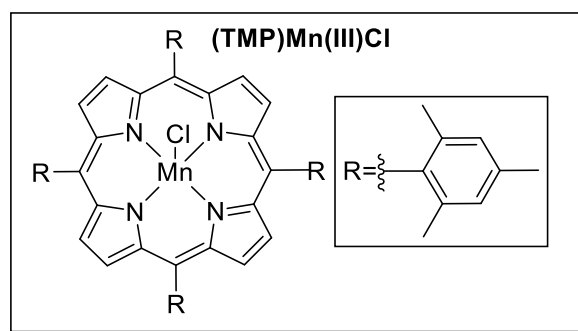

Figure 6.1: Structure of (TMP)Mn(III)Cl.

**6.3.1 Characterisation of (TMP)Mn(III)Cl**

To verify its purity, (TMP)Mn(III)Cl was characterised via UV-Vis spectroscopy and mass spectrometry. In fact, UV-Vis analysis represents a highly useful technique to identify (TMP)Mn(III)Cl and unreacted $TMPH_2$, which absorb at wavelengths of 475 nm and 416 nm, respectively. The spectrum observed for (TMP)Mn(III)Cl following

purification is in good agreement with the data present in literature, and also indicates that no residual TMPH$_2$ is present in the sample.[6]
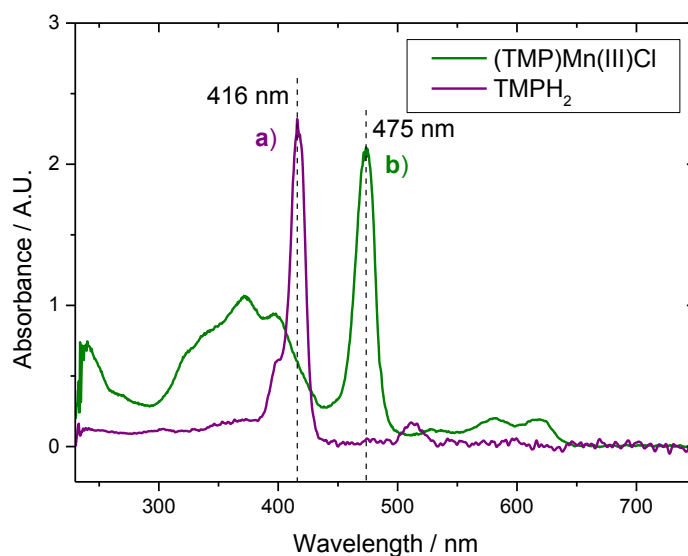
Figure 6.2: UV-Vis spectra of (TMP)Mn(III)Cl (green line) purified *via* column chromatography and TMPH$_2$ (purple line).
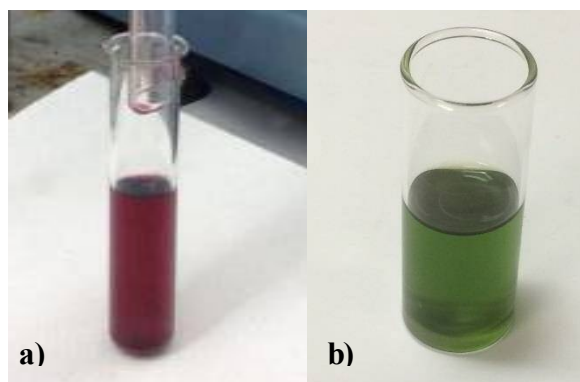
Figure 6.3: Pictures of (a) TMPH$_2$ and (b) (TMP)Mn(III)Cl.

To further confirm the coordination of Mn to the porphyrin and Cl, mass spectrometry of the purified compound was performed. Figure 6.4 shows the mass spectrum of the green solution reported in Figure 6.3(b); as can be seen in the mass spectrum, a molecular mass at 870 m/z is observed, confirming the formation of the species (TMP)Mn(III)Cl, with exact mass 870 u.
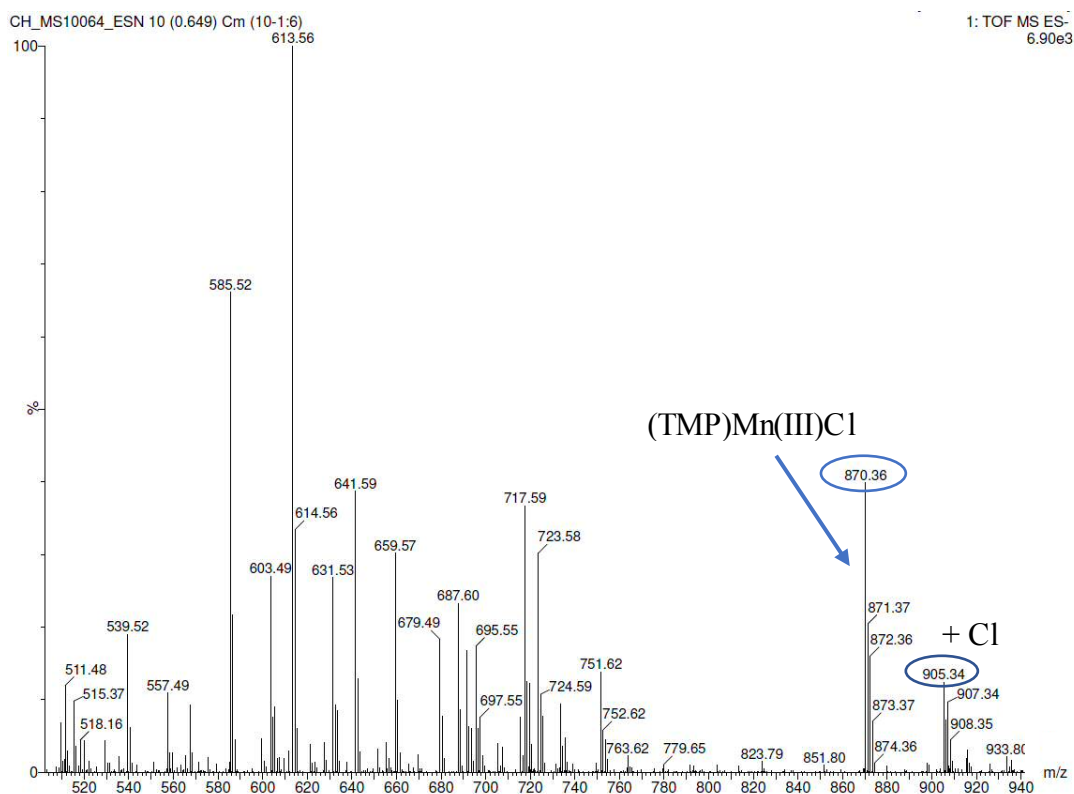
Figure 6.4: Electrospray Ionisation - Mass Spectrometry (ESI-MS) analysis of pure (TMP)Mn(III)Cl.

Following characterisation *via* ESI-MS, pure (TMP)MnCl was employed to perform alkane fluorination. Notably, cyclooctane was used as model substrate, due to its relatively high boiling point, 151°C, which is high enough to allow kinetic measurements without experiencing issues related to substrate evaporation. Conditions were otherwise identical to the ones reported by Groves system.[6]
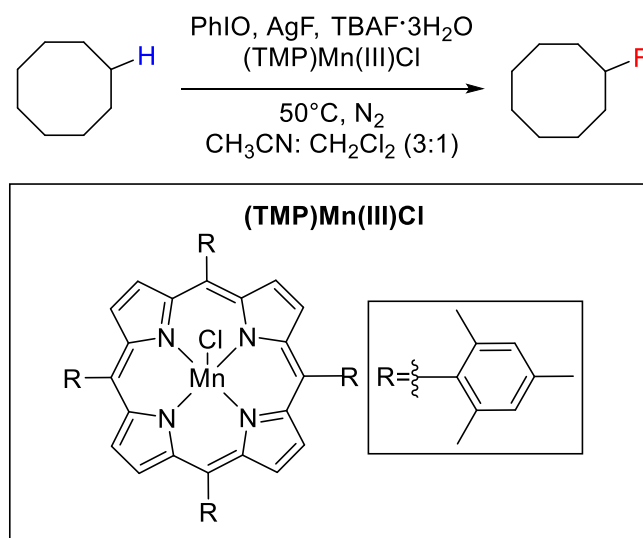
Figure 6.5: Direct cyclooctane fluorination catalysed by (TMP)Mn(III)Cl.

6.3.2 Optimisation of reaction conditions

In order to study the effect of different parameters on the catalytic performances of (TMP)Mn(III)Cl, on this model alkane fluorination system, essential for the screening of different catalysts, a thorough understanding of the catalytic system, in addition to the optimisation of reaction conditions, is essential.

In the original report, up to 10 mol. % of catalyst, (TMP)Mn(III)Cl, and up to 10 equivalents of oxidant were employed, during each reaction. However, as they were periodically added to the reaction mixture, thereby reforming the active catalytic species, true kinetic information was not provided. Therefore, to investigate the true kinetic of the reaction, an experiment was performed adding only 1 mol. % of catalyst and 1 equivalent of oxidant (PhIO), without further additions to the reaction mixture.
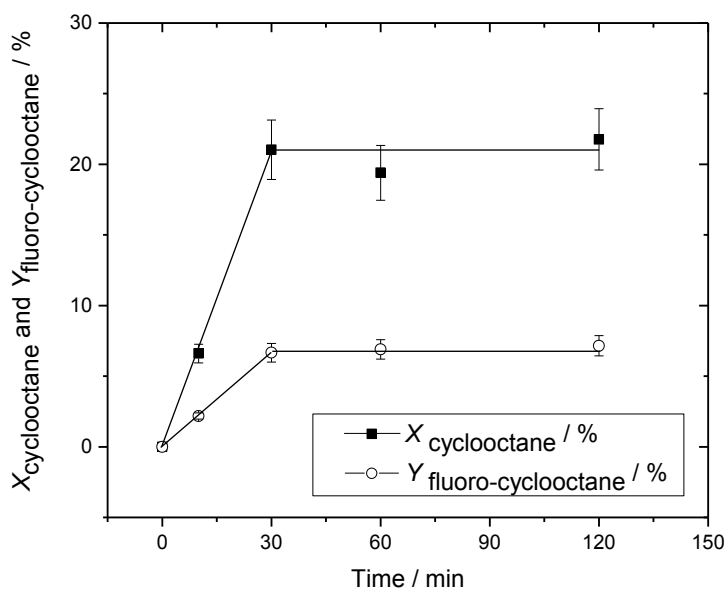
Figure 6.6: Cyclooctane conversion (shaded squares) and fluoro-cyclooctane yield (hollow circles) with time over (TMP)Mn(III)Cl with only one equivalent of PhIO added at the beginning of the reaction. Reaction conditions: 1.5 mmol of cyclooctane, 0.3 mmol of TBAF·3H$_2$O, 4.5 mmol of AgF, 0.015 mmol (TMP)Mn(III)Cl, 1.5 mL of CH$_3$CN anhydrous, 0.5 mL of CH$_2$Cl$_2$ anhydrous and 1.5 mmol of PhIO. The reaction was performed at 50°C in N$_2$ at 700 rpm.

As can been seen (Figure 6.6), a linear increase in cyclooctane conversion ($X_{cyclooctane}$), and fluoro-cyclooctane yield ($Y_{fluoro-cyclooctane}$), to 21 % of conversion and 7% of yield, was observed in the first 30 minutes of reaction. However, following 30 minutes of reaction, no further increase in either conversion or yield was observed following 120 minutes of reactions, thus indicating termination of the reaction. This might be due several effects, such as i) consumption of the oxidant (*i.e.* missing of active oxygen donor in solution) ii) deactivation of (TMP)Mn(III)Cl and iii) consumption of fluorinating agents (*i.e.* TBAF and AgF). Accordingly, turnover number (TON) and turnover frequency (TOF) were calculated over 30 minutes, giving TON = 21 and TOF = 42 h^{-1}, indicating that every (TMP)Mn(III)Cl molecule can catalyse an average of 21 catalytic cycles. Notably, poor fluoro-cyclooctane selectivity was observed, with a maximum of 32 % cyclooctane conversion to the desired fluorinated product, fluoro-cyclooctane, after 30 minutes of reaction. The low value of selectivity observed indicates the potential formation of by-products.

Notably, a control reaction in the absence of the catalyst was performed and no cyclooctane conversion was measured, demonstrating that the catalytic activity is completely due to the presence of (TMP)Mn(III)Cl.

6.3.3 Investigation of oxidant consumption

To investigate the possible reasons for termination of reaction at 30 minutes, a number of control experiments was performed. As briefly reported in the previous section, one of the possible reasons accountable for the termination of the reaction after 30 minutes, may be the excessive consumption of the oxidant.

Therefore, to investigate the role of the oxidant on the kinetics of the reaction, several equivalents of oxidant were periodically added to the reaction mixture; up to 5 equivalents of PhIO were added with delays of 30 minutes between each addition. Notably, the delay time was chosen according to the previous experiment, reported in Figure 6.6, showing termination of reaction after 30 minutes. For ease of comparison, the reaction with only one equivalent of PhIO is demonstrated by hollow circles.
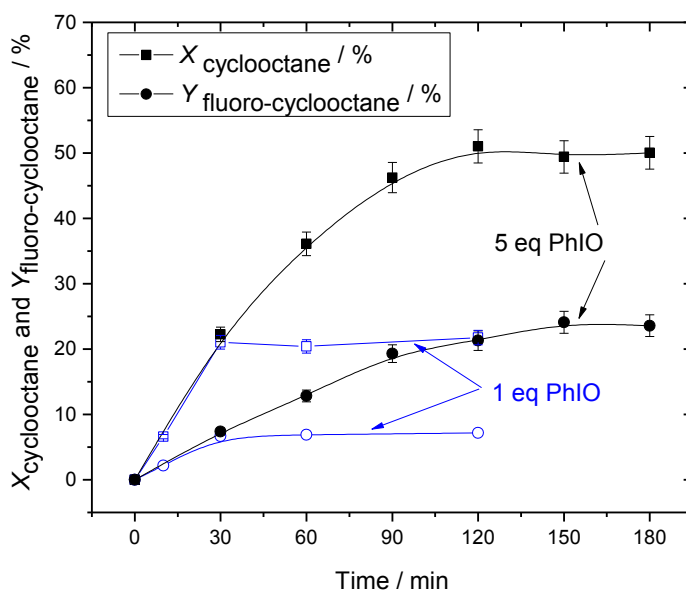
Figure 6.7: Cyclooctane conversion (squares) and fluoro-cyclooctane yield (circles) with time over (TMP)Mn(III)Cl with 5 equivalents of PhIO (black shaded symbols) and with only one equivalent of PhIO (blue hollow symbols). Reaction conditions: 1.5 mmol of cyclooctane, 0.3 mmol of TBAF·3H$_2$O, 4.5 mmol of AgF, 0.015 mmol (TMP)Mn(III)Cl, 1.5 mL of CH$_3$CN anhydrous, 0.5 mL of CH$_2$Cl$_2$ anhydrous and 7.5 mmol of PhIO (black squares) or 1.5 mmol of PhIO (black circles) (one equivalent, 1.5 mmol, respectively added at time 0, 30, 60, 90 and 120 min). The reaction was performed at 50°C in N$_2$ at 700 rpm.

Interestingly, when additional PhIO was added to the reaction mixture every 30 minutes, higher values of cyclooctane conversion and fluoro-cyclooctane yields were reached (Figure 6.7). In fact, 50 % conversion of cyclooctane and 24 % yield of fluoro-cyclooctane were observed at reaction times ≥ 150 min, thus indicating that adding fresh oxidant is essential for the reaction to proceed. However, no further increase (*i.e.* over 50 %) of cyclooctane conversion was observed after 120 minutes of reaction, despite the regular addition of fresh oxidant. The same effect was observed in terms of fluoro-cyclooctane yield, with no increase seen between 120 and 150 minutes of reaction time.

The substantially higher TON calculated for this experiment, TON = 50, clearly indicates that the lack of fresh oxidant, after 30 minutes from the addition, contributes to the termination of the standard reaction, suggesting that an excessive loss of the oxidant occurs (Figure 6.6). However, a maximum conversion of 50 % was achieved, even under these conditions, indicating that even adding fresh oxidant to the reaction

mixture, full conversion is not achieved. This clearly indicates that other parameters are also involved in the deactivation of the system.

Notably, similarly to the previous experiment reported earlier in this Chapter (*vide supra*), high selectivity towards fluoro-cyclooctane ($S_{\text{fluoro-cyclooctane}}$) was not observed. Relatively poor fluoro-cyclooctane selectivity may indicate the formation of by products, potentially formed by oxidation of cyclooctane, similarly to the findings of Chapter 5, where oxidised by-products were observed during fluorination. Further investigation on the formation of oxidised products will be discussed later in this Chapter.

6.3.4 Effect of addition of fresh fluorine sources (TBAF/AgF)

As observed in the previous section, although periodic addition of oxidant to the reaction mixture increases the overall yield of fluorinated product, it is still not sufficient to achieve full cyclooctane conversion. Termination of reaction at 50% of conversion could be due to two different reasons: i) consumption of fluorine sources (*i.e.* TBAF and AgF), and ii) deactivation of (TMP)Mn(III)Cl. In order to determine the cause of reaction termination, the effect of addition of: i) fluorine sources (TBAF/AgF), and ii) fresh (TMP)Mn(III)Cl, were studied.

First, the effect of potential consumption of fluorine sources was investigated. Thus, an experiment was performed under the same conditions described above (*i.e.* periodically adding 5 equivalents of PhIO), albeit adding fresh amounts of both AgF and TBAF at 90 minutes and 150 minutes. Notably, 90 minutes and 150 minutes were chosen to verify if cyclooctane conversion values higher than 50 % can be achieved after addition of fresh fluorine sources in the reaction mixture. To aid comparison with the previous experiment, the new experiment performed with addition of fluorine sources is shown in the following figure as hollow symbols:
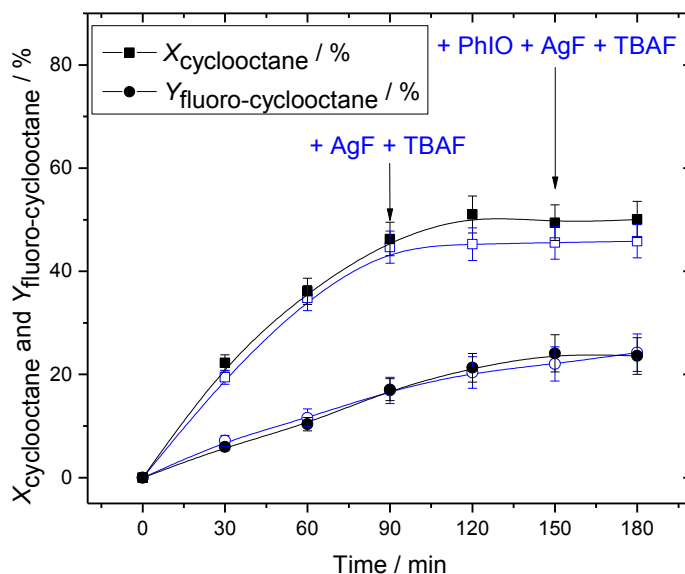
Figure 6.8: Cyclooctane conversion (squares) and fluoro-cyclooctane yield (circles) with time over (TMP)Mn(III)Cl without (black shaded symbols) and with addition of fresh AgF and TBAF at 90 minutes and 150 minutes (blue symbols). Reaction conditions: 1.5 mmol of cyclooctane, 0.9 mmol of TBAF·3H$_2$O, 13.5 mmol of AgF, 0.015 mmol (TMP)Mn(III)Cl, 1.5 mL of CH$_3$CN anhydrous, 0.5 mL of CH$_2$Cl$_2$ anhydrous and 9.0 mmol of PhIO (one equivalent, 1.5 mmol, added at time 0, 30, 60, 90, 120 and 150 min, respectively). The reaction was performed at 50°C in N$_2$ at 700 rpm.

As shown in Figure 6.8, similarly to the previous experiment (see Figure 6.7) conversion values higher than 50 % were not achieved, even when additional fluorine sources are added, suggesting that the termination of reaction at 150 minutes is not to be attributed to a lack of fluorine sources in the reaction. In fact, addition of fresh equivalents of both fluorine sources (*i.e.* TBAF and AgF) does not improve the catalytic performances of the systems, with similar kinetic observed in both Figure 6.8 and Figure 6.7.

6.3.5 Effect of addition of (TMP)Mn(III)Cl

After ruling out the effects of consumption of PhIO and consumption of fluorinating agents (*i.e.* TBAF and AgF), another effect that can be responsible for the termination of reaction at around 50 % of conversion may be the deactivation of the (TMP)Mn(III)Cl catalyst, thus suggesting that a TON higher than 50 cannot be achieved by the catalyst for this reaction. To first investigate eventual modification of

(TMP)Mn(III)Cl, including its decomposition, during reaction, UV-Vis analysis of the reaction mixture reported in Figure 6.8 at 180 minutes, was performed.
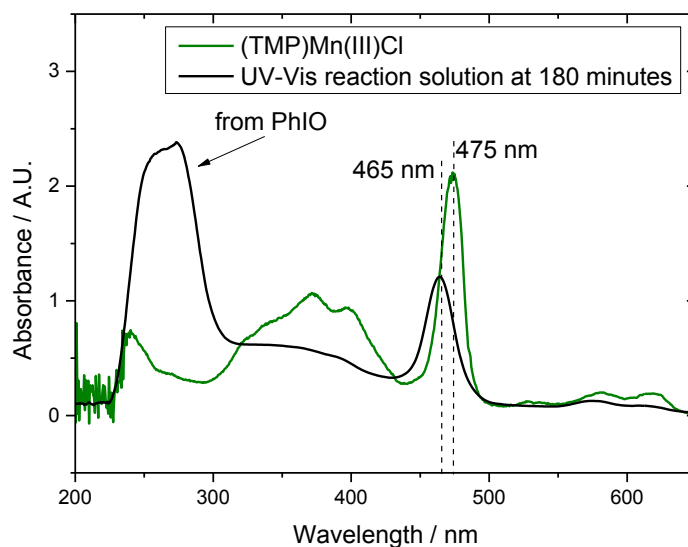
Figure 6.9: UV-Vis spectra of (TMP)Mn(III)Cl (green line) purified *via* column chromatography and reaction mixture at termination of reaction.

UV-Vis analysis of reaction mixture (back line figure 6.9) shows an absorption peak centred at 465 nm, slightly shifted from the absorption peak of fresh (TMP)Mn(III)Cl, 475 nm. This suggests that, although the Mn-porphyrin is still present in the reaction mixture (*i.e.* the Mn-porphyrin complex does not decompose during reaction), the Mn-porphyrin species formed after 180 minutes of reaction, absorbing at 465 nm may not be active for alkane fluorination.

Following the observation that reaction termination following 50% conversion at 150 minutes of reaction is not due to either the effect of i) consumption of fluorine sources and ii) consumption of active oxidant, 1 mol. % of fresh (TMP)Mn(III)Cl was added to the reaction mixture at 150 minutes, to determine if this may lead to a conversion > 50%.
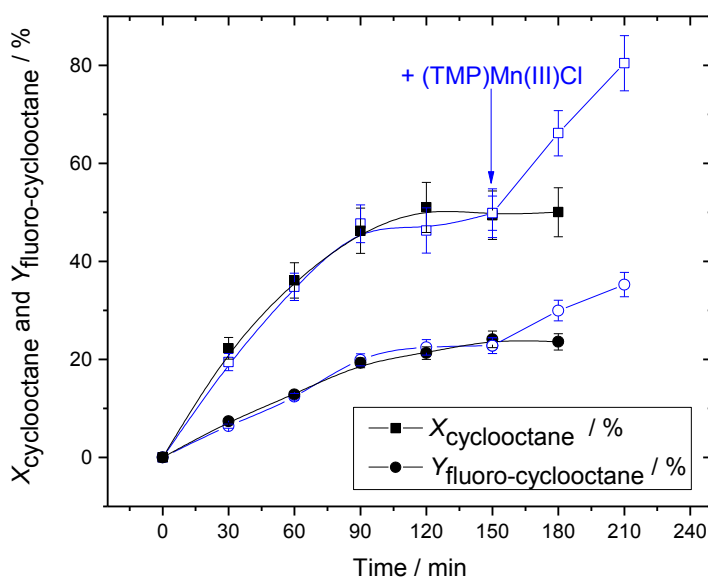
Figure 6.9: Cyclooctane conversion (squares) and fluoro-cyclooctane yield (circles) with time over (TMP)Mn(III)Cl i) without addition of fresh (TMP)Mn(III)Cl (black shaded symbols), and ii) with addition of 1 mol % of fresh (TMP)Mn(III)Cl at 150 minutes (hollow blue symbols). Reaction conditions: 1.5 mmol of cyclooctane, 0.9 mmol of TBAF·3H$_2$O, 13.5 mmol of AgF, 0.015 mmol (TMP)Mn(III)Cl, 1.5 mL of CH$_3$CN anhydrous, 0.5 mL of CH$_2$Cl$_2$ anhydrous and 10.5 mmol of PhIO (one equivalent, 1.5 mmol, added at time 0, 30, 60, 90, 120, 150 and 180 min, respectively). The reaction was performed at 50°C in N$_2$ at 700 rpm.

Interestingly, upon addition of fresh (TMP)Mn(III)Cl, additional cyclooctane conversion was observed, with 80 % of cyclooctane conversion after 210 minutes of reactions. This indicates that the reaction termination previously observed (black lines Figure 6.9) may be attributed to the deactivation of (TMP)Mn(III)Cl. Interestingly, a similar reaction rate was observed in the two ranges 0-60 minutes and 150-210 minutes, further suggesting that regular addition of (TMP)Mn(III)Cl is essential to achieve high cyclooctane conversion values. This experiment also indicates that TON higher than 50 cannot be achieved, with Mn-porphyrin deactivation occurring after an average of 50 catalytic cycles yielding to the Mn-porphyrin species absorbing at 465 nm in the UV-Vis spectrum observed in Figure 6.9.

Notably, in all the experiments reported so far, fluoro-cyclooctane selectivity higher than 50 % was not achieved. Therefore, a deeper investigation on the by-reactions and by-products occurring in this system is the focus of the next section of this Chapter.

6.3.6 Reaction selectivity, competition between oxidation and fluorination pathways

In the original report from Groves group, reactions were only reported as a function of yield of fluorinated products, up to a maximum of 50 - 60 %.[6] However, it is clear that the fluorination pathway is not the only reaction pathway possible under these reaction conditions. In fact, selectivity values lower than 50 % can be attributed to the presence of competitive reaction pathways. As M-containing porphyrins are well known to catalyse C-H abstraction reactions, reportedly *via* O-rebound type mechanisms, reminiscent of those of the MMO family, such as methane monooxygenase family, oxidised products are very likely to be formed as by-products throughout the entire reaction timescale.

To investigate the potential competition between oxidative reaction pathways and fluorination pathways a deeper investigation into the reaction products, focusing also on eventual oxidised product was performed.

To determine and quantify the possible by-products of cyclooctane fluorination, qualitative and quantitative analysis against pure standards was performed *via* GC analysis, using authentic standards of cyclooctene, cyclooctene oxide, cyclooctanol and cyclooctanone. As expected from the low values of fluoro-cyclooctane selectivity, a number of additional products were observed during reaction. Indeed, products such as cyclooctanol, cyclooctanone, cyclooctene and cyclooctanone oxide were observed during the reaction time (Figure 6.10).
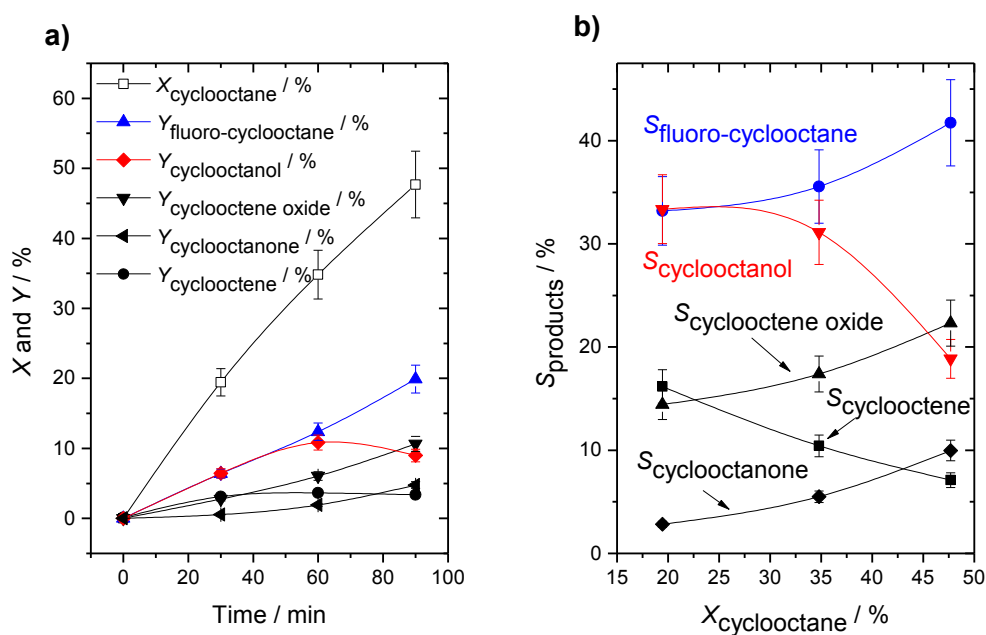
Figure 6.10 a) Cyclooctane conversion (hollow squares) and products yield (shaded symbols) with time over (TMP)Mn(III)Cl with 3 equivalents of PhIO; **b)** Products selectivity over cyclooctane conversion. Reaction conditions: 1.5 mmol of cyclooctane, 0.3 mmol of TBAF·3H$_2$O, 4.5 mmol of AgF, 0.015 mmol (TMP)Mn(III)Cl, 1.5 mL of CH$_3$CN anhydrous, 0.5 mL of CH$_2$Cl$_2$ anhydrous and 4.5 mmol of PhIO (one equivalent, 1.5 mmol, respectively added at time 0, 30 and 60 min).

The presence of these by-products clearly indicates the existence of a competitive oxidative pathway in which an oxygen is incorporated, yielding to cyclooctene oxide, cyclooctanol and cyclooctanone. Quantities of cyclooctene were also found to some extent, potentially formed *via* i) dehydration of cyclooctanol, ii) dehydrofluorination of fluoro-cyclooctane, and/or iii) direct cyclooctane dehydrogenation.

As shown in Figures 6.10 **a)** and **b)**, the selectivity of the reaction changes with reaction time and, thus, with cyclooctane conversion. Indeed, in the early stage of the reaction (first 30 and 60 minutes) relatively high selectivity towards cyclooctanol is observed, (almost identical to the selectivity for fluoro-cyclooctane) indicating that cyclooctanol is the favoured product of the oxidative route. Although formed in smaller quantities, cyclooctene and cyclooctene oxide were also present at some extent at 30 minutes of reaction, whilst only traces of cyclooctanone were observed *via* GC.

In biomimetic systems, the alcohol/ketone ratio is a key factor used to elucidate the nature of the mechanism involved in the reaction. In fact, in biomimetic systems, the alkyl radicals formed following H-abstraction, can potentially be oxidised *via* two different mechanisms: i) metal-based oxidation, and ii) radical chain autoxidation.[17] In the first mechanism, the metal complex is responsible for the oxidation of the substrate, yielding the hydroxylated substrate as a favoured product. Differently, for radical chain autoxidation, the metal complex is not involved in the oxidation of the alkyl radical species, and free radical species are present in the reaction mixture, leading to the formation of both alcohols and ketones, in similar yields. Therefore, whilst high alcohol/ketone ratios are indicative of metal-based oxidation reaction pathways, that favour the formation of the alcohols, low alcohol/ketone ratios (≤ 1) are indicative of radical chain autoxidation mechanisms.[17]

In order to understand if the mechanism governing the oxidative route is a metal-based oxidation or a radical chain autoxidation, the ratio between cycooctanol and cycooctanone was calculated in the early stage of reaction (30 minutes) and an alcohol/ketone ratio of 11.8 was calculated. This high alcohol/ketone ratio, is indicative of a metal-based oxidation mechanism, thus suggesting that the oxidative route is catalysed by a high oxidation state Mn-porphyrin, as opposed to a free radical chain autoxidation mechanism.

Although high cyclooctanol selectivity was observed during the first hour of reaction, a drop of selectivity from 31 % to 19 % occurred between 60 and 90 minutes. This drop in selectivity may be explained by further oxidation of cyclooctanol to cyclooctanone, catalysed by the presence of high amounts of oxidant present in the reaction mixture, thus explaining the increase in cyclooctanone selectivity shown in Figure 6.10. As previously reported, cyclooctene and cyclooctene oxide were also found amongst the by-products detected in solution. However, whilst decreasing of cyclooctene selectivity was observed, from 16 % to 7 % in a range 30 – 90 minutes, an increase selectivity towards cyclooctene oxide was detected, from 14 % to 22 %. This could be explained by oxidation of cyclooctene to cyclooctene oxide, due to the high amounts of oxidant present in the reaction mixture. However, whilst oxidised by-products were found in solution, confirming the presence of a competitive metal-based oxidation pathway, the major reaction product, characterised by higher

selectivity, was found to be fluoro-cyclooctane, reaching 41 % of selectivity at 47 % of cyclooctane conversion (blue line Figure 6.10). Further investigation of the reaction pathways and competition between oxidation and fluorination is therefore investigated further below.

6.3.7 Stability studies

To further investigate the reaction pathways, and to understand the rate of interconversion of product and by-products, (*e.g.* if fluoro-cyclooctane can be yielded by "decomposition" of the main oxidation product), stability studies on the main products were performed. Firstly, the stability of the fluorinated species was investigated using the fluoro-alkane as substrate instead of cyclooctane. Notably, due to the unavailability of commercial fluoro-cyclooctane, an analogous fluorine-alkane substrate, fluoro-cyclohexane, commercially available in high purity, was employed.
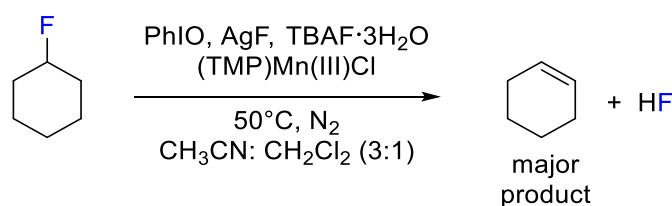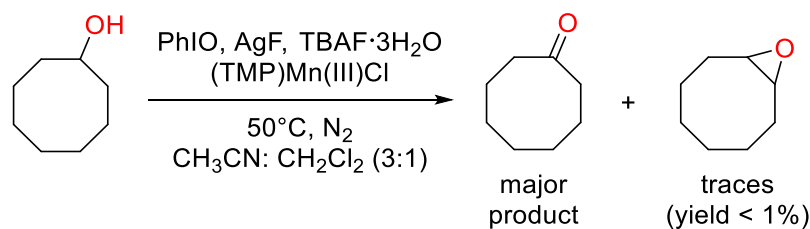

Figure 6.11: Fluoro-cyclohexane stability study under fluorination reaction conditions. Reaction conditions: 0.75 mmol of fluoro-cyclohexane, 0.15 mmol of TBAF·3H2O, 2.25 mmol of AgF, 0.0075 mmol (TMP)Mn(III)Cl, 0.75 mL of CH3CN anhydrous, 0.25 mL of CH2Cl2 anhydrous and 1.5 mmol of PhIO (one equivalent, 0.75 mmol, added at time 0, and 30 minutes, respectively).

Interestingly when fluoro-cyclohexane was used as substrate under general reaction conditions, 5.5 % and 21.5 % conversion values were found at 30 and 60 minutes, respectively, with the major product observed being cyclohexene. This suggests that the alkyl fluoride may undergo to dehydrofluorination yielding the corresponding alkene, releasing HF.[18,19] The alkene so formed, could subsequently be further oxidised under general reaction conditions, yielding the corresponding epoxide.[20]

In analogy to the stability test performed on the fluorinated product, stability studies on the main product of the oxidative pathway, cyclooctanol, were performed, in order to investigate the main decomposition pathway of the oxidative route.

Figure 6.12: Cyclooctanol stability study under fluorination reaction conditions. Reaction conditions: 0.75 mmol of cyclooctanol, 0.15 mmol of TBAF·3H$_2$O, 2.25 mmol of AgF, 0.0075 mmol (TMP)Mn(III)Cl, 0.75 mL of CH$_3$CN anhydrous, 0.25 mL of CH$_2$Cl$_2$ anhydrous and 1.5 mmol of PhIO (one equivalent, 0.75 mmol, added at time 0, and 30 minutes, respectively).

Substituting cyclooctane with cyclooctanol, interestingly, no fluoro-cyclooctane was found in the reaction mixture, thus indicating no interconversion between fluoro-cyclooctane and cyclooctanol occurs. This confirms that fluoro-cyclooctane and cyclooctanol are formed through two different reaction pathways. However, as previously observed in Figure 6.10, high decomposition of cyclooctanol was detected (43 % of cyclooctanol conversion was found after 60 minutes of reaction), with cyclooctanone obtained as major product and cyclooctene oxide formed in traces (yields ≤ 1%). Combining stability studies with the observations made in Section 6.3.6, a possible reaction scheme can be proposed (Figure 6.13). Following kinetic analysis of cyclooctane fluorination reaction, reported in the previous section (Figure 6.10) two main different reaction pathways can be identified, leading to the conversion of cyclooctane into fluoro-cycooctane and cyclooctanol. Also, according to the high ratio of cyclooctanol/cyclooctanone found in the early stage of the reaction (11.8), the oxidation pathway is likely to occur *via* a metal-based oxidation of cyclooctane to yield an alkyl radical intermediate, which yields cyclooctanol. Also, the fluorination pathway leading to the formation of fluoro-cyclooctane can be suggested to occur through a similar mechanism, due to the similar yield and selectivity exhibited by fluoro-cyclooctane and cyclooctanol (6.5 % yield and 33 % of selectivity for both products). Therefore, the selectivity of the reaction in terms of fluorination/oxidative route, may be controlled by the rate of fluorination/ hydroxylation of the alkyl radical species formed upon H-abstraction.

Following stability studies, it was also found that both cyclooctanol and fluoro-cyclooctane can further react under reaction conditions, yielding mainly to

cyclooctanone and cyclooctene, respectively. However, cyclooctene itself may also be oxidised under general reaction conditions, yielding to the corresponding epoxide.[20]

To further study the fluorination/oxidation competitive pathways, the pure oxidative pathway (*i.e.* in the absence of fluorine sources) will be further investigated in the following section.
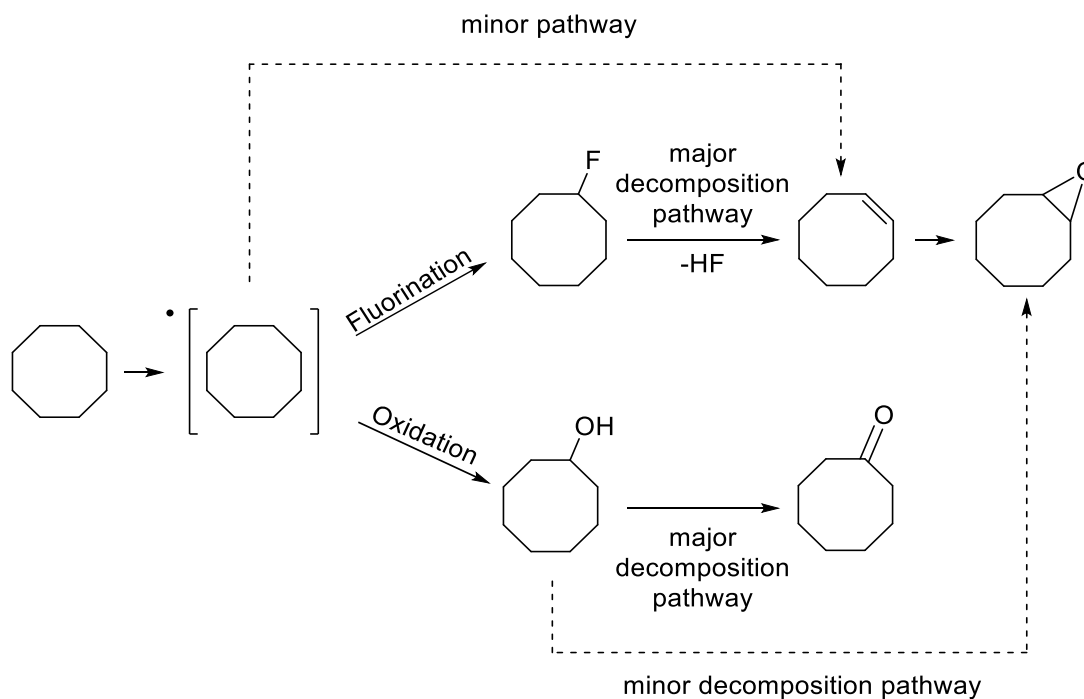
Figure 6.13: Competition oxidative / fluorinating pathways, with by-products and hypothesis on the by-products formation.

6.3.8 Time on line analysis of the oxidative pathway

To properly compare oxidation and fluorination pathways, the same reaction was performed under exactly the same conditions but without the presence of fluorine sources (*i.e.* without TBAF and without AgF).
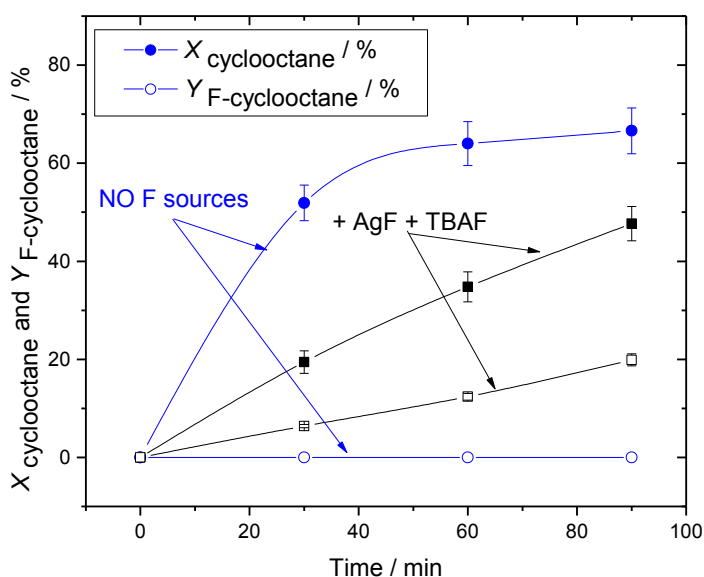
Figure 6.14: Cyclooctane conversion (shaded symbols) and F-cyclooctane yield (hollow symbols) with time over (TMP)Mn(III)Cl in normal conditions (black squares) and in the absence of AgF and TBAF·3H$_2$O (blue circles). Reaction conditions: 1.5 mmol of cyclooctane, 0.3 mmol of TBAF·3H$_2$O, 4.5 mmol of AgF, 0.015 mmol (TMP)Mn(III)Cl, 1.5 mL of CH$_3$CN anhydrous, 0.5 mL of CH$_2$Cl$_2$ anhydrous and 4.5 mmol of PhIO (one equivalent, 1.5 mmol, respectively added at time 0, 30 and 60 min). The reaction was performed at 50°C in N$_2$ at 700 rpm.

As shown in Figure 6.14, in the absence of fluorine sources, the catalyst exhibits good catalytic activity with only oxidised products being observed (Figure 6.15**b**). In line with the high alcohol/ketone ratio, cyclooctanol was mainly obtained, with 62 % of selectivity. Interestingly, TOFs calculated over the first 30 minutes of reaction, were found to be 40 h^{-1} with the fluorine sources (AgF and TBAF) and 104 h^{-1} without (Figure 6.15**a**).
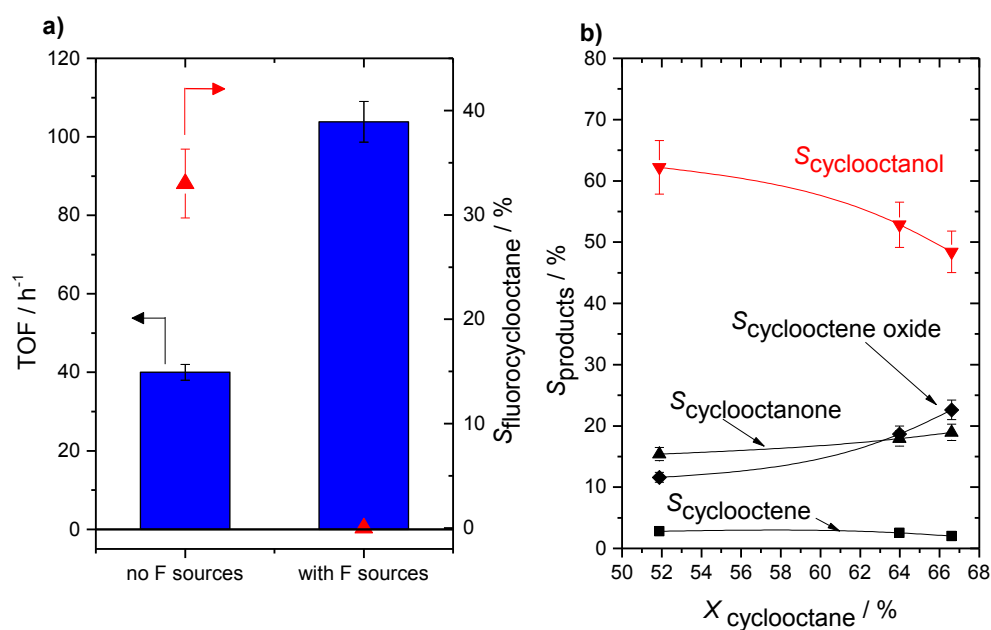
Figure 6.15 a) TOF (blue bars) and fluoro-cyclooctane selectivity (red triangles) with and without fluorine sources (AgF and TBAF); **b)** products selectivity over cyclooctane conversion with (TMP)Mn(III)Cl in the absence of AgF and TBAF·3H$_2$O. Reaction conditions: 1.5 mmol of cyclooctane, 0.015 mmol (TMP)Mn(III)Cl, 1.5 mL of CH$_3$CN anhydrous, 0.5 mL of CH$_2$Cl$_2$ anhydrous and 4.5 mmol of PhIO (one equivalent, 1.5 mmol, respectively added at time 0, 30 and 60 min). The reaction was performed at 50°C in N$_2$ at 700 rpm.

In good agreement with the reaction scheme reported in Figure 6.13, the main product at the initial stage of reaction is cyclooctanol. However, in the absence of fluorine sources, other oxidised products were observed, with cyclooctanone and cyclooctene oxide observed as main by-products and cyclooctene observed in traces (yields < 2 %). Although the formation of cyclooctanone as a by-product occurs, a cyclooctanol/cyclooctanone ratio of 5.4 was found following 30 minutes of reaction. As previously reported (Section 6.3.6, *vide supra*), cyclooctanol/cyclooctanone ratios higher than 1 are generally indicative of a metal-based oxidation mechanism, as reported for catalyst exhibiting bio-mimetic activity. In fact, this is in good agreement with the enzymatic activity of the monooxygenase family enzymes, able to catalyse the conversion of alkanes to alcohols. Furthermore, as previously reported in literature, overoxidation reactions may occur, leading to the synthesis of cyclooctanone.[21]

The higher reaction rate previously observed in the absence of fluorinating reagents, with greater than 50 % of substrate conversion in the first 30 min of reactions, against

20 % measured in the presence of AgF and TBAF, indicates the presence of fluorine sources as inhibitors to the activity of the catalyst. This difference of rate could potentially be attributed to different axial ligands bound to the metal. Indeed, according to the reaction mechanism hypothesised by Groves (Figure 6.16), the replacement of the axial chlorine ligand with a fluorine and the formation of a di-fluorinated species are essential for the fluorination pathway to occur.[6] Therefore, the type of ligand that binds to the metal might affect the catalytic performances of (TMP)Mn(III)Cl.[22]
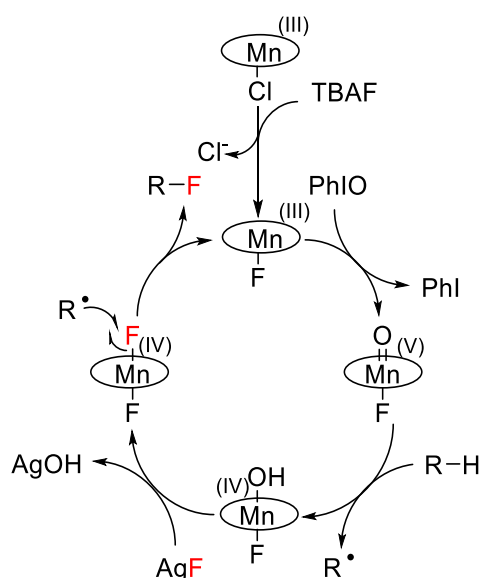

Figure 6.16 Reaction mechanism for alkane fluorination proposed by Groves.[6]

6.3.9 Mechanism

To further study and gain a better understanding of the reaction mechanism involved in this system, the influence of i) the axial ligand, ii) the oxidant, and iii) the oxidant and the substrate, on the catalyst, (TMP)Mn(III)Cl, were all investigated.

First, to investigate the possible modification of the axial ligands binding to the Mn site of the porphyrin, time resolved UV-Vis analysis was performed. (TMP)Mn(III)Cl was first dissolved into the reaction mixture (CH$_3$CN/CH$_2$Cl$_2$ 3:1) and an absorbance spectrum with the characteristic peak of the chlorinated Mn porphyrin was observed at a wavelength of 475 nm. After the addition of TBAF a blue shift toward higher energy was detected (457 nm), assigned to a (TMP)Mn(III)F by Groves.[6]

Subsequently, silver (I) fluoride was added to the reaction mixture and another shift at 440 nm was observed, potentially due to the coordination of another fluorine ligand to the Mn, giving an octahedral geometry, [(TMP)Mn(III)(F)$_2$]⁻. Clearly, changing the ligands present in solution has an impact on the speciation of the Mn centre.
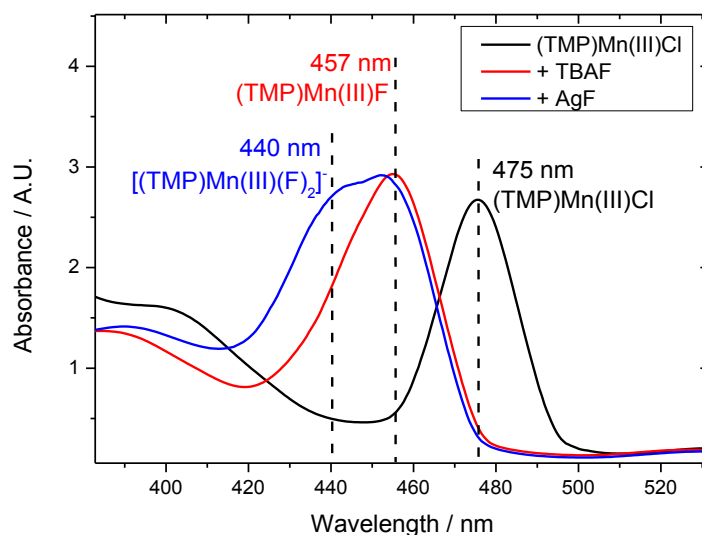
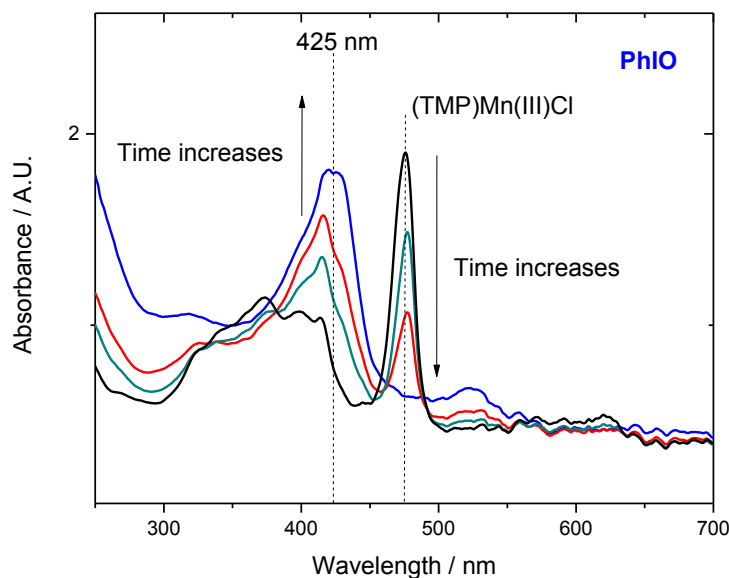**Figure 6.17:** UV-Vis analysis of a TMPMn(III)Cl solution in (CH$_3$CN/CH$_2$Cl$_2$ 3:1) following addition of first TBAF then AgF.
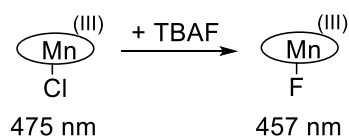
Scheme 6.18: Ligand exchange and UV shift observed upon interaction between (TMP)Mn(III) and TBAF.

To investigate the nature of the oxo-species formed upon interaction of the Mn-porphyrin with the oxidant, PhIO, two UV-Vis experiments were then performed: i) adding PhIO to a solution of (TMP)Mn(III)Cl in CH$_3$CN/CH$_2$Cl$_2$ (v/v 3:1), and ii) adding PhIO to a solution of (TMP)Mn(III)F in CH$_3$CN/CH$_2$Cl$_2$ (v/v 3:1).

Figure 6.19: UV-Vis analysis of a (TMP)MnCl solution in CH_3CN/CH_2Cl_2 (v/v 3:1) before (black line) and after the addition of PhIO.

As shown in Figure 6.19, following addition of PhIO to the UV cuvette, the absorption peak characteristic of (TMP)Mn(III)Cl decreases in intensity, indicating the formation of a different species which is formed upon interaction between (TMP)Mn(III)Cl and PhIO. In fact, in parallel to the decrease of the absorption band at 475 nm, another band appears in the range 415 - 428 nm. This wavelength range is typical of Mn(IV) species, as reported in literature, indicating the oxidation step of the Mn(III)-porphyrin following addition of the oxidant species.[23,24]

Thirdly, to investigate the effect of the fluorine sources (*i.e.* AgF and TBAF), and to therefore investigate the changes that appear when both oxidant and fluorine donors are present, PhIO, AgF and TBAF were all added to the same UV cuvette.
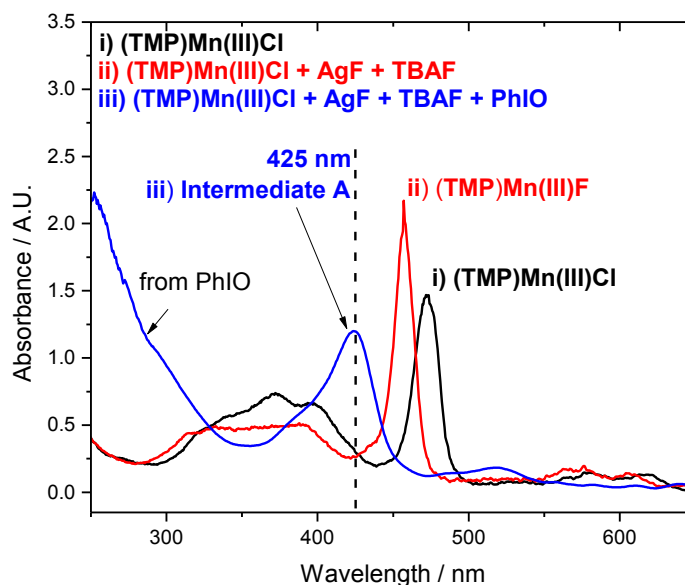
Figure 6.20 i) UV-Vis analysis of a (TMP)MnCl solution in CH_3CN/CH_2Cl_2 (v/v 3:1) before (black line) and after the addition of ii) AgF/TBAF (red line) and iii) PhIO (blue line).

As previously observed in Figure 6.17, following the addition of AgF and TBAF (red line) a shift was observed from 475 nm, characteristic of (TMP)Mn(III)Cl, to 457 nm, characteristic of (TMP)Mn(III)F. Following the formation of the (TMP)Mn(III)F species, PhIO was added to the UV cuvette (blue line Figure 6.20). Interestingly, following the addition of PhIO, the absorption band at 457 nm disappears, whilst a new band in the range 415 - 428 nm appeared, characteristic of a Mn(IV) complex, denoted as "intermediate A", in analogy with the absorption band observed in Figure 6.19. This indicates that similar intermediate species may be formed upon interaction between i) PhIO and (TMP)Mn(III)Cl, and ii) PhIO and (TMP)Mn(III)F. In fact, in both experiments an absorption band in a range 415 - 428 nm was observed, characteristic of a high valent Mn-porphyrin species, with oxidation state (IV), potentially indicating formation of the intermediate species Mn(IV)=O or Mn(IV)-OH. In fact, the formal reaction between a Mn(III) species and PhIO results in a 2 e⁻ oxidation step, yielding a Mn(V)=O species. However, it is well-known that porphyrins can stabilise high valent metals by e⁻ accepting, yielding to a Mn(IV) species with 1 e⁻ delocalised on the porphyrin ring [(TMP)Mn(IV)=O(X)]⁻.

In order to fully identify this intermediate species, UV-Vis analysis is not sufficient and further characterisation is required. Therefore, to fully characterise the intermediate species involved in this system, in depth *in-situ* and *ex-situ* analysis, including different techniques (such as Raman Resonance) will be the focus of future studies.

6.3.9.1 Effect of addition of substrate on the absorption band at 415 - 428 nm

To ensure the species at 415 - 428 nm (intermediate A) is in fact the real intermediate species, and, considering that the same type of intermediate was formed with and without the presence of fluorine sources, the behaviour of this band was investigated following addition of the substrate, cyclooctane. In fact, modification of the band related to intermediate A (415 - 428 nm) upon interaction with cyclooctane may indicate that intermediate A is the reaction intermediate species, potentially responsible of the H abstraction step. Given that same type of intermediate was found with and without fluorine sources (AgF and TBAF), the following experiments will be performed in the absence of fluorine sources, representing a model system to study the interaction between substrate and intermediate A.

Prior to studying addition of cyclooctane to the system, the solvothermal stability of intermediate A was investigated. In the following experiment, PhIO was added to a UV cuvette containing a solution of (TMP)Mn(III)Cl in CH_3CN/CH_2Cl_2 (v/v 3:1), and time on line UV-Vis analysis of the system was performed, in order to record the change of the absorption band characteristic of intermediate A (Figure 6.21).
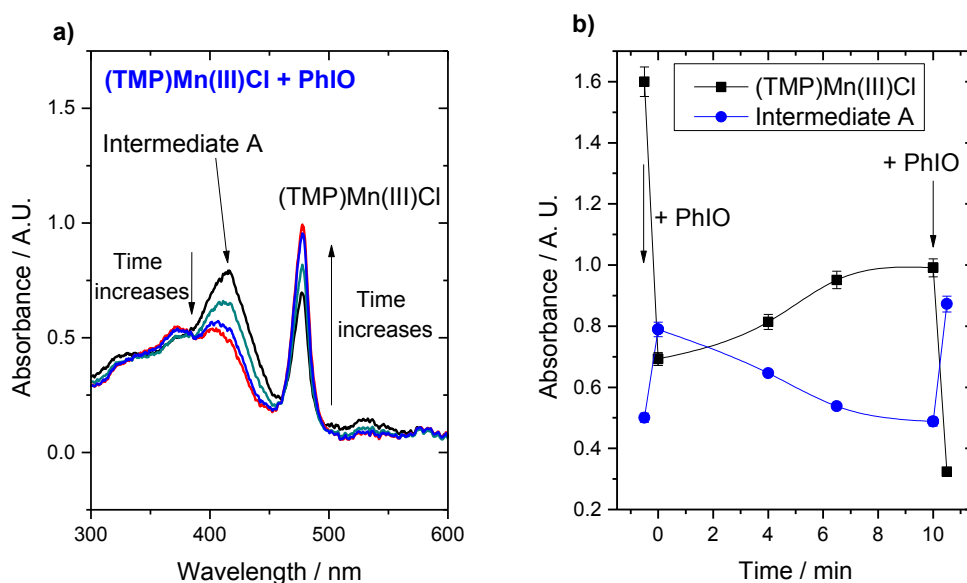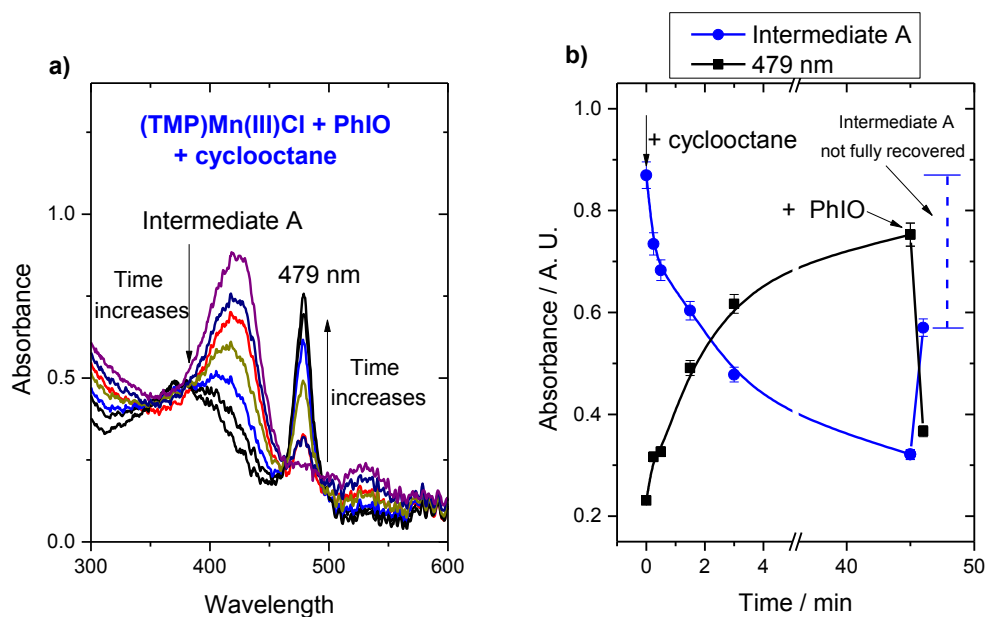
Figure 6.21: a) Time resolved UV-Vis analysis of a solution PhIO/(TMP)Mn(III)Cl in CH₃CN/CH₂Cl₂ (v/v 3:1); **b)** Intensity of λ_{475} (black squares) and λ_{425} (blue circles) over time for a solution PhIO/(TMP)Mn(III)Cl in CH₃CN/CH₂Cl₂ (v/v 3:1).

It is clear that a decrease in intensity of the absorption band at 425 nm (intermediate A) occurs with time. However, as the concentration of intermediate A decreases, the band centred at 475 nm increases in intensity. The simultaneous i) decreasing intensity of intermediate A, and ii) increasing intensity of (TMP)Mn(III)Cl, may indicate that a reduction from high valent Mn intermediate A, yielding back a Mn(III) species, occurs.

To better observe the relationship between the decreasing of the intermediate A absorption band and the increasing of the (TMP)Mn(III)Cl band, the intensity of these two wavelengths is plotted as a function of time, Figure 6.21**b**. The decreasing intensity of intermediate A with time, even in the absence of the substrate, may indicate that reduction of the high valent Mn intermediate A species occurs. The relatively low stability of intermediate A, with a lifetime ~ 10 minutes, may also explain the termination of reaction observed previously (Section 6.3.2, *vide supra*), with only one equivalent of PhIO. Interestingly, by adding fresh PhIO to the solution at 10 minutes, the absorption band at 425 nm is restored, indicating that intermediate A is reformed. This is also in line with the observation made earlier in this Chapter

(Section 6.3.3, *vide supra*), explaining the regenerated catalytic activity observed upon addition of new equivalents of PhIO.

Following an investigation of the intrinsic stability of intermediate A, the investigation of the effect of the substrate on this species was performed, by adding cyclooctane to a UV cuvette containing a solution of PhIO/(TMP)Mn(III)Cl solution.


Figure 6.22 a) Time resolved UV-Vis analysis of a solution PhIO/(TMP)Mn(III)Cl in CH$_3$CN/CH$_2$Cl$_2$ (v/v 3:1), following addition of cyclooctane; **b)** Intensity of λ_{475} (black squares) and λ_{425} (blue circles) over time for a solution PhIO/(TMP)Mn(III)Cl in CH$_3$CN/CH$_2$Cl$_2$ (v/v 3:1).

Following cyclooctane addition, intermediate A disappears to give the Mn(III) porphyrin at 479 nm. Also in this case, the intensity of λ_{max}, measured at 425 nm and 479 nm was reported as a function of time, demonstrating the relatively short lifetime of the high oxidation Mn-porphyrin species; around 45 % of conversion of this species (measured using the relative intensity of λ_{425}) was found 3 minutes after cyclooctane addition. In analogy to Figure 6.21, opposite behaviour is observed for the two absorption bands (blue line and black line in Figure 6.22) This may suggest that the high valent Mn intermediate A, absorbing in the range 415 - 428 nm, is reduced giving a Mn(III)-porphyrin species absorbing at 479 nm. In order to investigate the activity of the species formed at 479 nm, and its capability to restore the high oxidation Mn-porphyrin species at 415 - 428 nm, another equivalent of PhIO was added at 45 minutes. Interestingly, following addition of PhIO, the band assigned

to intermediate A increased in intensity, whilst a dramatic loss of intensity at 479 nm occurred. Nevertheless, although increasing intensity was observed following PhIO addition, a maximum intensity of 0.57 a.u. was achieved, substantially lower than the intensity observed at 0 minutes (0.87 a.u.), thus, suggesting that only partial restoring of intermediate A, can be achieved upon addition of fresh PhIO. This result may explain the decreasing activity previously observed by (TMP)Mn(III)Cl (Section 6.3.3, *vide supra*), in which cyclooctane conversion higher than 50 % was not achieved, even after the periodic addition of new equivalents of PhIO.

To understand the effect of the addition of cyclooctane to the system, in particular to investigate the interactions between cyclooctane and the high valent Mn species, intermediate A, the rate of decomposition of intermediate A was compared with and without cyclooctane (Figure 6.23).
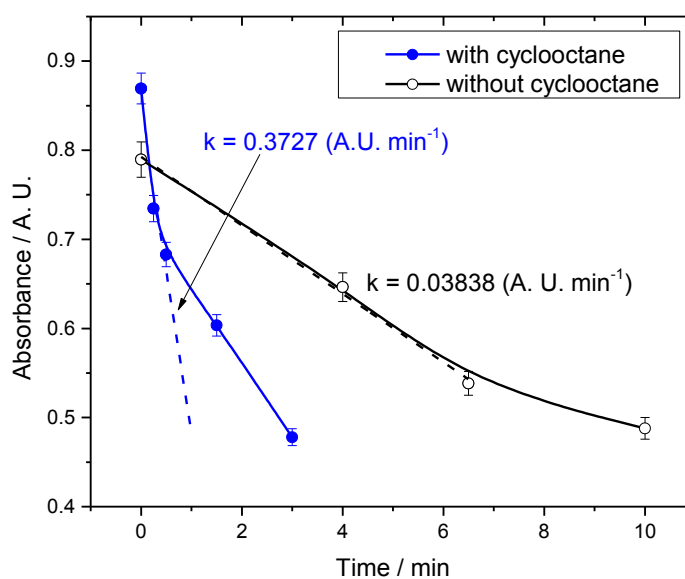
Figure 6.23 Intensity of λ_{425} over time for a solution PhIO/(TMP)Mn(III)Cl in CH$_3$CN/CH$_2$Cl$_2$ (v/v 3:1), with (shaded blue circles) and without (hollow black circles) cyclooctane.

The rate of decomposition of intermediate A was measured in the range of linearity (early stage). Comparing the rate of decrease of the high valent Mn intermediate A in the presence and absence of cyclooctane, it is clear that this species decomposes much faster in the presence of the substrate, cyclooctane. Indeed, a decomposition rate one

order of magnitude higher was found in the presence of cyclooctane (blue line figure 6.23); 0.3727 A.U. min^{-1} against 0.03838 A.U. min^{-1}. The faster rate of decomposition observed following addition of cyclooctane to the system, may indicate the reaction between the substrate and intermediate A. In fact, the high oxidation Mn-porphyrin species may react with cyclooctane through an H-abstraction mechanism, forming the alkyl radical species R· and reforming the Mn(III)-porphyrin species absorbing at 479 nm. In order to investigate the identity of the Mn(III)-porphyrin species absorbing at 479 nm, the UV-Vis spectrum previously observed upon decomposition of intermediate A in the presence of cyclooctane, was compared with the UV-Vis spectrum of pure (TMP)Mn(III)Cl (black line Figure 6.24).
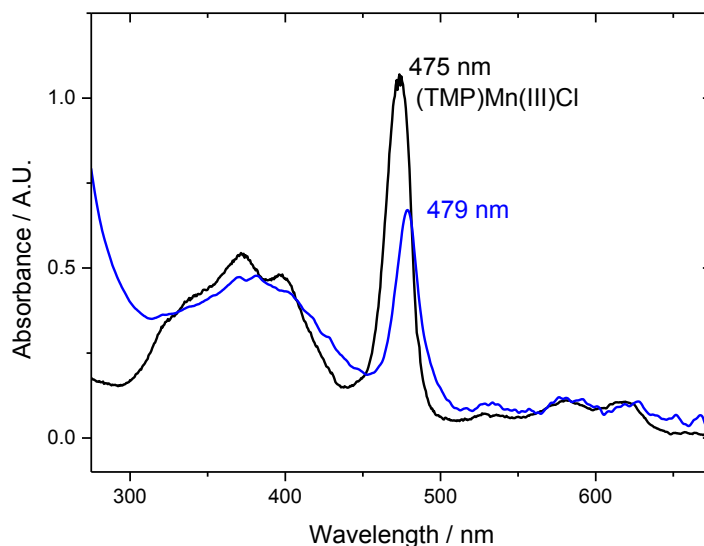

Figure 6.24 UV-Vis spectrum of a pure solution of (TMP)Mn(III)Cl in CH_3CN/CH_2Cl_2 (v/v 3:1) (black like), and UV-Vis spectrum of PhIO/(TMP)Mn(III)Cl solution following decomposition of intermediate A in the presence of cyclooctane (blue line).

As shown in figure 6.24, the two species with λ_{max} centred at 475 and 479 nm appear to be different, showing an isosbestic point around 481 nm and differences in the range 300 - 450 nm. This may suggest that the intermediate A could potentially react with cyclooctane yielding a Mn porphyrin species different from (TMP)Mn(III)Cl. However, to ensure the nature of this species and to understand if is really different from (TMP)Mn(III)Cl, more detailed analysis is required.

Although the identification of intermediate A as a potentially active intermediate species for both oxidation and fluorination, more detailed spectroscopic analysis of the system is required to observe and assign all the intermediate species involved in the system. However, a number of conclusions can already be made. The same intermediate species is formed with and without fluorine sources (AgF and TBAF), thus suggesting that the first steps of reaction are similar for both fluorination and oxidation pathways. The active intermediate species (intermediate A) is relatively unstable and a decomposition rate of 0.038 A.U. min^{-1} is found. In the presence of the substrate a higher decomposition rate of intermediate A is found, 0.37 A.U. min^{-1}, suggesting reaction between cyclooctane and intermediate A, thus potentially indicating intermediate A to be the true reactive intermediate species. Also, intermediate A can be partially restored following addition of fresh amount of oxidant.

The observation of a similar high valent Mn intermediate species for both oxidation and fluorination routes, may suggest that a similar substrate activation mechanism exists for both the fluorination and oxidation routes. Considering the high cyclooctanol/cyclooctanone ratio found at short reaction times, a metal-based oxidation route is suggested for the oxidation pathway, and, consequently also for the fluorination pathway. These hypotheses suggest that both fluorination and oxidation pathways follow the same reaction mechanism for the formation of the alkyl radical species (same H-abstraction mechanism). However, following formation of the alkyl radical species R· two different pathways may occur for oxidation and fluorination, respectively; i) the (TMP)Mn(IV)(OH)X species, generated by H-abstraction, can quickly react with the R· radical yielding to the R-OH species, and ii) the (TMP)Mn(IV)(OH)X species may undergo to ligand exchange with AgF, forming a (TMP)Mn(IV)(F)X species, responsible for the F-rebound mechanism, giving the R-F product. The hypothesis of the additional step (ligand exchange) for the fluorination pathway, may explain the different TOF exhibited by (TMP)Mn(III)Cl with and without fluorine sources (AgF and TBAF), potentially suggesting a different rate limiting step for the fluorination pathway. In fact, whilst TOF of 40 h^{-1} was found in the presence fluorine sources (AgF and TBAF), a TOF of 104 h^{-1} was found in the absence of the fluorine sources.
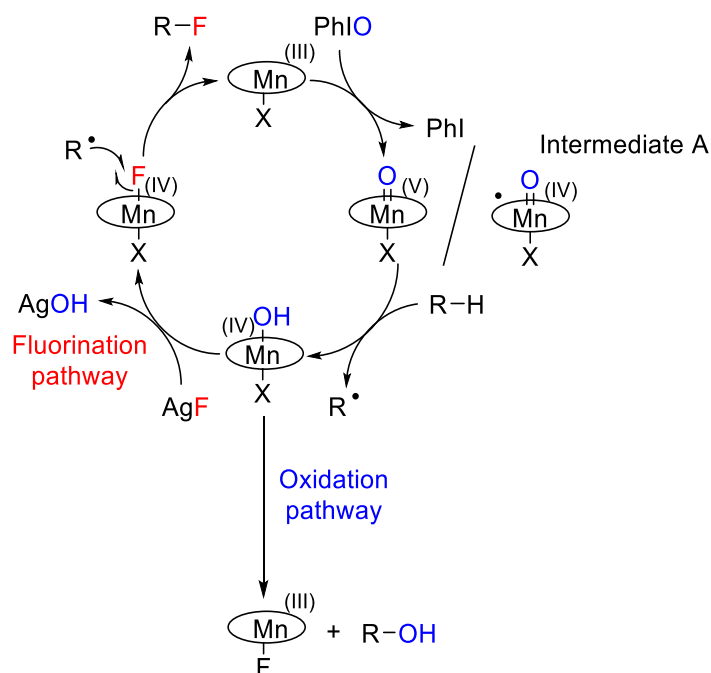
**Figure 6.25:** Possible reaction mechanism showing competition between oxidation and fluorination pathways.
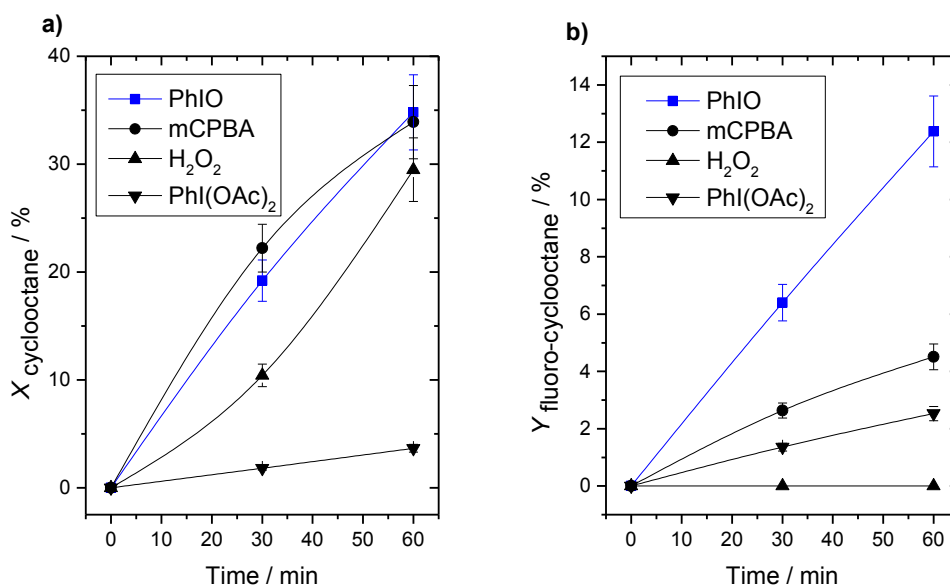
6.3.10 Effect of different oxygen donors

From the kinetic studies performed in the previous sections, competition between oxidation and fluorination clearly occurs under general alkane fluorination conditions with (TMP)Mn(III)Cl and PhIO. Therefore, to investigate the possibility to modulate the selectivity among the two pathways, the performance of the system in terms of oxidation versus fluorination (*i.e.* O-based selectivity vs. F-based selectivity), was studied using a variety of other oxidants instead of PhIO.

Therefore, cyclooctane fluorination reaction was performed under general reaction conditions, albeit using i) $PhI(OAc)_2$, ii) H_2O_2, and iii) mCPBA, instead of PhIO (Figures 6.26 and 6.27).
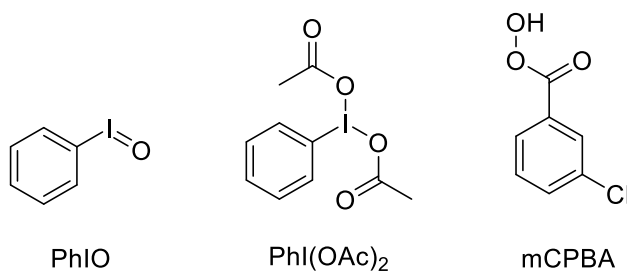
**Figure 6.26:** Structures of PhIO, PhI(OAc)₂ and mCPBA.

Figure 6.27: a) Cyclooctane conversion and **b)** fluoro-cyclooctane yield with time over (TMP)Mn(III)Cl with different oxygen donors. Reaction conditions: 1.5 mmol of cyclooctane, 0.3 mmol of TBAF·3H₂O, 4.5 mmol of AgF, 0.015 mmol (TMP)Mn(III)Cl, 1.5 mL of CH₃CN anhydrous, 0.5 mL of CH₂Cl₂ anhydrous and 3.0 mmol of oxygen donor reagent (one equivalent, 1.5 mmol, respectively added at time 0 and 30 min). The reaction was performed at 50°C in N₂ at 700 rpm.

As shown in Figures 6.27, the employment of different types of oxygen donors leads to drastic modifications in terms of cyclooctane conversion and fluoro-cyclooctane yield.

Interestingly, whilst similar conversion values are achieved after 30 minutes with PhIO, mCPBA and H₂O₂, very different fluoro-cyclooctane yields were observed. This indicates that although similar activity was observed amongst the various oxidants, completely different selectivity was found. In fact, despite the fact that relatively high conversion was achieved after half an hour of reaction, no fluoro-cyclooctane yield was detected at all with H₂O₂ as oxidant, thus indicating that this

type of oxidant is exclusively active for oxidation, and totally inactive for fluorination. However, it is worth noticing that the presence of H_2O_2 involves the presence of water (solution 50 % in water) in the system, which may also influence the balance between oxidation and fluorination. Nevertheless, the complete absence of the desired fluorinated product is an indication that the fluorination path does not occur at all in these conditions.
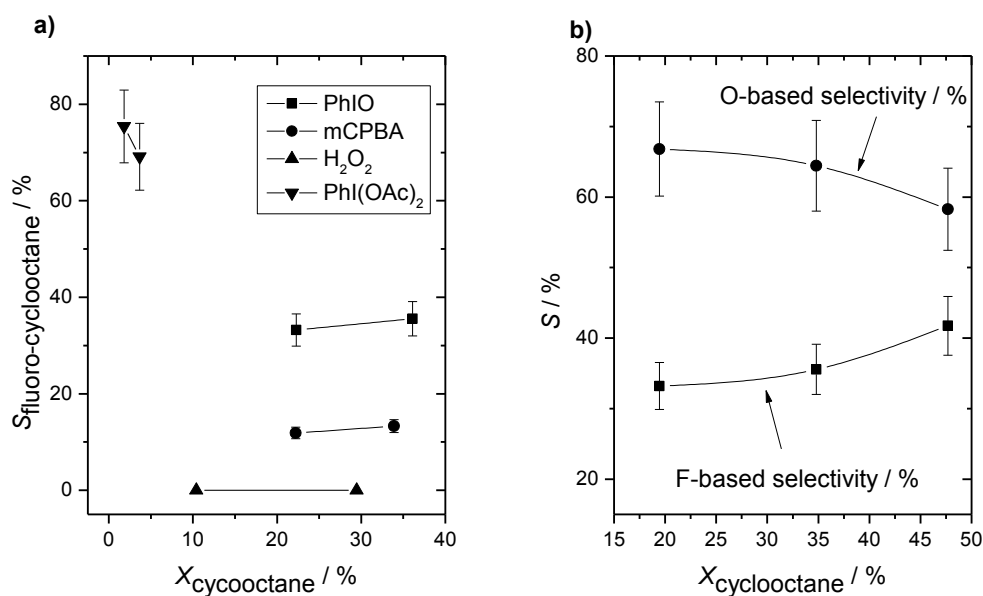
Figure 6.28: a) Fluoro-cyclooctane selectivity over cyclooctane conversion for cyclooctane fuorination reaction with different oxidants; **b)** Selectivity against conversion for O-based selectivity (black circles) and F-based selectivity (black squares), for PhIO.

Plotting fluoro-cyclooctane selectivity over cyclooctane conversion (Figure 6.28**a**), highlights the large impact that the nature of the oxidant has on the balance between fluorination and oxidation. In fact, even though the same activity is reported for PhIO and mCPBA (Figure 6.27), higher fluoro-cyclooctane selectivity is observed with PhIO, (35 % and 13 % observed for PhIO and mCPBA respectively) hence demonstrating that oxidative pathways are more favourable with mCPBA. On the other side, although poor activity was found substituting PhIO with its precursor, (PhI(OAc)$_2$), the highest selectivity was obtained in these conditions (greater than 60 % selectivity), albeit at lower levels of conversion.

This study clearly demonstrates that the type of oxidant employed for the reaction highly affects the selectivity of the process, thus, indicating that the relative rate for

fluorination and oxidation pathway can be tuned by varying the nature of the oxidant species. Nevertheless, whilst the fluorination pathway can easily be completely removed using H_2O_2 as oxidant, elimination of the oxidative pathway, exclusively leading to fluorinated product, is yet to be observed. In fact, although up to 75 % selectivity to fluoro-cyclooctane was found for $PhI(OAc)_2$, very poor activity was observed, with cyclooctane conversion below 4 % seen.

To understand if it is possible to remove the oxidative pathway from the reaction, a plot showing selectivity over conversion for both fluorine selectivity and oxygen selectivity, using the best conditions, PhIO as oxidant is shown in Figure 6.28**b**. Notably total oxygen selectivity (O-based selectivity) was calculated as a sum of the single selectivity value obtained for each oxidised product.

Plotting both F-based selectivity and O-based selectivity over cyclooctane conversion it looks clear that under these reaction conditions, oxidation is favoured over fluorination. In fact, although increasing F-based selectivity (up to 40 %) was found and near 50 % of cyclooctane conversion demonstrated, O-based selectivity is higher than the F-based one. Thus, indicating that, even though alkane fluorination occurs using (TMP)Mn(III)Cl porphyrin and fluorine sources, the competitive oxidation pathway cannot be eliminated under these reaction conditions (*i.e.* using oxygen donor species as oxidants).

Despite this, these observations indicate that the catalytic activity and selectivity toward oxidation and fluorination can be tuned by varying the nature of the oxidant. Therefore, future studies will focus on the screening of other types of oxidant species different from the classic oxygen donor species (such as PhIO), in order to investigate if higher fluorination selectivity can be achieved.

6.3.11 UV-Vis analysis with different oxidants

To begin to study the reasons responsible for the different activity and selectivity observed in the presence of the different oxidants, time on line UV-Vis analysis was performed using $PhI(OAc)_2$ and H_2O_2, in order to investigate the intermediate species formed upon interaction between i) (TMP)Mn(III)Cl and $PhI(OAc)_2$, and ii) (TMP)Mn(III)Cl and H_2O_2. In fact, although poor activity was observed using

PhI(OAc)$_2$, the highest fluoro-cyclooctane selectivity was observed. Therefore, the species formed upon interactions with PhI(OAc)$_2$ can be used as reference model for the fluorination pathway. In contrast to the (TMP)Mn(III)Cl - PhI(OAc)$_2$ system, the interactions between (TMP)Mn(III)Cl and H$_2$O$_2$ can be investigated as a model system for a pure oxidative system (*i.e.* in the absence of the fluorination pathway).

Firstly, PhI(OAc)$_2$ was added to a UV cuvette containing a solution of (TMP)Mn(III)Cl in CH$_3$CN/CH$_2$Cl$_2$ (v/v 3:1) and time on line UV-Vis analysis was performed and reported in Figure 6.29:
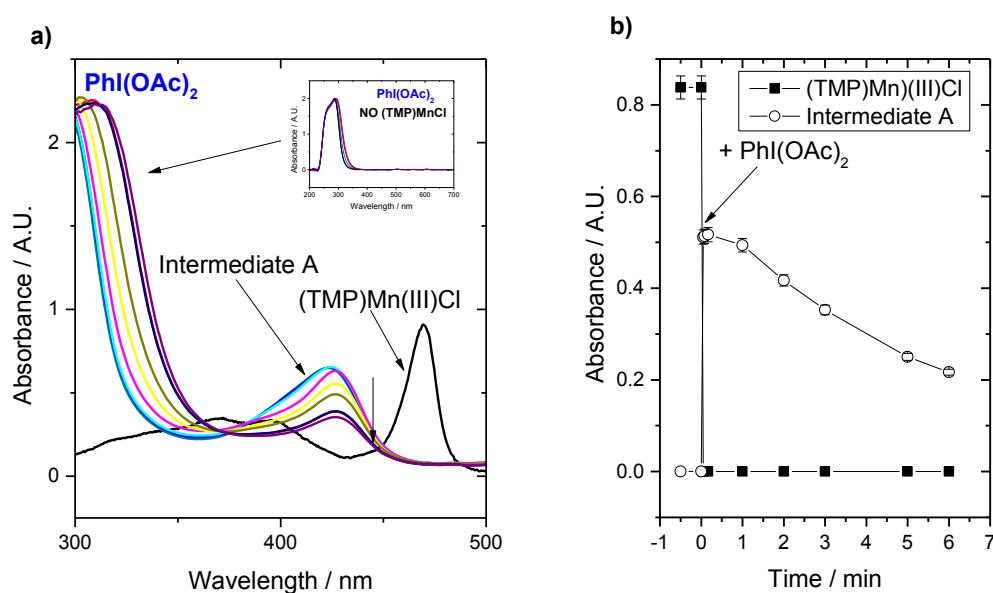
Figure 6.29: a) Time resolved UV-Vis analysis of a (TMP)MnCl solution in CH$_3$CN/CH$_2$Cl$_2$ (v/v 3:1) before (black line) and after the addition of PhI(OAc)$_2$. **Right top inset:** UV-Vis analysis of a solution of PhI(OAc)$_2$ in CH$_3$CN/CH$_2$Cl$_2$ (v/v 3:1), in the absence of (TMP)Mn(III)Cl; **b)** Intensity of λ_{475} (shaded squares) and λ_{425} (hollow circles) over time before and after PhI(OAc)$_2$ addition (at t = 0).

As shown in Figure 6.29, following addition of PhI(OAc)$_2$, the absorption band characteristic of (TMP)Mn(III)Cl totally disappears, whilst a new absorption band appears at 425 nm, indicating the formation of intermediate A, as found for PhIO. However, the absorption band at 425 nm was found to be highly unstable, quickly decreasing in intensity after only a few minutes as reported in Figure 6.29**b**, plotting the intensity of λ_{max} over time for 475 and 425 nm.

Despite the decreasing intensity of the species absorbing at 425 nm with time, no new features related to a Mn-porphyrin species were observed, potentially indicating: i) formation of a Mn-porphyrin species not visible at UV-Vis or ii) decomposition of the Mn-porphyrin complex. Although further analysis, including MS analysis of the solution, are essential to identify the species formed upon decomposition of the species at 425 nm, this result may explain the poor activity observed in these reaction conditions (*i.e.* replacing PhIO with PhI(OAc)$_2$). In fact, in contrast to PhI(OAc)$_2$, when PhIO was used as oxidant, decreasing of the intensity of the band centred at 425 nm was shown to be related to an increase in the band at 478 - 479 nm, re-establishing a Mn(III)-porphyrin species, subsequently oxidised again upon addition of new amounts of PhIO, subsequently re-establishing the species at 425 nm.

Notably, UV-Vis analysis of a solution of PhI(OAc)$_2$ in CH$_3$CN/CH$_2$Cl$_2$ (v/v 3:1), in the absence of (TMP)Mn(III)Cl, was performed, and an intense absorption band in a range 225 - 400 nm was observed, demonstrating that the intense absorption band at λ < 380 nm observed in Figure 6.29**a** is due to pure PhI(OAc)$_2$ and/or its decomposition products.

Following preliminary UV-Vis analysis of (TMP)Mn(III)Cl interactions with PhI(OAc)$_2$, the same experiment was repeated using H$_2$O$_2$ as oxidant.
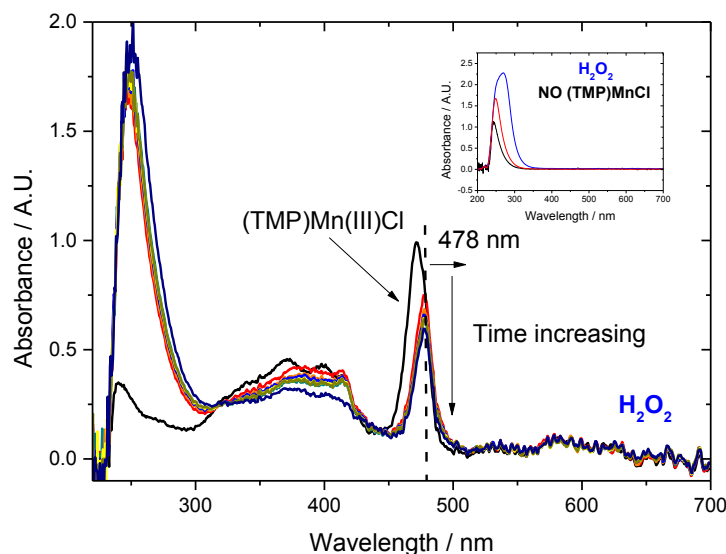
Figure 6.30: Time resolved UV-Vis analysis of a (TMP)MnCl solution in CH_3CN/CH_2Cl_2 (v/v 3:1) before (black line) and after the addition of H_2O_2. Inset: Time on line UV-Vis analysis of a solution of PhI(OAc)$_2$ in CH_3CN/CH_2Cl_2 (v/v 3:1), in the absence of (TMP)Mn(III)Cl.

Interestingly, upon adding H_2O_2 to a solution of (TMP)Mn(III)Cl in CH_3CN/CH_2Cl_2 (v/v 3:1), although no oxidised species absorbing at wavelength 425 nm was observed, a small red shift (from 475 nm to 478 nm) occurred. This shift, may suggest an exchange of the axial ligand (Cl⁻) with an oxygen based ligand derived from the addition of H_2O_2/H_2O. Also, a small decreasing of intensity of the absorption band at 478 nm was observed, potentially indicating: i) formation of a new species with a different extinction coefficient (ε) or ii) partial decomposition/conversion of Mn-porphyrin into a species not absorbing in the UV-Vis region.

To properly compare the different species formed upon interaction of the various oxidants with (TMP)Mn(III)Cl, the different UV-Vis spectra observed straight after the addition of the respective oxidant to the solution of (TMP)MnCl are reported in Figure 6.31. As shown in the following figure, whilst similar high oxidation state Mn species with wavelength in the range 415 - 428 nm are observed following PhIO and PhI(OAc)$_2$ addition, only a very light shift toward higher wavelengths was observed with H_2O_2, clearly indicating that a different oxidation pathway that does not lead to fluorination is involved in these conditions (with H_2O_2).

Whilst PhIO and PhI(OAc)$_2$ give the same type of intermediate species, intermediate A, reversible interconversion between intermediate A and (TMP)Mn(III)X occurs in the presence of PhIO, thus potentially explaining the high activity observed with PhIO. However, with H$_2$O$_2$, intermediate A is not observed at all, thus suggesting that the reaction occurs *via* a different mechanism with different type of intermediates, exclusively leading to oxidation. From these observations it can be concluded that the formation of intermediate A is thought to be essential for the fluorination pathway.
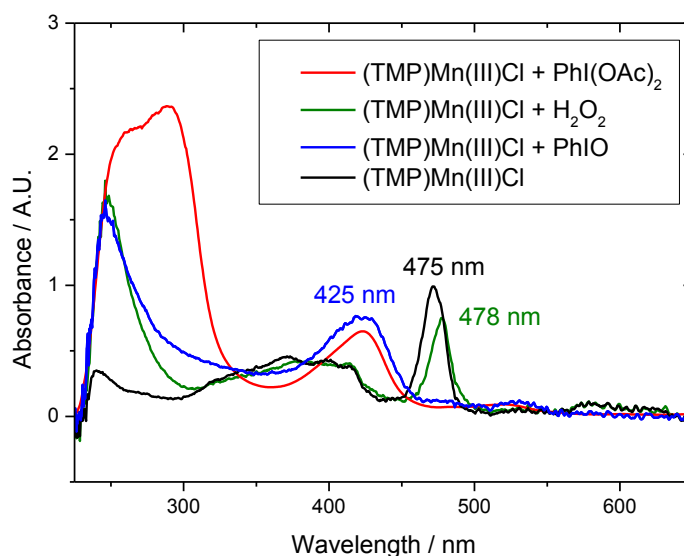
Figure 6.31: UV-Vis spectra of (TMP)Mn(III)Cl solution in CH$_3$CN/CH$_2$Cl$_2$ (v/v 3:1) before (black line) and after the addition of i) PhI(OAc)$_2$ (red line), ii) H$_2$O$_2$ (green line), and iii) PhIO (blue line).

6.3.12 Strategy to prepare a heterogeneous catalyst for alkane fluorination

Following a basic kinetic and mechanistic study, in order to have a better understanding of the model system, a preliminary approach toward the design and the catalytic testing of a heterogeneous catalyst active for alkane fluorination will be the focus of this section. In fact, as previously reported in Chapter 1, heterogeneous catalysts are generally preferred to homogeneous ones for industrial applications, mainly due to their ease of separation from reaction mixtures, leading to the development of simpler and less expensive processes. Therefore, the development of a robust heterogeneous catalyst active for alkane fluorination, never reported in

literature so far, would represent a significant breakthrough from both mechanistic and industrial perspective.

However, the choice of the metallic source (in this case the type of ligand coordinating the Mn centre) plays a central role in the design of an active heterogeneous catalyst. Therefore, to investigate the role of the porphyrin on the catalytic activity of Mn, the catalytic activity of simple Mn(II) and Mn(III) complexes was investigated, performing the reaction with: i) Mn(acac)$_2$ and ii) Mn(acac)$_3$. Nevertheless, with both catalysts, no conversion and yield were observed, demonstrating that the porphyrin scaffold is essential to stabilise the high oxidation states of Mn(V) and (IV) due to electron exchanges with the porphyrin ring.

Considering that the porphyrin scaffold is essential for catalytic activity to be observed, a preliminary strategy for the preparation of a heterogeneous catalyst able to perform alkane fluorination reaction was identified by supporting (TMP)Mn(III)Cl. Therefore, a preliminary attempt to support (TMP)Mn(III)Cl was performed, supporting (TMP)Mn(III)Cl on silica, SiO$_2$. Notably, SiO$_2$ is a readily available support, reported to be an efficient support for one bio-mimetic complex, used as catalyst for methane selective oxidation to methanol following doping of μ-nitrido diiron tetra-tert-butylphthalocyanine (FePctBu$_4$)$_2$N, a biomimetic compound.[15,25]

Pure (TMP)Mn(III)Cl was supported on SiO$_2$ according to the procedure reported in literature by Sorokin *et al.*,[15] yielding to a green solid, denoted (TMP)Mn(III)Cl@SiO$_2$ and characterised *via* solid UV-Vis analysis (Figure 6.32). Notably, the (TMP)Mn(III)Cl loading on SiO$_2$ was determined *via* UV-Vis analysis of the (TMP)Mn(III)Cl solution prior and following impregnation on SiO$_2$, giving a (TMP)Mn(III)Cl loading of 28.4 μmol/g. Indeed, starting and final (TMP)Mn(III)Cl concentration values, were measured using the Beer-Lambert law (Equation 6.1) through previous UV-Vis calibration with standard (TMP)Mn(III)Cl solution.
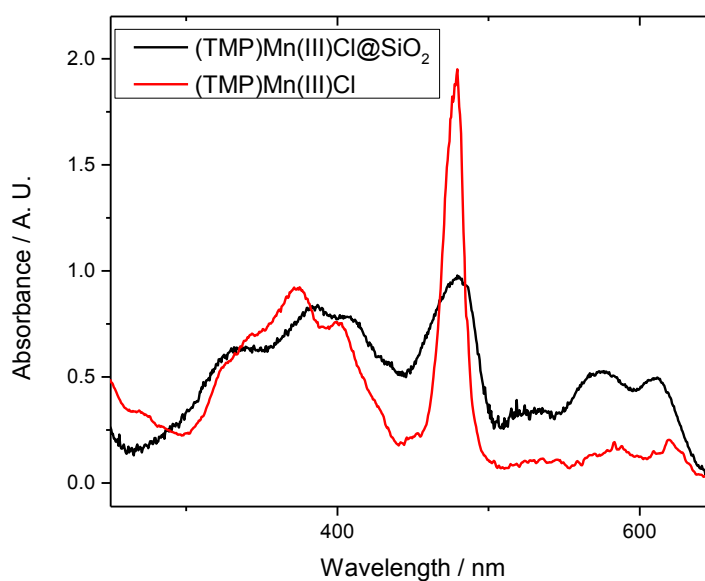
$$A = \varepsilon[C]l$$

Equation 6.1: Beer-Lambert Law

Where: A = absorbance
ε = molar extinction coefficient
[C] = concentration
l = path length of the sample cell

Figure 6.32 Liquid UV-Vis spectrum of (TMP)Mn(III)Cl solution in CH_3CN/CH_2Cl_2 (v/v 3:1) (red line), and solid Diffusive Reflectance UV-Vis spectrum of (TMP)Mn(III)Cl@SiO_2.

Solid UV-Vis analysis of (TMP)Mn(III)Cl@SiO_2 (black line Figure 6.32), clearly demonstrates the presence of (TMP)Mn(III)Cl on SiO_2, as shown by the presence of an absorption pattern similar to the one reported for a solution of pure (TMP)Mn(III)Cl (red line Figure 6.32). Also, the broadening of the absorption bands of (TMP)Mn(III)Cl, could indicate that the porphyrin is bound to the support.

The investigation of the catalytic performances of the supported material so prepared, for cyclooctane fluorination reactions, are detailed below.

6.3.13 Catalytic performances of (TMP)Mn(III)Cl@SiO₂

Following preparation and preliminary characterisation of (TMP)Mn(III)Cl@SiO$_2$, a study of the catalytic performances exhibited by this material for cyclooctane fluorination reaction was performed. Notably, to properly compare supported and unsupported (TMP)Mn(III)Cl, (TMP)Mn(III)Cl@SiO$_2$ was tested under identical reaction conditions of unsupported (TMP)Mn(III)Cl.
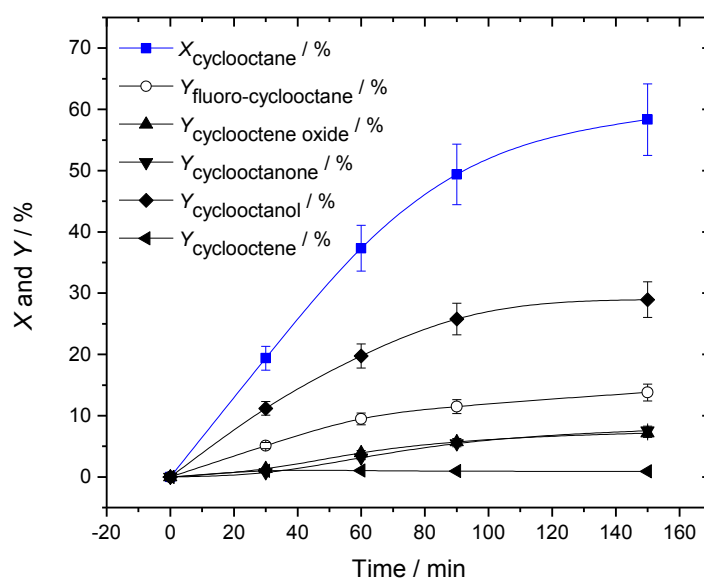

Figure 6.33: Cyclooctane conversion (blue line) and products yield (black line) with time over (TMP)Mn(III)Cl@SiO$_2$. Reaction conditions: 1.5 mmol of cyclooctane, 0.3 mmol of TBAF·3H$_2$O, 4.5 mmol of AgF, 0.015 mmol (TMP)Mn(III)Cl (TMP)Mn(III)Cl@SiO$_2$), 1.5 mL of CH$_3$CN anhydrous, 0.5 mL of CH$_2$Cl$_2$ anhydrous and 3.0 mmol of PhIO (one equivalent, 1.5 mmol, respectively added at time 0 and 30 min). The reaction was performed at 50°C in N$_2$ at 700 rpm.

As shown in Figure 6.33, good catalytic activity, similar to the one exhibited by unsupported (TMP)Mn(III)Cl, was observed in these conditions. Nevertheless, although formation of 14 % of fluoro-cyclooctane yield was detected (hollow circles in Figure 6.33), higher selectivity for cyclooctanol (rhombus in Figure 6.33) was observed, with cyclooctanol obtained as major product (29 % of cyclooctanol yield and 14 % of fluoro-cyclooctane yield detected at 150 minutes). The higher selectivity for cyclooctanol observed in these conditions could be explained by: i) the presence of

hydroxyl groups present as impurities on SiO_2 surface, or ii) modifications of the axial ligand bound to the Mn, as an effect of the coordination of (TMP)Mn(III)Cl to the support (SiO_2).

Nevertheless, although good catalytic activity observed, high leaching of (TMP)Mn(III)Cl in the solution was detected, suggested by green colour of the reaction mixture. To verify the presence of the Mn-porphyrin leached into the reaction mixture, UV-Vis analysis of the solution at t_0 (before the addition of PhIO), following removal of the solid catalyst, was performed.
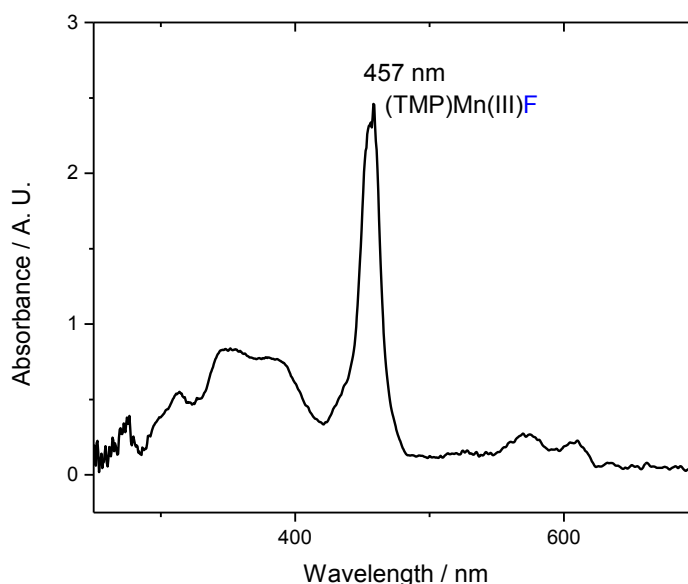
Figure 6.34: UV-Vis spectrum of reaction solution of cyclooctane fluorination with (TMP)Mn(III)Cl@SiO2, before the addition of PhIO, following removal of the solid catalyst, (TMP)Mn(III)Cl@SiO2.

As shown in Figure 6.34, UV-Vis of the solution following removal of the solid catalyst, shows that an intense absorption band at 457 nm, previously assigned to (TMP)Mn(III)F, formed by exchange of the Cl$^-$ ligand with a F$^-$ (from TBAF), is present in solution. This confirms the instability of the supported (TMP)Mn(III)Cl@SiO_2 heterogeneous catalyst under reaction conditions. Notably, by determining the concentration of Mn-porphyrin present in solution *via* the Beer-Lambert law, it could be estimated that approximately 59 % of the initially supported (TMP)Mn(III)Cl was found in solution. Considering this, an estimation of the

heterogeneous contribution to the reaction (*i.e.* the catalytic performance of non-leached (TMP)Mn(III)Cl@SiO$_2$), could be performed. Therefore, the activity and selectivity towards the main products, fluoro-cyclooctane and cyclooctanol, was reported as a function of cyclooctane conversion (Figure 6.35) for both supported and unsupported (TMP)Mn(III)Cl.
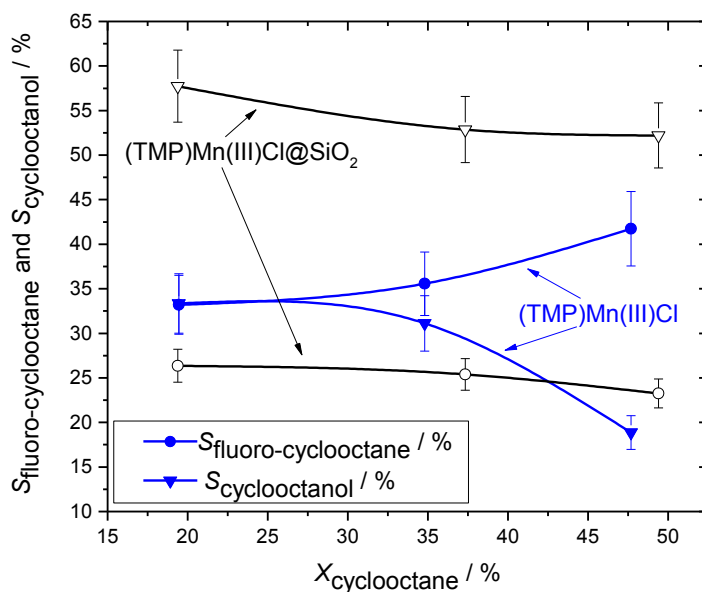
Figure 6.35: Fluoro-cyclooctane (circles) and cyclooctanol (triangles) selectivity against cyclooctane conversion with unsupported (TMP)Mn(III)Cl (shaded blue symbols) and (TMP)Mn(III)Cl@SiO$_2$ (hollow black symbols).

As shown in Figure 6.35, similar activity was observed for both unsupported and supported (TMP)Mn(III)Cl, in terms of substrate conversion achieved per unit time. Since only 59 % of the complex was found in solution by UV-Vis analysis, the similar levels of substrate conversion achieved indicates that at least some activity (up to 40 %) is obtained from the supported complex, presuming a first order relationship between (TMP)Mn(III)Cl concentration and activity. Although the high level of leaching is obviously undesirable, achieving some contribution of activity from the supported complex clearly indicates the possibility that future catalysts, based on supported and/or encapsulated (TMP)Mn(III)Cl, could be developed.

However, although similar activity was found, it is notable that different selectivity was observed with unsupported (TMP)Mn(III)Cl and supported

(TMP)Mn(III)Cl@SiO$_2$. Indeed, whereas fluoro-cyclooctane was formed as major product with unsupported (TMP)Mn(III)Cl, increased selectivity to cyclooctanol was observed for the heterogeneous catalyst, supported (TMP)Mn(III)Cl@SiO$_2$. This indicates that the supported complex is somewhat more selective to cyclooctanol than fluoro-cyclooctane. The higher cyclooctanol selectivity observed with (TMP)Mn(III)Cl@SiO$_2$ could be due to several reasons, such as: i) the possible presence of hydroxyl groups on the material, which may participate in the reaction mechanism, and ii) the coordination of (TMP)Mn(III)Cl with the support, which may prevent the formation of the (TMP)Mn(F)$_2^-$ species reported by Groves[6,22] to be responsible for the F-rebound chemistry, through occupation and/or steric blocking of the axial positions. In the latter case, it may be necessary for future studies to focus on other methods of immobilisation, such as encapsulation of (TMP)Mn(III)Cl within a porous network, in order to achieve high levels of stability without negatively impacting the intrinsic chemistry of the porphyrin and therefore hindering its ability to perform fluorination. Nevertheless, further studies to properly investigate the activity and selectivity of immobilised materials are clearly required.

6.4 Conclusions

In this chapter, kinetic and mechanistic investigation of alkane fluorination reactions catalysed by a biomimetic catalyst, (TMP)Mn(III)Cl, was performed. In contrast to the system investigated in Chapter 5, where electrophilic/radical fluorine sources were employed (*i.e.* Selectfluor®), the model system studied in this chapter is proposed to occur *via* H-abstraction mechanism, catalysed by a high oxidation state Mn-porphyrin species, followed by a F-rebound step. Considering the promising nature of this system, kinetic studies, using cyclooctane as model substrate were then performed, using PhIO as oxidant. Under these conditions, using 1 mol % of (TMP)Mn(III)Cl and only one equivalent of PhIO, termination of reaction after 30 minutes occurred with no further conversion seen. Following investigation of the effects responsible for the termination of reaction after 30 minutes, it was found that periodic addition of fresh amounts of PhIO could partially restore the catalytic activity of the catalyst, indicating that decomposition of active oxidant agent typically occurs in < 30 minutes. However, whilst addition of other equivalents of fluorine sources (*i.e.* AgF and TBAF) did not affect the kinetics of the reaction, the addition of fresh amounts of

(TMP)Mn(III)Cl was found to be essential to achieve cyclooctane conversion values > 50. This indicates that decomposition of (TMP)Mn(III)Cl occurred after an average of 50 catalytic cycles (maximum TON = 50). Nevertheless, although consistent cyclooctane conversion values were achieved, fluoro-cyclooctane selectivity higher than 50 % was never achieved. This is in line with the report previously published by Groves group[6], where maximum yields were achieved in a range 50 - 60%, albeit the authors utilised a periodic addition of PhIO and (TMP)Mn(III)Cl. More detailed reaction mixture analysis, in fact, revealed the presence of oxidised by-products in solution, (such as cyclooctanol, cyclooctanone, cyclooctene oxide and cyclooctene) demonstrating competition between a fluorination pathway and an oxidative reaction pathway (this is in line with the findings of Chapter 5 where competition between fluorination/oxidation was found to some extent). Time on line analysis of all the products formed in solution, revealed cyclooctanol to be the main product of the oxidative route, formed with similar yields of fluoro-cyclooctane. However, stability studies revealed that the fluoro alkyl product can undergo to de-hydrofluorination, forming small amounts of cyclooctene, subsequently further oxidised to cyclooctene oxide. Stability studies were also performed on cyclooctanol, demonstrated that high amount of cyclooctanol can be oxidised to give cyclooctanone as major product.

To further investigate the competition between fluorination and oxidation, mechanistic studies focusing on UV-Vis analysis were performed. Following UV-Vis analysis several conclusions can be made: i) an intermediate species at 425 nm related to a high oxidation state Mn-porphyrin species was formed upon addition of PhIO to a solution of (TMP)Mn(III)Cl, ii) the same species was found with and without fluorine sources (*i.e.* AgF and TBAF), suggesting the same intermediate species exists for both oxidation and fluorination pathways. Further investigation of the intermediate species at 425 nm was then performed, investigating the behaviour of this absorption band with and without the substrate. In both cases, the species at 425 nm was found to decompose, giving a Mn(III)-porphyrin species at 475 - 479 nm, however, in the presence of cyclooctane, a decomposition rate 1 order of magnitude higher was observed. This may suggest interactions between cyclooctane and the intermediate high valent Mn species at 425 nm.

Despite the preliminary analysis reported in this Chapter, more detailed analysis, using complementary techniques (such as Resonance Raman and Mass Spectrometry), are required for a full identification of the intermediate species involved in the reaction mechanism.

From the previous studies, is clear that competition between oxidation and fluorination occurs under general alkane fluorination conditions with (TMP)Mn(III)Cl and PhIO. Therefore, the possibility to modulate the selectivity amongst the two pathways, was investigated using a variety of other oxidants instead of PhIO. Interestingly, it was found that in changing the type of oxidant is possible to modulate the selectivity of the system in terms of fluorination/oxidation selectivity. The observation that the catalytic activity and selectivity of this type of biomimetic compound, (TMP)Mn(III)Cl, can be tuned by varying the type of oxidant is indeed promising, and more detailed studies, aimed to the discovery of an oxidant ideally able to switch on only the fluorination route, will be performed in future studies. However, whilst the findings that the selectivity of fluorination versus oxidation pathways are tuneable upon changing the oxidant, the oxidative route was ultimately found to be the favoured route under the reaction conditions explored, with a maximum of fluoro-cyclooctane selectivity of 50% achieved when PhIO was used as oxidant at 50 % of cyclooctane conversion. This further indicates that more detailed investigation of the system, in order to optimise the fluorination versus oxidation selectivity favouring the fluorination route is required.

Following optimisation studies of the model system, a preliminary attempt toward the design of a heterogeneous catalyst active for alkane fluorination was performed by supporting (TMP)Mn(III)Cl on SiO_2. However, although good catalytic activity (58 % of cyclooctane conversion observed at 150 minutes) was demonstrated by this material, higher oxidation selectivity was found, with cyclooctanol observed as main product. Also, high levels of (TMP)Mn(III)Cl leaching were observed by UV-Vis analysis of the reaction solution, with (TMP)Mn(III)F found present in solution. Clearly, future work should be focused upon identifying alternative methods of supporting or encapsulating the Mn-porphyrin catalyst (see Chapter 7 for further discussion).

6.5 References

1 [1]K. L. Hull, W. Q. Anani, M. S. Sanford, *J. Am. Chem. Soc*. 2006, **128**, 7134−7135.

2 W. Liu, J. T. Groves, *Angew. Chem., Int. Ed*. 2013, **52**, 6024−6027.

3 S. Bloom, A. Sharber, M. G. Holl, J. L. Knippel, T. Lectka, *J. Org. Chem*. 2013, **78**, 11082−11086.

4 J.-B. Xia, C. Zhu, C. Chen, *J. Am. Chem. Soc*. 2013, **135**, 17494−17500.

5 S. Bloom, M. McCann, T. Lectka, *Org. Lett*. 2014, **16**, 6338−6341.

6 W. Liu, X. Y. Huang, M. J. Cheng, R. J. Nielsen, W. A. Goddard, J. T. Groves, *Science*, 2012, **337**, 1322 −1325.

7 P.R. Ortiz de Montellano, *Chem. Rev*. 2010, **110** (2), 932-948.

8 J. T. Groves, *J. Chem. Educ.*, 1985, **62** (11), 928-931.

9 C. N. Neumann, T. Ritter, *Nature Chemistry*, 2016, **8** (9), 822-823.

10 S. Bloom, J. L. Knippel, T. Lectka *Chem. Sci.*, 2014, **5**, 1175–1178.

11 J.-B. Xia, C. Zhu and C. Chen, *Chem. Commun.*, 2014, **50**, 11701-11704.

12 C. R. Pitts, S. Bloom, R. Woltornist, D. J. Auvenshine, L. R. Ryzhkov, M. A. Siegler, T. Lectka, *J. Am. Chem. Soc*. 2014, **136**, 9780−9791.

13 H. Volz, T. Barth, *Liebigs Ann. Chem.*, 1989, 171-175.

14 K. Fisher, D. Mcphee, F. X. Woolard, Patent N° WO 2009/088404, 2009.

15 A. B. Sorokin E. V. Kudrik, L. X. Alvarez, P. Afanasiev, J. M. M. Millet, D. Bouchu, Catal. Today, 2010, **157**, 149-154.

16 N. Havare, D. A. Plattner, *Org. Lett.*, 2012, **14**, 5078−5081.

17 J. Kim, R. G. Harrison, C. Kim, L. Que, Jr. *J. Am. Chem. Soc.*, 1996, **118** (18), 4373–4379.

18 S. Fetzner, F. Lingens, *Microbiol Rev*. 1994, **58** (4), 641–685.

19 J. V. Beach, K. J. Shea, *J. Am. Chem. Soc.*, 1994, **116** (1), 379–380.

20 J. P. Collman, J. I. Brauman, B. Meunier, T. Hayashi, T. Kodadek, Sc. A. Raybuck *J. Am. Chem. Soc*. 1985, **107**, 2000-2005.

21 A. De Mico, R. Margarita, L. Parlanti, A. Vescovi, G. Piancatelli, *J. Org. Chem.*, 1997, **62** (20), 6974–6977.

22 W. Liu, J. T. Groves, *Acc. Chem. Res*. 2015, **48**, 1727−1735.

23 R. D. Arasasingham, T. C. Bruice, *Inorg. Chem.*, 1990, **29**, 1422-1427.

24 J. T. Groves, M. K. Stern, *J. Am. Chem. Soc.*, 1988, **110**, 8628–8638.

[25] M. M. Forde, B. C. Grazia, R. Armstrong, R. L. Jenkins, M. Hasbi Ab Rahim, A. F. Carley, N. Dimitratos, J. A. Lopez-Sanchez, S. H.Taylor, N. B. McKeown, G. J. Hutchings, *J. Catal.*, 2012, **290**, 177-185.

Conclusions and Pertaining Challenges

7

7.1 Conclusions

In this thesis, the viability of heterogeneous catalysts to perform $C(sp^3)$-F bond formation has been studied.

In the first chapters of the thesis (Chapter 3 and 4), the formation of $C(sp^3)$-F bonds from activated substrates, such as carboxylic acids, was investigated. Despite difficulties related to the stability of heterogeneous materials in the harsh reaction conditions typically required for fluorination reactions with electrophilic/radical fluorine sources, such as Selectfluor®, it was found that stable and active heterogeneous materials can be employed for decarboxylative fluorination reactions. In particular, as reported in Chapter 3, mechanochemically-prepared 1 wt. % Ag_2O/TiO_2 was found to be an efficient and reusable heterogeneous catalyst for the decarboxylative fluorination of various carboxylic acids. Impressively, higher turnover numbers (TON) and turnover frequencies (TOF) to those reported for the corresponding homogeneous catalyst ($AgNO_3$) were obtained under otherwise identical reaction conditions. Optimisation and spectroscopic characterisation of the mechanochemically-prepared materials was performed, showing that phase transformations between two different oxides (Ag_2O and Ag_2O_2) can occur, and an optimal milling frequency in terms of activity and stability occurs at 15 Hz. Indeed, with suitable regeneration between cycles, up to five catalytic cycles without loss in activity were achieved for the mechanochemically prepared catalyst, resulting in TON over one order of magnitude higher than has been previously observed being obtained by homogeneous analogues with specific substrates. Curiously, heat treatments of the materials also led to the discovery that mechanochemical milling gives rise to light sensitive materials.

In view of the development of light sensitive Ag_2O/TiO_2 materials, Chapter 4 focused upon the photocatalytic decarboxylative fluorination reaction, in the presence of UV light. During these studies, it was found that even in the absence of Ag, pure,

unmodified TiO$_2$ is an active heterogeneous catalyst for photocatalytic decarboxylative fluorination. Indeed, as reported in Chapter 4, the activation of TiO$_2$, resulted in a highly active photocatalytic decarboxylative fluorination reaction, yielding TOFs up to 1113 h^{-1} when 2,2-dimethylglutaric acid was used as substrate. Impressively, these TOFs, which are twice those previously reported in the literature, could potentially be further increased, should more detailed optimisation of the reaction conditions be performed. In Chapter 4, detailed mechanistic studies with several kinetic and spectroscopic techniques (XPS, MAS NMR, DRIFTS), allowed detailed study of the reaction mechanism, and based on these studies, a tentative reaction mechanism was proposed.

The employment of non-toxic and readily available TiO$_2$ to perform photo-catalysed selective C(sp^3)-F bond formation, in the presence of Selectfluor® and with high TOFs, represents a significant finding in the field of fluorination chemistry. Indeed, this finding could lead to the development of a more industrially amenable fluorination process for the synthesis of highly desirable fluorinated compounds. Moreover, the employment of water as solvent, the absence of additional metal into the reaction solution (e.g. Ag) and the facile recovery of TiO$_2$, efficiently reused up to 4 times, dramatically increases the sustainability of this method over those previously reported in the literature. Combined, Chapters 3 and 4 clearly demonstrate the viability of solid materials to act as heterogeneous catalysts for C(sp^3)-F bond forming reactions.

Following this achievement, a more difficult strategy was also explored, investigating the performance of heterogeneous catalysts to achieve direct C(sp^3)-H fluorination. Indeed, whilst decarboxylative fluorination represents an interesting system for the formation of new C(sp^3)-F bonds, pre-activated substrates are always required, leading to decreased atom efficiency. However, although direct C(sp^3)-H fluorination represents an elegant and desirable approach, this strategy is also far more challenging, due to the greater stability of C(sp^3)-H bonds relative to C(sp^3)-COOH bonds.

Nevertheless, when performing decarboxylative fluorination reactions with TiO$_2$ and Ag$_x$O/TiO$_2$ with different substrates (malonic acid, citric acid), it was found that particular, activated C(sp^3)-H bonds (such as benzylic C-H), resulted in competition

between decarboxylative fluorination and direct $C(sp^3)$-H fluorination occurring. Building upon this observation, a preliminary investigation of the catalytic performances of heterogeneous catalysts, such as Ag_xO/TiO_2 to perform direct $C(sp^3)$-H fluorination was thus performed, using the fluorination of ethylbenzene as a model reaction. However, although the heterogeneous material was found to possess some levels of activity for this reaction, thus demonstrating that heterogeneous catalysts can in principle be active also for direct $C(sp^3)$-H fluorination, this system was also found to exhibit several, major disadvantages. Indeed, several drawbacks were found, such as: i) poor selectivity for the fluorinated compound, ii) undesirable competition between oxidation and fluorination, iii) poor stability of the fluorinated compound, resulting in competitive reactions, and iv) poor selectivity with respect to Selectfluor® (4 to 8 equivalents required for acceptable levels of activity and selectivity to be observed). Moreover, it was found that the requirement for excessive quantities of Selectfluor® resulted from the non-catalytic reaction between Selectfluor® and the solvent, acetone, which resulted in the generation of a highly toxic compound, fluoroacetone. Unfortunately, avoiding the use of acetone, used as a co-solvent to solubilise the substrates, could not be achieved over the time frame of this work, thus limiting the immediate viability of the system.

Considering the poor viability of direct $C(sp^3)$-F systems with electrophilic/radical fluorine sources, such as Selectfluor®, an alternative approach for direct $C(sp^3)$-H fluorination was subsequently explored, specifically using Groves[1] system as model system for alkane fluorination reaction. Indeed, unlike previous systems, this alkane fluorination route is reported to be catalysed by a biomimetic compound, (TMP)Mn(III)Cl, and requires nucleophilic fluorine sources such as AgF and TBAF, instead of radical/electrophilic sources. To optimise the reaction conditions, an essential task prior to the screening of different heterogeneous catalysts for alkane fluorination, detailed kinetic studies were first reported. Following investigation of this system it was found that: i) the active oxidant species has a lifetime $\leq$ 30 minutes, therefore, periodic addition of PhIO was essential, ii) (TMP)Mn(III)Cl exhibits a maximum TON = 50 for alkane fluorination, iii) competition between oxidation and fluorination occurs, with maximum 50 % of selectivity observed for the $C(sp^3)$-F product.

To better understand the system, stability studies were also performed, allowing a reaction scheme to be proposed. Within this scheme, competition between fluorination and oxidation is observed. Preliminary mechanistic studies have been performed, *via* UV-Vis analysis, and the formation of an intermediate high valent Mn-porphyrin species was observed at 415 - 428 nm. The interaction of this species with the substrate was also analysed, further confirming that this species is a Mn-porphyrin intermediate, actively involved in the reaction mechanism.

By changing the type of oxidant in the Groves[1] system, it was found that the selectivity of the system in terms of fluorine/oxygen selectivity could be tuned. This represents an interesting finding, suggesting that the development of a catalyst with tuneable selectivity, ideally active solely for alkane oxidation or alkane fluorination, depending from the reaction conditions, could in principle be achieved. However, despite this finding, it was noted that the oxidation route was generally preferred to the fluorination pathway, under the conditions optimised during this study.

In parallel with kinetic and mechanistic investigation of the system, a preliminary approach for the preparation of a heterogeneous catalyst for alkane fluorination reaction has also been performed by supporting (TMP)Mn(III)Cl on SiO$_2$. However, although good activity was observed, the material is not stable under reaction conditions, and significant leaching of (TMP)Mn(III)Cl was found to occur.

7.2 Pertaining challenges

This thesis has provided good insight into the applicability of heterogeneous catalysts to perform fluorination reactions, focusing on $C(sp^3)$-F formation, demonstrating that: i) active, ii) stable, iii) reusable, and iv) truly heterogeneous catalysts can be employed for $C(sp^3)$-F formation, especially when pre-activated substrates such as carboxylic acids are employed. Despite this, several challenges and hurdles remain to be overcome, and these should represent the focus of future research studies.

Despite the good results presented in Chapters 3 and 4, more detailed analysis on the reusability of the catalytic materials could be pursued, in order to further improve the stability and reusability properties of the materials designed in this research. In fact, given that stability of a catalyst is often more commercially determining than its

intrinsic activity, developing robust heterogeneous catalysts, particularly those capable of continuous operation, is an important task.[2]

Similarly, more detailed analysis on the versatility of the systems, could also be interesting to explore in future studies. Indeed, developing a robust and versatile catalyst could dramatically increase the suitability of the heterogeneous catalysts developed in this research for intensified operation. Of particular interest is the development of catalysts capable of converting additional substrates, particularly those possessing additional functional groups.

Preliminary mechanistic studies, in order to study the reaction mechanism, especially focusing on the interaction between TiO_2 and carboxylic acids, under photocatalytic conditions, were also investigated in this work. Although preliminary mechanisms have been proposed, the radical nature of decarboxylative fluorination systems means that further analysis, with radical sensitive techniques such as EPR, aimed to the identification of the intermediate radical species participating to the reaction mechanism, could be performed. Likewise, considering the high impact and the radical-involving nature of all the systems reported so far, mechanistic studies including: i) isotope effects, ii) experiments with radical clocks, and iii) effect of radical scavenger, could also be the focus of future studies. Moreover, considering the good photocatalytic performances exhibited by TiO_2, the applicability of this system could be further investigated for other classes of substrates, such as alkanes.

This thesis also provides preliminary investigations of different fluorinating systems, for direct $C(sp^3)$-H fluorination. However, although heterogeneous materials were found to be active to some extent also for type of reactions such as benzylic fluorination, the employment of electrophilic/radical fluorinating agents such as Selectfluor® has exhibited several problems, suggesting that the system under investigation is not viable. However, further studies in order to develop a viable benzylic fluorination system, especially desirable for many pharmaceutical applications, are definitely worthy of attention. This thesis also provides a valuable insight into alkane fluorination reactions catalysed by (TMP)Mn(III)Cl. Indeed, preliminary kinetic and mechanistic insight have revealed competition between fluorination and oxidation. However, the relative rate of both pathways has been shown to be tuneable. Therefore, further studies will be focused on the optimisation of

this system in order to achieve the highest selectivity toward fluorination. Also, a preliminary attempt toward the preparation of a heterogeneous material containing (TMP)Mn(III)Cl, has demonstrated that simple supporting procedures do not provide sufficient stability to the catalyst. Considering the instability of simple supported catalyst, (TMP)Mn(III)Cl, encapsulated materials, where the porphyrin can be trapped within a cage of a porous material, may prove to be suitable alternatives for the preparation of a heterogenous material containing (TMP)Mn(III)Cl, to perform alkane fluorination reactions. Alternatively, more functionalised porphyrin backbones, such as 5,10,15,20-tetrakis(1-methyl-4-pyridinio)porphyrin tetra(p-toluenesulfonate), TMPyP, may prove to be more amenable to coordination to a solid support, given their higher degree of functionalisation. Thus, future studies will also focus on preparation and catalytic investigation of these new types of Mn(III)-porphyrin containing catalysts, in order to design a robust heterogeneous catalyst active for alkane fluorination reactions.

7.3 References

[1] W. Liu, X. Huang, M. J. Cheng, R. J. Nielsen, W. A. Goddard, J. T. Groves. *Science*, 2012, **337**, 1322-1325.

[2] C. Hammond, *Green. Chem.*, 2017, **12**, 2711-2728.

Appendix

8

8.1 pXRD analysis of TiO₂ supported catalysts and pure TiO₂

The average crystallite size for anatase and rutile phases of TiO_2 supported heterogeneous catalysts were calculated using the Scherrer equation and are reported below in Tables 8.1. For anatase and rutile, reflections centred at 25.5 and 27.7 °, respectively, were used to determine the average crystallite size. The relative composition between the two phases is also reported for all catalysts.

Catalyst	Anatase (Å)	Rutile (Å)	% Anatase	% Rutile
Unsupported TiO_2	209	245	86	14
$1Ag_2O/TiO_{2(MM)}$ 3 Hz	208	241	86	14
$1Ag_2O/TiO_{2(MM)}$ 7.5 Hz	220	227	86	14
$1Ag_2O/TiO_{2(MM)}$ 15 Hz	209	234	82	18
$1Ag_2O/TiO_{2(MM)}$ 22.5 Hz	189	287	82	18
$1Ag_2O/TiO_{2(MM)}$ 7.5 Hz	174	292	73	27

Table 8.1a: Average crystallite size and relative ratio for anatase and rutile phases of: i) unsupported TiO_2 and ii) TiO_2 supported heterogeneous catalysts following preparation at different milling frequencies.

TiO_2	Anatase (Å)	Rutile (Å)	% Anatase	% Rutile
1st cycle	209	245	86	14
2nd cycle	210	302	84	16
3rd cycle	201	273	82	18
4th cycle	228	261	78	22

Table 8.1b: Average crystallite size and relative ratio for anatase and rutile phases of fresh and used TiO_2 (P25) during photocatalytic decarboxylative fluorination (Chapter 4 p. 143)

Catalyst	Anatase (Å)	Rutile (Å)	% Anatase	% Rutile
$1Ag_2O/TiO_{2(SI)}$ Not calcined	209	278	82	18
$1Ag_2O/TiO_{2(SI)}$ Calcined at 350°C	212	292	81	19

Table 8.1c: Average crystallite size and relative ratio for anatase and rutile phases of TiO_2 supported heterogeneous catalysts prepared *via* sol immobilisation.

8.2 BET analysis of TiO_2 supported catalysts and pure TiO_2

BET analysis of Ag_2O/TiO_2 mechanochemical mixtures prepared at different milling frequencies:

$1Ag_2O/TiO_{2(MM)}$	Specific Surface Area (m^2/g)
3 Hz	57
7.5 Hz	59
15 Hz	65
30 Hz	55

Table 8.2a: Specific surface areas of $1Ag_2O/TiO_2$ catalysts following preparation at different milling frequencies.

BET analysis of TiO$_2$ (P25) before and after photocatalytic decarboxylative fluorination:

Catalyst	Specific Surface Area (m^2/g)
Fresh TiO$_2$	55
Used TiO$_2$	55

Table 8.2b: Specific surface area of TiO$_2$ (P25) prior and after photocatalytic decarboxylative fluorination (Chapter 4 p. 143).

8.3 GC calibration equations

GC calibration equations for benzylic fluorination reaction:
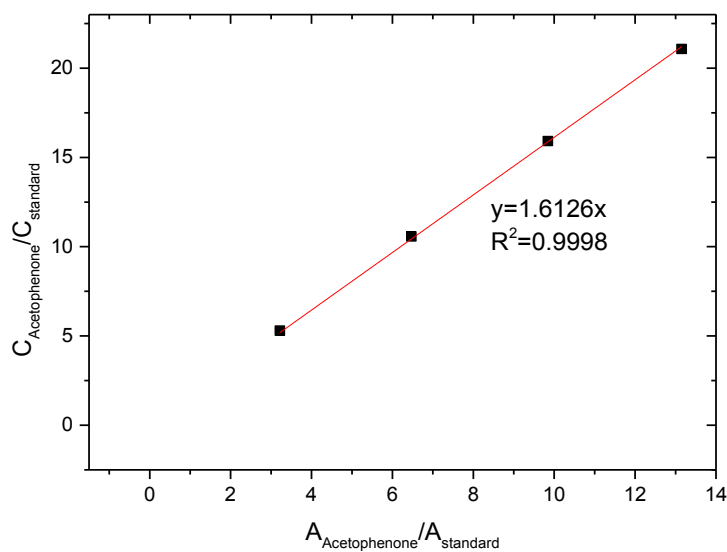
Figure 8.1: Calibration line for acetophenone performed with the GC using biphenyl as internal standard.
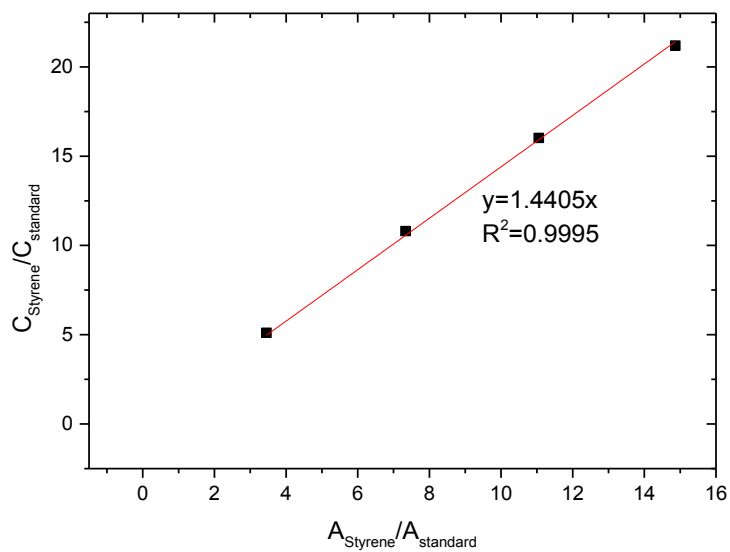
Figure 8.2: Calibration line for styrene performed with the GC using biphenyl as internal standard.
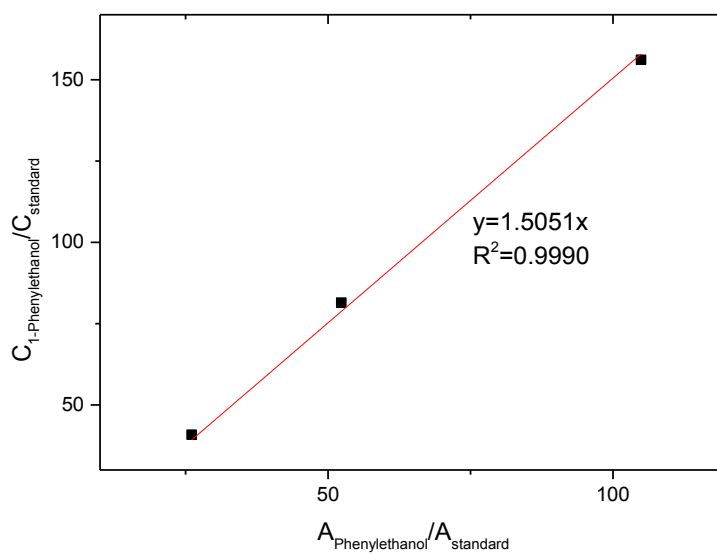
Figure 8.3: Calibration line for 1-phenyl-ethanol performed with the GC using biphenyl as internal standard.

GC calibration equations for cyclooctane fluorination:
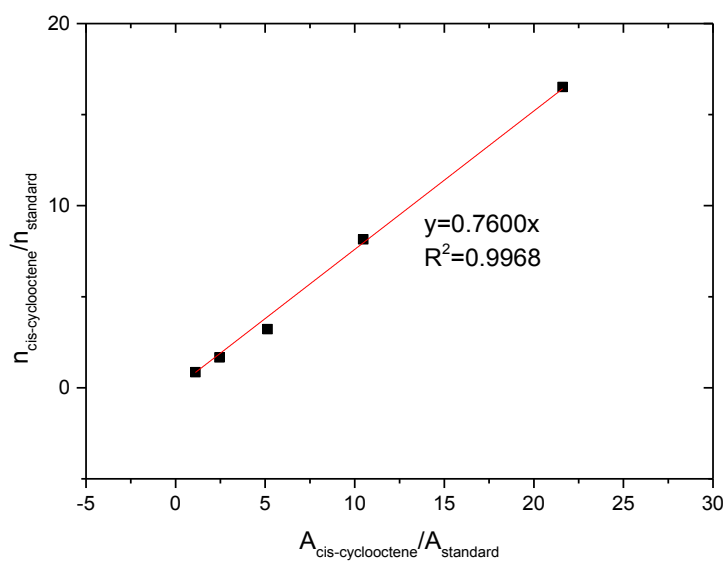
Figure 8.4: Calibration line for cis-cyclooctene performed with the GC using α,α,α-trifluorotoluene as internal standard.
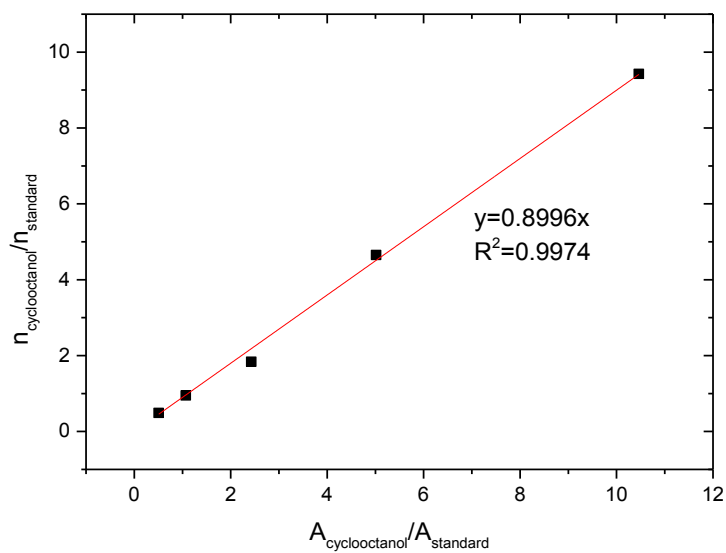
Figure 8.5: Calibration line for cyclooctanol performed with the GC using α,α,α-trifluorotoluene as internal standard.
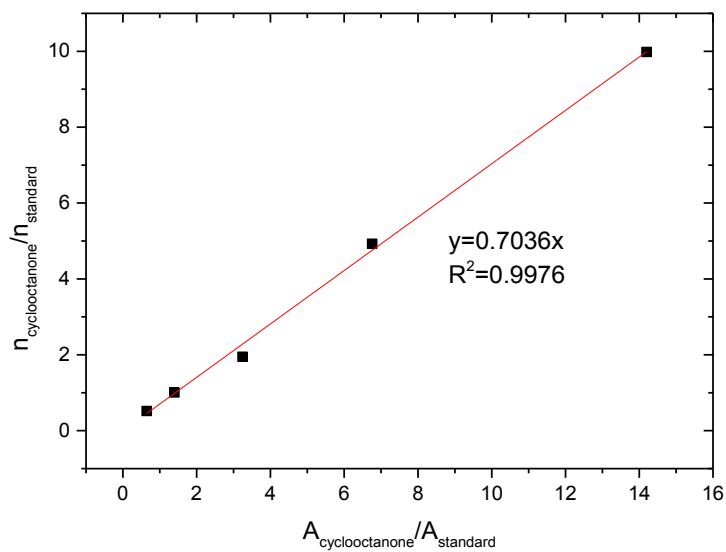
Figure 8.6: Calibration line for cyclooctanone performed with the GC using α,α,α-trifluorotoluene as internal standard.
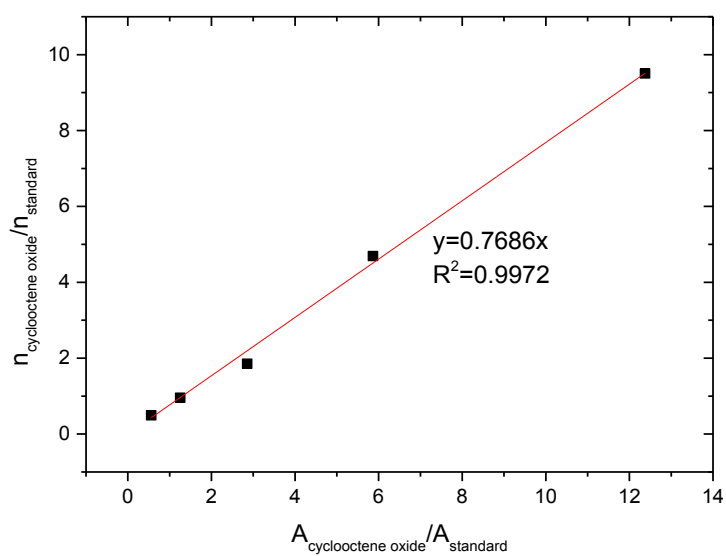
Figure 8.7: Calibration line for cyclooctene oxide performed with the GC using α,α,α-trifluorotoluene as internal standard

8.4 NMR spectra

In this section are reported NMR spectra for the products involved in this work. ^{19}F spectra were run on a JEOL Eclipse (+) 300M Hz equipped with a 5mm autotunable BBO probe and on a 400 MHz Bruker UltraShield^{TM} using α,α,α-trifluorotoluene as reference (δ=-63.72 ppm), ^{1}H of pure 4-fluoro-4-methylpentanoic acid was run on a 400 MHz Bruker UltraShield^{TM} spectrometer using TMS as reference (δ=0 ppm).

HOOC ⟍⟍ F **(1)**
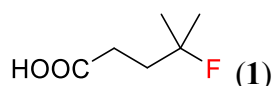
Figure 8.8: Chemical structure of 4-fluoro-4-methylpentanoic acid (**1**).

4-fluoro-4-methylpentanoic acid (**1**) was prepared from 2,2-dimethylglutaric acid according to the general procedures described in Chapter 3 and Chapter 4. ^{19}F NMR (CDCl$_3$, 283 MHz): δ −141.29 (m, 1F). ^{19}F NMR (H$_2$O/(CH$_3$)$_2$CO, 283 MHz): -135.19 (m, 1F). ^{19}F NMR (D$_2$O, 283 MHz) δ -137.21 (m, 1F), in agreement with the values found in literature.[1]
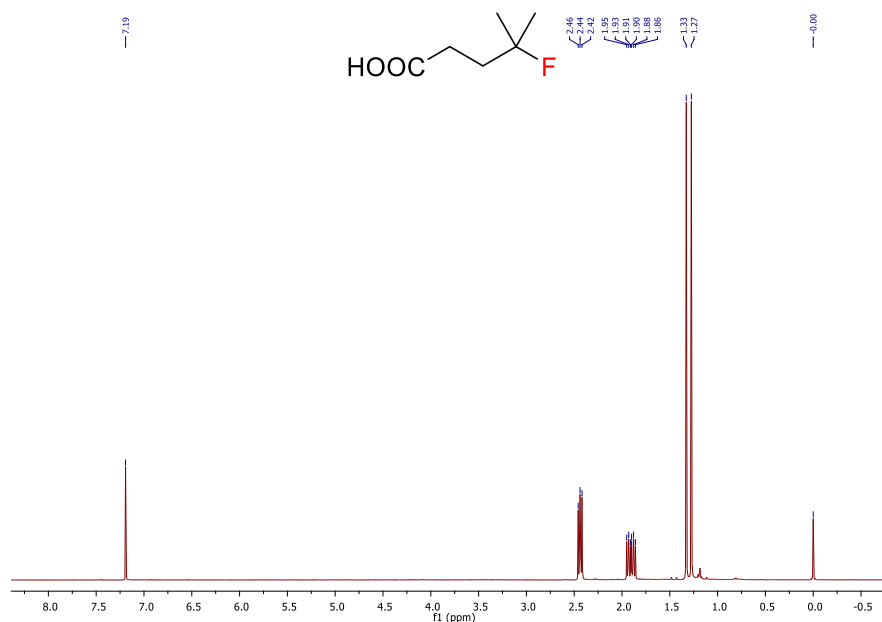
Figure 8.9: ^{1}H NMR spectra of 4-fluoro-4-methylpentanoic acid (**1**) in CDCl$_3$.
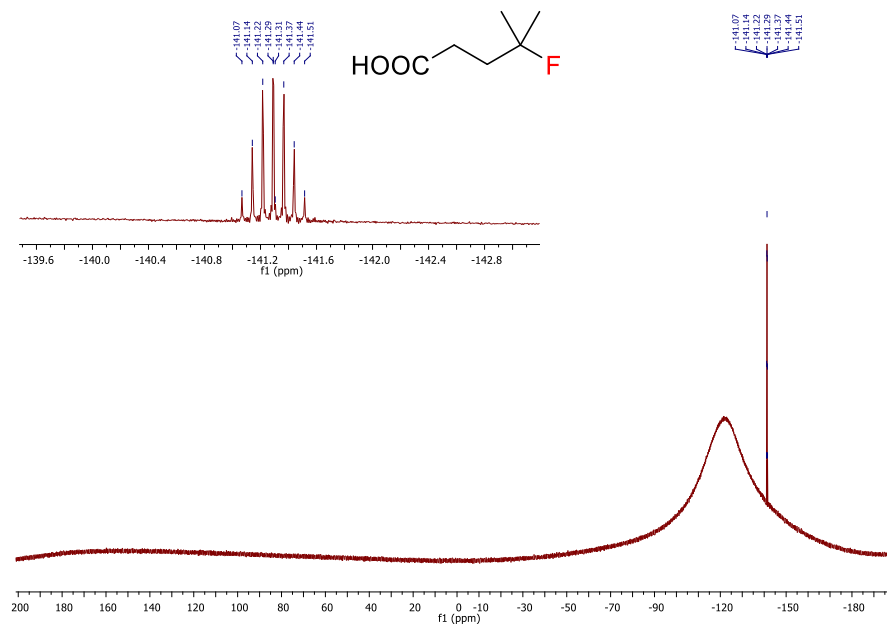
Figure 8.10: ^{19}F NMR spectra of 4-fluoro-4-methylpentanoic acid (**1**) in CDCl$_3$.
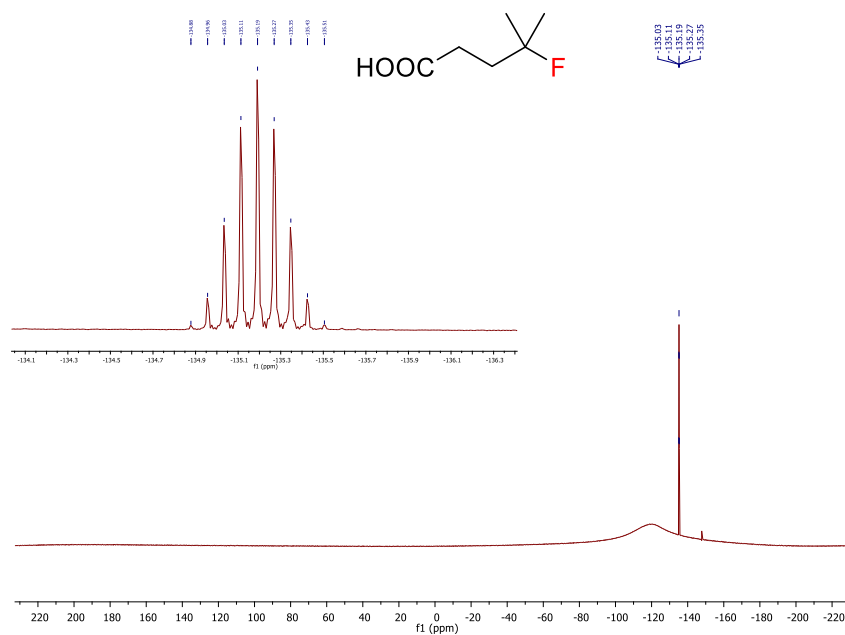
Figure 8.11: ^{19}F NMR spectra of 4-fluoro-4-methylpentanoic acid (**1**) in H$_2$O/(CH$_3$)$_2$CO.
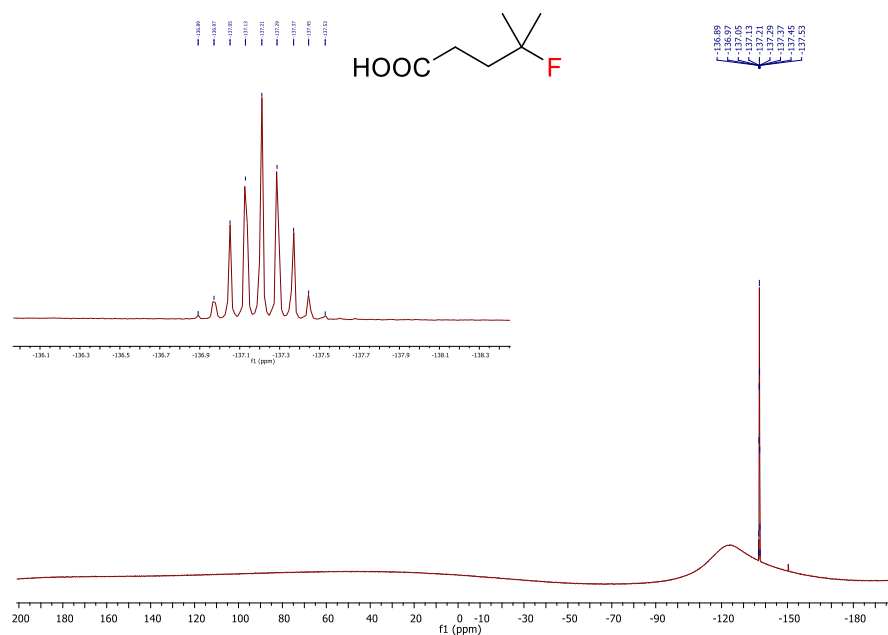
**Figure 8.12:** ^{19}F NMR spectra of 4-fluoro-4-methylpentanoic acid (**1**) in D$_2$O.
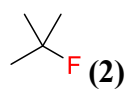
Figure 8.13: Chemical structure of 2-fluoro-2-methylpropane (**2**).

2-Fluoro-2-methylpropane (**2**) was prepared from pivalic acid according to the general procedures described in Chapter 3 and Chapter 4. ^{19}F NMR (no solvent, 376 MHz) δ − 129.35 (m, 1F), in agreement with the value found in literature.[2]
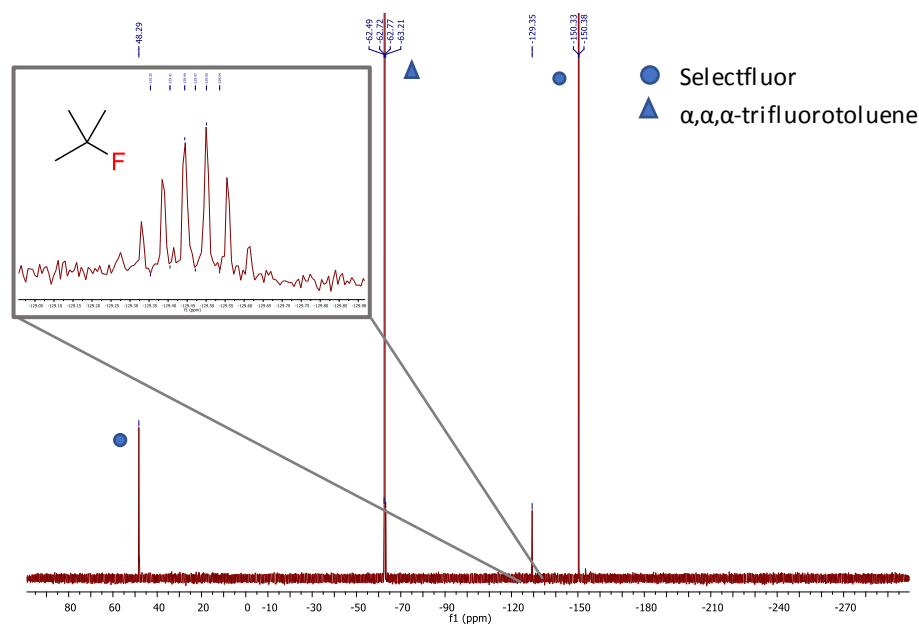
Figure 8.14: ^{19}F NMR spectra of crude reaction with pivalic acid as substrate.
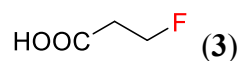
Figure 8.15: Chemical structure of 3-fluoropropanoic acid (**3**).

3-Fluoropropanoic acid (**3**) was prepared from succinic acid according to the general procedures described in Chapter 3 and Chapter 4. ^{19}F NMR (no solvent, 376 MHz): δ – 217.29 (m, 1F), in agreement with the value found in literature.[3]
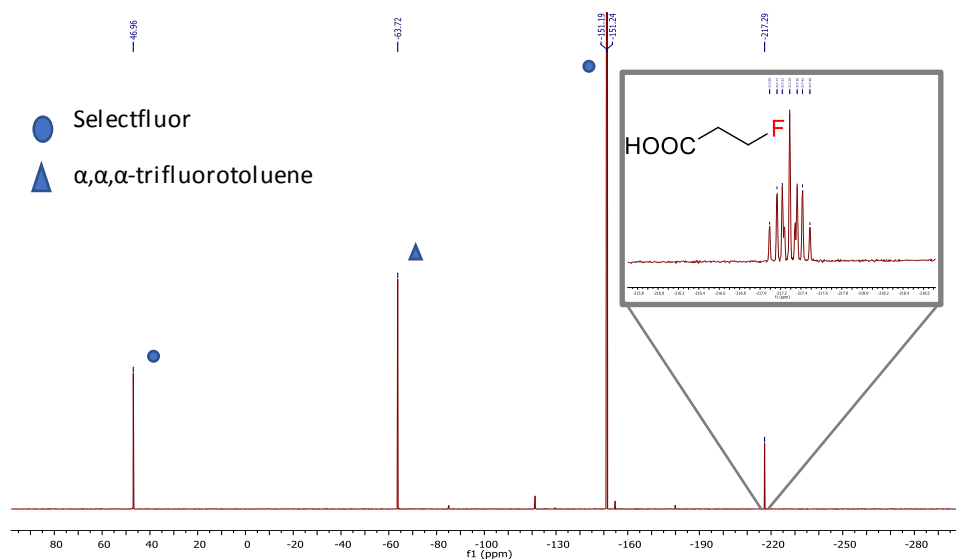
Figure 8.16: ^{19}F NMR spectra of crude reaction using succinic acid as substrate.
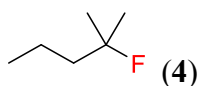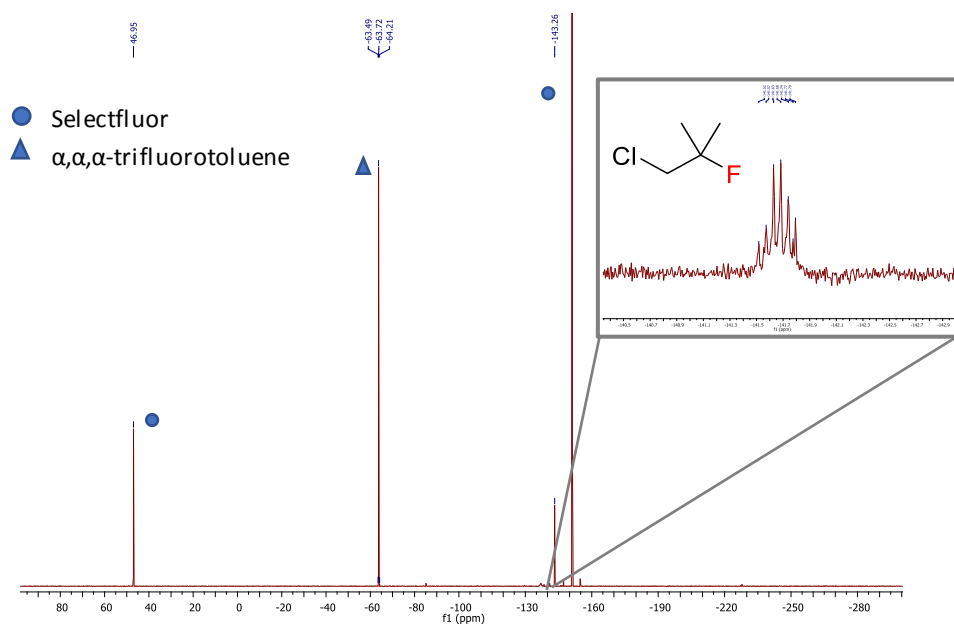

Figure 8.17: Chemical structure of 2-fluoro-2-methylpentane (**4**).

2-Fluoro-2-methylpentane (**4**) was prepared from 2,2-dimethylvaleric acid according to the general procedures described in Chapter 3 and Chapter 4. ^{19}F NMR (CDCl$_3$, 376 MHz): δ −136.94 (m, 1F), in agreement with the value present in literature.[2,3]
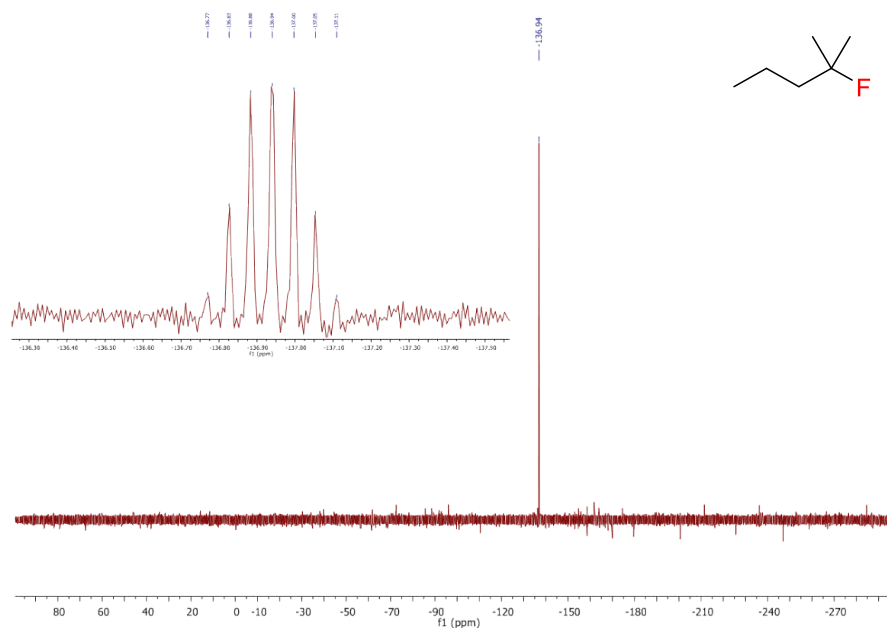
Figure 8.18: ¹⁹F NMR spectra of 2-fluoro-2-methylpentane (**5**) in CDCl₃.

(**5**)
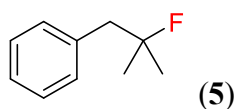
Figure 8.19: Chemical structure of (2-fluoro-2-methylpropyl)benzene (**5**).

(2-Fluoro-2-methylpropyl)benzene (**5**) was prepared from 2,2-dimethyl-3-phenylpropionic acid according to the general procedure described in Chapter 3. ¹⁹F NMR (no solvent, 376 MHz) δ –137.89 (m, 1F), in agreement with the value found in literature.[3]
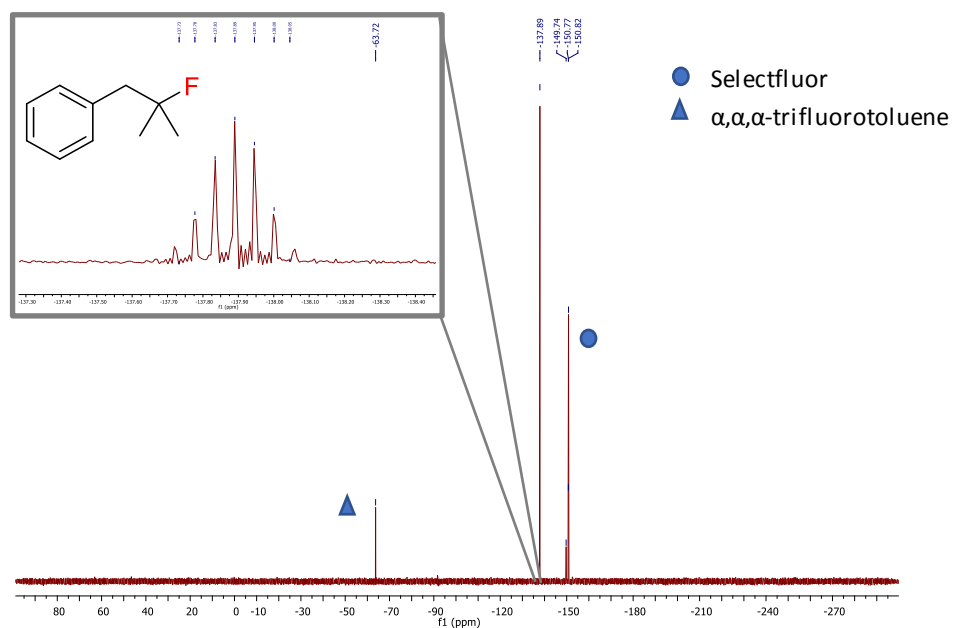
**Figure 8.20:** ^{19}F NMR spectra of crude reaction with 2,2-dimethyl-3-phenylpropionic acid as substrate.
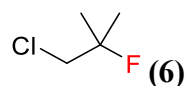
Figure 8.21: Chemical structure of 3-chloro-2-fluoro-2-methylpropane (**6**).

3-Chloro-2-fluoro-2-methylpropane (**6**) was prepared from 3-chloro-2,2-dimethylpropionic acid according to the general procedure described in Chapter 4. ^{19}F NMR (no solvent, 376 MHz) δ −143.26 (m, 1F).
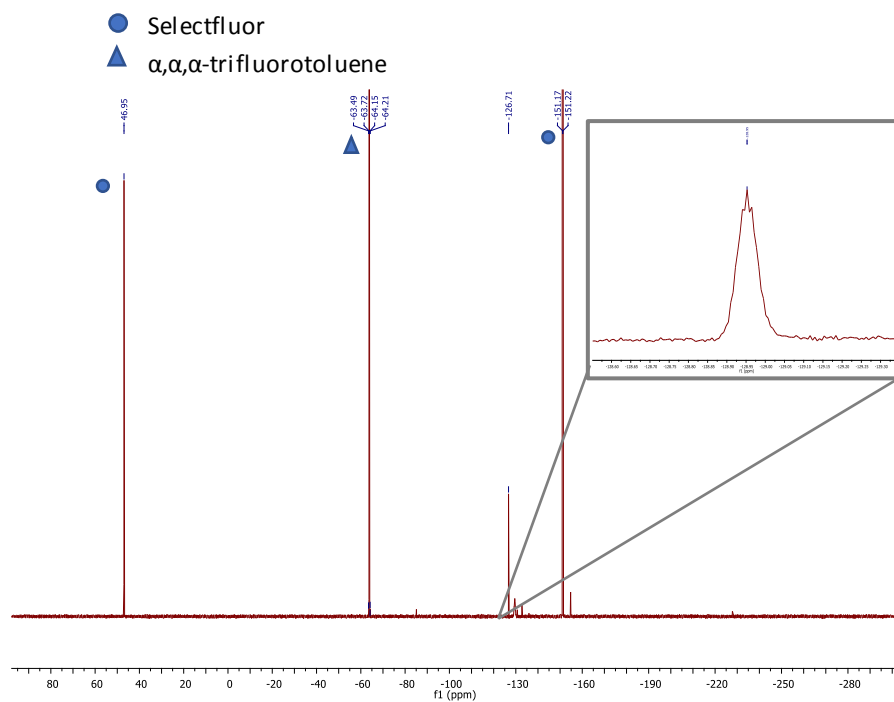
Figure 8.22: ^{19}F NMR spectra of crude reaction with 3-chloro-2,2-dimethylpropionic acid as substrate.
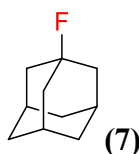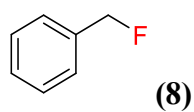

Figure 8.23: Chemical structure of 1-fluoroadamantane (**7**).

1-Fluoroadamantane (**7**) was prepared from 1-adamantane carboxylic acid according to the general procedure described in Chapter 4. ^{19}F NMR (no solvent, 376 MHz) δ = - 126.71 (s, 1F), in agreement with the value found in literature.[2]
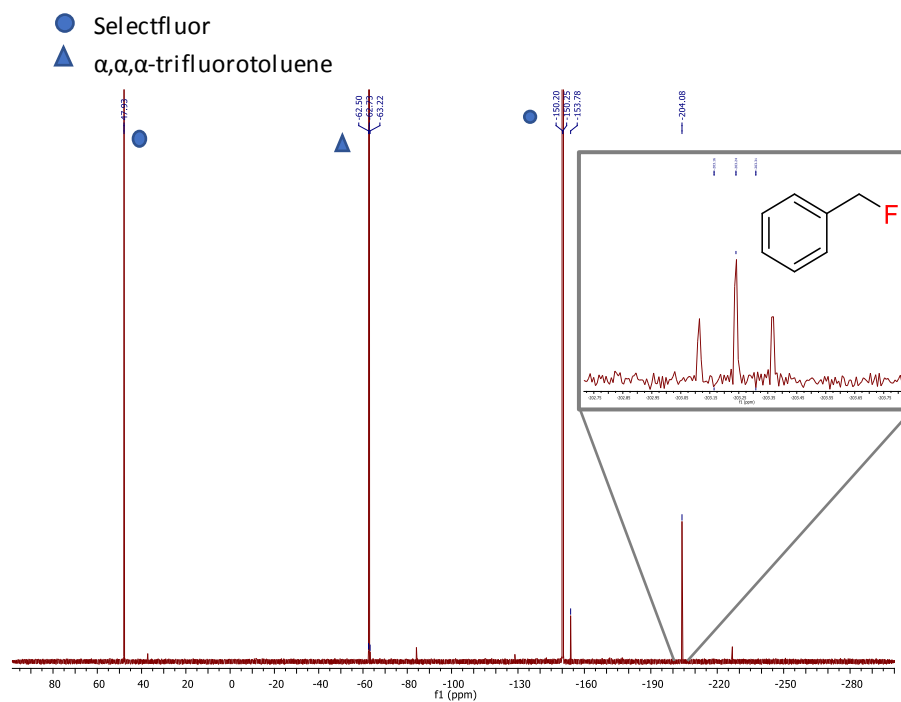
Figure 8.24: ^{19}F NMR spectra of crude reaction with 1-adamantane carboxylic acid as substrate.

Figure 8.25: Chemical structure of benzyl fluoride (**8**).

Benzyl fluoride (**8**) was prepared from phenylacetic acid according to the general procedure described in Chapter 4. ^{19}F NMR (no solvent, 376 MHz) δ −204.08 (t, $^{2}J_{H-C-F}$ = 48 Hz, 1F), in agreement with the value found in literature.[2]

Figure 8.26: ^{19}F NMR spectra of crude reaction with phenylacetic acid as substrate.

8.5 References for known compounds

[1] N. R. Patel, R. A. Flowers. *J. Org. Chem.*, 2015, **80**, 5834-5841.

[2] F. J.Weigert, *J. Org. Chem.,* 1980, **45** (17), 3476-3483.

[3] J.-B. Xia, C. Zhu, C. Chen, *Chem. Commun.*, 2014, **50**, 11701-11704.